國立臺灣大學生命科學院動物學研究所

碩士論文

Institute of Zoology
College of Life Science
National Taiwan University
Master Thesis

以大量平行定序資料推估果蠅的種化歷史

Inferring speciation history of *Drosophila* by massive parallel sequencing

何韋進

Wei-Chin Ho

指導教授：丁照棣

Advisor: Chau-Ti Ting

中華民國 99 年 6 月

June, 2010

誌謝

人生用旅行來比喻再恰當不過了(正確說來，旅行亦是人生中的一段較短的時間，而這較短的時間讓我們比較容易想像罷了)。這旅途上總有岔路，因著選擇的岐異，會遇到形形色色的人、事、物。你我若有緣，便能相視而笑，甚或長程陪伴；若無緣，則見面不識，無處往來。對於我有緣在人生中所能碰到的人們，我都將由衷的感謝。

不論緣份這套道理對你們是否管用，我的現實人生，確實有了一個小小的段落。那便是到了台大動物所，做了一些事，寫了一些文章。在這一段小小的旅行中，我要特別感謝丁照棣老師，給了我一個馳騁的舞台，願意花很多的時間帶著我想問題、討論分析方法，也能夠包容我的糊塗與不成熟。感謝李壽先老師過去在族群遺傳學課上的教學，算是我這段路程的起點。感謝于宏燦老師的金玉良言，字字發人深省。過去大學時代亦曾上過阮雪芬老師的生物資訊課，也許是讓我踏上這段旅程的遠因。謝文萍老師的統計知識淵博，有機會的話我還想向老師討教。感謝眾口試委員願意抽空讀我的論文初稿，以及在口試時給我的許多寶貴建議。另外，感謝曹順成老師和方淑老師關於我研究工作上的討論幫忙，以及日常生活上的協助。也感謝張慧羽老師，每次的討論都讓我獲益良多。同時，也感謝同樣在族群遺傳學課堂上帶給我很多背景知識的王弘毅老師。

除了眾多老師外，朝夕相處的實驗室夥伴也對我很有幫助。感謝小春，你是除了老師外，我最有力的知識來源，非常懷念你在實驗室時，能夠和你討論的日子。感謝雅仁，雖然你每次都說對我的研究幫不上忙，但對於我學術背景和心理素質的幫助都甚大。感謝承叡，沒有你在分析方法上打先鋒的話，我的研究工作想必會遇到更多困難。感謝文喬和心彥，兩位散發出的母愛雨露均霑，各方面的照顧都無微不至。感謝小菊，和你聊天真的很有趣。感謝其駿，和你的討論常常能刺激我多方面的思考。感謝士又，你在學術研究和流行資訊上的學問，讓我學到很多。感謝姵君和莞儒，進入實驗室受到兩位學姊很多的幫助和鼓舞，不會忘記我們一起去清大上課的日子。感謝筱涵，這一段小小的旅

行的最初和最後都收到你的鼓勵，非常感動。感謝景賀，你跟我的討論常常都很受用，讓我學習到不少。感謝凱文，有你在讓實驗室的生活增色不少。另外也要感謝實驗室的生力軍：家翔、宇謙、瑾瑜、芷筠、詩凡、佳蓉、家宣（雖然你說不要寫你，但我硬是要寫），和你們一起談天說地，讓我這一趟旅程很開心。

走在旅程的先端，回頭望望總會看到初始的地方。感謝我的爸媽和弟弟，處處包容我，時時支持我，讓我有機會夠做我自己最想要做的事情而無後顧之憂，謝謝你們。

最後，真的感謝所有人生路途上我碰過的人們，幫助過我的人們。我願將此感謝，化為貢獻丁點知識於全人類的誠心，繼續接下來的旅程。

各位，旅程上後會有期了！

韋進 於 2010 年夏

摘要

如何能使一個新物種形成，對演化生物學家來說仍然是有趣且重要的待解決問題。雖然已經有很多理論被提出，對於種化的進程的瞭解和能夠支持的適當例子仍相當有限。最近隨著大量平行定序技術的發展，比起以往我們能夠更容易的得到大量序列資料。這些充足的序列資料提供了一個絕佳的機會來研究過去缺乏序列資料時所難以回答的種化問題。此篇論文中，有兩個系統藉著大量平行序列資料來研究種化的問題。其一，為了演示種化的基因觀點，擬黃果蠅類群被作為研究的對象。藉由 4348 個基因序列資料，種化模型檢定揭露了這些基因間分歧時間有顯著的不同。此外，也發現了不同演化樹型的支持度鑲嵌在基因體中的現象。這些結果演示了基因體層次上的演化樹型不一致，且提出了在這個類群的種化過程中，扮演重要角色的候選基因。其二，為了分析造成種化的機制，黃果蠅的初期種化模型成為研究的對象。這個模型由具有行為隔離的全球型與辛巴威型組成。藉由族群基因體序列，分析出在各行為種中可能在演化歷史上經歷過適應的位點。另外藉由全轉錄體定序，分析得到在兩不同行為種間表現量有顯著歧異的基因。有趣的是，在辛巴威型果蠅中有顯著較高表現量的基因中，被發現和視覺有關功能的基因占有顯著的比例，而在全球型果蠅中有顯著較高表現量的基因，則是和代謝有關的基因。這些結果不僅提供研究行為隔離的遺傳基礎，也建議了種族分化的可能機制。

關鍵字：大量平行定序、種化、擬黃果蠅類群、全球型／辛巴威型分化

Abstract

To evolutionary biologist, how a new species arise remains an interesting and important question to solve. Though many hypothetical scenarios were proposed, it is still limited to understand how speciation progresses and discover proper cases to support. Currently, it is easier to sample the considerable sequences with the development of massive parallel sequencing (MPS). These abundant sequences provide a superior opportunity to approach speciation questions which were hard to assay before. Here, two systems with speciation questions were studied via the help of MPS. First, to demonstrate the genic view of speciation, *Drosophila simulans* clade were used as a model to analyze. With the sequences of 4348 genes, significantly heterogeneous divergence was revealed by the speciation model test. In addition, the genome-wide mosaic nature of phylogeny inference was also discovered. These results demonstrate the discordance of topologies among loci at the genomic level and proposed the candidates which can be crucial during speciation. Second, to assay the mechanisms which play an important roles in speciation, the incipient speciation model of *Drosophila melanogaster* were analyzed. This model comprises two behavioral isolated races, M (for cosmopolitan) and Z (for Zimbabwe). In each race, the adaptive loci were suggested by using population genome sequence. Moreover, the differentially expressed genes were found by using RNA-seq. Interestingly, the genes upregulated in the Z race are enriched for vision whereas genes upregulated in the M race are enriched in metabolic processes. These results not only provide the genetic basis of behavior isolation but also suggest the driving force underlying racial differentiation.

Keywords: massive parallel sequencing, speciation, *Drosophila simulans* clade, Z/M differentiation

Contents

誌謝 ……i

中文摘要 ……iii

Abstract ……v

Chapter 1 General Introduction ……1

Chapter 2 Inferring the Speciation History by Massive Gene Trees in *Drosophila simulans* clade

Introduction ……9

Materials and Methods ……14

Results ……19

Discussion ……37

Chapter 3 Sequence and Expression Divergence between Two *Drosophila melanogaster* Races in Incipient Speciation

Introduction ……41

Materials and Methods ……46

Results ……51

Discussion ……88

References ……94

Appendix ……104

Supplementary Tables ……107

List of Tables

Table 2.1 Speciation model test of each paired species……24

Table 2.2 Branch-specific d_N and d_S categorized by their inference via maximum likelihood method……25

Table 2.3 Speciation model test of each paired species based on X chromosome genes……26

Table 2.4 Branch-specific d_N and d_S on chromosome arms via maximum likelihood method……27

Table 2.5 The number of candidate regions based on clustered windows with posterior probability > 0.8……28

Table 3.1 List of M-type and Z-type sample in genome data analysis……50

Table 3.2 Averaged population parameters of each chromosome in different populations……56

Table 3.3 The number of candidate regions suggested by different methods on each chromosome arm……57

Table 3.4 Distribution of high F_{ST} sites in genome data……58

Table 3.5 Summary of the mapping result of each sample……59

Table 3.6 Correlation coefficients between the RPKMs in each paired lines……60

Table 3.7 The number of DEGs depends on two kinds of multiple test corrections……61

Table 3.8 The GO terms enrich in Z>M DEGs based on Bonferroni's correction……62

Table 3.9 The GO terms enrich in M>Z DEGs based on Bonferroni's correction……63

Table 3.10 Distribution of High F_{ST} sites in RNA-seq data……64

Table 3.11 Distribution of Shared High F_{ST} sites in two datasets……65

(Supplementary Tables)

Table s2.1 Representative GO terms of sampled genes in chapter 2……108

Table s3.1 The list of low diversity regions in Z-type race……111

Table s3.2 The list of low diversity regions in M-type race……113

Table s3.3 The list of regions with clustered high F_{ST} sites……116

Table s3.4 Z>M DEG based on Bonferroni's correction……117

Table s3.5 M>Z DEGs based on Bonferroni's correction……123

Table s3.6 Z>M DEGs based on FDR correction……129

Table s3.7 M>Z DEGs based on FDR correction……138

Table s3.8 The GO terms enrich in Z>M DEGs based on FDR correction……146

Table s3.9 The GO terms enrich in M>Z DEGs based on FDR correction……147

Table s3.10 List of shared high F_{ST} sites summarized by their belonging transcripts ……148

Table s3.11 The list of regions with clustered high F_{ST} sites by RNA-seq data …151

List of Figures

Figure 2.1 Three possible topologies……29

Figure 2.2 genome-wide pattern of phylogeny……30

Figure 2.3 The Discordant pattern on chromosomes and candidate regions……31

Figure 2.4 Distributions of within-species distance and distances between species……33

Figure 2.5 The number of genes with positive-selected lineage……34

Figure 2.6 The proportion of windows supporting each of the topologies on chromosomal arms……35

Figure 2.7 GO slim for the first level of biological process terms for the dataset……36

Figure 3.1 Hypothetical multi-loci scheme in Z/M isolation……45

Figure 3.2 The distribution of population parameters (θ, π, and Tajima's D) in different chromosome arms in two races (Z and M)……67

Figure 3.3 The distribution of nucleotide diversity (π), normalized nucleotide diversity (Z score), and differences between two Z scores in Z race and M race along chromosome arm……77

Figure 3.4 The genome-wide F_{ST} pattern on different arms……83

Figure 3.5 The correlations of expression levels between each races……84

Figure 3.6 The fold changes versus the p-values of Fisher's exact test in four comparisons between Z races and M races……85

Figure 3.7 The genome-wide clustered F_{ST} pattern on different arms by RNA-seq data ……87

Chapter 1

General Introduction

Speciation increases the current species diversity. To evolutionary biologist, how a new species arise is an interesting and important question to solve. According to the biological species concept (BSC), species are "groups of interbreeding natural populations that are reproductively isolated from other such groups" (Mayr 1963). Based on BSC, a strong barrier to prevent gene flow between two species is essential in speciation. Therefore, understanding isolation mechanisms is crucial in the studies of speciation and diversity.

Barriers to gene flow

There are usually two time points to categorizing these barriers to gene flow. One is mating, when males and females bump into each other and transfer their gametes, and the other one is zygote formation, when the fertilization occurs and the hybrid zygote is on the way to develop to a new individual. According to these two time points, three kinds of isolations are named: premating isolation, postmating and prezygotic isolation, as well as postzygotic isolation. Each isolation category has their own examples as introduced in the following sections.

Premating isolation describes that the male in one species and the females in another species have no or few opportunities to meet each other or meet without mating, so the gene flow between these two species are blocked. The separation can be due to the different habitat (habitat isolation). For example, the meeting occurrence between two close species of ladybird beetles, *Epilachna niponica* and *E. yasutomii,* is few because they have different preferred plants, thistles and blue cohosh (Katakura

and Hosogai 1994). In addition, the isolation can be caused by different breeding seasons or times of a day (temporal isolation). An example is that the different seasons (fall and spring) to reaching reproductive age of two field crickets, *Gryllus pennsylvanicus* and *G. veletis* (1979). Besides, another example is that several hours apart between the spawning time of two Atlantic corals, *Montastraea annularis and M. franksi* (Knowlton et al. 1997) . These two examples explicate the temporal isolation can occur no matter the time difference is long or short.

In addition, the premating isolation can form because the discriminated preference toward the mating signals. The mating signals are various and at least include visual signals, acoustic signals, and chemical signals. For instance, Martinez Wells and Henry (1992) reported that there are three specific kinds of courtship songs in green lacewings (*Chrysoperla plorabunda* complex) are used by males to attract females. Moreover, the ultraviolet pattern and pheromones play important roles in sexual isolation between two sulfur butterflies, *Colias eurytheme* and *C. philodice* (Silberglied and Taylor 1978).

Postmating, prezygotic isolation means that the zygote does not form even though the mating really occurs. The zygote formation is not guaranteed by mating behavior due to some mechanisms which inhibit or decrease the heterospecific hybridization. A better-studied example is that the specificity of egg and sperm in several abalones (*Haliotis*) from California is very high, and it has been suggested to be due to interaction between sperm protein lysine and envelop receptors in egg (Kresge, Vacquier, and Stout 2001).

Postzygotic isolation is the character that reduces survival rates (inviability) or reproductive rates (sterility) of hybrids. For example, hybrid females between two

parrots (*Agapornis roseicollis* and *A. personata fischeri*) have lower reproductive rate because of their very slow response to male courtships (Buckley 1969). Another case is the hybridized F_2 progeny between two yeasts (*Saccharomyces cerevisiae* and *S. bayanus*) suffer sporulation defects due to the incompatibility of their nuclear and mitochondrial genomic materials (Lee et al. 2008).

It is noted that these isolating mechanisms are not exclusive with each other. While there can be a lot of isolation mechanisms between the species can be discovered, it is still absorbing to assay their time order. During speciation, the isolating mechanisms occurred from very beginning stage may drive the formation of other isolating mechanisms. To reveal the speciation history, these isolating mechanisms should be dissected in detail.

Geographic Speciation Modes

When we plan to approach the beginning of speciation, we can not ignore the mode of biogeography no matter what kind of isolating mechanism serve as initiating force. According to the geographic distribution of ancestor and derived species, at least three kinds of speciation model were proposed including allopatric speciation, sympatric speciation, and parapatric speciation.

The central idea of allopatric specition is that the evolution of reproductive isolation is due to geographical separation. When geographical separation forms, the gene flow of two populations decrease severely, and then the populations evolve independently. Two kinds of allopatric speciation are categorized are allopatric speciation by vicariance and peripatric speciation based on the sizes of separated populations. While the two separated populations are equally large in allopatric speciation by vicariance, the small population from ancestors diverges in peripatric

speciation. For example, many speciation events of several cricket (*Laupala*) species in Hawaiian archipelagos are suggested to be peripatric (Shaw 2002).

When sympatric speciation occurs, there are no geographic barriers to prohibit gene flow between populations. The reproductive isolation between two populations evolves even with their abundant gene flow initially. This mode of speciation is more difficult theoretically due to the abundant gene flow and competition of coexistence. A remarkable example of sympatric speciation is the cichlid fish (*Amphilophus zaliosus*) evolved from an acestral species (*A. citrinellus*) in Lake Apoyo, Nicaragua and this is suggested by their morphology and dietary differentiation as well as phylogeographic analysis (Barluenga et al. 2006).

In the middle of allopatric and sympatric speciation, parapatric speciation means the reproductive isolation forms with limited gene flow. Theoretically, it can occur in two adjacent populations with different selective pressures or with evolved reproductive incompatibility. Though this is an available model theoretically, it is difficult to demonstrate by rejecting allopatric and sympatric speciation.

Molecular data in speciation study

With the advance in molecular biology, the molecular data can be obtained easier. Besides the morphological, ecological and behavioral observation, molecular data becomes an important approach to study speciation. For example, to study the phylogeny, which helps the clarification of species and their speciation, molecular characters have advantages than morphological characters because the unambiguity, abundance and clocklikeness. Additionally, the polymorphism and divergence, which can be observed in molecular level, provide accesses to study adaptation and demography applying the knowledge of population genetics.

In addition, when we approach the genetic basis of isolation mechanism, the mapping between phenotype and genotype can be difficult. Rather than piecewise approaches, larger-scale approaches like quantitative trait loci (QTL) mapping or genome-wide association study (GWAS) are more efficient rationally. Therefore, the more genomic sequences are available, the more information in speciation study we can obtain.

Massive parallel sequencing providing new opportunities in speciation study

Nowadays, a new era in biological studies comes due to the development of massive parallel sequencing (MPS), or known as next-generation sequencing. By MPS, the sequences can be obtained sooner and cheaper than the ones by Sanger sequencing. These gigantically abundant sequence data undoubtedly helps extend our knowledge of genomes and many genomic-level studies in areas like medicine, agriculture, and of course, evolutionary biology.

There are three kinds of MPS platforms commercially released in current (Mardis 2008). The first one is Roche/454 FLX Pyrosequencer. In this platform, after the library is constructed, it is amplified on emulsify beads (known as emulsion PCR) and then sequenced by pyrosequecing. In pyrosequecing, the pyrophosphate discarded in nucleotide polymerization is utilized as the energy to react with luciferase for producing light. The amount of light correlates the amount of incorporated nucleotides. The second one is Illumina genome analyzer, which use bridge amplification to clone sequences on a chip, and then these cloned clustered are sequenced by florescence-marked bases. The third one is Applied Biosystems SOLiD^{TM} Sequencer. This platform is also used emulsion PCR, but the sequencing process is based on ligation of a universal primer and a labeled detecting primer

which have specificity of two nucleotides. Finally, the sequences are decoded by these two-base codes. No matter which platform is used, the outputs are short read sequences (about tens to hundreds base pairs). Before further analysis, assembly is the first and time-consuming step.

As mentioned above, these massive molecular data are very helpful in speciation study. For example, Hittinger et al. (2010) suggested ancient balanced polymorphisms existed in a multi-locus gene network correlated to the metabolism of sugars in some *Saccharomyces kudriavzevii* strains. In this study, with whole-genome sequences of *S. kudriavzevii* strains done by Solexa genome analyzer, the significantly higher divergence was shown in the region including these loci by comparing to the rest of genome and by reconstructing phylogenetic trees. Another example is that Rubin et al. (2010) revealed the loci such as thyroid stimulating hormone receptor are under selection during chicken domestication. Their work was done by scanning low diversity regions in whole genome, where the population sequences were obtained by ABSoLid sequencer.

Not only genomic sequences, the expression profiles (kinds and levels) can be available by MPS if total-RNA is extracted and sequenced. This is achieved by counting the number of sequenced reads, which measure the expression level for a transcript directly. When measuring expression levels, the differences between performances of sequencing are needed to be corrected. In addition, because all the transcripts are fragmentized first, the amount of short reads for one transcript also correlates with its length. Generally, RPKM is a good index because length and all number of generated reads are rationally considered as normalizing factors (Mortazavi et al. 2008).

With massive genomic sequences, we can assay the adaptive and demographic history in species genome-widely. Moreover, the genome sequences and expression profiles are helpful to search the candidate genes contribute as isolation barriers. In this study, I utilized the sequences generated by Illumina sequence analyzer to infer speciation history in two different groups, *D. simulans* clade and behavioral races of *D. melanogaster.* In chapter 2, I demonstrated using massive gene trees can approach the speciation history in *D. simulans* clade, which is a species complex and the speciation events occurs in a short time window. In chapter 3, I assayed the incipient speciation of two behavioral races of *D. melanogaster* by finding sequence and expression divergence. Both studies not only show the role of MPS in speciation study, but also increase our knowledge in the possible speciation mechanisms.

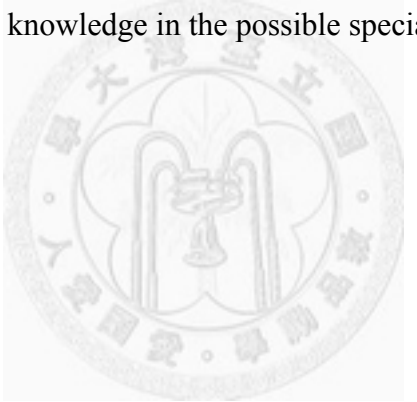

Chapter 2

Inferring the Speciation History by Massive Gene Trees in *Drosophila simulans* clade

Introduction

According to the biological species concept (BSC), the speciation accomplishes when a reproductive barrier is constructed. Based on BSC, Wu (2001) proposed the genic view of speciation. If some genes contribute the driving forces of speciation, the gene flows in these genes should be cease in the very early stage of speciation. With the progress of speciation, the region where the gene flow does not exist becomes larger. After a solid reproductive barrier is formed, the flows of all genes are not allowed and the mutations are accumulated in their lineages independently. In this view, each gene has different inference for evolutionary history because of their different properties during speciation. Therefore, when several speciation events occurred in a very narrowed time window, the discordance among genes can be severely higher. Accompanying, while there are many genes can not directly be indications, those genes which play important roles in speciation have more potential to reflect the evolutionary history.

The *Drosophila simulans* clade, which comprises *D. simulans* and its two sibling species, *D. sechellia* and *D. mauritina*, serves as a good model to speciation study for a long time. While *D. simulans* is a cosmopolitan species, the other two species are endemic island species. *D. sechellia* was collected only from several small islands of Seychelles archipelagos, and *D. mauritina* was discovered in Mauritius island most. There is still no evidence that any two of them are sympatric distributed (Lachaise et al. 1988).

Another lower-scale habitat isolation was revealed in *D. sechellia.* The distribution of *D. sechellia* is strictly associated to the fruit of rubiaceous shrub, *Morinda citrifolia*. This fruit is noxious and repulsive to other insects including *D. simulans* and *D. mauritina* implying that this fruit helps *D. sechellia* outcompete its sibling species or avoid the invasion by parasitoid wasp such as *Leptopilina* species (Rkha, Capy, and David 1991). Several genomic fragments have been suggested to be related to resistence in *D. sechellia* adults and larvae (Jones 2005)

One of the advantages for using this species complex to study speciation is its very closeness to *D. melanogaster*, which serves as a good model animal in genetics study. Therefore, the genetic assays are easier than other non-model organisms. These genetic tools can expand our study from phenotype level to genetic level. An example which was just mentioned above is mapping the adaptation loci to toxic plants in *D. sechellia*.

Moreover, through genetic assay, abundant loci were reported to cause hybrid inviability or sterility between *D. simulans* and *D.mauritiana* (Coyne 1984; True, Weir, and Laurie 1996; Wu, Johnson, and Palopoli 1996; Tao and Hartl 2003; Tao et al. 2003a; Tao et al. 2003b), between *D.simulans* and *D. sechellia* (Coyne and Kreitman 1986; Cabot et al. 1994; Hollocher and Wu 1996), as well as between *D.mauritiana* and *D. sechellia* (Masly and Presgraves 2007). Interestingly, the F_1 hybrid sterility usually occurs asymmetrically in two sexes: sterile male but fertile female. This finding supports Haldane's rule, which states that when one sex of hybridized offspring is absent, rare, or sterile, the sex is usually heterogametic one (Haldane 1922).

Among those loci, *Odysseus* (*OdsH*) is a remarkable gene which cause male hybrid sterility between *D. simulans* and *D. mauritiana*. *Ods* site was named first by Perez et al. (1993), who discovered that the sterile male in *D. simulans* background can be induced by the introgression of *Ods* fragment from *D. mauritiana*. With finer mapping, the coding gene which resides in this loci was found by Ting et al. (1998). The protein produced from this coding gene comprises 349 amino acids and has a homeobox domain, which make this gene named as *OdsH* (*Ods*-site homeobox gene). In addition, the significantly higher d_N/d_S proportion between *D. simulans* and *D. mauritiana* are revealed. Though the general functions of *OdsH* are still not uncovered clearly, the expression pattern in wild type flies and the mutant phenotype of $OdsH^0$ *D. melanogaster* suggest that its potential function is related to sperm maturation in young males (Sun, Ting, and Wu 2004; Ting et al. 2004). Currently, the diverged heterochromatin binding of *OdsH* in *D. simulans* clade were discovered and suggested to contribute on hybrid sterility (Bayes and Malik 2009).

As a hotspot model to study speciation, several characters of speciation history in this complex are roughly highlighted by previous population genetics studies. First, the species complex was suggested to diverge in just less than one million years (Kliman et al. 2000; Tamura, Subramanian, and Kumar 2004; McDermott and Kliman 2008) while the divergence time of this species complex from *D. melanogaster* was suggested to be about 5 million years (Tamura, Subramanian, and Kumar 2004). When analyzing the divergence time between *D. simulans* and *D. sechellia* as well as the one between *D. simulans* and *D. mauritina* respectively, the former one is few longer (Kliman et al. 2000). Second, the effective population sizes of two island species are very different. The population size of *D. sechellia* is much smaller than the one of *D. mauritina* (Kliman et al. 2000; Legrand et al. 2009).

The phylogeny issue of *D. simulans* clade is also studied by many different loci with population sequence data. Several genes that do not support the same phylogeny and even the populations of each species can not be in one monophyletic unit (Hey and Kliman 1993; Kliman and Hey 1993; Hilton, Kliman, and Hey 1994; Kliman et al. 2000). Among this discordant pattern, there are still two genes to provide a clear phylogeny of this species complex and cluster the populations in each species well. The first one is *OdsH*, which was mentioned to be able to cause male hybrid sterility between *D. simulans* and *D. mauritiana.* By applying maximum parsimony, the relationship, ((*simulans* and *mauritiana*), *sechellia*), was inferred clearly (Ting, Tsaur, and Wu 2000). However, when the same method was applied to a region which is 1.8 kb apart from *OdsH*, the phylogenetic relationship become unclear, and an umbrella-like tree was proposed by populations of three species. Another gene which provides a clear phylogenetic relationship among these three species' populations is *Iris* (Malik and Henikoff 2005). *Iris* was derived from a retrovirus gene, *envelope* and was also suggested to be under positive selection. However, the relationship suggested by this gene is ((*simulans* and *sechellia*), *mauritiana*), which is different from the one suggested by *OdsH*.

According to the knowledge of *D. simulans* clade including its short divergence time and revealed discordant pattern, it provides us a good model to demonstrate the genic view of speciation. In this study, I first assay the distribution of divergence time by the speciation model test. Next, the genome-wide incongruence patterns among gene trees are uncovered by several different algorithms. The incongruent patterns on the chromosomes are also revealed. Finally, I propose candidate genes by two properties, the clustered windows with high posterior probabilities to support one

topology and their monophyletic relationship among populations in one species. These genes will help us to infer the history of speciation in this clade.

Materials and Methods

Sequence mapping and assembly

The program MAQ 0.6.3 (Li, Ruan, and Durbin 2008), which could incorporate both sequencing and mapping quality, was used to map Solexa reads against reference sequences and assemble the mapping results. The reference sequences, which are obtained from FlyBase (http://flybase.bio.indiana.edu/), are the coding regions of *D. sechellia* (release 1.0, FB2008_02) and *D. simulans* (release 1.0, FB2008_02). In addition, orthology information (FB2008_02) was also obtained from FlyBase.

The set of short reads were first mapped against *D. sechellia* and the rest against *D. simulans* coding regions. The result with mapping quality score less than 20, which indicated that the probability of the mapping to be wrong is higher than 1%, is excluded. Two versions of *D. mauritiana* transcripts, one from the reads mapped to *D. sechellia* and the other from those mapped to *D. simulans*, were then assembled respectively.

Error exclusion

Before alignment, each gene was checked for frame and premature stop codon first. Of the remaining ortholog sets, the coding regions of *D. melenogaster*, *D. sechellia*, and *D. simulans* were translated into amino acid sequences and aligned using ClustalW 2.0.5 (Thompson, Higgins, and Gibson 1994). The alignment of nucleotides was then obtained based on the amino acid alignment. Abridged sequences were then obtained by excluding sites with gap in either of the three species. Ortholog sets were excluded when the abridged sequence is shorter than half of the original whole-length alignment with gaps. Furthermore, branch lengths in the

D. melanogaster-D. sechellia-D. simulans three-species phylogeny were calculated maximum likelihood method with GTR+Γ model implemented by PAUP 4.0 (Swofford 2003). Ortholog sets with shorter *D. melenogaster* branches than other branches were regarded as wrong alignment and excluded.

Sequence alignments and quality control

Based on the aligned *D. sechellia* and *D. simulans* sequences, the two versions of *D. mauritiana* assembled results were matched to the corresponding target species and then combined into one final *D. mauritiana* transcript. For each gene in the four species alignment, codons with nucleotides in "N" (ambiguous sites in *D. melenogaster*, *D. simulans*, and *D. sechellia*; lack of Solexa reads in *D. mauritiana*) or "-" (gaps) in any species were excluded from all sequences.

Any codon with the sequencing depth of any nucleotide lower than 3x was also removed for preventing possible bias caused by the sequencing error. To avoid analyzing genes with insufficient sequence information after these abridging, those shorter than 300 bp were excluded from further analyses.

The aligned sequences of *D. simulans* populations (Begun et al. 2007) replaced the *D. simulans* sequence in original alignment for preventing potential problems of *D. simulans* released sequence due to admixed sampling. *w501* population was chosen as the representation for *D. simulans*. In the end, 4348 ortholog sets were used in all the analyses.

Speciation model test

In speciation model test (see appendix), a likelihood ratio test is constructed by two likelihood functions which are the probability of numbers of silent substitutions

between two in-group species when the numbers of silent substitutions between in-group species and out-group species are given. The maximum likelihood estimators for distribution of divergence times of loci are different in two competitive hypotheses. The null hypothesis suggests a constant time in all loci while the alternative hypothesis suggests a gamma distribution. These likelihood ratio tests were implemented by R 2.5.1.

By C++ code, 1000 subsamples are random generated. In each sample, the number of genes is 485, which is equal to the number of sampled genes on X chromosome in our dataset.

Informative sites analysis

For a four-species tree (*D. melenogaster*, *D. simulans*, *D. sechellia*, and *D. mauritiana*), a nucleotide site is informative if and only if this site has 2-2 states (e.g. A, A, G, and G). Using C++ code, the number of informative sites can be calculated. The resolution of each locus is decided by absolute majority (>50%).

To recognize sites which are possibly affected by incomplete lineage sorting very possibly, the aligned *D. simulans* subgroups sequences are applied. One site is ambiguous if there is a polymorphic state between *D. simulans* subgroups in this site. This work is also implemented by C++ code.

Maximum-likelihood (ML) method for gene trees and d_N and d_S estimation

The codeml program of the PAML package (ver. 4) (Yang 2007) was implemented to suggest maximum-likelihood (ML) based topologies and branch-specific nonsynonymous substitution rate (d_N) and synonymous substitution rate (d_S). Two runs of analyses were used for each locus. In the first run, the topologies were

inferred without given trees, and then in the second run, d_N and d_S were estimated with given trees which had resulted from the first run. The models of all analyses are free-ratio model (Yang 1998) and F3X4 model (Goldman and Yang 1994).

Bayesian inference (BI) method

For each locus or each window along chromosome arms (see Large-scale Topologies Analysis section), the topology based on Bayesian algorithm is inferred by using MrBayes (ver. 3.1) (Ronquist and Huelsenbeck 2003) with GTR model. The posterior probability for each possible topology is summarized from 10 runs of MCMC with 100,000 generations. A locus has resolved topology if the posterior probability of dominant topologies is larger than 80%

Large-scale topologies analysis

All sequences are linked together according to annotated physical position in five chromosome arms. These linked sequences are divided into hundreds of 1kb size window. To see which topologies these windows support, Bayesian inference method is applied.

If there are more than three continuous windows support the same tree, these windows are recognized as a "cluster" which support that tree. Similarly, we checked all arms and only focused on the window with dominant posterior probability > 80%.

Distance estimation

The distance matrix between six *D. simulans* subgroups, *D. sechellia*, and *D. mauritiana* are calculated via Dnadist program of PHYLIP (ver. 3.6) with F84 substitution model (Felsenstein 2005). The distance is used in following analysis only when the total number of compared sites are larger than 300. To search loci where six

D. simulans subgroups are clustered in one clade, following two groups of estimation were compared: (1) the distances between any pair of *D. simulans* subgroups and (2) the distances between all *D. simulans* subgroups and the two species (*D. sechellia* and *D. mauritiana*) individually. The candidate loci are the ones where all the available distances in (2) must be larger than the ones in (1).

Gene Ontology (GO) analysis

To show the functional overview for the datasets I analyzed, "GO slimmer" was be used to calculate the number of genes which belongs to given biological process GO terms. This tool can be used in AmiGo website (Carbon et al. 2009). In my study, only the first level terms are considered.

Another method to analyze the representativeness of our datasets is via "GO Term Enrichment" tool, which can also be implemented in AmiGo website. The algorithm compared the number of genes in each GO term in our dataset with the one in FlyBase databank by chi-square tests, and then significantly enriched GO terms are suggested.

Results

Speciation model test rejects the constant divergence time hypothesis

To study the geographic origin of speciation, the speciation model test was applied. The rationale of this speciation model test is based on the distributions of divergence time of all loci. While the null hypothesis assuming constant (strictly allopatric model), the alternative hypothesis have more parameters to describe the distribution of divergence time of loci fitting gamma distribution. This test was performed between *D. simulans* & *D. sechellia, D. simulans* & *D. mauritiana,* and *D. sechellia* & *D. mauritiana* independently. The results of these three paired species are suggested to reject the null hypothesis as shown in Table 2.1.

Discordance of gene trees

To study the genome-wide pattern of phylogenetic trees among these three species, 4348 gene trees were reconstructed. There are three possible topologies for an unrooted three species tree shown in Figure 1. According to the absolute majority of informative sites, 848 (19.6%) genes support tree1, 724 (16.9%) genes support tree2, 770 (17.3%) genes support tree3, and the rest are marked as non-resolved ones. These gene trees have no concordant one obviously and all three trees contribute to the pie chart very equally (Figure 2.2a).

To show this incongruence is not method-biased, the other two common methods to reconstruct phylogenetic relationship were used. By maximum likelihood method, there are 1359 (31.3%) genes support tree1, 1178 (27.1%) genes support tree2, and 1257 (28.9%) genes support tree3. In addition, 930 (21.4%) genes support tree1, 760 (17.5%) genes support tree2, and 862 (19.8%) genes support tree3 via Bayesian

inference method (posterior probability > 0.8). A very equally distributed pattern could be observed no matter which method is used (Figure 2.2b & 2.2c).

The incongruence is also not biased toward the cutoff criterion. With posterior probability larger than 0.5 as cutoff, 1261 (29.0%) genes support tree1, 1080 (24.8%) genes support tree2, and 1238 (28.5%) genes support tree3. In addition, 700 genes (16.1%) support tree1, 552 (12.7%) genes support tree2, and 645 (14.8%) genes support tree3.

Phylogeny of informative sites

Besides, the distribution of informative sites to support each possible topology is also equally distributed (Figure 2.2d). Among 14524 informative sites, 5069 (34.9%) sites support tree1, 4619 (31.8%) sites support tree2, and 4836 (33.3%) sites support tree3. In the end, the discordance pattern can be observed not only by counting genes but also counting sites.

One of sources of phylogenetic incongruence is incomplete lineage sorting, which indicates the contributions of ancestral polymorphisms. To find out whether the polymorphism would interfere the reconstruction of phylogenetic relationship between these three species, the polymorphism between *D. simulans* subgroups are took into consideration. After removing ambiguous (polymorphic among *D. simulans* populations) sites, there are 7274 unambiguous sites left. Among these unambiguous sites, 2657 (36.5%) sites support tree1, 2357 (32.4%) sites support tree2, and 2260 (31.1%) sites support tree3. The percentage of sites supporting treel increases slightly (34.9% to 36.5%) while the percentage of sites supporting tree3 decreases (33.3% to 31.1%).

Chromosomal-scale phylogenetic pattern

To confirm that the incongruence is exactly a genome-wide pattern, I perform the analysis of posterior probability distribution along different chromosome arms. Each window contains the same number of sites (1kb), so the windows are expected with the same topology-resolving power and the comparison among windows are rational. Consequently, the high level of discordance is revealed on each chromosome arm in Figure 2.3.

The close divergences of intra-species and inter-species

Here I provide another way to show the genome-wide discordance pattern. I analyze the following three distributions of distances: (1) between *D. simulans* subgroups, (2) between *D. simulans* subgroups and *D. sechellia*, and (3) between *D. simulans* subgroups and *D. mauritiana*. The distributions are shown in Figure 2.4. Applying pairwise Kolmorogov-Smirnov tests, I can not reject the null hypothesis that these distributions are the same (*p*-values between (1) & (2): 0.1686; between (1) & (3): 0.2317; between (2) & (3): 0.9506).

Faster-evolving lineage of two endemic species

To compare the selection efficacy for each species in this clade, the nonsynonymous divergence and synonymous divergence (d_N and d_S) were calculated and assigned to each branch according to its maximum-likelihood inferred phylogeny. The results are shown in Table 2.2. The synonymous divergence of *D. sechellia* lineage is slightly larger than the one of *D. mauritiana* lineage and *D. simulans* lineage, but all are about one-fifth to one-fourth of the one of *D. melanogaster* lineage. This proportion is consistent with the pervious study (Tamura, Subramanian,

and Kumar 2004). Intriguingly, *D. mauritiana* and *D. sechellia* have higher d_N/d_S ratio than its sibling *D. simulans* lineage. These lineage effects are independent of the underlying trees.

To identify genes under positive selection, the genes with lineage where d_N/d_S larger than one were recognized. The number of these genes are summarized in Figure 2.5. There are 518 genes with positive-selected lineage and the order of each lineage is in *D. mauritina* > *D.sechelia* > *D. simulans.*

Different pattern on X chromosome

I compared the distribution of windows which supports each tree on different arms. Intriguingly, we found that the pattern of autosomal arms are very similar to what we discovered in whole-genome analysis, but the pattern of X chromosome are very different as shown in Figure 2.6. There are about 23.3 % windows supports tree 3 and more than the percentages which supports tree 1 and tree2 separately.

To reveal whether the selection efficacies of X chromosome and autosomes are different, averaged d_N and d_S were calculated. The striking differences between d_N/d_S of X chromosome and autosomes are revealed in Table 2.4. Moreover, while the d_N/d_S in *D. sechellia* lineage is still larger than the ones in other lineage on four autosomal arms, the d_N/d_S in *D. mauritiana* lineage is largest on X chromosome.

Furthermore, only using genes on X chromosome, we apply speciation model tests again. The significant levels are marginal (Table 2.5). Comparing with the distribution of significant level of tests which is based on random subsamples, the test based on X chromosome genes are not so significant to reject the null hypothesis. The

percentiles are 0.010, 0.001 and 0.001 in *D. simulans* & *D. sechellia, D. simulans* & *D. mauritiana,* and *D. sechellia* & *D. mauritiana*.

Candidate genes suggested under the genic view of speciation

Based on the genic view of speciation, the genes which play important role in reproductive isolation should be strong in inferring phylogenetics trees. Here two methods were proposed to find these candidate genes. First, by the criterion that the phylogeny *D. simulans* populations are clustered in a monophyletic group, 220 genes are recognized. Second, the clustered regions supporting one topologies are plotted in the gray-background spectrum in Figure 2.3. The numbers of clustered regions supporting one topology are shown in Table 2.6. Consequently, 39 clustered regions support tree1, 22 clustered regions support tree2, and 30 clustered regions support tree3.

Representation of dataset

To see whether our dataset represent all genome in a functional view, the annotated first-class biological process GO terms of the genes in our dataset are categorized and shown in Figure. 2.7. I also did GO enrichment analysis, and the dominant terms are shown in Table s2.1. These representative terms are roughly related to metabolic pathway.

Table 2.1 Speciation model test of each paired species

	-ln *L*	*p* value
((*D. sim*, *D. sec*), *D. mel*)		
L1: constant	12352.26	<1E-15
L2: gamma distribution	12206.59	
((*D. sim*, *D. mau*), *D. mel*)		
L1: constant	12004.88	<1E-15
L2: gamma distribution	11902.56	
((*D. sec*, *D. mau*), *D. mel*)		
L1: constant	12349.13	<1E-15
L2: gamma distribution	12223.55	

Note- For each pair of species, *L* is the likelihood of each model. The distribution of divergence times is constant in the first model and a gamma distribution in the second model. The *p* value is based on the likelihood ratio test of two models.

Table 2.2 Branch-specific d_N and d_S categorized by their inference via maximum likelihood method

	D. sim	*D. sec*	*D. mau*	*D. mel*	internal
Tree 1 (1359)					
d_S	0.0211	0.0260	0.0208	0.1051	0.0086
d_N	0.0015	0.0025	0.0020	0.0099	0.0007
d_N/d_S	0.0690	0.0963	0.0971	0.0944	0.0856
Tree 2 (1178)					
d_S	0.0224	0.0252	0.0228	0.1032	0.0083
d_N	0.0015	0.0025	0.0021	0.0091	0.0006
d_N/d_S	0.0647	0.0991	0.0921	0.0886	0.0724
Tree 3 (1257)					
d_S	0.0199	0.0256	0.0220	0.1042	0.0081
d_N	0.0015	0.0030	0.0022	0.0103	0.0008
d_N/d_S	0.0760	0.1155	0.0987	0.0987	0.0948
Not Resolved (554)					
d_S	0.0137	0.0187	0.0146	0.0984	-
d_N	0.0009	0.0019	0.0014	0.0075	-
d_N/d_S	0.0685	0.0995	0.0950	0.0766	-

Note- Tree1 is ((*D. sim*, *D. sec*), *D. mau*, *D. mel*) and 1359 genes support tree1, tree2 is ((*D. sim*, *D. mau*), *D. sec*, *D. mel*) and 1178 genes support tree2, tree3 is ((*D. sec*, *D. mau*), *D. sim*, *D. mel*) and 1257 genes support tree3, and 554 genes support neither.

Table 2.3 Speciation model test of each paired species based on X chromosome genes

	-ln *L*	*p* value
((*D. sim*, *D. sec*), *D. mel*)		
L1: constant	1244.76	0.0005
L2: gamma distribution	1239.40	
((*D. sim*, *D. mau*), *D. mel*)		
L1: constant	1163.11	0.0267
L2: gamma distribution	1161.24	
((*D. sec*, *D. mau*), *D. mel*)		
L1: constant	1228.99	0.0280
L2: gamma distribution	1227.16	

Note- For each pair of species, *L* is the likelihood of each model. The distribution of divergence times is constant in the first model and a gamma distribution in the second model. The *p* value is based on the likelihood ratio test of two models.

Table 2.4 Branch-specific d_N and d_S on chromosome arms via maximum likelihood method

	D. sim	*D. sec*	*D. mau*	*D. mel*	internal
X (485)					
d_S	0.0151	0.0206	0.0149	0.1173	0.0054
d_N	0.0015	0.0027	0.0023	0.0123	0.0008
d_N/d_S	0.1021	0.1323	0.1515	0.1048	0.1405
2L (891)					
d_S	0.0203	0.0252	0.0216	0.1029	0.0084
d_N	0.0015	0.0027	0.0020	0.0099	0.0008
d_N/d_S	0.0741	0.1058	0.0942	0.0962	0.0905
2R (896)					
d_S	0.0219	0.0263	0.0218	0.1033	0.0080
d_N	0.0013	0.0026	0.0019	0.0089	0.0006
d_N/d_S	0.0605	0.0991	0.0864	0.0860	0.0696
3L (885)					
d_S	0.0203	0.0250	0.0213	0.1000	0.0075
d_N	0.0014	0.0026	0.0021	0.0093	0.0006
d_N/d_S	0.0695	0.1029	0.0963	0.0929	0.0829
3R (1191)					
d_S	0.0216	0.0256	0.0226	0.1031	0.0077
d_N	0.0014	0.0025	0.0021	0.0092	0.0006
d_N/d_S	0.0659	0.0969	0.0910	0.0894	0.0781

Note- The numbers of sampled size on different arms are listed in parentheses.

Table 2.5 The number of candidate regions based on clustered windows with posterior probability > 0.8

	arm				
	X	2L	2R	3L	3R
((*D. sim*, *D. sec*), *D. mau*, *D. mel*)	1	4	7	14	13
((*D. sim*, *D. mau*), *D. sec*, *D. mel*)	2	5	5	6	4
((*D. sec*, *D. mau*), *D. sim*, *D. mel*)	2	3	8	5	12

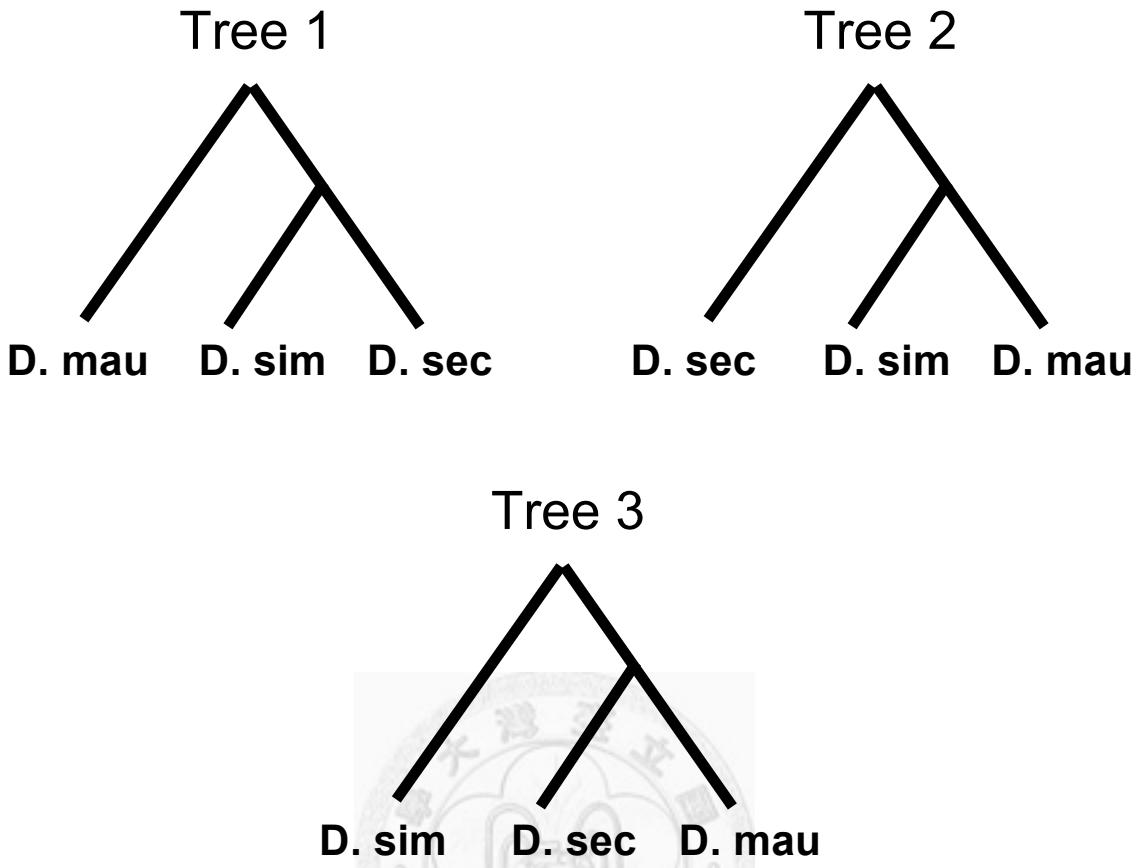

Figure 2.1 Three possible topologies There are three possible topologies for three species, *D. simulans* (*D. sim*), *D. sechellia* (*D. sec*), and *D. mauritiana* (*D. mau*).

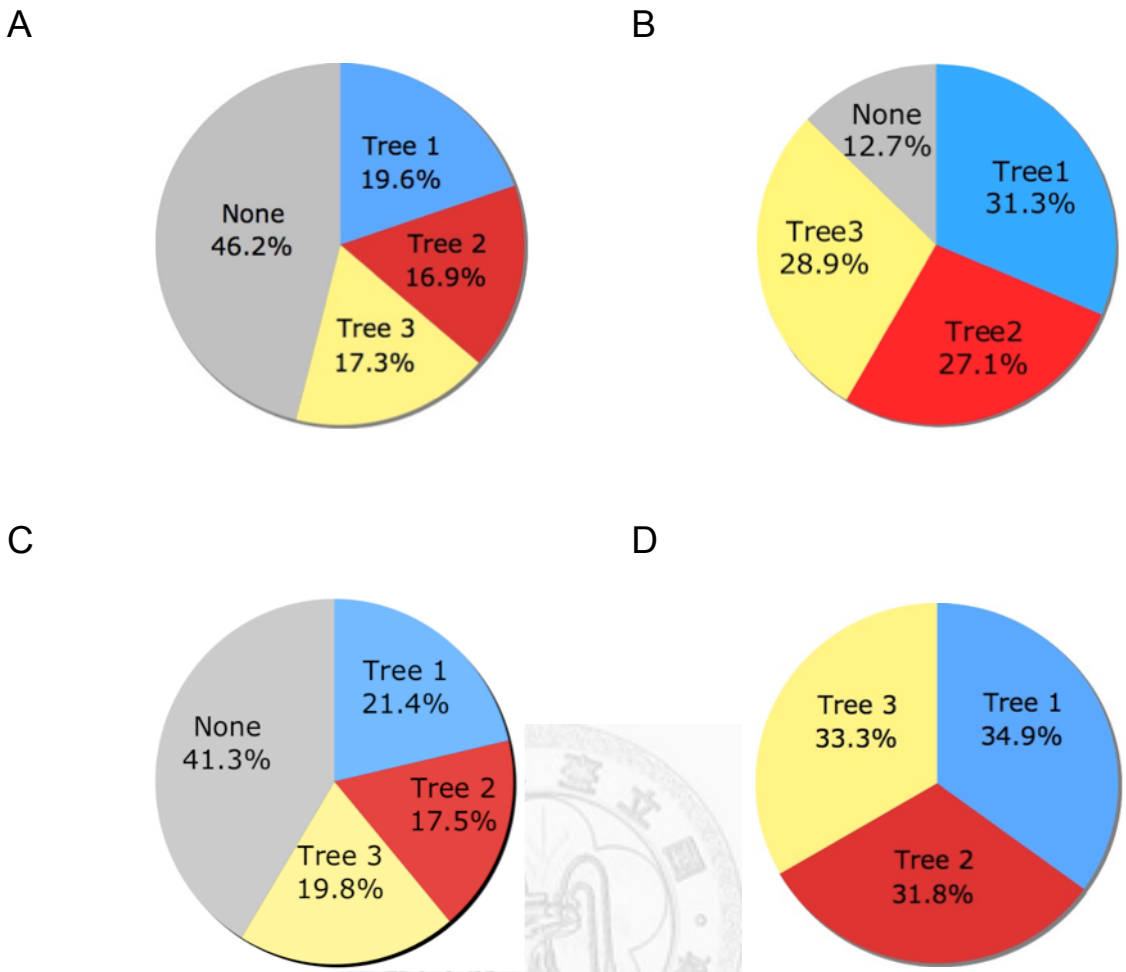

Figure 2.2 Genome-wide pattern of phylogeny a) the propotion of genes supporting each of the topologies based on the majority of informative sites **b)** the propotion of genes supporting each of the topologies based on maximum likelihood method **c)** the propotion of genes supporting each of the topologies based on bayesian inferance **d)** the propotion of informative sites supporting each of topologies

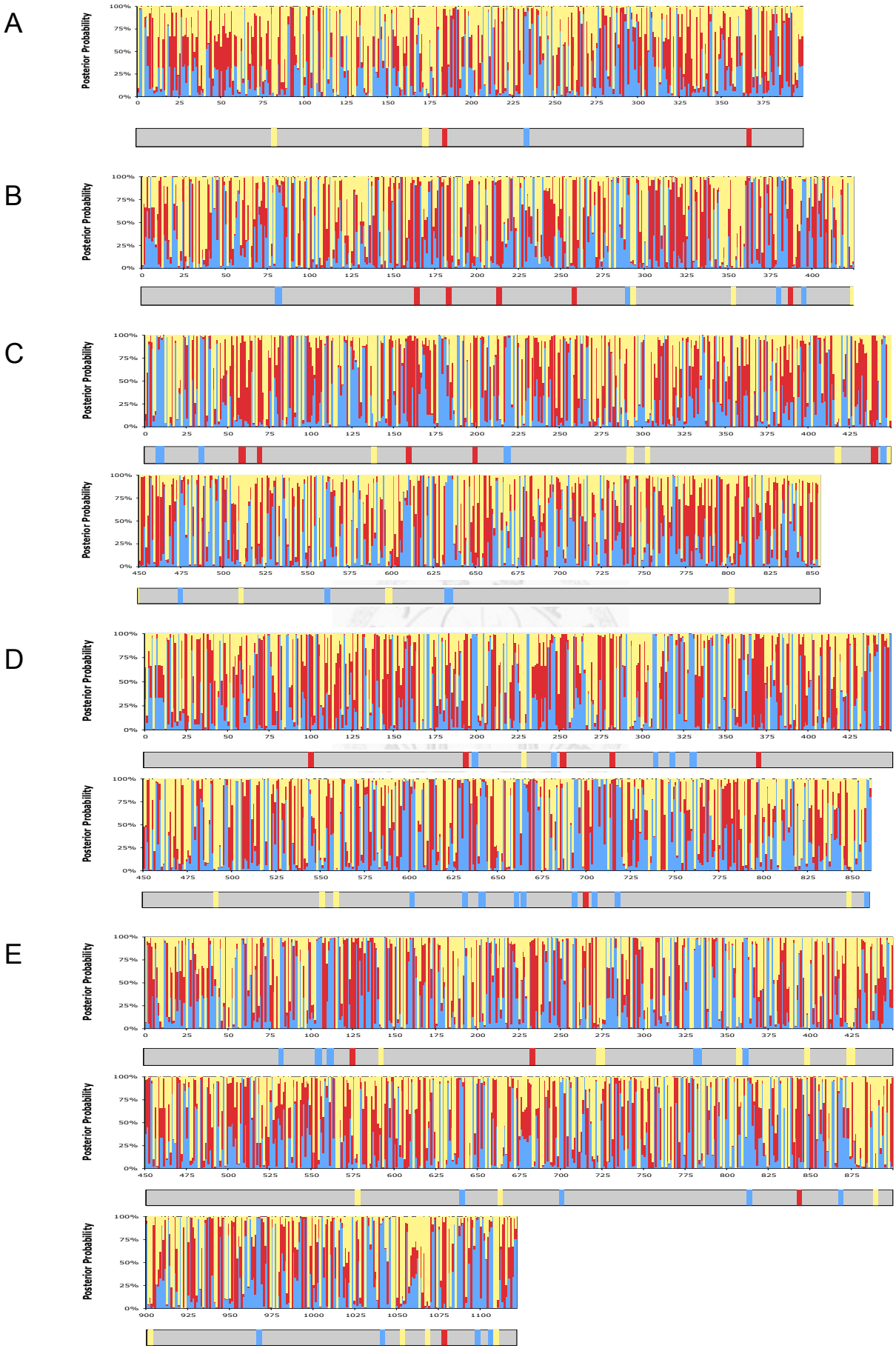
A
B
C
D
E
Posterior Probability
100%
75%
50%
25%
0%

Figure 2.3 The discordant pattern on chromosomes and candidate regions For each arm, the upper histogram are posterior probability distribution supporting each of the topologies (blue for tree1, red for tree2, yellow for tree3) on each 1kb window. The clustered >0.8 windows are also shown in lower one. **a)** on chromosome X **b)** on chromosome 2L **c)** on chromosome 2R **d)** on chromosome 3L **e)** on chromosome 3R

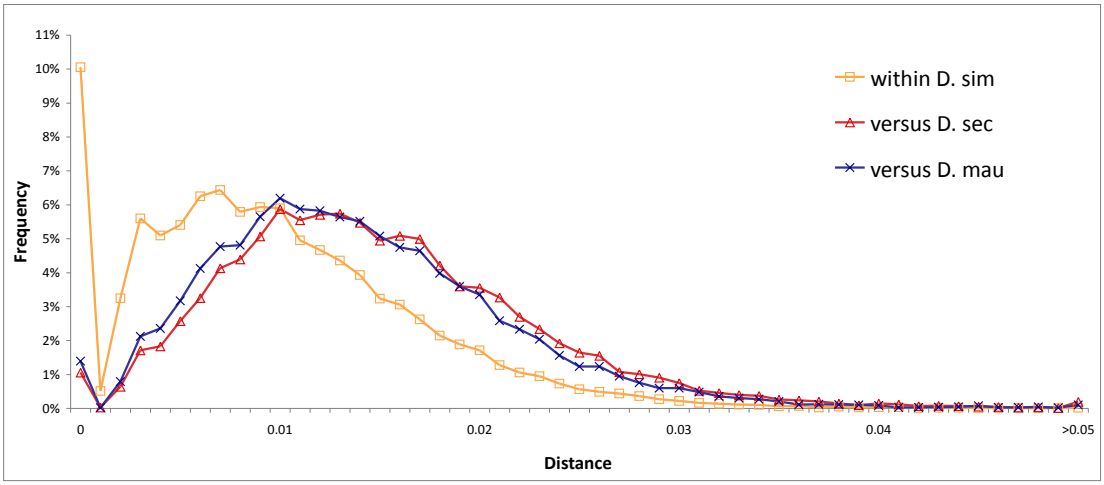

Figure 2.4 Distributions of within-species distance and distances between species

Here differences compare *w501* population and other *D. simulans* populations (within *D. sim*), *D. sechellia* (versus *D. sec*) as well as *D. mauritina* (versus *D. mau*) individually.

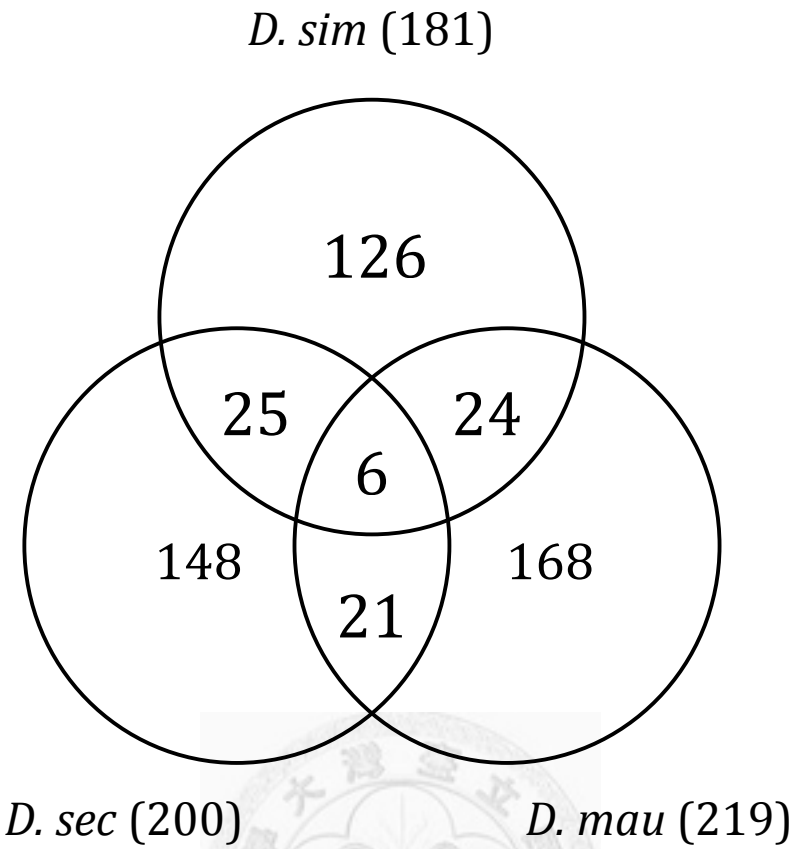

Figure 2.5 The number of genes with positive-selected lineage

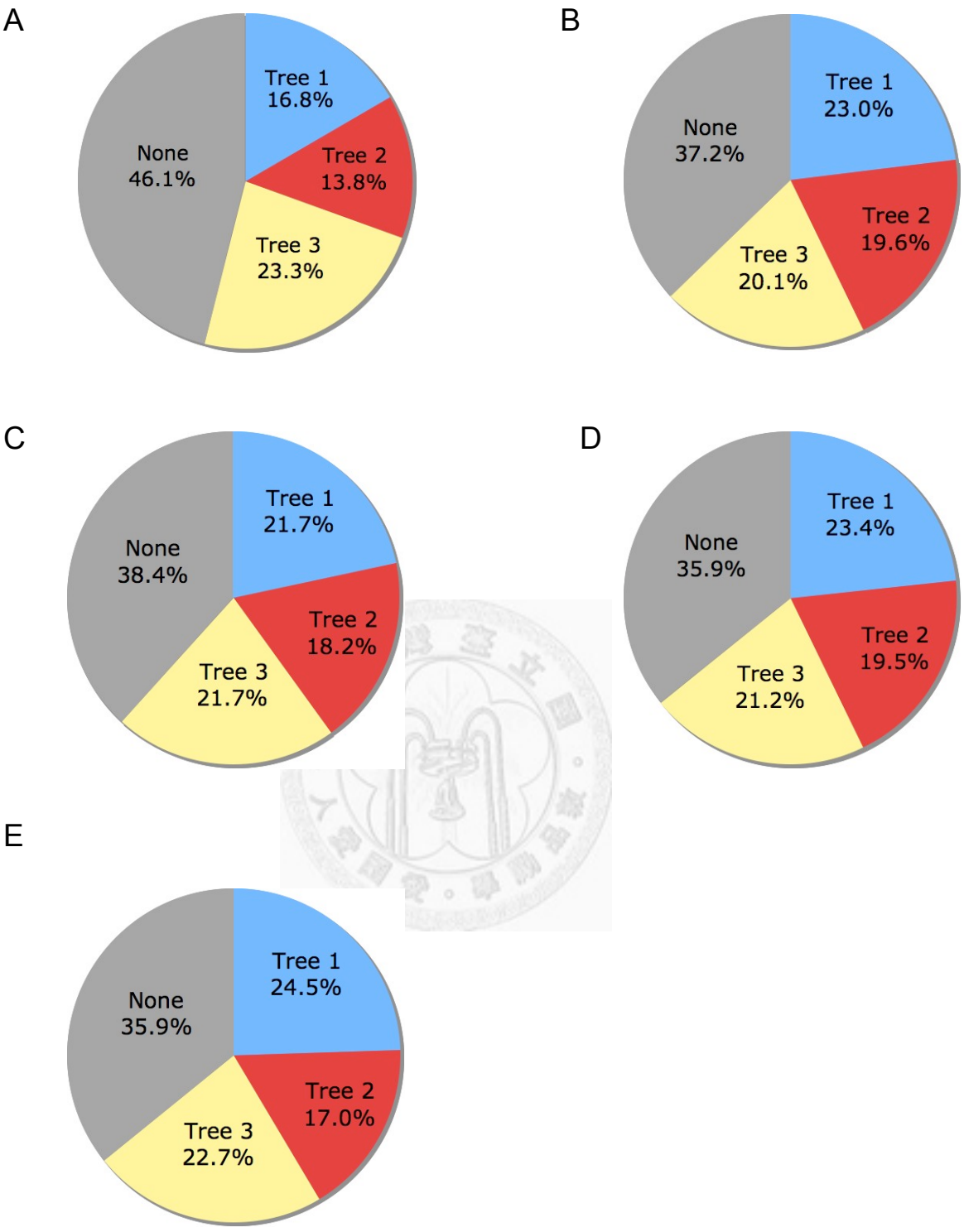

Figure 2.6 The proportion of windows supporting each of the topologies on chromosomal arms a) on chromosome X (sample size: 398) **b)** on chromosome 2L (sample size: 829) **c)** on chromosome 2R (sample size: 854) **d)** on chromosome 3L (sample size: 860) **e)** on chromosome 3R (sample size: 1121)

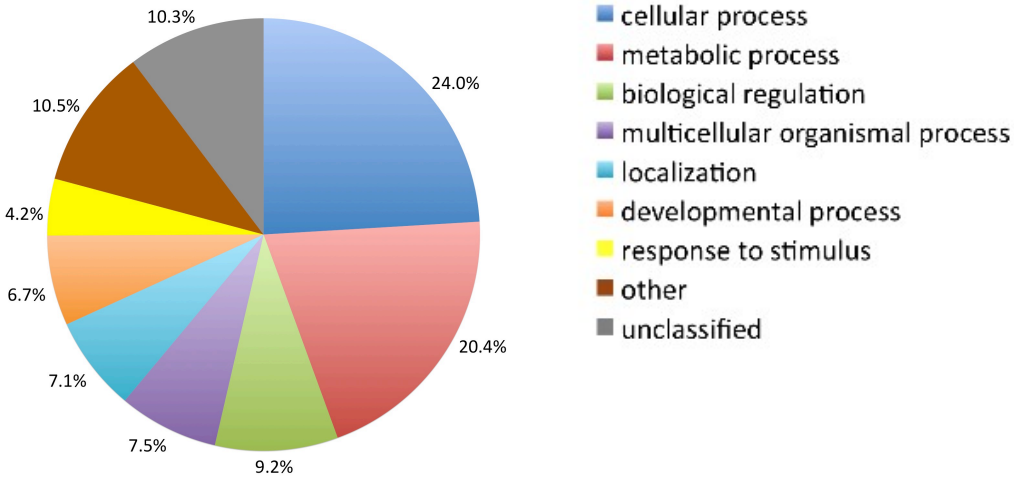

Figure 2.7 GO slim for the first level of biological process terms for the dataset

Discussion

In this chapter, the distributions of divergence time are significantly not constant so that the allopatric speciation model is rejected by the speciation model test. I reveal the discordant pattern in many different methods. The incongruent pattern does not depend on methods including different algorithms and different scales. Moreover, the faster-evolution in two endemic species and the specialties of X chromosome during speciation are revealed. Finally, according to the genic view of speciation, some candidates can be suggested.

Explanation to the incongruence

Generally, the complexity of inferring speciation can be explained by two factors: incomplete lineage sorting due to ancient polymorphism and the long-term introgression during speciation (Degnan and Rosenberg 2009). When there are several speciation events occurs in a very short time window, the contribution of these two factors can be amplified. In *D. simulans* clade, the speciation events which cause these three species occurs in a very time window was inferred. This inference contributes as a remote cause of incongruence. The corresponding evidence can be found in my study. The short time window can be suggested by very close divergence time. In table 2.2, the synonymous divergence of each species estimated by d_S are very close. In addition, in figure 3.4, the distribution of two kinds of divergence can not be discriminate easily. Even the polymorphism and the divergence are so close.

One caveat on divergence estimation is that due to the methodology of aligning short reads sequence, the divergence of *D. mauritiana* may be underestimated. The aligning algorithm is reference-based and the reads with too many mismatched are excluded. These discard sequences become the source of underestimation.

I tried to assay the contribution of incomplete lineage sorting by removing ambiguous sites and the result is not remarkably changed. This may suggest the role of incomplete lineage sorting is not so much. However, the polymorphic data I considered are limited. The resolving power can increase much if I have more populational sequence data.

By the speciation model test, I reject the null hypothesis that the distribution of divergence time of all loci is constant in three pairs of species. The remarkable variance of divergence time suggests the gene flow between these three species did not cease completely soon. Therefore, the "speciation with introgression" scenario is suggested. This scenario not only makes the genic view of speciation considerable but also explains the incongruence in whole-genome.

Speciation events in two island species

With the result of speciation model test, we now have new clues to discuss the geographic origin of two island species, *D. sechellia* and *D. mauritiana*. A simple model to explain the speciation of island species is peripatric model. If the speciation follows peripatric model, which means it was achieved by one founder event, the distribution of isolation time between loci should be like the one in strictly allopatric model. According to the test results, the strictly allopatric model is rejected. It indicates abundant gene flows during speciation and the parapatric model is more possible than peripatric model.

Moreover, both two island species show higher d_N/d_S and more d_N/d_S >1 lineages than *D. simulans* in my analytical results. This may reflect the adaptation history during successful colonization. During colonization, effective population size decrease and the accompanying drift can make the genetic variability increased and

then provide the materials which can be worked on by natural selection. Several genes have been revealed as fast-evolving genes in this clade such as smell and taste receptor genes in *D. sechellia* (McBride 2007), as well as *Acp26Aa* (Tsaur, Ting, and Wu 2001) and *OdsH* (Ting et al. 2004) in *D. mauritiana.* These genes are potentially related to speciation events. While the former plays important roles in host specificity, the latter can contribute on reproductive isolation.

The effect of X chromosome

In my study, several characters are revealed to be different between X chromosome and autosomes. First, the windows on X chromosomes support tree3 are more while the number of autosomal windows support three trees are roughly equally. Therefore, there seems be more shared divergence between two island species on X chromosome than on autosomes no matter these shared divergent sites are from ancestral polymorphism or parallelism. The driving force of this phenomenon may be related to the construction of post-mating isolation because more hybrid sterility genes on X chromosome.

Interestingly, the introgression levels suggested by comparing the speciation model test for resampled autosome data and X chromosome data separately provide more information. The just marginal significance level in X chromosomes suggests that the introgression in genes in X chromosome is less. Moreover, the significant level between different species pair is also different. The genes in X chromosome may be not so important in speciation between *D. simulans* & *D. sechellia* comparing to *D. simulans* & *D. mauritina and D. mauritiana* & *D. sechellia.*

Furthermore, the higher d_N/d_S in *D. mauritina* lineage also suggest the substitution on X chromosome may play a more important role in *D. mauritina* than in other two

species. It is reminded that *OdsH*, which was suggested to be speciation gene, cause the male hybrid sterility between *D. simulans* and *D. mauritiana* and has d_N/d_S larger than two. My finding at least suggest the speciation may be drived by elements on X chromosome and may reinforce the hypothesis that *OdsH* can be speciation gene. Admittedly, there can be more genes involved in speciation remain to be uncovered.

Suggested Candidates

Under this senario, the genes with important roles in speciation should cease gene flow early so that they have the two properties I used to propose candidates. If people want to figure out the speciation mechanism, those candidates are worthy of further study. Remarkably, a region containing *OdsH* is proposed by the clustered region with posterior probability larger than 0.8 to support tree2.

The final remark is the sequence data provided from transcriptome may be limited so that the overall pattern may not be revealed. Based on the GO term analysis, the metabolic genes are over-represented. The genes with function related to behavior or reproduction may be lost in my data set. Besides, there are no good reference sequences for *D. mauritina* so far. It is reasonable that the main questions here can be dissected more clearly after the good reference sequences for *D. mauritina* are released. In that time, the methods presented here will be very helpful.

Chapter 3

Sequence and Expression Divergence between Two *Drosophila melanogaster* Races in Incipient Speciation

Introduction

While analyzing a species complex (e.g. *D. simulans* clade in chapter 2), which has evolved in a period, to study speciation, the goal of inferring the speciation mechanism can be more unattainable because the pivot may be covered with time being. The other mutations, which are not related to speciation but accumulated in derived lineage, can interfere the analysis results. Therefore, if a very beginning stage of speciation is observed, addressing speciation mechanism of this system is not difficult as in a species complex.

A remarkable incipient speciation stage in M-type (for cosmopolitan) and Z-type (for Zimbabwe) races of *Drosophila melanogaster* could provide a great model to study the speciation mechanism as the aforesaid reason. Begun and Aquadro (1993) first discovered the uniqueness of flies in Zimbabwe. Comparing to the divergence of American populations, the one of Zimbabwe populations is much higher in several nuclear genes. Afterward, the behavioral difference in the populations from Zimbabwe was also revealed (Wu et al. 1995). In this study, the females in several Zimbabwe populations were reported to strongly prefer the males from the same population than from other places worldwide while the females from worldwide have no or weak preference. However, no significant hybrid inviability or sterility was discovered. The polymorphism of this sexual trait was further studied in more Southern African lines (Hollocher et al. 1997a). The polymorphic sexual isolation suggests that these populations undergo speciation at a very beginning stage.

After an incipient speciation model was established, the next movement should be dissecting the isolation in genetic level. As a model organism, there are many available genetic tools in *D. melanogaster*. For example, genetic mapping is easier and faster through the phenotypic markers. In addition, the abundant genome sequences make whole-genome screening approach possible.

A series of genetic mapping have provided the clues to Z/M isolation. The different magnitudes of contribution on different chromosomes were revealed by chromosome substitution lines. The results show that the effect of third chromosome is larger than the one of the second chromosome and much larger than the one of X chromosome (Hollocher et al. 1997b). Moreover, three loci on the third chromosome were suggested to be responsible for Z-type female preference and four others control Z-type male mating success (Ting, Takahashi, and Wu 2001). This mapping result also suggests that the interaction between these loci are existing by finding that the contribution to Z/M isolation of one candidate locus is usually smaller than the one of a larger fragment which contains the same locus and other loci. In addition, several loci on the second chromosome were also suggested to contribute to Z/M isolation (Ting, Tsaur, and Wu 2000; Takahashi and Ting 2004).

These observations support a hypothetical multi-loci scheme in this behavioral isolation (Takahashi and Ting 2004). There may be many loci which contribute on the isolation. However, the state of these sites might not be fixed in all lines which have the same preference. The pattern is illustrated by Figure 3.1. In hypothesized two Z-type races, loci #1 fixes only in Z race #1 while loci #2 is fixed in Z race #2. There are still some but not all the contributed loci are completely fixed.

Among the reasonable candidates for Z/M isolation, *desat2* is a well-studied case. The role of *desat2* in cuticular hydrocarbon (CHs) polymorphism between *D. melanogaster* populations was first uncovered by (Dallerac et al. 2000). Because CHs play an important role in mate recognition, *desat2* turned to be a target to understand sexual isolation between Z-type and M-type races. In sequence analysis, several sites had been proposed to highly correlate with behavior (Takahashi et al. 2001), and a deletion in promoter region was suggested to cause inactivation of desat2 in M-type races (Fang, Takahashi, and Wu 2002). Moreover, the phenotype of M-type allele is more resistant to cold and sensitive to starvation than the one of Z-type allele (Greenberg et al. 2003). The adaption to ecological factors may drive sexual isolation which is caused by accompanying CHs difference.

The discovery of *desat2* provokes the researchers to attach the importance of the regulatory region, which may cause the different expression level in Z/M isolation. By studying the variant expression levels in different chromosome substitution lines between Z-type and M-type races, both the contribution of *cis*-elements and *trans*-elements are important (Osada, Kohn, and Wu 2006; Wang et al. 2008). Furthermore, Wang et al. (2008) revealed that the third chromosome and X chromosome contribute more on the expression difference than the second chromosome no matter the location of differentially expressed genes.

According to the multi-loci scheme, more candidate genes for behavioral differentiation remain to be discovered. In order to propose the more candidate genes which involve in this complex trait, a genome-wide search is an inevitable step. In this study, two whole-genome datasets were applied. First, we used a set whole genome sequence of M-type lines from Raleigh, U.S. and Z-type lines from Malawi to search the low-diversity regions, which can be current selective sweeps. Second,

we found the differentially expressed genes (DEGs) between Z-type lines from Zimbabwe and M-type lines from U.S. and France by RNA-seq. These candidates and fixation patterns will provide hints to discuss this incipient speciation process.

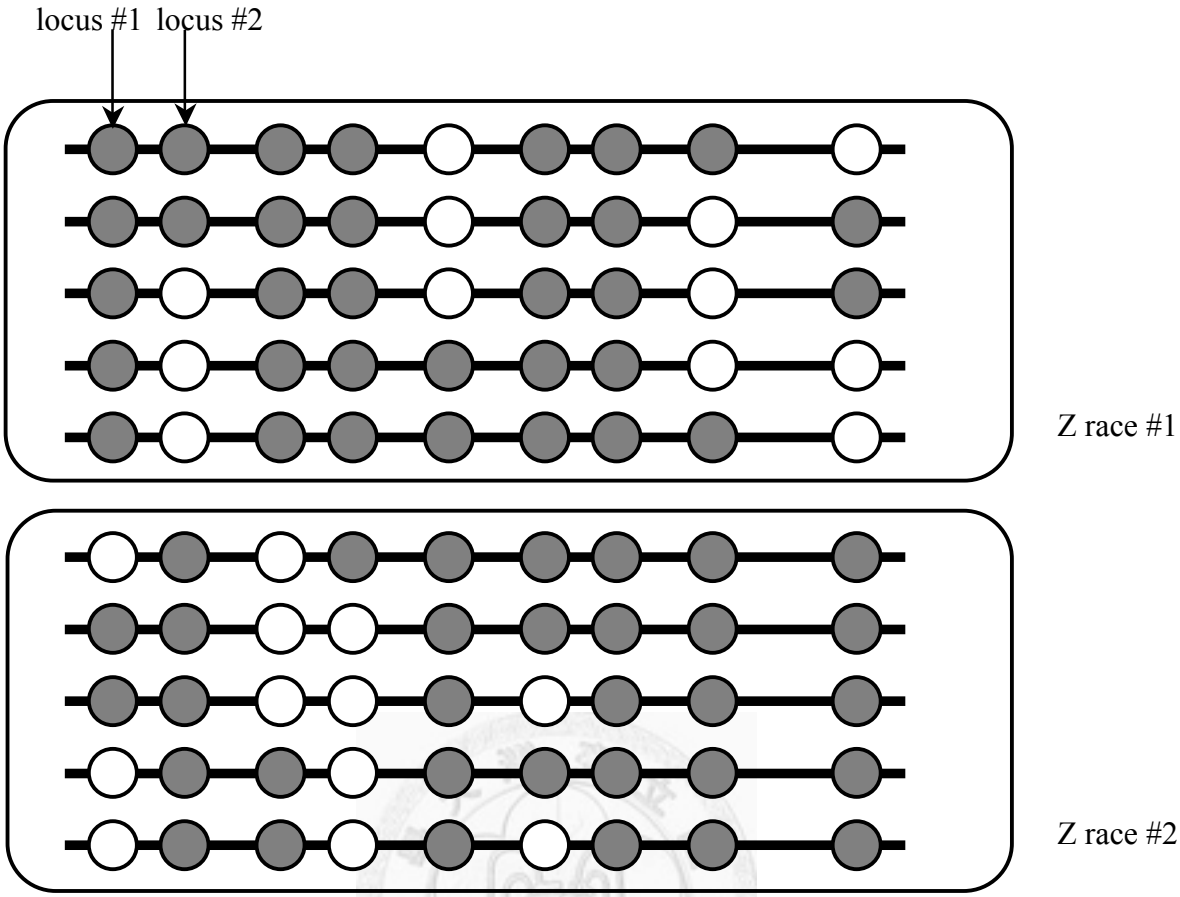

Figure 3.1 Hypothetical multi-loci scheme in Z/M isolation Each line stands for an individual and each circle stands for a locus. The close circles stand for Z-type alleles while the open circles stand for M-type alleles. The Z-type behavior is contributed by many different loci. Each locus can not be fixed among all Z-type races. For example, locus #1 is fixed among all individuals of Z race #1, but is polymorphic in Z race #2. However, locus #2 is fixed in Z race #2 but polymorphic in Z race #1. This figure is modified from Takahashi and Ting (2004).

Material and Method

Analysis of genome sequences

The genome sequences of *D. melanogaster* sampled in Raleigh, North Carolina and Malawi are downloaded from the 50 *D. melanogaster* genome project release 1.0 (website: http://www.dpgp.org/). Some sequences are removed based on the online notes. All of Raleigh lines were M-type lines. Based on the behavior data, the Z-type Malawi lines were recognized. The M-type races and Z-type races which were used in following analysis are listed in table 3.1.

To calculate fixation index (F_{ST}) for each site, the formula $F_{ST} = 1- (H_S/H_T)$ was applied, where H_S is the averaged heterozygosity of Z group and M group (H_Z and H_M) and H_T is the heterozygosity in hypothetically mixed population. H_Z and H_M were estimated based on formula 1 and 2, where $f_{Z,i}$ and $f_{M,i}$ are the sampled frequency of nucleotide state i (A, T, G or C) as well as i and j stand for nucleotide states. H_T was calculated by formula 3, where the averaged frequency (f_T) is equal to $(f_Z+f_M)/2$.

$$H_Z = 2\sum_{i<j} f_{Z,i} f_{Z,j} \quad (1)$$

$$H_M = 2\sum_{i<j} f_{M,i} f_{M,j} \quad (2)$$

$$H_T = 2\sum_{i<j} f_{T,i} f_{T,j} \quad (3)$$

The annotations of these high F_{ST} sites are based on genome sequences in FlyBase (release 5.22). A site recognized to locate on introns means that it locate on the genic region but does not locate on any released transcripts. If more than one gene or alternative splicing forms are annotated to one site, the longest transcript will be assigned.

The nucleotide diversity (π), Watterson's theta (θ) and Tajima's D in each 10kb window are calculated by variscan (ver 2.0.2) (Vilella et al. 2005). Only the sites in M-type races which have larger than 30 samples, and the sites in Z-type races which have 4 samples are used. The windows with less than 1000 sampled sites (i.e. sample proportion <10%) are discarded. To search the low diversity region in M-type races or Z-type races, first the π values are normalized to Z scores by subtracting the sample mean and being divided by the sample standard deviation. Then, the windows where the differences of Z score between M and Z are larger than 2 were chosen as candidate regions.

Short reads sequence assembly

The Illumina short sequence reads were assembled by MAQ (version 0.7.1), which can map the reads to a reference set of sequences by the phred-scaled quality scores (Li, Ruan, and Durbin 2008). The reference set we used comprises *D. melanogaster* transcripts downloaded from FlyBase (release 5.22). Only the splicing form with longest length was used in the reference set. In mapping stage, the maximum number of mismatched bases was raised to 200 in order to avoid that high quality differences between our data and reference sequences were discarded. In the following analysis, only uniquely-mapped reads (with mapping quality larger than zero) were involved.

Identification of differentially-expressed genes (DEGs)

For each transcript, we examined whether there is a homogeneous trend of expression levels differences between Z groups and M groups first. By comparing RPKM (reads per kilobase per million mapped reads) of all combinations between two Z lines and two M lines (i.e. Z30 vs. FR, Z56 vs. FR, Z30 vs. CS, and Z56 vs. CS), the gene with homogeneous trend which is Z larger than M (Z>M) or M>Z were

considered. The RPKM for one transcript is equal to $10^9 x/ML$, where x is the number of uniquely-mapped reads, M is total number of uniquely-mapped reads in one line, and L is the length of transcript (Mortazavi et al. 2008).

The significance levels of expression level differences between four Z-M line pairs were done by Fisher's exact test according to the number of uniquely-mapped reads of each line. To find the set of Z>M DEGs and M>Z DEGs, only four comparisons with Bonferroni's corrected p-values smaller than 0.01 were accepted. Besides, the adjusted p-values by step-up FDR (Benjamini and Hochberg 1995), which was calculated by multtest package of R, were also applied.

Gene ontology (GO) term enrichment analysis

To see the composition of gene sets in functional view, "GO Term Enrichment" tool, which can be implemented in AmiGo (ver 1.7) website (Carbon et al. 2009), can be used. The algorithm compared the number of GO terms in our dataset with the one in FlyBase databank by chi-square tests, and then significantly shared GO terms are suggested.

Finding high F_{ST} sites in RNA-seq data

After mapping, the sequences generated by RNA-seq can also be used for finding high F_{ST} sites. Only the sequence with sequencing phred-scale quality larger than 10 are used. In addition, the sites with depth smaller than five in any sample are not involved because they may bias this frequency based analysis. The average of each nucleotide state within group (f_Z, f_M, and f_T) are calculated by the frequency in each line (f_{Z30}, f_{Z56}, f_{FR}, *and* f_{CS}) as formula 4 to 6 first, and then the heterozygosities were estimated based on these average frequencies as formula 1 to 3. With heterozygosity

of Z group (H_Z) and M group (H_M), averaged heterozygosity (H_S) is equal to (H_Z $+H_M$)/2. Finally, F_{ST} is equal to 1-(H_S/H_T). All these works were implemented by C++ codes.

$$f_Z = \left(f_{Z30} + f_{Z56}\right)/2 \quad (4)$$

$$f_M = \left(f_{FR} + f_{CS}\right)/2 \quad (5)$$

$$f_T = \left(f_{FR} + f_{CS} + f_{Z30} + f_{Z56}\right)/4 \quad (6)$$

Table 3.1 List of M-type and Z-type sample in genome data analysis

Type	Name	X	2L	2R	3L	3R
	MW6	v	v	v	v	v
	MW11	v				
Melawi	MW28	v	v	v	v	v
	MW56		v	v	v	v
	MW63	v	v	v	v	v
	RAL-301	v	X	v	v	v
	RAL-303	X	v	v	v	v
	RAL-304	X	v	v	X	X
	RAL-306	v	v	v	X	X
	RAL-307	v	v	v	v	v
	RAL-313	v	v	v	v	v
	RAL-315	v	v	v	v	v
	RAL-324	v	v	v	v	v
	RAL-335	v	v	v	v	v
	RAL-357	v	v	v	v	v
	RAL-358	v	v	v	v	v
	RAL-360	v	v	v	v	v
	RAL-362	v	v	v	v	v
	RAL-365	v	v	v	v	v
	RAL-375	v	v	v	v	v
	RAL-379	v	v	v	v	v
	RAL-380	v	v	v	v	v
	RAL-391	v	v	v	v	v
Raleigh	RAL-399	v	v	v	v	v
	RAL-427	v	v	v	v	v
	RAL-437	v	v	v	v	v
	RAL-486	v	v	v	v	v
	RAL-514	v	v	v	v	v
	RAL-517	v	v	v	v	v
	RAL-555	v	v	v	v	v
	RAL-639	v	v	v	v	v
	RAL-705	v	v	v	v	v
	RAL-707	v	v	v	v	v
	RAL-714	v	v	v	v	v
	RAL-730	v	v	v	v	v
	RAL-732	v	v	v	v	v
	RAL-765	v	v	v	v	v
	RAL-774	v	v	v	v	v
	RAL-786	v	v	v	v	v
	RAL-799	v	v	v	v	v
	RAL-820	v	v	v	v	v
	RAL-852	v	v	v	v	v

Note- In 50 *D. melanogaster* genome project (website: http://www.dpgp.org/), five Z-type lines from Malawi and 37 M-type lines from Raleigh were sequenced. For each arm, the names of available lines are listed here. v: used in analysis, X: available online but entirely removed according to the suggestion on the website, blank: not sampled.

Results

Recent selective sweeping regions suggested by population genomic sequences

With the aligned genome sequence of four Z-type lines from Malawi and thirties of M-type lines from Raleigh, I started my analysis with the genome-wide plot of nucleotide diversity (π) and Watterson's θ in Raleigh M population and Malawi Z population. Moreover, by comparing these two population parameters, Tajima's *D* can be calculated. These parameters are widely used to infer the population history.

The plots of π, θ and Tajima's *D* are shown in Figure 3.2. A striking pattern is discovered that the differences between π and θ are obvious in Raleigh M populations, especially in X chromosome, while the one in Malawi Z populations are not easily observed (Table 3.2). This observation is also confirmed by the distributions of Tajima's *D*. While the most values of Tajima's *D* in Malawi Z populations are narrowed between (0, -1), the more negative values can be discovered in Raleigh M populations.

Rather than genome-wide consistent pattern, the recipe to solve the isolation question is to search the genomic region which might endure adaptive selection in each population. The adaptive selection may make local heterozygosity lower than expectation because of hitchhiking effect (known as selective sweep). Therefore, I comparing the normalized nucleotide diversity (Z score of π) in two races, the low diversity which is specific in one race can be revealed. The comparison of π in two populations is also shown in Figure 3.3. Apparently again, the pattern of X chromosome is very different from other autosomal arms. The nucleotide diversity is reduced much in M-type races on X chromosome while the reduction is less on autosomes.

Using Z score difference larger than two as criterion, we found 22 windows which have low diversity in Z races and 59 windows which have low diversity in M races (Table 3.3). The detailed lists are in Table s3.1 and Table s3.2. The location of windows which have low diversity in M races are bias to X chromosome (42 on X, six on 2L, three on 2R, one on 3L, and 7 on 3R) while the location of windows which have low diversity in Z races are not (two on X, five on 2L, four on 2R, one on 3L, and 10 on 3R).

The whole-genome pattern of high F_{ST} sites and their clustering

While the genome-wide pattern of nucleotide diversity was suggested, the fixed different sites between two races can also be proposed. By calculating the fixation index (F_{ST}) of each site, 16008 sites with F_{ST} larger than 0.9 were revealed. Their distribution on different chromosome arms was summarized in Table 3.4. The locations of these sites are biased on the X chromosome (44%) and on the 3R arm (27%).

Because of the hitchhiking effect, the window with clustered high F_{ST} sites can also be recognized as candidates. The pattern is also shown as Figure 3.4. It is clear that high F_{ST} sites are abundant through X and 3R independently but very rare in 2L and 2R. The candidate regions, which have larger than 30 high F_{ST} sites, were summarized in Table 3.3.

Finding differentially expressed genes by RNA-seq

Besides in sequence level, to find candidates in expression level is also very informative. The transcriptome of two Z lines from Zimbabwe (Z30 and Z56) and two worldwide lines (FR and CS) are sampled. The numbers of reads generated by

sequencing platform and the mapped percentages to *D. melanogaster* transcripts are shown in Table 3.5. All of their mapped percentages are little higher than 80%. Afterwards, I used RPKM as the references of the expression level of each gene. In Table 3.6 and Figure 3.5, the correlations of expression levels in each paired lines are shown. The correlations within Z groups and within M group are larger than the ones between two groups. This observation suggests that the expression level differences within Z or M group are smaller than between two groups.

With Fisher's exact test and Bonferroni's correction, the differently-expressed genes (DEGs) between Z groups and M groups were found. In the intersection set of corrected *p*-values smaller than 0.01 in four comparisons, there are 246 genes in which the expression level in Z group is significantly larger than in M group (Z>M), and 243 genes which have significant M>Z expression pattern (listed in Table s3.4 and Table s3.5). The relationship between testing results and expression fold changes are shown in Figure 3.6. In addition, the distribution of DEGs among chromosome arms is shown in Table 3.7. Among these DEGs, the number of DEGs in the third chromosome and second chromosome is larger than X chromosome (216 and 190 vs. 82).

To see whether there is a dominated biological process involved in the expression differentiation, the enriched GO terms were inferred (see Table 3.8 and Table 3.9). The representative terms in both sets are inter-consistent but not similar with each other. The enriched terms in Z>M set are related to vision and the detection or response to other kinds of stimulus. The importance of sight is shown in the three terms with smallest *p*-values such as phototransduction (1st place), detection of light stimulus (2nd), and response to light stimulus (3rd). However, the representative

terms in M>Z set are related to catabolic pathway of small molecules (1st), especially of oxoacid and carboxylic acid (both 2nd).

The results are independent with the method of multiple test correction

We also used false discovery rate (FDR), a less stringent way to do multiple tests correction. 392 significantly Z>M genes and 353 significantly M>Z genes are found (listed in Table s3.6 and Table s3.7). These two sets included all of the DEGs which were found by Fisher's exact test and Bonferroni's correction. In addition, the distribution on chromosomes is shown in Table 3.7. The patterns of representative terms are also very alike to the data set using Bonferonni's correction (Table s3.8 and Table s3.9).

The genome-wide pattern of high F_{ST} sites suggested by RNA-seq data

With these mapped abundant sequences, F_{ST} of each site can also be measured. The number of high F_{ST} sites on different chromosome arms was summarized in Table 3.10. Among five arms, X and 3L are occupied most (31% and 29%) while 2L, 2R, and 3R are equally less (15%, 13%, and 12%).

To search more evident high F_{ST} sites, the two sets of high F_{ST} sites proposed by two different dataset are compared although the intergenic and intronic regions are lost in RNA-seq data. 150 shared high F_{ST} sites were discovered (listed in Table s3.10 by transcripts). Their distributions on chromosomes are summarized in Table 3.11.

In addition, the number of high F_{ST} sites in 10 kb sliding windows on each arms are also shown as Figure 3.7. The regions with clustered high F_{ST} sites were summarized in Table s3.11. There are 18 regions on 3R, 14 regions on X, 3 regions on 2L, 1 region on 2R and 1 region on 3R. Only one in X (7175001..7185000)

overlaps with the candidate windows which were proposed by genome data (7179001..7197000 by clustered F_{ST} sites).

Table 3.2 Averaged population parameters of each chromosome in different populations

	Z-type		M-type	
	π	θ	π	θ
X	0.0107	0.0111	0.0060	0.0106
2L	0.0096	0.0098	0.0082	0.0116
2R	0.0092	0.0094	0.0077	0.0113
3L	0.0095	0.0097	0.0074	0.0108
3R	0.0076	0.0078	0.0063	0.0095
A[#]	0.0089	0.0091	0.0073	0.0107

[#]A means averaged values among autosomes.

Table 3.3 The number of candidate regions suggested by different methods on each chromosome arm

	lower π value in MW population	lower π value in RA population	clustered high F_{ST} sites by MW/RA genome data	clustered high F_{ST} sites by Z/M RNA-seq
X	2	42	7	14
2L	5	6	0	3
2R	4	3	1	1
3L	1	1	2	18
3R	10	7	5	1

Note- MW = Melawi, RA = Raleigh, Z=Zimbabwe, M=French and Canton-S

Table 3.4 Distribution of high F_{ST} sites in genome data

	Location and type of F_{ST}								Total
	intergenic region	pseudo -gene	intron	UTR		CDS*			
				5' end	3' end	R	S	U	
X	2734	15	3099	140	241	175	675	3	7082
2L	534	0	545	20	39	31	153	0	1322
2R	453	2	438	32	51	52	117	1	1146
3L	924	3	822	56	53	62	154	0	2074
3R	1489	2	2102	99	128	111	451	2	4384
Total	6134	22	7006	347	512	431	1550	6	16008

* R for replacement substitution, S for synonymous substitution, and U for undetermined substitution between R and S

Table 3.5 Summary of the mapping result of each sample

	FR	CS	Z30	Z56
Uniquely mapped reads number	10,179,229	10,202,837	10,268,143	11,825,426
Total reads number	12,356,410	12,390,828	12,444,019	14,293,998
Uniquely mapped percentage	82.38%	82.34%	82.51%	82.73%

Table 3.6 Correlation coefficients between the RPKMs in each paired lines

	CS	Z30	Z56
FR	0.9682	0.9444	0.9621
CS	-	0.9156	0.9471
Z30	-	-	0.9807

Table 3.7 The number of DEGs depends on two kinds of multiple test corrections

	Bonferroni correction		FDR	
	Z>M	M>Z	Z>M	M>Z
X	39	43	63	59
2L	40	53	63	73
2R	44	53	70	71
3L	57	38	96	64
3LHet	0	0	0	1
3R	65	56	97	83
3RHet	0	0	1	0
4	0	0	1	2
U	1	0	1	0
Total	246	243	392	353

Table 3.8 The GO terms enrich in Z>M DEGs based on Bonferroni's correction

rank	Terms		p-values	sampled frequency	background frequency
1	GO:0007602	phototransduction	3.71E-13	15/193	48/12665
2	GO:0009583	detection of light stimulus	1.99E-12	15/193	53/12665
3	GO:0009416	response to light stimulus	4.07E-12	19/193	108/12665
4	GO:0009582	detection of abiotic stimulus	8.85E-12	15/193	58/12665
5	GO:0009581	detection of external stimulus	3.40E-11	15/193	63/12665
6	GO:0009314	response to radiation	4.21E-11	19/193	122/12665
7	GO:0007601	visual perception	6.42E-11	13/193	43/12665
8	GO:0050953	sensory perception of light stimulus	8.99E-11	13/193	44/12665
9	GO:0016056	rhodopsin mediated signaling pathway	1.42E-10	10/193	20/12665
10	GO:0050896	response to stimulus	5.59E-09	55/193	1345/12665
11	GO:0007603	phototransduction, visible light	8.79E-09	9/193	20/12665
12	GO:0009605	response to external stimulus	2.36E-08	20/193	194/12665
13	GO:0051606	detection of stimulus	2.74E-08	15/193	97/12665
14	GO:0007186	G-protein coupled receptor protein signaling pathway	4.54E-08	20/193	201/12665
15	GO:0009586	rhodopsin mediated phototransduction	8.94E-08	8/193	17/12665
16	GO:0009584	detection of visible light	1.51E-07	9/193	26/12665
17	GO:0009628	response to abiotic stimulus	2.58E-07	21/193	246/12665
18	GO:0050908	detection of light stimulus involved in visual perception	1.10E-06	8/193	22/12665
19	GO:0022400	regulation of rhodopsin mediated signaling pathway	1.63E-06	7/193	15/12665
19	GO:0016059	deactivation of rhodopsin mediated signaling	1.63E-06	7/193	15/12665
21	GO:0050962	detection of light stimulus involved in sensory perception	1.67E-06	8/193	23/12665
22	GO:0008277	regulation of G-protein coupled receptor protein signaling pathway	2.47E-06	8/193	24/12665
23	GO:0007165	signal transduction	2.99E-06	20/193	254/12665
24	GO:0003008	system process	8.08E-06	31/193	623/12665
25	GO:0023060	signal transmission	9.83E-06	29/193	557/12665
26	GO:0050877	neurological system process	1.05E-05	30/193	594/12665
27	GO:0023046	signaling process	1.07E-05	29/193	559/12665
28	GO:0006952	defense response	2.65E-05	16/193	181/12665
29	GO:0023052	signaling	1.33E-04	44/193	1248/12665
30	GO:0050906	detection of stimulus involved in sensory perception	3.80E-04	8/193	43/12665
31	GO:0007166	cell surface receptor linked signaling pathway	4.38E-04	27/193	587/12665
32	GO:0042051	compound eye photoreceptor development	6.11E-04	9/193	62/12665
33	GO:0042462	eye photoreceptor cell development	7.04E-04	9/193	63/12665
34	GO:0019731	antibacterial humoral response	7.82E-04	8/193	47/12665
35	GO:0007600	sensory perception	9.04E-04	17/193	263/12665
36	GO:0050890	cognition	1.23E-03	20/193	365/12665
37	GO:0042461	photoreceptor cell development	1.99E-03	9/193	71/12665
38	GO:0042742	defense response to bacterium	3.57E-03	9/193	76/12665
39	GO:0051716	cellular response to stimulus	3.95E-03	19/193	359/12665
40	GO:0006955	immune response	6.09E-03	13/193	180/12665
41	GO:0009617	response to bacterium	8.31E-03	9/193	84/12665

Table 3.9 The GO terms enrich in M>Z DEGs based on Bonferroni's correction

rank	Terms		p-values	sampled frequency	background frequency
1	GO:0044281	small molecule metabolic process	1.57E-17	54/221	715/12665
2	GO:0043436	oxoacid metabolic process	2.23E-12	29/221	263/12665
2	GO:0019752	carboxylic acid metabolic process	2.23E-12	29/221	263/12665
2	GO:0006082	organic acid metabolic process	2.23E-12	29/221	263/12665
5	GO:0055114	oxidation reduction	1.49E-11	37/221	473/12665
6	GO:0042180	cellular ketone metabolic process	1.56E-11	29/221	283/12665
7	GO:0005975	carbohydrate metabolic process	9.27E-08	28/221	373/12665
8	GO:0032787	monocarboxylic acid metabolic process	2.37E-07	14/221	84/12665
9	GO:0044242	cellular lipid catabolic process	2.79E-07	9/221	25/12665
10	GO:0044282	small molecule catabolic process	6.56E-07	15/221	107/12665
11	GO:0016042	lipid catabolic process	8.99E-07	10/221	38/12665
12	GO:0006066	alcohol metabolic process	1.16E-06	18/221	169/12665
13	GO:0044262	cellular carbohydrate metabolic process	3.24E-06	18/221	180/12665
14	GO:0008152	metabolic process	5.36E-06	131/221	5060/12665
15	GO:0006635	fatty acid beta-oxidation	1.55E-05	6/221	11/12665
16	GO:0009062	fatty acid catabolic process	3.05E-05	6/221	12/12665
16	GO:0019395	fatty acid oxidation	3.05E-05	6/221	12/12665
18	GO:0034440	lipid oxidation	5.58E-05	6/221	13/12665
19	GO:0005996	monosaccharide metabolic process	9.70E-05	12/221	93/12665
20	GO:0006629	lipid metabolic process	1.75E-04	20/221	285/12665
21	GO:0019318	hexose metabolic process	1.77E-04	11/221	80/12665
22	GO:0044106	cellular amine metabolic process	5.17E-04	15/221	174/12665
23	GO:0044283	small molecule biosynthetic process	1.30E-03	18/221	266/12665
24	GO:0044271	cellular nitrogen compound biosynthetic process	1.32E-03	17/221	239/12665
25	GO:0046395	carboxylic acid catabolic process	1.52E-03	8/221	46/12665
25	GO:0016054	organic acid catabolic process	1.52E-03	8/221	46/12665
27	GO:0009156	ribonucleoside monophosphate biosynthetic process	1.57E-03	6/221	21/12665
27	GO:0009161	ribonucleoside monophosphate metabolic process	1.57E-03	6/221	21/12665
29	GO:0009056	catabolic process	1.93E-03	23/221	424/12665
30	GO:0006519	cellular amino acid and derivative metabolic process	3.44E-03	15/221	202/12665
31	GO:0006520	cellular amino acid metabolic process	3.45E-03	13/221	152/12665
32	GO:0046040	IMP metabolic process	4.14E-03	4/221	7/12665
32	GO:0006188	IMP biosynthetic process	4.14E-03	4/221	7/12665
34	GO:0009308	amine metabolic process	4.34E-03	19/221	319/12665
35	GO:0030258	lipid modification	4.83E-03	6/221	25/12665
36	GO:0006006	glucose metabolic process	8.19E-03	8/221	57/12665

Table 3.10 Distribution of High F_{ST} sites in RNA-seq data

	Location and type of F_{ST}					
	UTR		CDS*			
	5' end	3' end	R	S	U	Total
X	269	591	467	3414	182	4923
XHet	0	2	0	2	0	4
2L	144	213	254	1666	66	2343
2R	125	251	207	1351	53	1987
2RHet	0	0	1	2	0	3
3L	280	490	529	3238	142	4679
3LHet	0	1	1	2	0	3
3R	102	206	221	1264	83	1876
3RHet	1	0	3	1	0	5
4	3	8	19	21	2	53
mt	0	0	2	2	0	4
Total	924	1762	1704	10963	528	15881

* R for replacement substitution, S for synonymous substitution, and U for undetermined substitution between R and S

Table 3.11 Distribution of Shared High F_{ST} sites in two datasets

	Location and type of F_{ST}					
	UTR		CDS*			
	5' end	3' end	R	S	U	Total
X	8	18	10	51	5	92
2L	0	3	1	6	0	10
2R	0	1	0	5	0	6
3L	1	1	3	11	0	16
3R	5	1	4	16	0	26
Total	14	24	18	89	5	150

* R for replacement substitution, S for synonymous substitution, and U for undetermined substitution between R and S

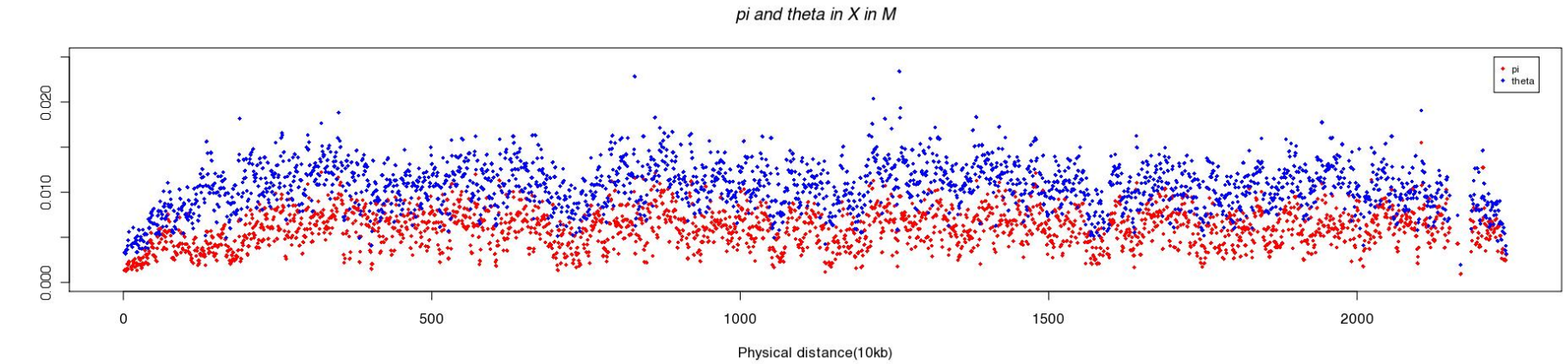
pi and theta in X in M
pi
theta
0.000
0.010
0.020
0
500
1000
1500
2000
Physical distance(10kb)

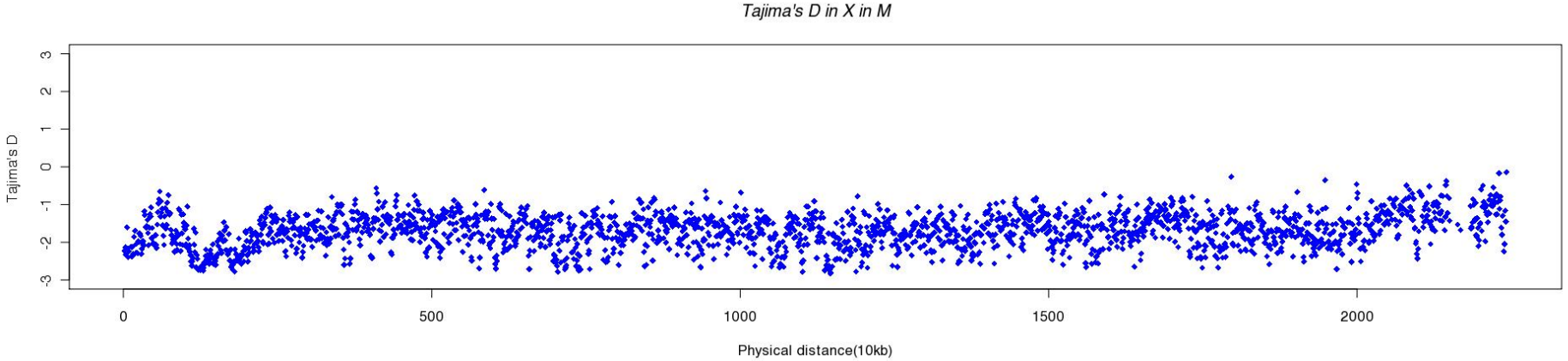
Tajima's D in X in M
Tajima's D
-3
-2
-1
0
1
2
3
0
500
1000
1500
2000
Physical distance(10kb)

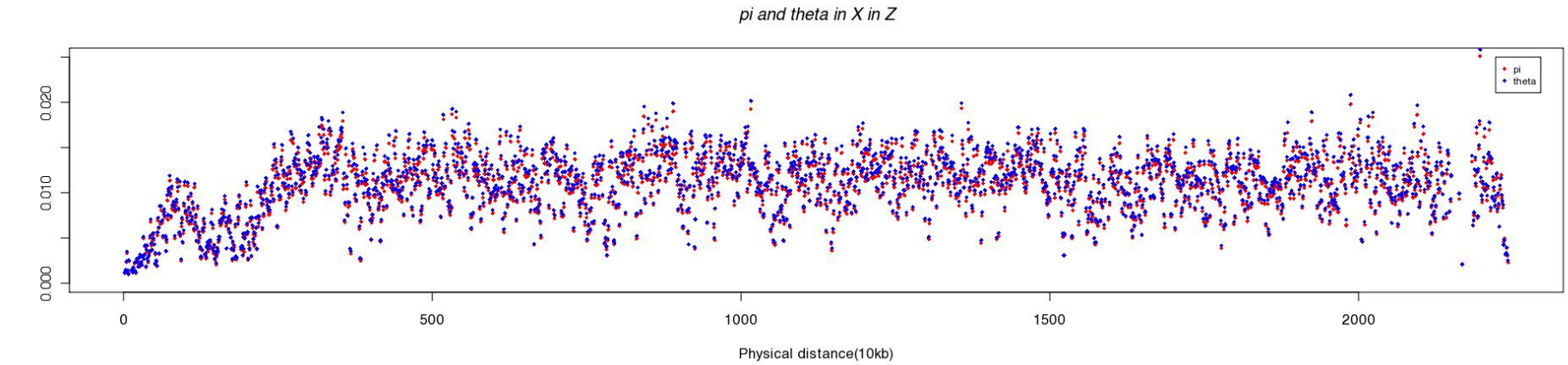
pi and theta in X in Z
pi
theta
0.000
0.010
0.020
0
500
1000
1500
2000
Physical distance(10kb)

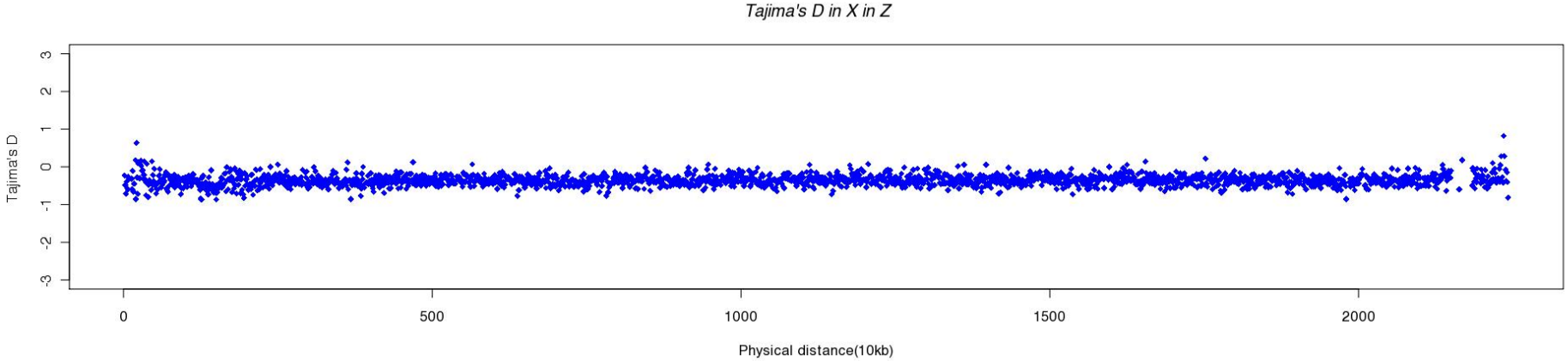
Tajima's D in X in Z
Tajima's D
-3
-2
-1
0
1
2
3
0
500
1000
1500
2000
Physical distance(10kb)

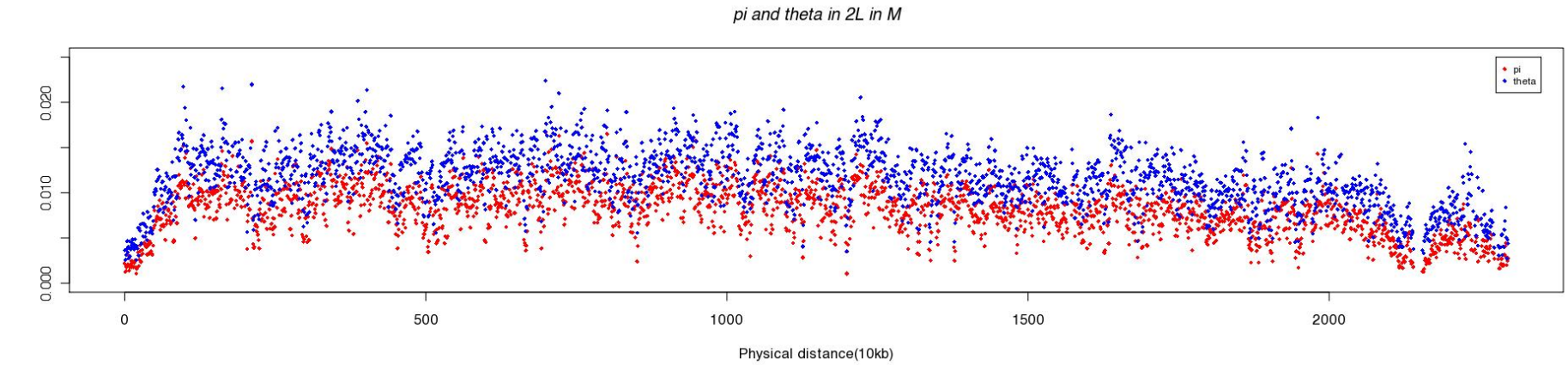
pi and theta in 2L in M
pi
theta
0.000
0.010
0.020
0
500
1000
1500
2000
Physical distance(10kb)

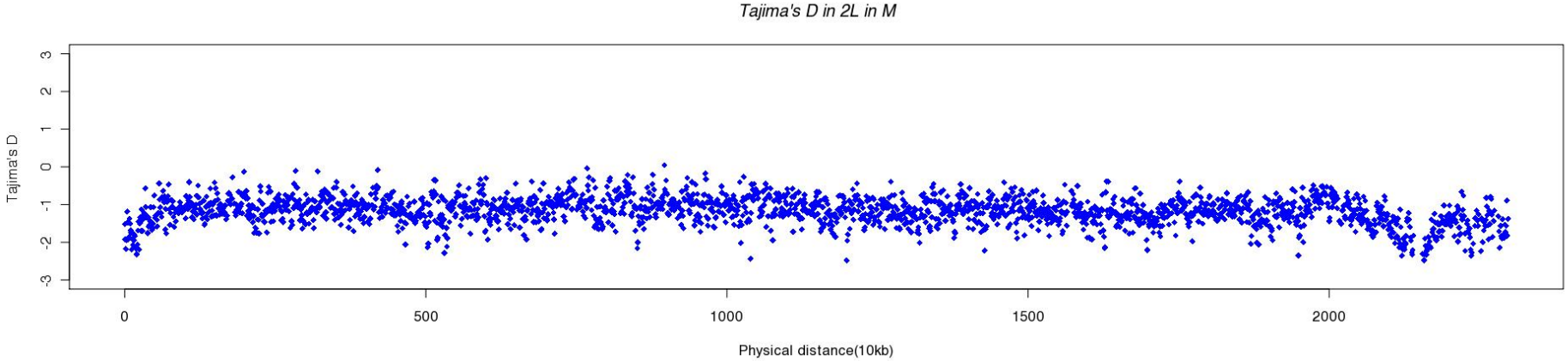
Tajima's D in 2L in M
Tajima's D
-3
-2
-1
0
1
2
3
0
500
1000
1500
2000
Physical distance(10kb)

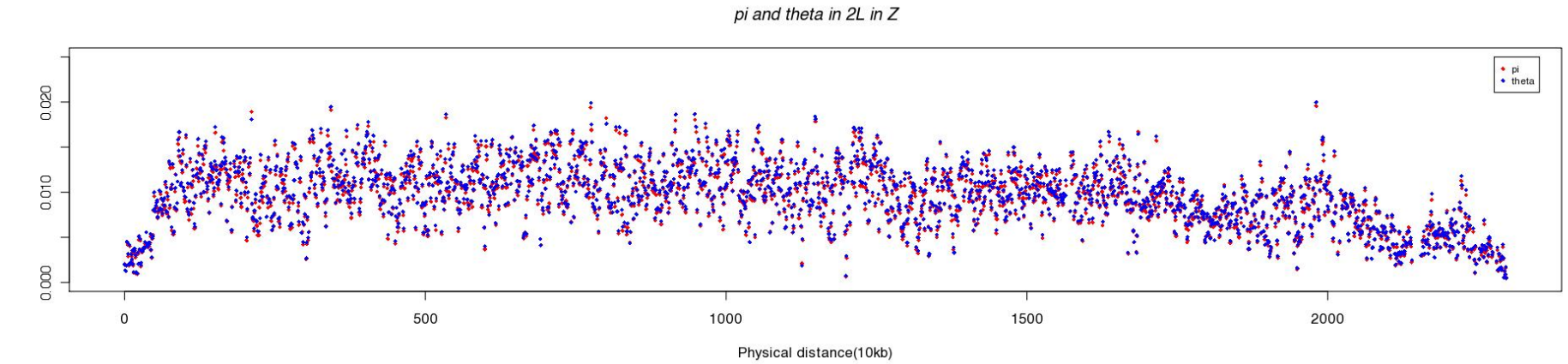
pi and theta in 2L in Z
pi
theta
0.000
0.010
0.020
0
500
1000
1500
2000
Physical distance(10kb)

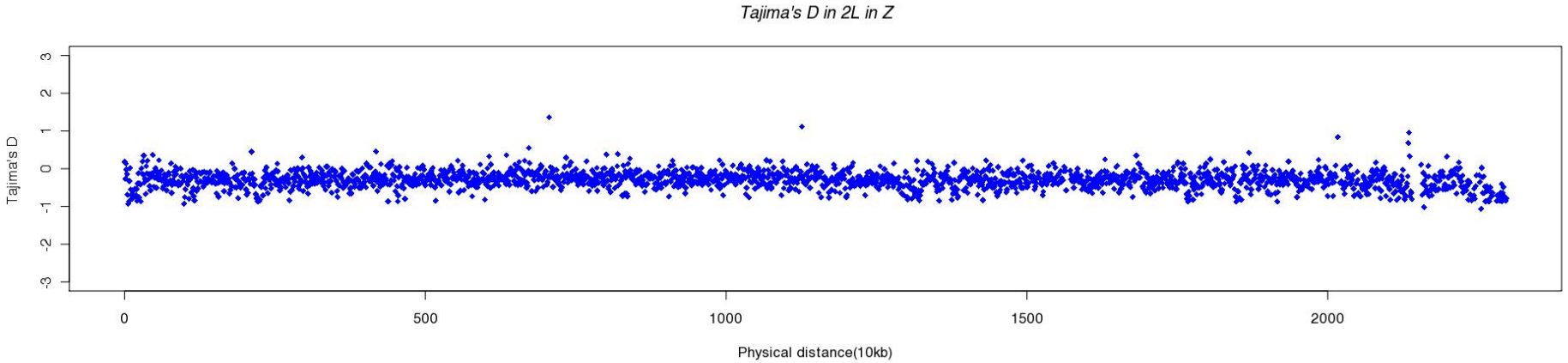
Tajima's D in 2L in Z
Tajima's D
-3
-2
-1
0
1
2
3
0
500
1000
1500
2000
Physical distance(10kb)

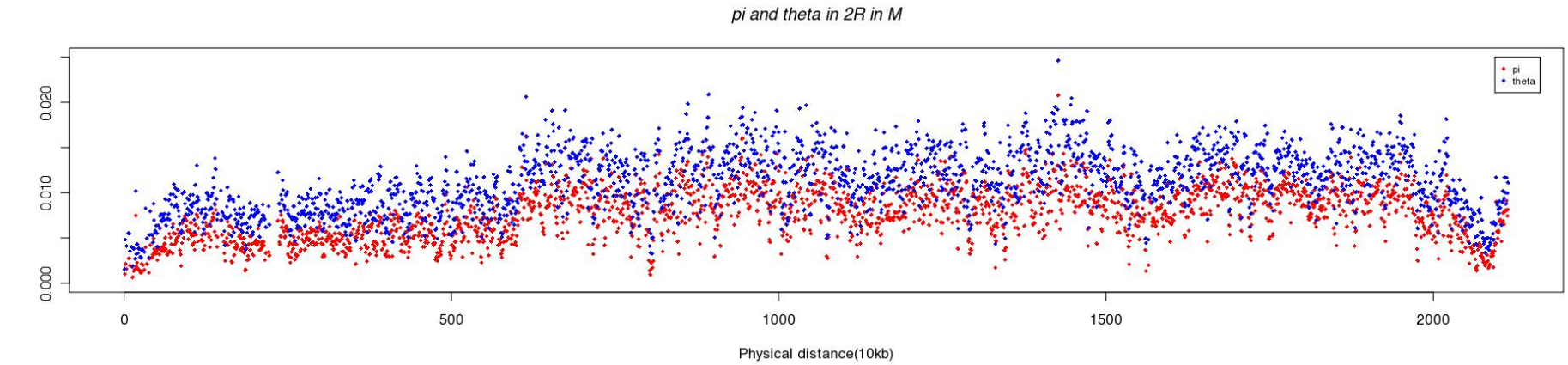
pi and theta in 2R in M
pi
theta
0.000
0.010
0.020
0
500
1000
1500
2000
Physical distance(10kb)

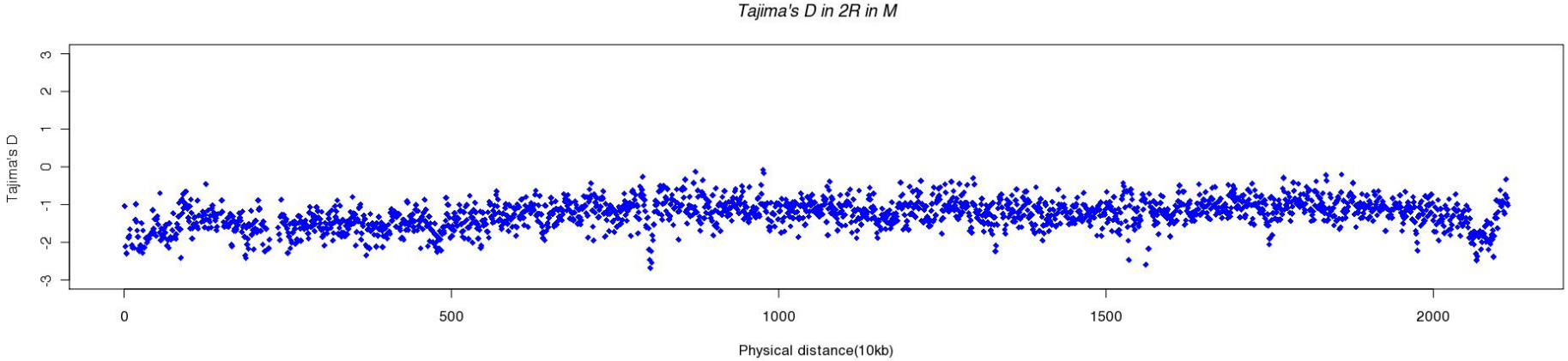
Tajima's D in 2R in M
Tajima's D
-3
-2
-1
0
1
2
3
0
500
1000
1500
2000
Physical distance(10kb)

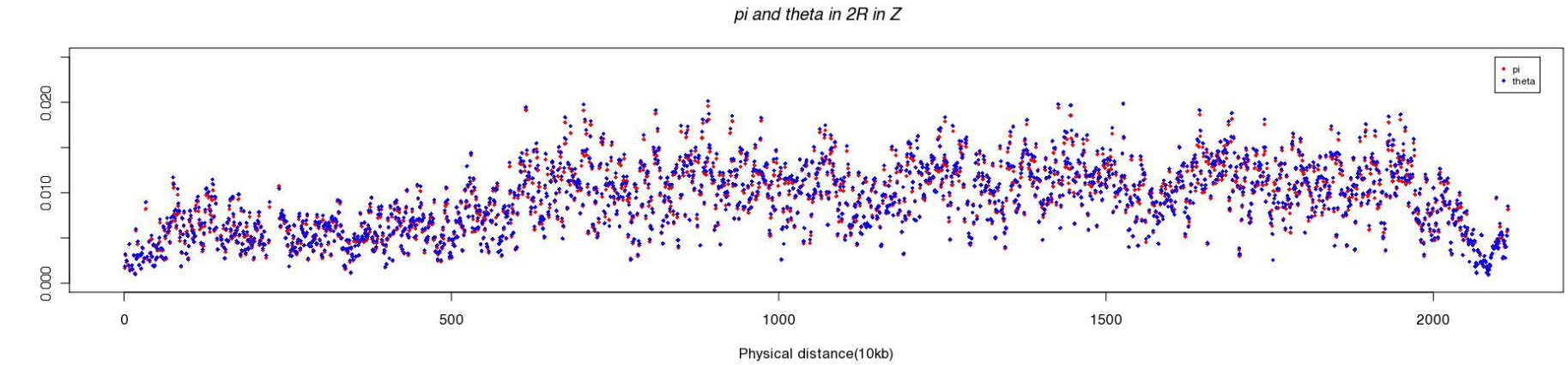
pi and theta in 2R in Z
pi
theta
0.000
0.010
0.020
0
500
1000
1500
2000
Physical distance(10kb)

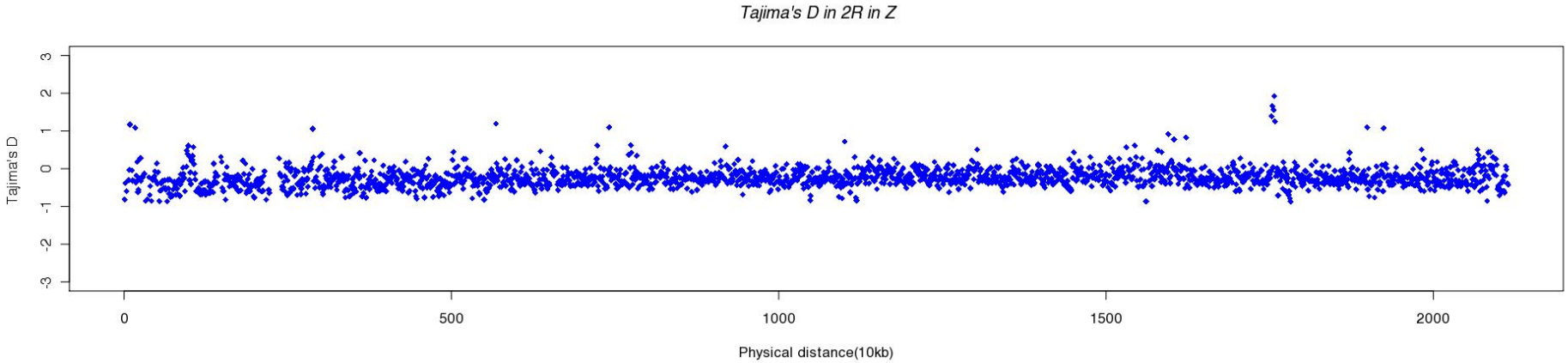
Tajima's D in 2R in Z
Tajima's D
-3
-2
-1
0
1
2
3
0
500
1000
1500
2000
Physical distance(10kb)

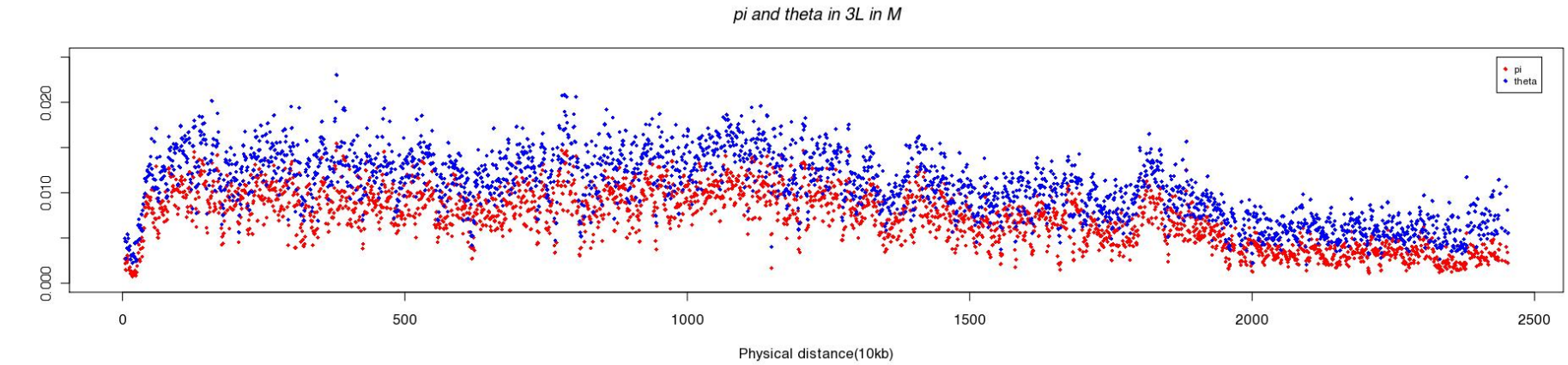
pi and theta in 3L in M
pi
theta
0.000
0.010
0.020
0
500
1000
1500
2000
2500
Physical distance(10kb)

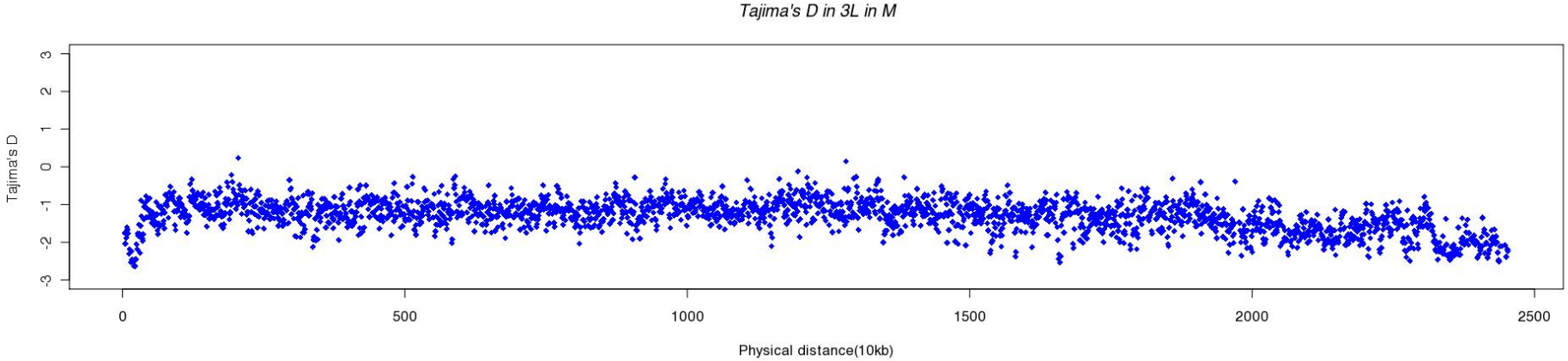
Tajima's D in 3L in M
Tajima's D
-3
-2
-1
0
1
2
3
0
500
1000
1500
2000
2500
Physical distance(10kb)

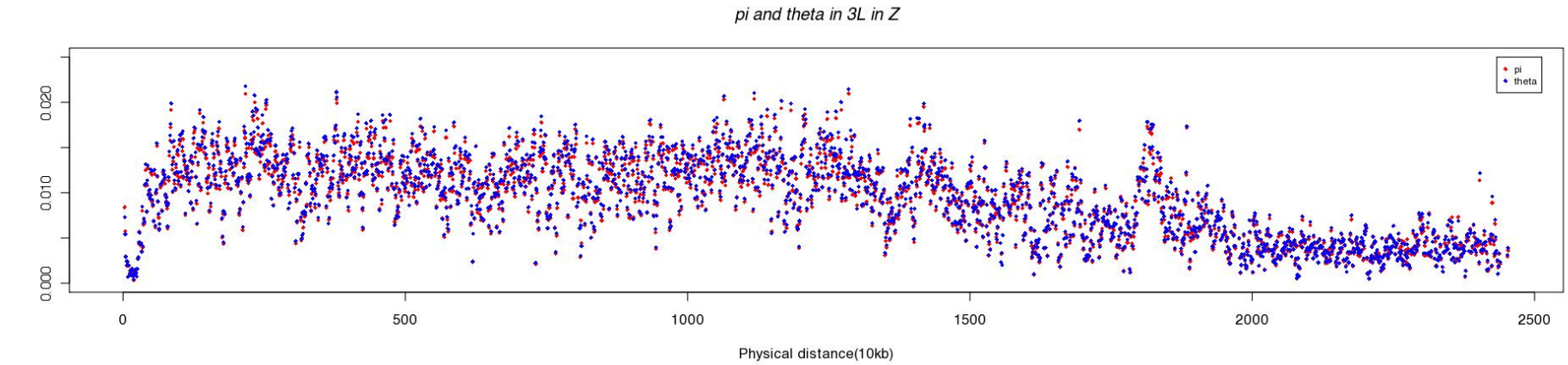
pi and theta in 3L in Z
pi
theta
0.000
0.010
0.020
0
500
1000
1500
2000
2500
Physical distance(10kb)

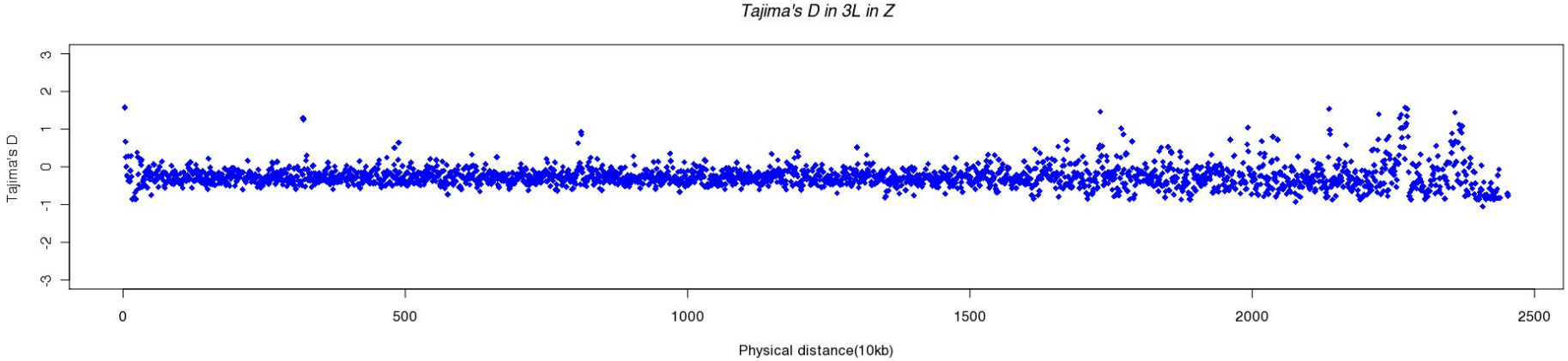
Tajima's D in 3L in Z
Tajima's D
-3
-2
-1
0
1
2
3
0
500
1000
1500
2000
2500
Physical distance(10kb)

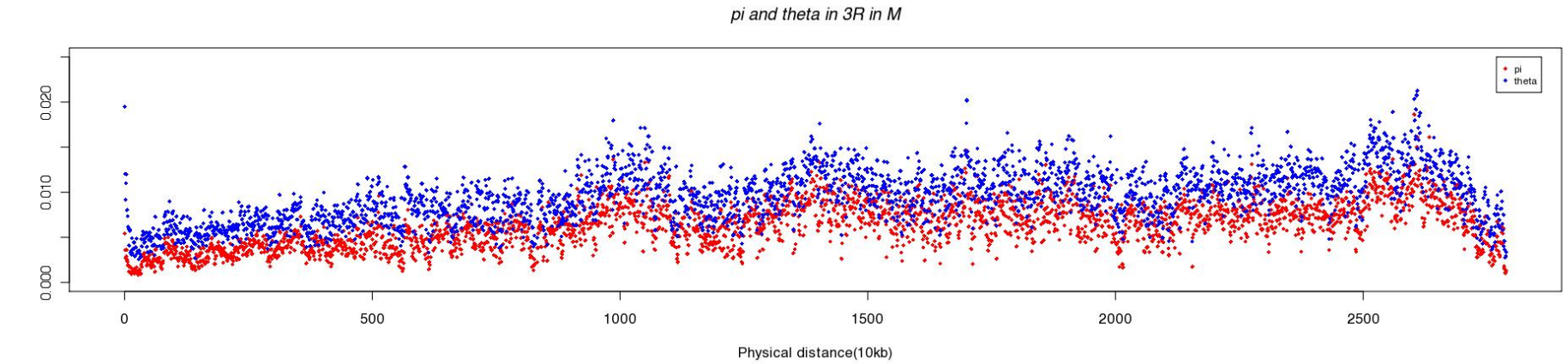
pi and theta in 3R in M
pi
theta
0.000
0.010
0.020
0
500
1000
1500
2000
2500
Physical distance(10kb)

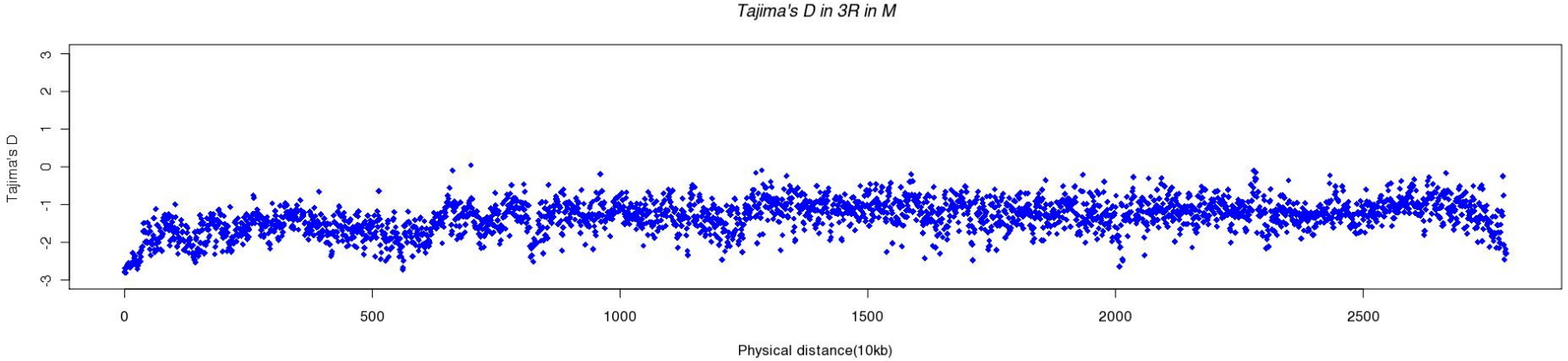
Tajima's D in 3R in M
Tajima's D
-3
-2
-1
0
1
2
3
0
500
1000
1500
2000
2500
Physical distance(10kb)

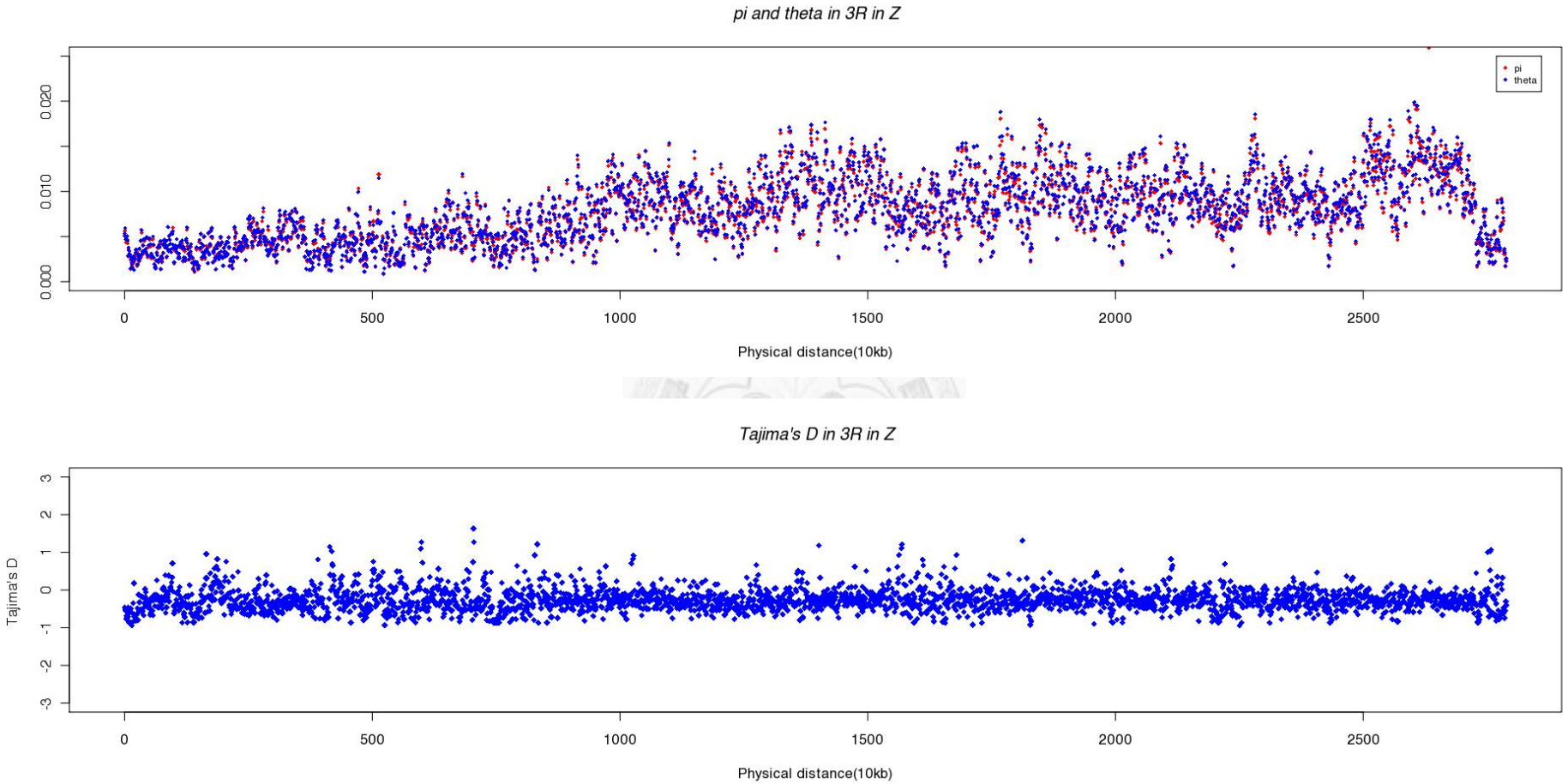

Figure 3.2 The distribution of population parameters (θ, π, and Tajima's D) in different chromosome arms in two races (Z and M)

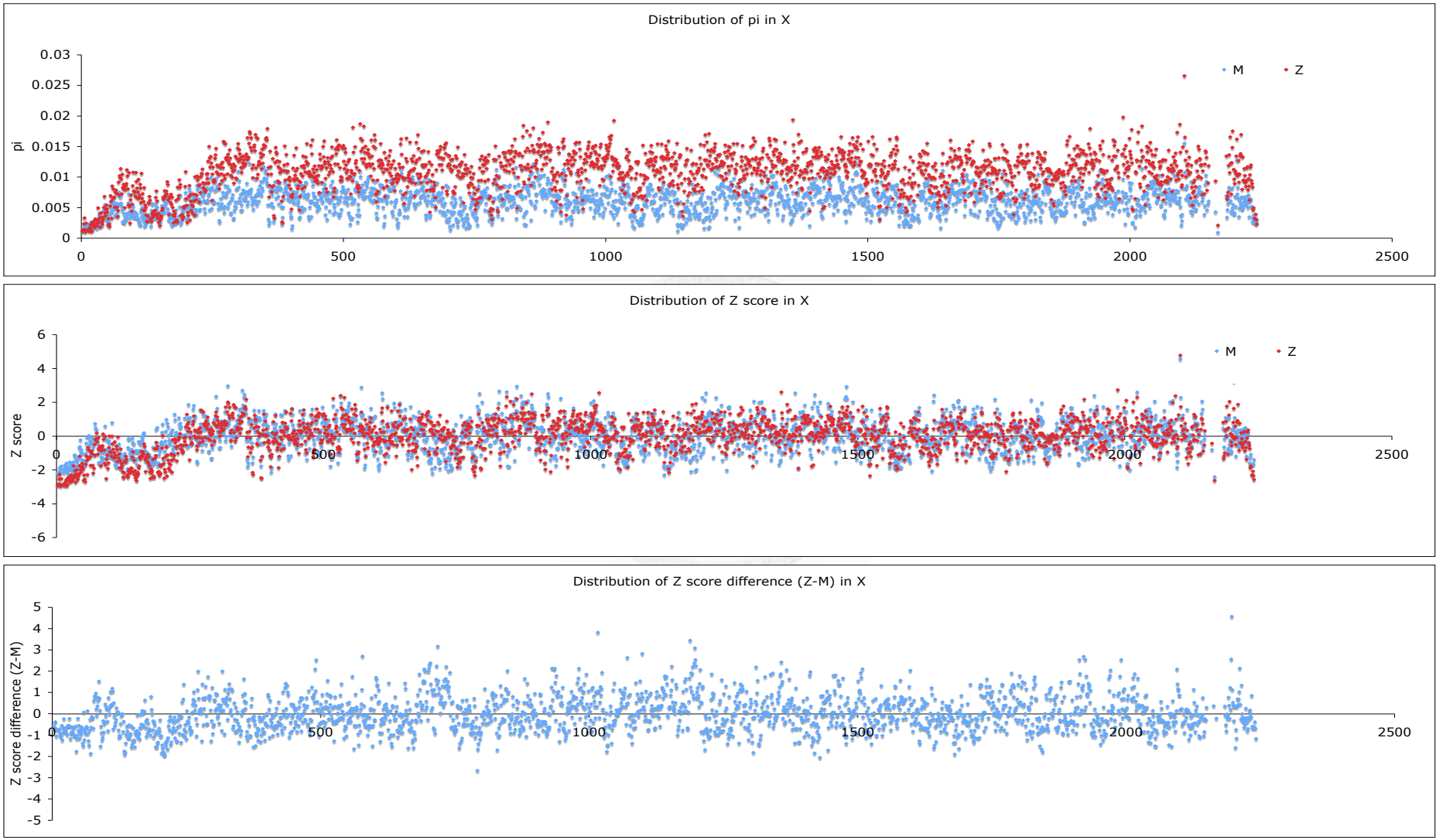
Distribution of pi in X
pi
0.03
0.025
0.02
0.015
0.01
0.005
0
0
500
1000
1500
2000
2500
M
Z
Distribution of Z score in X
Z score
6
4
2
0
-2
-4
-6
0
500
1000
1500
2000
2500
M
Z
Distribution of Z score difference (Z-M) in X
Z score difference (Z-M)
5
4
3
2
1
0
-1
-2
-3
-4
-5
0
500
1000
1500
2000
2500

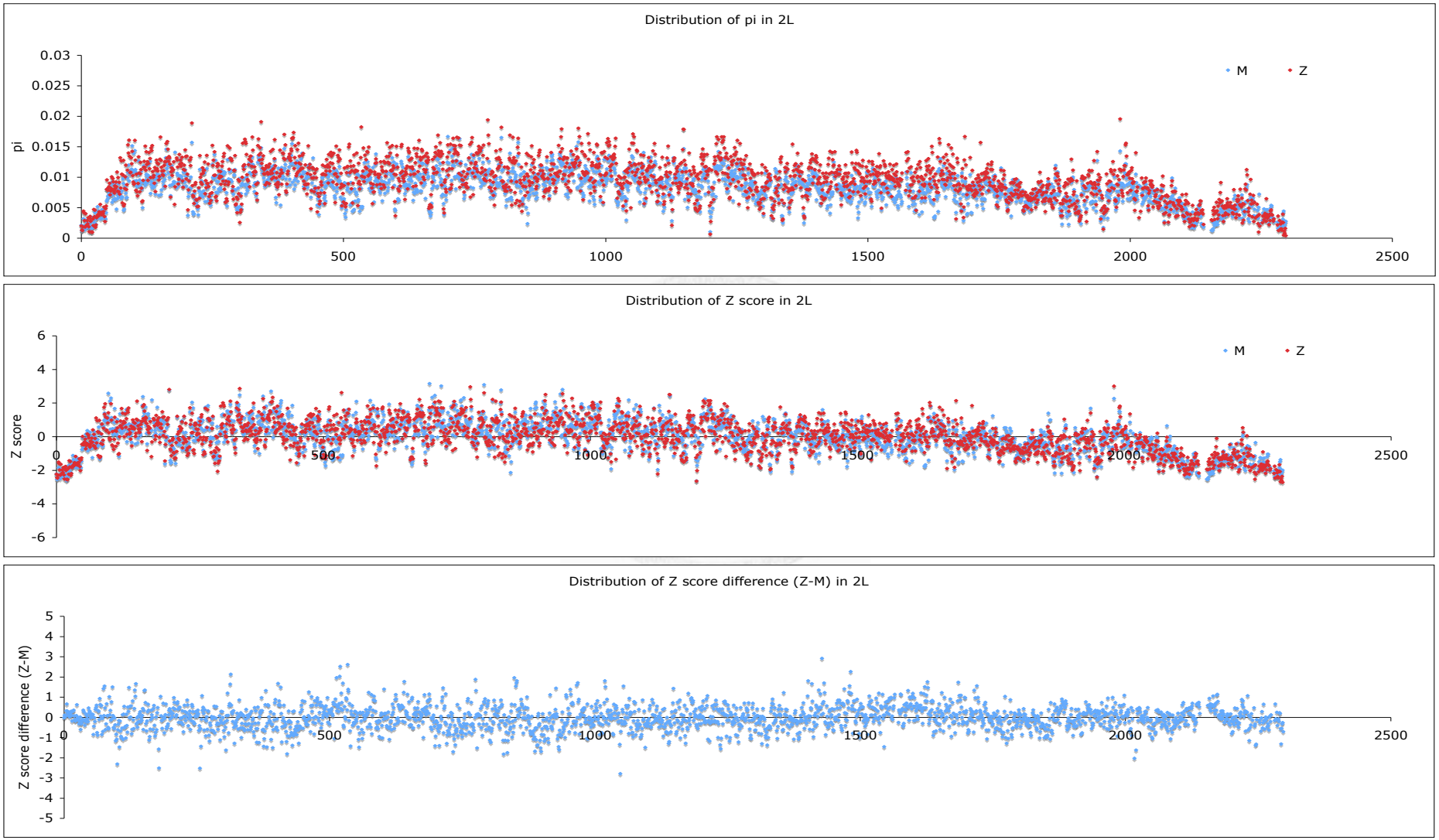
Distribution of pi in 2L
pi
0.03
0.025
0.02
0.015
0.01
0.005
0
0
500
1000
1500
2000
2500
M
Z
Distribution of Z score in 2L
Z score
6
4
2
0
-2
-4
-6
0
500
1000
1500
2000
2500
M
Z
Distribution of Z score difference (Z-M) in 2L
Z score difference (Z-M)
5
4
3
2
1
0
-1
-2
-3
-4
-5
0
500
1000
1500
2000
2500

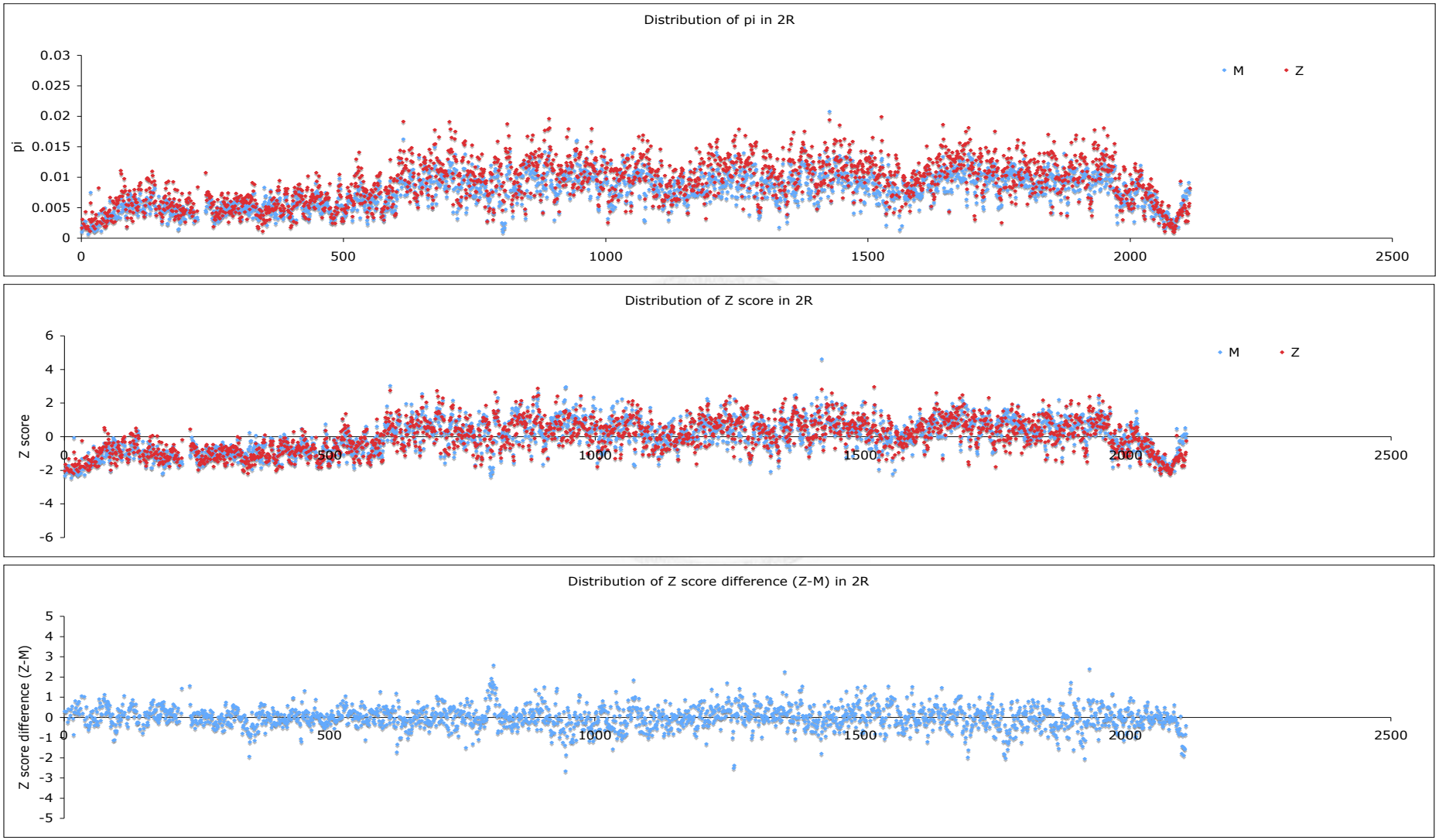
Distribution of pi in 2R
pi
0.03
0.025
0.02
0.015
0.01
0.005
0
0
500
1000
1500
2000
2500
M
Z
Distribution of Z score in 2R
Z score
6
4
2
0
-2
-4
-6
0
500
1000
1500
2000
2500
M
Z
Distribution of Z score difference (Z-M) in 2R
Z score difference (Z-M)
5
4
3
2
1
0
-1
-2
-3
-4
-5
0
500
1000
1500
2000
2500

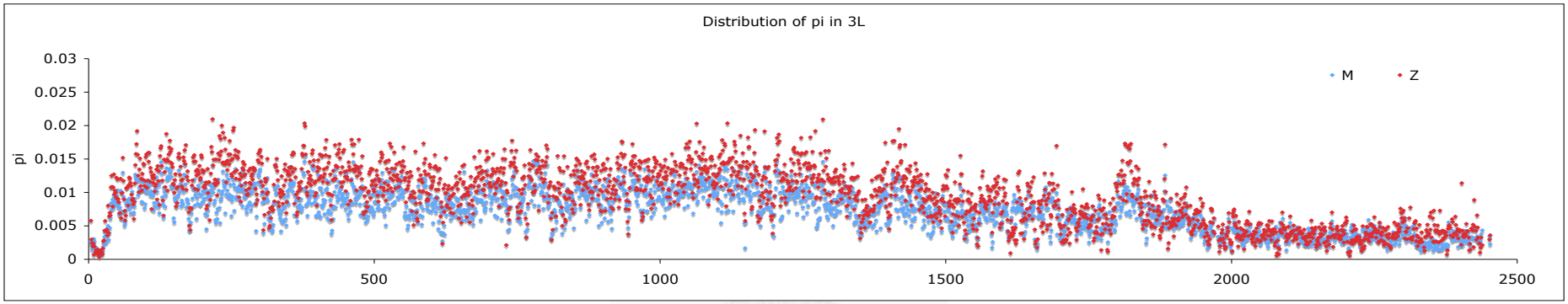
Distribution of pi in 3L
pi
0.03
0.025
0.02
0.015
0.01
0.005
0
0
500
1000
1500
2000
2500
M
Z

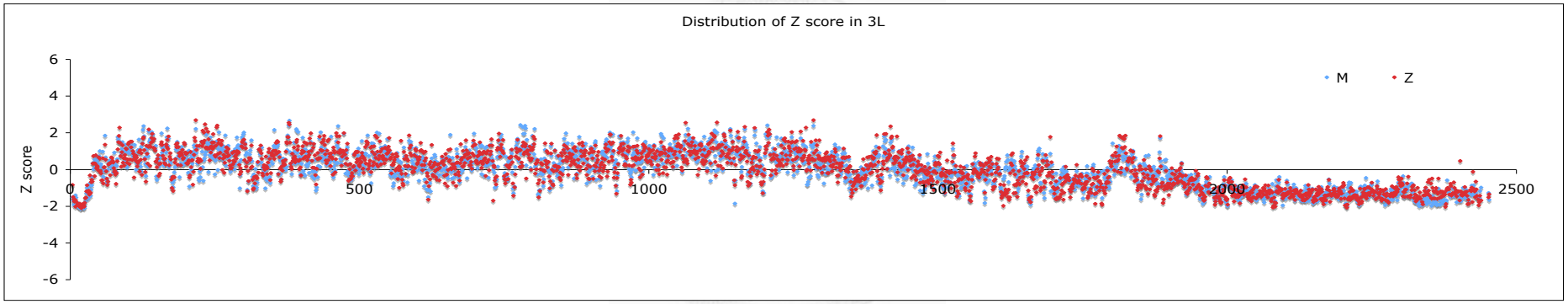
Distribution of Z score in 3L
Z score
6
4
2
0
-2
-4
-6
0
500
1000
1500
2000
2500
M
Z

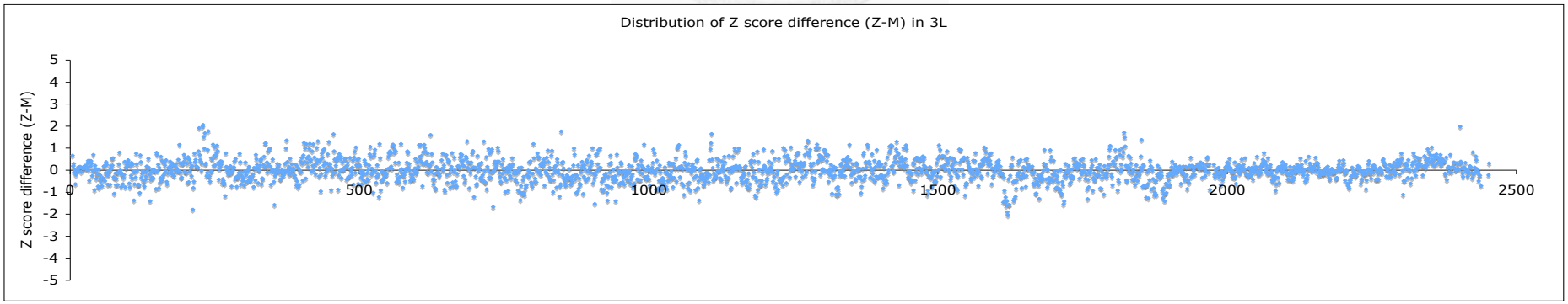
Distribution of Z score difference (Z-M) in 3L
Z score difference (Z-M)
5
4
3
2
1
0
-1
-2
-3
-4
-5
0
500
1000
1500
2000
2500

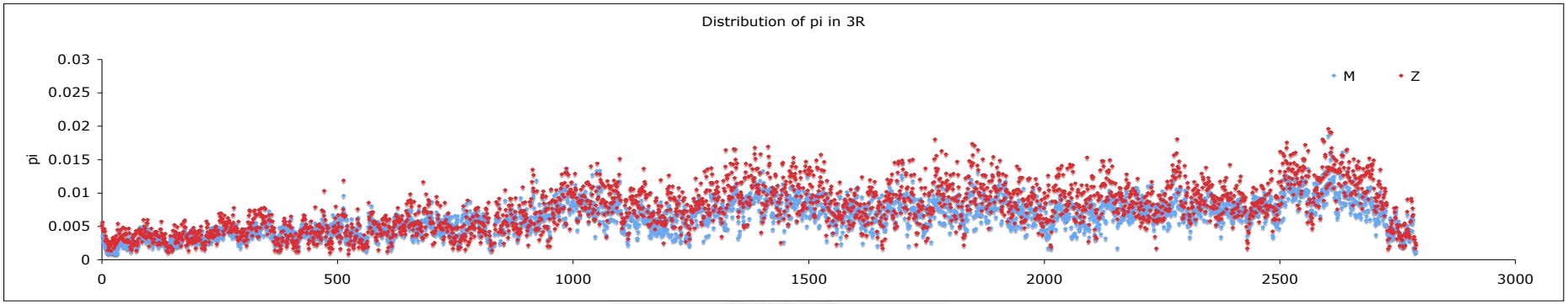
Distribution of pi in 3R
pi
0.03
0.025
0.02
0.015
0.01
0.005
0
0
500
1000
1500
2000
2500
3000
M
Z

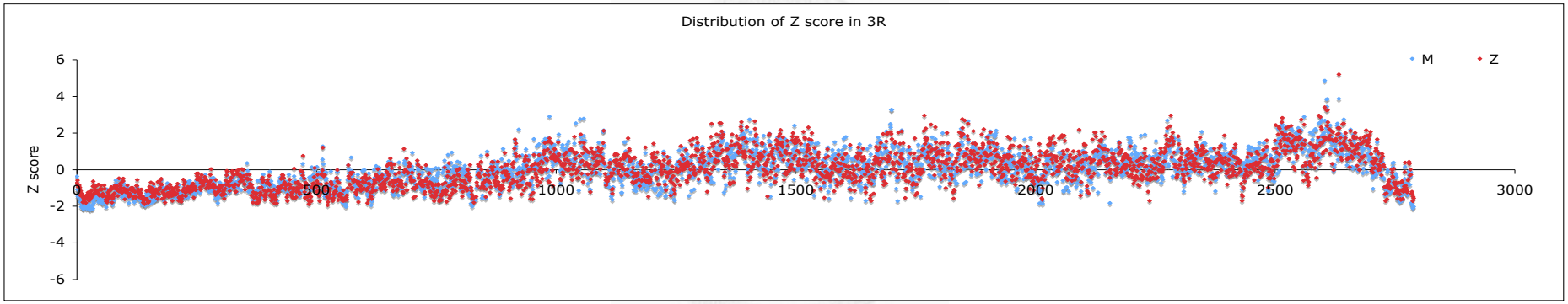
Distribution of Z score in 3R
Z score
6
4
2
0
-2
-4
-6
0
500
1000
1500
2000
2500
3000
M
Z

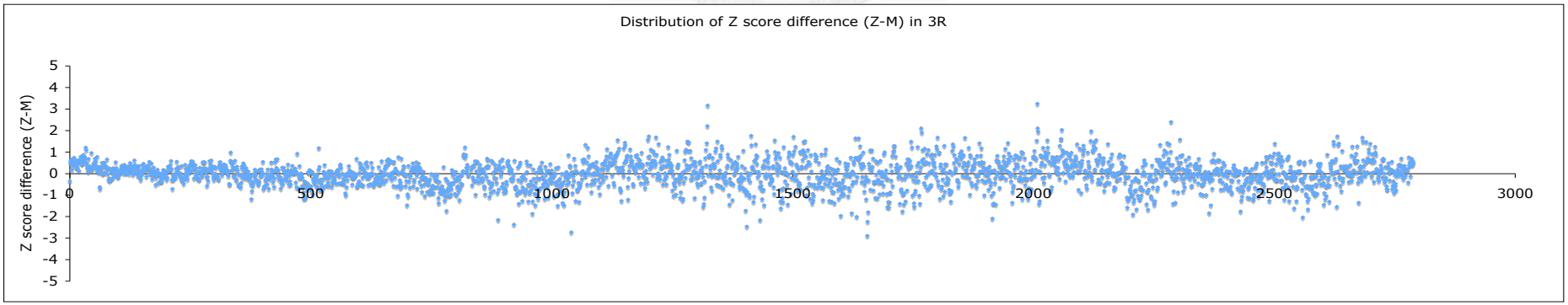
Distribution of Z score difference (Z-M) in 3R
Z score difference (Z-M)
5
4
3
2
1
0
-1
-2
-3
-4
-5
0
500
1000
1500
2000
2500
3000

Figure 3.3 The distribution of nucleotide diversity (π), normalized nucleotide diversity (Z score), and differences between two Z scores in Z race and M race along chromosome arm The units of x-axes are 10kb. Each point stands for one 10 kb window.

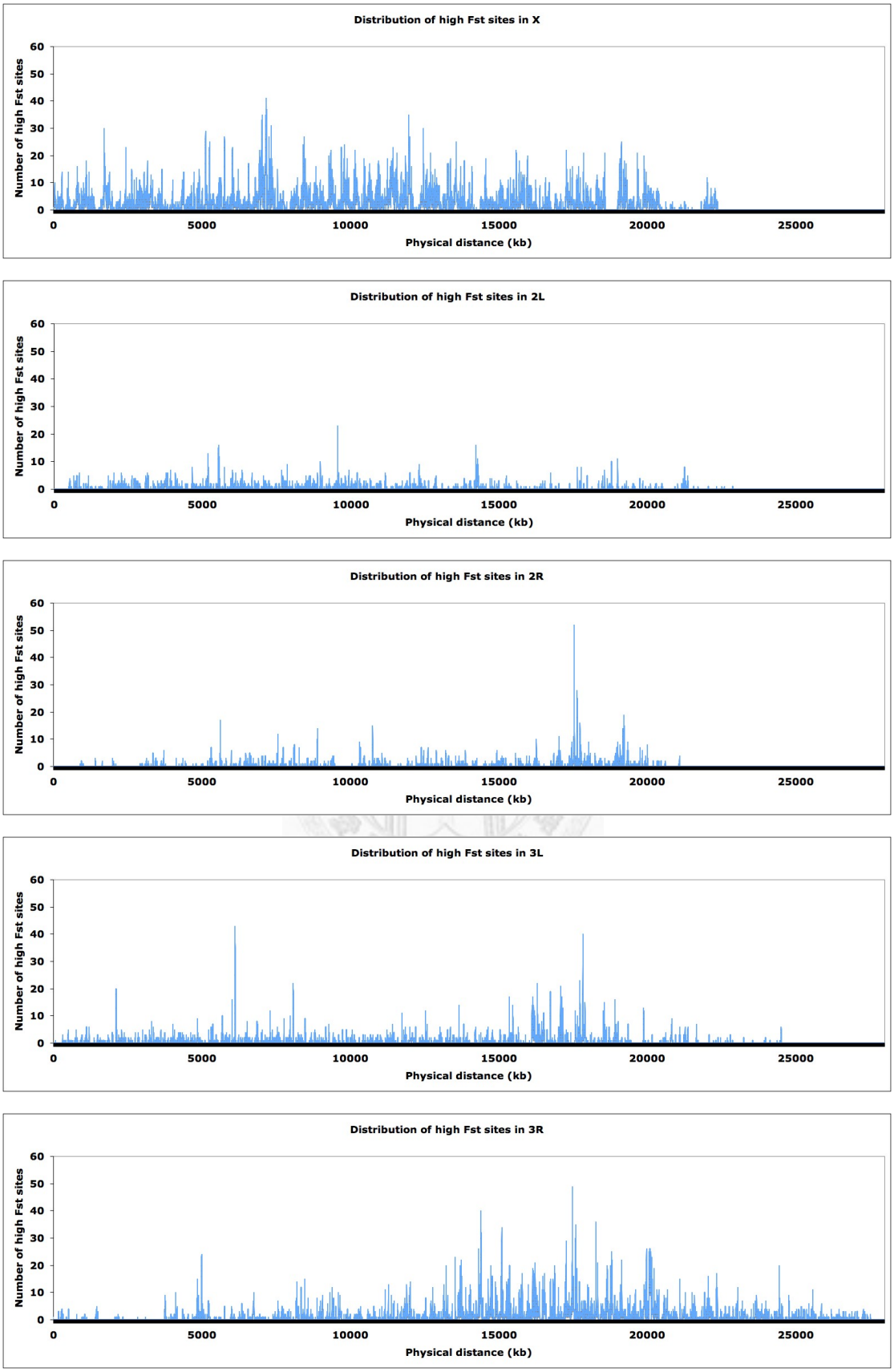

Figure 3.4 The genome-wide F_{ST} pattern on different arms The size of each window is 10 kb and the one sliding movement is 1 k

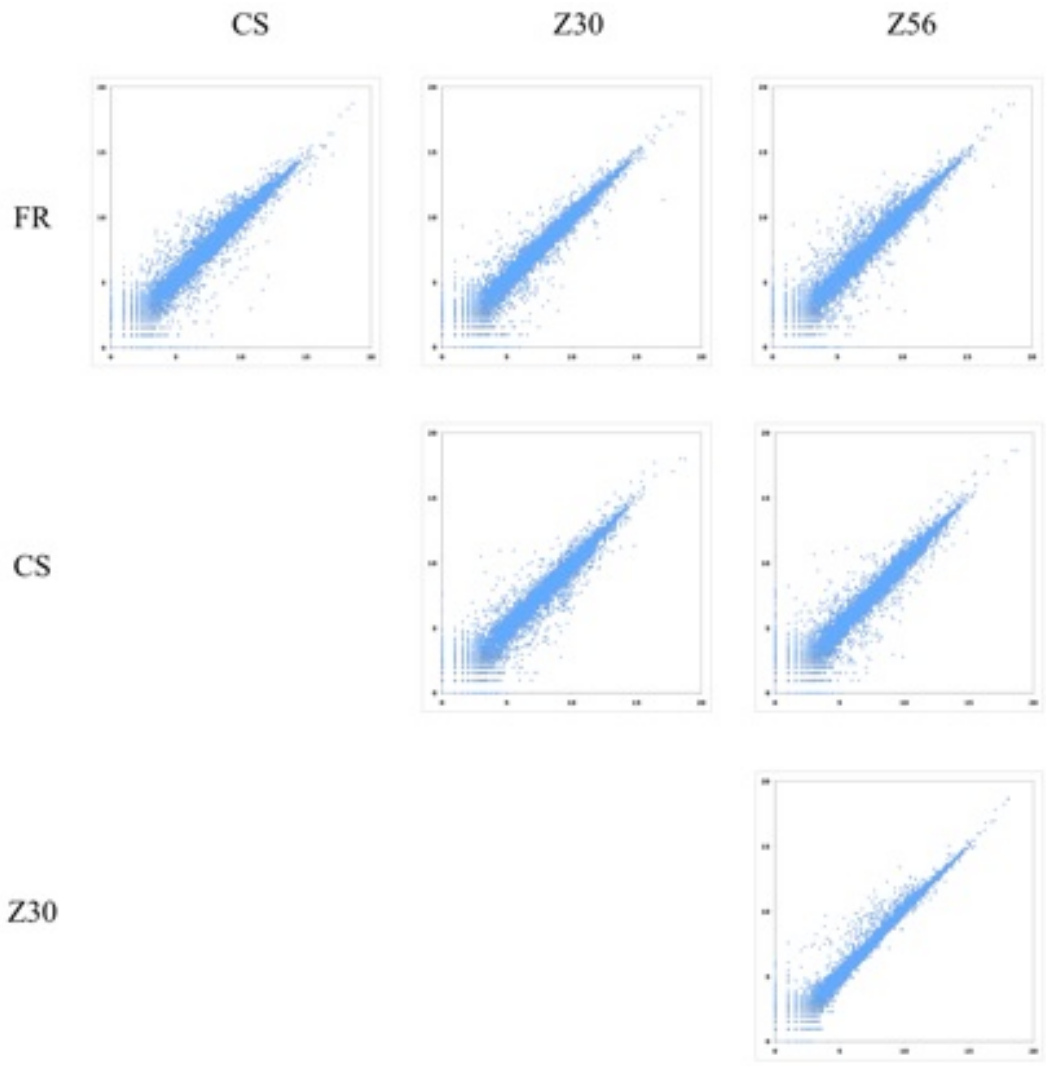

Figure 3.5 The correlations of expression levels between each races (unit: $\log_2$ [RPKM])

A

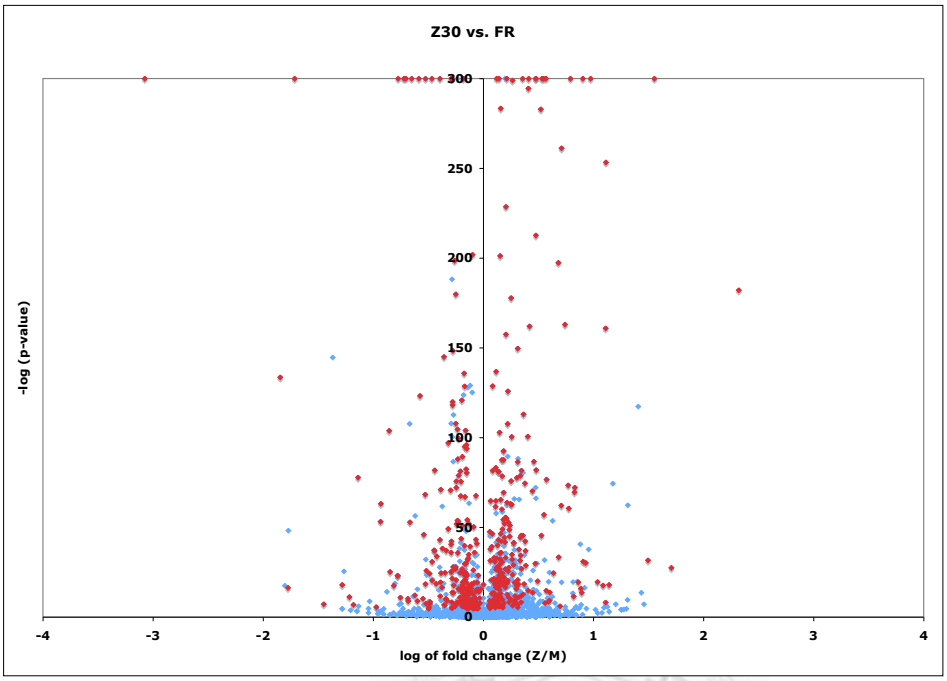
Z30 vs. FR
-log (p-value)
300
250
200
150
100
50
0
-4
-3
-2
-1
0
1
2
3
4
log of fold change (Z/M)

B

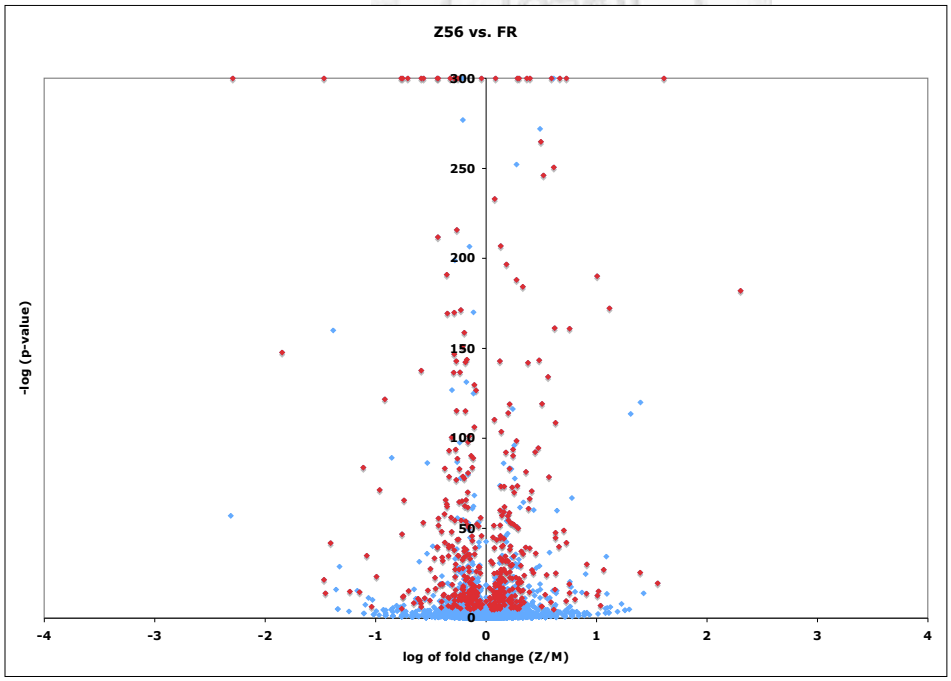
Z56 vs. FR
-log (p-value)
300
250
200
150
100
50
0
-4
-3
-2
-1
0
1
2
3
4
log of fold change (Z/M)

C

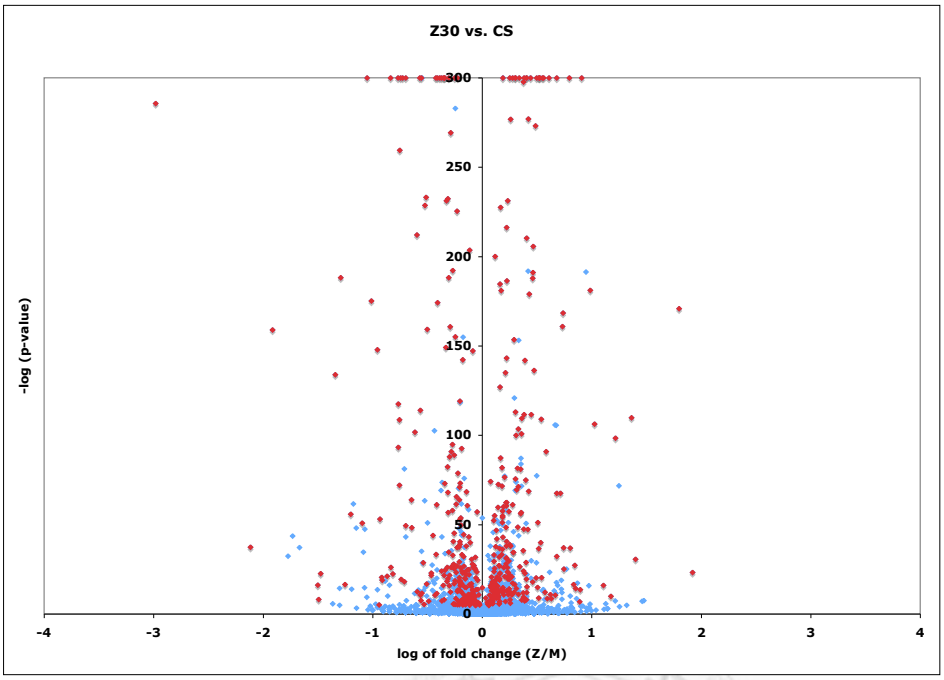

D

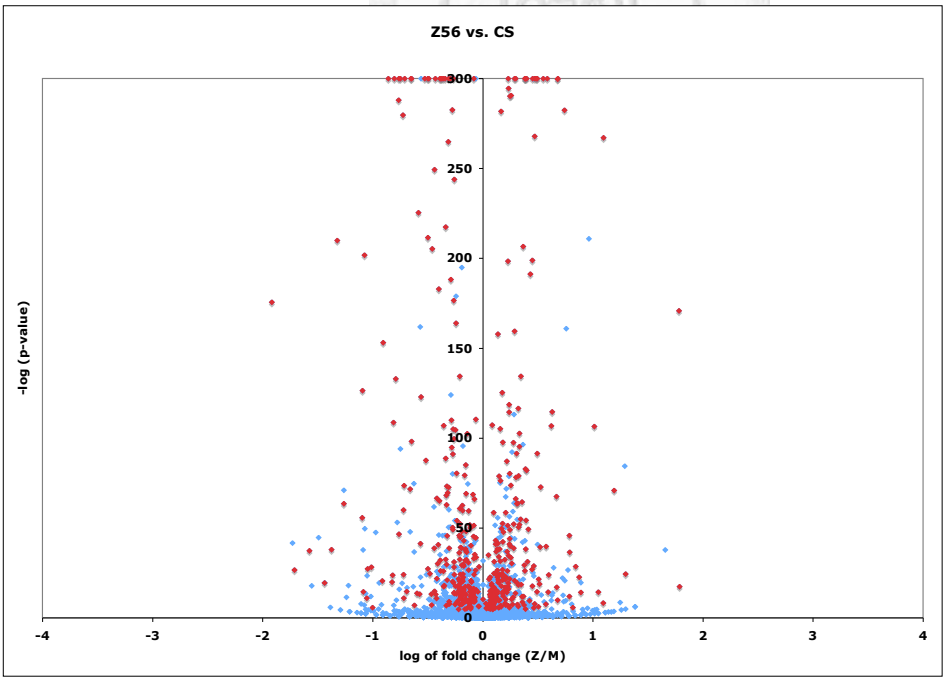

Figure 3.6 The fold changes versus the *p*-values of Fisher's exact test in four comparisons between Z races and M races The positive x-axis is Z/M fold change while the negative x-axis is M/Z fold change. Both axes are in $\log_{10}$ scale. Red points stands for DEGs.

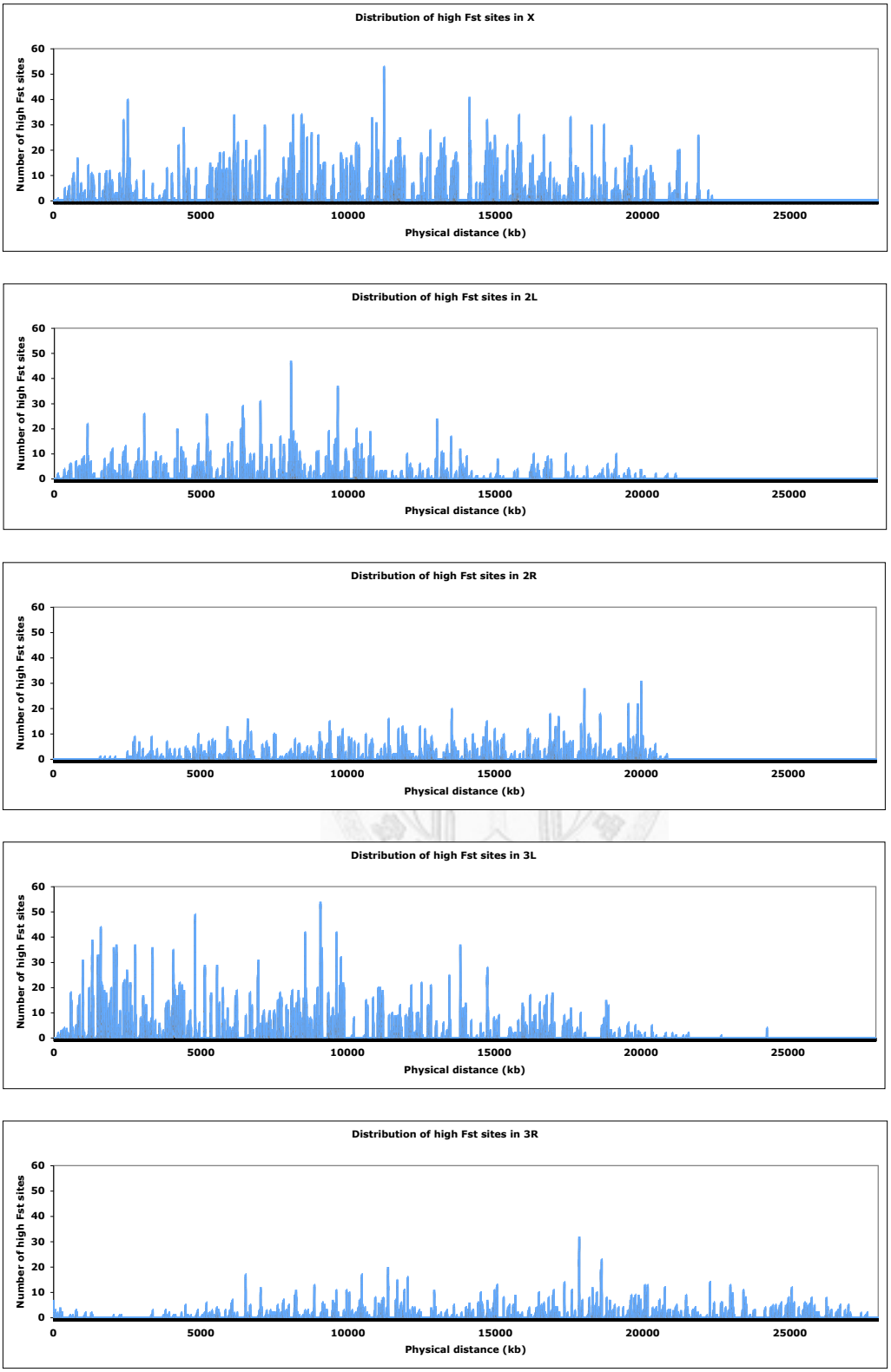

Figure 3.7 The genome-wide clustered F_{ST} pattern on different arms by RNA-seq data The size of each window is 10 kb and the one sliding movement is 1 kb.

Discussion

In this study, the differentiation between Z races and M races in two different levels was assayed: sequence level and expression level. In the former, several regions with low diversity or clustered high F_{ST} sites were recognized as candidate regions. Additionally, the hundreds of DEGs were also proposed to be candidate genes in the latter. To summarize the general pattern among these candidates or study the functions of these candidates in detail will be expected to help us figuring out the biology of Z/M system.

Demographic events: African vs. non-African lines

Even though we focus on the differences between two behavioral races, it can not be ignored that the Z races reside in Africa and most M races reside in the worldwide including Africa. When the *Drosophila melanogaster* speared out of Africa, a severe bottleneck was suggested by observing lower nucleotide diversity in non-African lines. The reduced diversity can be observed in X chromosome and autosome but the reduction is much stronger in X chromosome (Andolfatto 2001). My data is consistent with these revealed results. Comparing the diversity between Malawi Z and Raleigh M races, which can be representative for African lines and non-African lines, I observed a strong reduction of π in M races' X chromosome and a weak reduction in autosomes, which was shown in Table 3.2.

These differences can be explained by at least two properties (Mousset and Derome 2004). The first one is that the autosomal inversion polymorphism is abundant in African populations . The inversion can cease crossing over, which is helpful for harboring mutation even with weakly deleterious effect, so cause the diversity reduction. The

second one is less effective population size of X chromosome. Assuming 1:1 sex ratio, the effective population size of X chromosome should be 3/4 of the one of autosomes. Therefore, during the population shrinkage, the X chromosome, which has smaller effective population size, can be affected more by accompanying drift. Based on the second hypothesis, when I observed the excess candidates in X chromosome, the drift may play more important roles than selection. This idea may be supported by extreme excess of candidate regions with low diversity in Raleigh M population's X chromosome. However, whether these sequence differences are neutral or not remains more studies.

However, this reduction pattern does not hold when the values of Watterson's θ of my data are considered. The θ in Raleigh M population does not reduce much in X chromosome and increase in autosomes. Except for the two reasons, the other one reason can be the ascertainment bias because of very limited sample size of Malawi Z races. When the sample number is low, the frequency spectrum can be more uniform rather than exponential decay under neutral expectation. Therefore, the low-frequency sites can be affected much. That is the reason why π, rather than θ_W, was chosen as estimators for the variance level. Moreover, we discovered a genome-wide pattern of less Tajima's *D* in Malawi Z races (Figure 3.2), which is supported by our knowledge to the demographic history between African and non-African races, but it still can be questionable because of limited sample size.

Candidate distributions in different chromosome arms

Hollecher et al. (1997b) revealed that the contributions of Z/M isolation on autosomes are larger than the ones on X chromosome. In my results, the pattern of expression

divergence is consistent with this previous study. However, when examining the fixed differences in sequence level, the results are usually not only bias to the third chromosome, but also to X chromosome. In fact, there are many cases that X chromosome is occupied most by these candidate genomic regions. Reminding that the expression levels are affected on X and the third chromosome much (Wang et al. 2008), these fixed differences on X chromosome may play important roles in Z/M isolation by synergic function for regulating expression levels of other protein rather than their protein products.

This differentiate pattern may be explained by the lower effective population size of X chromosome again. The expression levels, which belongs to higher-level characters in genotype-phenotype mapping network, are not easily be affected easily such as single nucleotide site does. Therefore, the lower effective population size cause excess high F_{ST} sites but not excess DEGs.

Another noticeable differentiate pattern can be discovered between the candidate genomic regions suggested by Malawi/Raleigh data and Zimbabwe/M data generated by RNA-seq. Though X chromosome is occupied most, the occupied second places for two datasets are different (3R and 3L). These two dataset are different in sampling method and sampling place. While the evidence to support how the former one involves in this pattern is not clear, the latter one can be supported by the multi-loci scheme (Figure 3.1). Sampling more Z lines in different African regions are helpful to assay this question.

Candidates proposed by the genome-wide approaches

Reviewing some candidate regions proposed in Malawi/Raleigh population data, some especially intriguing ones can be found. For example, some regions with olfactory receptor genes (*Or*) or gustatory receptor genes (*Gr*) are proposed. These differences of pheromone sensing may directly involve mating preference because of the important roles of pheromone cues in *Drosophila* mating behavior (Greenspan and Ferveur 2000). Noting that there are many genes in these regions which are not studied in detail, we are expected to have more information to solve Z/M isolation if the functions of these genes are known.

A caveat on this genome-wide approach is noted here. The selected regions can be just regulatory machinery rather than functional protein. Because eukaryotes have complex regulation machinery, regulated region can be far from the adaptive regulation elements. Therefore, the real candidate genes may locate on adjacent regions rather than within "candidate" regions. The bias occurs if only the genes in the candidate regions are considered. However, so far we do not have general rule to handle this question, the extended regions can be arbitrary.

The role of sight in behavioral isolation

While several main biological processes can be recognized as eye development, visual-related signaling pathway in M>Z DEGs, it is noted that the sight plays an important role and the effect spreads from molecular level to developmental level. The node in the deepest level according the hierarchical relationship among those terms related to sight is GO:0016059, deactivation of rhodopsin mediated signaling (19th place).

The expression level of genes which deactivate the rhodopsin mediated signaling can be induced in darkness (Landry et al. 2007). In Landry et al.'s study, the authors first have systematically assayed the variation of expression levels of genes in phototransduction network between different species and different treatments of darkness. Among the genes which were proposed in this study, Gβ76C and TPR, which was suggested to be induced in darkness, was significantly up-regulate in Z-type races. In addition, retinal degeneration C (RDGC), which have significantly differential expressed pattern between *D. melanogaster* and *D. simulans,* was also have Z>M pattern. This study provides a case to infer the genes which deactivate the rhodopsin mediated signaling can potentially play a role in differentiation and a possible environmental factor driving the up-regulation.

Though in *D. melanogaster*, visual stimuli in the courtship sequence are thought not crucial as the acoustic or phermonal signals (Greenspan and Ferveur 2000). The success mating in darkness is discovered by Spieth and Hsu (1950). However, the up-regulation of eye development genes and recovery genes still has potential to cause the choosy behavior of Z-type females. More researches are needed to see whether the darkness drives the behavioral isolation.

The role of metabolic adaptation in behavioral isolation

While the Z>M genes are related to sight, the representative genes in M>Z sets are related to metabolism. All the terms roughly covered by the pathway involving fatty acid, purine (and its precursor IMP), hexose and cellular amino acid. It is reminded that the candidate *desat2* is a gene involved in metabolism. Greenberg et al. (2003) have reported

the M-type allele is more resistant to cold and sensitive to starvation. This mutation may make flies able to adapt the new environment when the flies spread out of Africa. This scenario is supported by the differentiated pattern in whole-transcriptome level between European and Africa populations proposed by Hutter et al. (2008). By microarray approaches, the representative terms among DEGs were also be revealed to relate to carbohydrate metabolic process, monocarboxylic acid metabolic process, and fatty acid metabolic process. If there are more genes related to adaptation in metabolism and thus involve in behavioral isolation is an interesting question and remains more study to these candidate genes.

References

Andolfatto, P. 2001. Contrasting patterns of X-linked and autosomal nucleotide variation in *Drosophila melanogaster* and *Drosophila simulans*. Molecular Biology and Evolution **18**:279-290.

Barluenga, M., K. Stolting, W. Salzburger, M. Muschick, and A. Meyer. 2006. Sympatric speciation in Nicaraguan crater lake cichlid fish. Nature **439**:719-723.

Bayes, J. J., and H. S. Malik. 2009. Altered heterochromatin binding by a hybrid sterility protein in *Drosophila* sibling species. Science **326**:1538-1541.

Begun, D., and C. Aquadro. 1993. African and north-American populations of *Drosophila melanogaster* are very different at the DNA level. Nature **365**:548-550.

Begun, D. J., A. K. Holloway, K. Stevens, L. W. Hillier, Y. P. Poh, M. W. Hahn, P. M. Nista, C. D. Jones, A. D. Kern, C. N. Dewey, L. Pachter, E. Myers, and C. H. Langley. 2007. Population genomics: Whole-genome analysis of polymorphism and divergence in *Drosophila simulans*. Plos Biology **5**:2534-2559.

Benjamini, Y., and Y. Hochberg. 1995. Controlling the false discovery rate - a practical and powerful approach to multiple testing. Journal of the Royal Statistical Society Series B-Methodological **57**:289-300.

Buckley, P. A. 1969. Disruption of species-typical behavior patterns in F1 hybrid Agapornis parrots. Zeitschrift fur Tierpsychologie **26**:737-743.

Cabot, E., A. Davis, N. Johnson, and C. Wu. 1994. Genetics of reproductive isolation in the *Drosophila simulans* clade - complex epistasis underlying hybrid male sterility. Genetics **137**:175-189.

Carbon, S., A. Ireland, C. J. Mungall, S. Shu, B. Marshall, S. Lewis, A. Hub, and W. P. W. Grp. 2009. AmiGO: online access to ontology and annotation data. Bioinformatics **25**:288-289.

Coyne, J. 1984. Genetic-basis of male-sterility in hybrids between 2 closely related species of *Drosophila*. Proc Natl Acad Sci USA **81**:4444-4447.

Coyne, J. A., and M. Kreitman. 1986. Evolutionary genetics of two sibling species, *Drosophila simulans* and *D. sechellia*. Evolution **40**:673-691.

Dallerac, R., C. Labeur, J. Jallon, D. Knippie, W. Roelofs, and C. Wicker-Thomas. 2000. A Delta 9 desaturase gene with a different substrate specificity is responsible for the cuticular diene hydrocarbon polymorphism in *Drosophila melanogaster*. Proc Natl Acad Sci USA. **97**:9449-9454.

Degnan, J. H., and N. A. Rosenberg. 2009. Gene tree discordance, phylogenetic inference and the multispecies coalescent. Trends Ecol Evol **24**:332-340.

Fang, S., A. Takahashi, and C. Wu. 2002. A mutation in the promoter of desaturase 2 is correlated with sexual isolation between Drosophila behavioral races. Genetics **162**:781-784.

Felsenstein, J. 2005. PHYLIP (Phylogeny Inference Package). Pp. Distributed by the author. Department of Genome Sciences, University of Washington, Seattle.

Goldman, N., and Z. H. Yang. 1994. Codon-based model of nucleotide substitution for protein-coding DNA sequences. Molecular Biology and Evolution **11**:725-736.

Greenberg, A., J. Moran, J. Coyne, and C. Wu. 2003. Ecological adaptation during incipient speciation revealed by precise gene replacement. Science **302**:1754-1757.

Greenspan, R. J., and J. F. Ferveur. 2000. Courtship in *Drosophila*. Annual Review of Genetics **34**:205-232.

Haldane, J. B. S. 1922. The part played by recurrent mutation in evolution. American Naturalist **67**:5-19.

Harrison, R. G. 1979. Speciation in north American field crickets: evidence from electrophoretic comparisons. Evolution **33**:1009-1023.

Hey, J., and R. M. Kliman. 1993. Population genetics and phylogenetics of DNA sequence variation at multiple loci within the *Drosophila Melanogaster* species complex. Molecular Biology and Evolution **10**:804-822.

Hilton, H., R. M. Kliman, and J. Hey. 1994. Using hitchhiking genes to study adaptation and divergence during speciation within the *Drosophila melanogaster* species complex. Evolution **48**:1900-1913.

Hittinger, C. T., P. Goncalves, J. P. Sampaio, J. Dover, M. Johnston, and A. Rokas. 2010. Remarkably ancient balanced polymorphisms in a multi-locus gene network. Nature **464**:54-U61.

Hollocher, H., C. Ting, F. Pollack, and C. Wu. 1997a. Incipient speciation by sexual isolation in *Drosophila melanogaster*: Variation in mating preference and correlation between sexes. Evolution **51**:1175-1181.

Hollocher, H., C. Ting, M. Wu, and C. Wu. 1997b. Incipient speciation by sexual isolation in *Drosophila melanogaster*: Extensive genetic divergence without reinforcement. Genetics **147**:1191-1201.

Hollocher, H., and C. Wu. 1996. The genetics of reproductive isolation in the *Drosophila simulans* clade: X vs autosomal effects and male vs female effects. Genetics **143**:1243-1255.

Hutter, S., S. S. Saminadin-Peter, W. Stephan, and J. Parsch. 2008. Gene expression variation in African and European populations of *Drosophila melanogaster*. Genome Biol **9**:R12.

Jones, C. 2005. The genetics of adaptation in *Drosophila sechellia*. Genetica **123**:137-145.

Katakura, H., and T. Hosogai. 1994. Performance of hybrid ladybird beetles (*Epilachna* spp) on the host plants of parental species. Entomol Exp Appl **71**:81-85.

Kliman, R., P. Andolfatto, J. Coyne, F. Depaulis, M. Kreitman, A. Berry, J. McCarter, J. Wakeley, and J. Hey. 2000. The population genetics of the origin and divergence of the *Drosophila simulans* complex species. Genetics **156**:1913-1931.

Kliman, R. M., and J. Hey. 1993. DNA sequence variation at the period locus within and among species of the *Drosophila melanogaster* complex. Genetics **133**:375-387.

Knowlton, N., J. L. Maté, H. M. Guzmán, R. Rowan, and J. Jara. 1997. Direct evidence for reproductive isolation among the three species of the *Montastraea annularis* complex in Central America (Panamá and Honduras). Marine Biology **127**:705-711.

Kresge, N., V. D. Vacquier, and C. D. Stout. 2001. Abalone lysin: the dissolving and evolving sperm protein. Bioessays **23**:95-103.

Lachaise, D., M. L. Cariou, J. R. David, F. Lemeunier, L. Tsacas, and M. Ashburner. 1988. Historical biogeography of the *Drosophila melanogaster* species subgroup. Evolutionary Biology **22**:159-225.

Landry, C. R., C. I. Castillo-Davis, A. Ogura, J. S. Liu, and D. L. Hartl. 2007. Systems-level analysis and evolution of the phototransduction network in *Drosophila*. Proc Natl Acad Sci USA **104**:3283-3288.

Lee, H.-Y., J.-Y. Chou, L. Cheong, N.-H. Chang, S.-Y. Yang, and J.-Y. Leu. 2008. Incompatibility of nuclear and mitochondrial genomes causes hybrid sterility between two yeast species. Cell **135**:1065-1073.

Legrand, D., M. I. Tenaillon, P. Matyot, J. Gerlach, D. Lachaise, and M.-L. Cariou. 2009. Species-wide genetic variation and demographic history of *Drosophila sechellia*, a species lacking population structure. Genetics **182**:1197-1206.

Li, H., J. Ruan, and R. Durbin. 2008. Mapping short DNA sequencing reads and calling variants using mapping quality scores. Genome Research **18**:1851-1858.

Malik, H., and S. Henikoff. 2005. Positive selection of *Iris*, a retroviral *envelope*-derived host gene in *Drosophila melanogaster*. Plos Genet **1**:429-443.

Mardis, E. R. 2008. Next-generation DNA sequencing methods. Annu Rev Genom Hum G **9**:387-402.

Masly, J. P., and D. C. Presgraves. 2007. High-resolution genome-wide dissection of the two rules of speciation in *Drosophila*. Plos Biology **5**:1890-1898.

Mayr, E. 1963. Animal species and evolution. Belknap Press, Cambridge, MA.

McBride, C. S. 2007. Rapid evolution of smell and taste receptor genes during host specialization in *Drosophila sechellia*. Proc Natl Acad Sci USA **104**:4996-5001.

McDermott, S. R., and R. M. Kliman. 2008. Estimation of isolation times of the island species in the *Drosophila simulans* complex from multilocus DNA sequence data. Plos One **3**:e2442.

Mortazavi, A., B. A. Williams, K. Mccue, L. Schaeffer, and B. Wold. 2008. Mapping and quantifying mammalian transcriptomes by RNA-Seq. Nature Methods **5**:621-628.

Mousset, S., and N. Derome. 2004. Molecular polymorphism in *Drosophila melanogaster* and *D. simulans*: what have we learned from recent studies? Genetica **120**:79-86.

Osada, N., M. H. Kohn, and C.-I. Wu. 2006. Genomic inferences of the *cis*-regulatory nucleotide polymorphisms underlying gene expression differences between *Drosophila melanogaster* mating races. Molecular Biology and Evolution **23**:1585-1591.

Perez, D., C. Wu, N. Johnson, and M. Wu. 1993. Genetics of reproductive isolation in the *Drosophila simulans* clade - DNA marker-assisted mapping and characterization of a hybrid-male sterility gene, *Odysseus* (*Ods*). Genetics **134**:261-275.

Rkha, S., P. Capy, and J. R. David. 1991. Host plant specialization in the *Drosophila melanogaster* species complex - a physiological, behavioral, and genetic-analysis. Proc Natl Acad Sci USA **88**:1835-1839.

Ronquist, F., and J. P. Huelsenbeck. 2003. MrBayes 3: Bayesian phylogenetic inference under mixed models. Bioinformatics **19**:1572-1574.

Rubin, C. J., M. C. Zody, J. Eriksson, J. R. S. Meadows, E. Sherwood, M. T. Webster, L. Jiang, M. Ingman, T. Sharpe, S. Ka, F. Hallbook, F. Besnier, O. Carlborg, B. Bed'hom, M. Tixier-Boichard, P. Jensen, P. Siegel, K. Lindblad-Toh, and L.

Andersson. 2010. Whole-genome resequencing reveals loci under selection during chicken domestication. Nature **464**:587-U145.

Shaw, K. 2002. Conflict between nuclear and mitochondrial DNA phylogenies of a recent species radiation: What mtDNA reveals and conceals about modes of speciation in Hawaiian crickets. Proc Natl Acad Sci USA **99**:16122-16127.

Silberglied, R. E., and O. R. Taylor. 1978. Ultraviolet Reflection and Its Behavioral Role in Courtship of Sulfur Butterflies *Colias eurytheme* and *Colias philodice* (Lepidoptera, Pieridae). Behavioral Ecology and Sociobiology **3**:203-243.

Spieth, H. T., and T. C. Hsu. 1950. The influence of light on the mating behavior of 7 species of the *Drosophila melanogaster* species group. Evolution **4**:316-325.

Sun, S., C. Ting, and C. Wu. 2004. The normal function of a speciation gene, Odysseus, and its hybrid sterility effect. Science **305**:81-83.

Swofford, D. L. 2003. PAUP*. Phylogenetic Analysis Using Parsimony. Sinauer Associates, Sunderland, Massachusetts.

Takahashi, A., and C. Ting. 2004. Genetic basis of sexual isolation in *Drosophila melanogaster*. Genetica **120**:273-284.

Takahashi, A., S. Tsaur, J. Coyne, and C. Wu. 2001. The nucleotide changes governing cuticular hydrocarbon variation and their evolution in *Drosophila melanogaster*. Proc Natl Acad Sci USA. **98**:3920-3925.

Tamura, K., S. Subramanian, and S. Kumar. 2004. Temporal patterns of fruit fly (*Drosophila*) evolution revealed by mutation clocks. Molecular Biology and Evolution **21**:36-44.

Tao, Y., and D. Hartl. 2003. Genetic dissection of hybrid incompatibilities between *Drosophila simulans* and *D. mauritiana* III. Heterogeneous accumulation of hybrid incompatibilities, degree of dominance, and implications for Haldane's rule. Evolution **57**:2580-2598.

Tao, Y., S. Xhen, D. Hartl, and C. Laurie. 2003a. Genetic dissection of hybrid incompatibilities between *Drosophila simulans* and *D. mauritiana* I. Differential accumulation of hybrid male sterility effects on the X and autosomes. Genetics **164**:1383-1397.

Tao, Y., Z. Zeng, J. Li, D. Hartl, and C. Laurie. 2003b. Genetic dissection of hybrid incompatibilities between *Drosophila simulans* and *D. mauritiana* II. Mapping hybrid male sterility loci on the third chromosome. Genetics **164**:1399-1418.

Thompson, J. D., D. G. Higgins, and T. J. Gibson. 1994. Clustal-W - Improving the sensitivity of progressive multiple sequence alignment through sequence weighting, position-specific gap penalties and weight matrix choice. Nucl Acids Res **22**:4673-4680.

Ting, C., A. Takahashi, and C. Wu. 2001. Incipient speciation by sexual isolation in *Drosophila*: Concurrent evolution at multiple loci. Proc Natl Acad Sci USA. **98**:6709-6713.

Ting, C., S. Tsaur, S. Sun, W. Browne, Y. Chen, N. Patel, and C. Wu. 2004. Gene duplication and speciation in Drosophila: Evidence from the Odysseus locus. P Natl Acad Sci Usa **101**:12232-12235.

Ting, C., S. Tsaur, and C. Wu. 2000. The phylogeny of closely related species as revealed by the genealogy of a speciation gene, *Odysseus*. Proc Natl Acad Sci USA **97**:5313-5316.

Ting, C., S. Tsaur, M. Wu, and C. Wu. 1998. A rapidly evolving homeobox at the site of a hybrid sterility gene. Science **282**:1501-1504.

True, J., B. Weir, and C. Laurie. 1996. A genome-wide survey of hybrid incompatibility factors by the introgression of marked segments of *Drosophila mauritiana* chromosomes into *Drosophila simulans*. Genetics **142**:819-837.

Tsaur, S., C. Ting, and C. Wu. 2001. Sex in *Drosophila mauritiana*: A very high level of amino acid polymorphism in a male reproductive protein gene, *Acp26Aa*. Molecular Biology and Evolution **18**:22-26.

Vilella, A. J., A. Blanco-Garcia, S. Hutter, and J. Rozas. 2005. VariScan: Analysis of evolutionary patterns from large-scale DNA sequence polymorphism data. Bioinformatics **21**:2791-2793.

Wang, H. Y., Y. G. Fu, M. S. McPeek, X. M. Lu, S. Nuzhdin, A. L. Xu, J. Lu, M. L. Wu, and C. I. Wu. 2008. Complex genetic interactions underlying expression differences between Drosophila races: Analysis of chromosome substitutions. Proceedings of the National Academy of Sciences of the United States of America **105**:6362-6367.

Wells, M. M., and C. S. Henry. 1992. The Role of Courtship Songs in Reproductive Isolation among Populations of Green Lacewings of the Genus Chrysoperla (Neuroptera, Chrysopidae). Evolution **46**:31-42.

Wu, C. 2001. The genic view of the process of speciation. J Evolution Biol **14**:851-865.

Wu, C., H. Hollocher, D. Begun, C. Aquadro, Y. Xu, and M. Wu. 1995. Sexual isolation in *Drosophila melanogaster*: a possible case of incipient speciation. Proc Natl Acad Sci USA. **92**:2519-2523.

Wu, C., N. Johnson, and M. Palopoli. 1996. Haldane's rule and its legacy: Why are there so many sterile males? Trends Ecol Evol **11**:281-284.

Yang, Z. H. 2007. PAML 4: Phylogenetic analysis by maximum likelihood. Molecular Biology and Evolution **24**:1586-1591.

Yang, Z. H. 1998. Likelihood ratio tests for detecting positive selection and application to primate lysozyme evolution. Molecular Biology and Evolution **15**:568-573.

Appendix: Rationale of speciation model test

Under the genic view of speciation (Wu 2001), in the beginning stage of speciation, few loci which contribute as driving force flow have already had no gene flows. With the progress of speciation, the region where the gene flow does not exist gradually expends to whole genome. Therefore, the divergence time among loci should be heterozygous. To test whether the heterozygous divergence time is a real case, Huang and Wu (personal communication) proposed a speciation model test.

The deduction of this test is beginning with the probability of the divergence in one locus. Assume the divergence time between two species is t, the effective population size of the common ancestor is N, the length of this locus is l, and the nucleotide substitution rate is μ. Takahata et al. (1995) proposed the probability of observing k substitutions as

$$p(k) = \frac{1}{1+4N\mu l} e^{-2t\mu l} \sum_{d=0}^{k} \frac{(2t\mu l)^d}{d!} \left(\frac{4N\mu l}{1+4N\mu l} \right)^{k-d} . \quad (1)$$

To study the pattern of divergence among loci, Osada and Wu (2005) first describe the log-likelihood function of m loci with the same nucleotide substitution rate μ is

$$L(\tau,\theta) = \ln \prod_{i=1}^{m} \left[\frac{1}{1+\theta l_i} e^{-\tau l_i} \sum_{d=0}^{k_i} \frac{(\tau l_i)^d}{d!} \left(\frac{\theta l_i}{1+\theta l_i} \right)^{k_i - d} \right], \quad (2)$$

where $\theta = 4N\mu$ and $\tau = 2\mu t$.

Moreover, they refer outgroup to filter out the variation of nucleotide substitution rate among loci. Assume the number of substitution with outgroup $K_i = 2T\mu_i l$ if the

divergence time between the outgroup and the targeted group (T) is large enough to let us ignore the coalescent part, the log-likelihood function becomes

$$L(\alpha,\gamma \mid K_i = 2T\mu_i l_i) = \ln \prod_{i=1}^{m} \left[\frac{1}{1+\gamma K_i} e^{-\alpha K_i} \sum_{d=0}^{k_i} \frac{(\alpha K_i)^d}{d!} \left(\frac{\gamma K_i}{1+\gamma K_i} \right)^{k_i - d} \right], \qquad (3)$$

where $\alpha = t/T$ and $\gamma = 2N/T$.

Wu and Huang tried to describe the heterogeneous divergence time by a gamma distribution. Assume t follows gamma(a, b), the log-likelihood function is

$$L(\alpha,\beta,\gamma \mid K_i = 2T\mu_i l_i) = \frac{1}{1+4N\mu_i l_i} \left(\frac{4N\mu_i l_i}{1+4N\mu_i l_i} \right) \sum_{d=0}^{k} \int_0^{\infty} \frac{(2tul)^d}{d!} \cdot e^{-2tul} \cdot \frac{t^{a-1} e^{\frac{-t}{b}}}{b^a \Gamma(a)} dt \qquad (4)$$

$$= \frac{1}{(\beta K_i + 1)^{\alpha} (1+\gamma K_i)} \left[\sum_{d=0}^{k_i} \frac{1}{d} \frac{1}{B(d,\alpha)} \left(\frac{\beta K_i}{\beta K_i + 1} \right)^d \left(\frac{\gamma K_i}{\gamma K_i + 1} \right)^{k_i - d} + \left(\frac{\gamma K_i}{\gamma K_i + 1} \right)^{k_i} \right] \qquad (5)$$

where $\alpha = a$, $\beta = b/T$, and $\gamma = 2N/T$.

While likelihood function (3) describes constant divergence time among all loci, function (5) describes the divergence time among all loci follows a gamma distribution. With two likelihood functions, a likelihood ratio test can be constructed and the distribution of $-2\Delta \ln L$ is a mixture of 0 and chi-square distribution with degree of freedom equal to one.

References:

Osada, N., and C. I. Wu. 2005. Inferring the mode of speciation from genomic data: A study of the great apes. Genetics **169**:259-264.

Takahata, N., Y. Satta, and J. Klein. 1995. Divergence Time and Population-Size in the Lineage Leading to Modern Humans. Theoretical Population Biology **48**:198-221.

Wu, C. 2001. The genic view of the process of speciation. J Evolution Biol **14**:851-865.

Supplementary Tables

Table s2.1 Representative GO terms of sampled genes in chapter 2 Only the terms with *p*-value less than 0.01 are listed.

GO Terms		*p*-value	Sample frequency	Background frequency
GO:0008152	metabolic process	3.88E-52	1764/3460	4976/12505
GO:0044237	cellular metabolic process	1.66E-38	1312/3460	3612/12505
GO:0044238	primary metabolic process	3.00E-27	1409/3460	4104/12505
GO:0009987	cellular process	2.85E-23	2068/3460	6510/12505
GO:0044248	cellular catabolic process	9.10E-23	186/3460	340/12505
GO:0044267	cellular protein metabolic process	1.46E-15	553/3460	1466/12505
GO:0044260	cellular macromolecule metabolic process	8.81E-15	954/3460	2783/12505
GO:0043412	macromolecule modification	9.76E-13	294/3460	708/12505
GO:0055114	oxidation reduction	1.21E-12	213/3460	475/12505
GO:0044265	cellular macromolecule catabolic process	1.41E-12	109/3460	198/12505
GO:0006810	transport	2.36E-12	535/3460	1455/12505
GO:0019538	protein metabolic process	1.20E-11	708/3460	2026/12505
GO:0006464	protein modification process	1.52E-11	278/3460	673/12505
GO:0051234	establishment of localization	1.57E-11	547/3460	1506/12505
GO:0043170	macromolecule metabolic process	4.71E-11	1143/3460	3502/12505
GO:0034660	ncRNA metabolic process	4.20E-09	67/3460	112/12505
GO:0007010	cytoskeleton organization	8.32E-09	209/3460	498/12505
GO:0000278	mitotic cell cycle	8.66E-09	182/3460	420/12505
GO:0043687	post-translational protein modification	1.02E-08	223/3460	540/12505
GO:0046907	intracellular transport	2.33E-08	150/3460	333/12505
GO:0044257	cellular protein catabolic process	5.01E-08	66/3460	114/12505
GO:0051603	proteolysis involved in cellular protein catabolic process	5.01E-08	66/3460	114/12505
GO:0000226	microtubule cytoskeleton organization	6.48E-08	143/3460	317/12505
GO:0019752	carboxylic acid metabolic process	9.65E-08	123/3460	263/12505
GO:0006082	organic acid metabolic process	9.65E-08	123/3460	263/12505
GO:0043436	oxoacid metabolic process	9.65E-08	123/3460	263/12505
GO:0016044	membrane organization	1.59E-07	144/3460	323/12505
GO:0007052	mitotic spindle organization	1.64E-07	99/3460	200/12505
GO:0034641	cellular nitrogen compound metabolic process	3.61E-07	109/3460	229/12505
GO:0016043	cellular component organization	4.15E-07	682/3460	2031/12505
GO:0009056	catabolic process	5.56E-07	359/3460	980/12505
GO:0015031	protein transport	6.66E-07	116/3460	250/12505
GO:0008104	protein localization	7.31E-07	156/3460	363/12505
GO:0007051	spindle organization	1.04E-06	110/3460	235/12505
GO:0016192	vesicle-mediated transport	1.07E-06	172/3460	411/12505

Table s2.1 (Continued)

GO Terms		*p*-value	Sample frequency	Background frequency
GO:0034613	cellular protein localization	1.23E-06	95/3460	195/12505
GO:0006886	intracellular protein transport	1.97E-06	93/3460	191/12505
GO:0034470	ncRNA processing	2.18E-06	43/3460	67/12505
GO:0045184	establishment of protein localization	2.38E-06	117/3460	257/12505
GO:0044085	cellular component biogenesis	2.73E-06	250/3460	650/12505
GO:0042180	cellular ketone metabolic process	3.01E-06	126/3460	283/12505
GO:0051179	localization	3.93E-06	616/3460	1833/12505
GO:0022613	ribonucleoprotein complex biogenesis	4.16E-06	50/3460	84/12505
GO:0033036	macromolecule localization	5.71E-06	197/3460	493/12505
GO:0044262	cellular carbohydrate metabolic process	5.81E-06	74/3460	144/12505
GO:0019941	modification-dependent protein catabolic process	6.10E-06	56/3460	99/12505
GO:0043632	modification-dependent macromolecule catabolic process	1.02E-05	56/3460	100/12505
GO:0051649	establishment of localization in cell	1.26E-05	189/3460	473/12505
GO:0006996	organelle organization	1.32E-05	397/3460	1125/12505
GO:0006897	endocytosis	1.79E-05	118/3460	267/12505
GO:0010324	membrane invagination	1.79E-05	118/3460	267/12505
GO:0006796	phosphate metabolic process	1.85E-05	234/3460	612/12505
GO:0006793	phosphorus metabolic process	1.85E-05	234/3460	612/12505
GO:0006399	tRNA metabolic process	1.96E-05	48/3460	82/12505
GO:0051641	cellular localization	2.14E-05	222/3460	576/12505
GO:0006520	cellular amino acid metabolic process	2.20E-05	75/3460	150/12505
GO:0043933	macromolecular complex subunit organization	2.20E-05	130/3460	302/12505
GO:0044255	cellular lipid metabolic process	2.60E-05	92/3460	196/12505
GO:0006511	ubiquitin-dependent protein catabolic process	2.61E-05	54/3460	97/12505
GO:0006260	DNA replication	3.26E-05	53/3460	95/12505
GO:0007017	microtubule-based process	3.33E-05	173/3460	430/12505
GO:0006629	lipid metabolic process	5.91E-05	122/3460	283/12505
GO:0051716	cellular response to stimulus	6.12E-05	144/3460	347/12505
GO:0006457	protein folding	6.85E-05	54/3460	99/12505
GO:0042254	ribosome biogenesis	7.21E-05	34/3460	52/12505
GO:0006519	cellular amino acid and derivative metabolic process	8.98E-05	92/3460	200/12505
GO:0070271	protein complex biogenesis	9.11E-05	81/3460	170/12505
GO:0006461	protein complex assembly	9.11E-05	81/3460	170/12505
GO:0044106	cellular amine metabolic process	1.75E-04	81/3460	172/12505
GO:0070727	cellular macromolecule localization	2.97E-04	119/3460	281/12505
GO:0065003	macromolecular complex assembly	4.37E-04	107/3460	248/12505

Table s2.1 (Continued)

GO Terms		*p*-value	Sample frequency	Background frequency
GO:0006091	generation of precursor metabolites and energy	4.55E-04	90/3460	200/12505
GO:0033554	cellular response to stress	4.66E-04	109/3460	254/12505
GO:0006807	nitrogen compound metabolic process	4.66E-04	625/3460	1914/12505
GO:0006139	nucleobase, nucleoside, nucleotide and nucleic acid metabolic process	4.85E-04	537/3460	1619/12505
GO:0006367	transcription initiation from RNA polymerase II promoter	5.54E-04	40/3460	69/12505
GO:0051128	regulation of cellular component organization	1.17E-03	119/3460	287/12505
GO:0006950	response to stress	1.23E-03	212/3460	570/12505
GO:0016310	phosphorylation	2.05E-03	181/3460	477/12505
GO:0051726	regulation of cell cycle	2.24E-03	74/3460	161/12505
GO:0006909	phagocytosis	2.77E-03	88/3460	201/12505
GO:0006396	RNA processing	2.97E-03	131/3460	327/12505
GO:0006259	DNA metabolic process	3.75E-03	97/3460	228/12505
GO:0006974	response to DNA damage stimulus	4.71E-03	82/3460	186/12505
GO:0006911	phagocytosis, engulfment	5.14E-03	84/3460	192/12505
GO:0065008	regulation of biological quality	5.38E-03	218/3460	599/12505
GO:0006732	coenzyme metabolic process	6.53E-03	44/3460	84/12505
GO:0000022	mitotic spindle elongation	6.75E-03	42/3460	79/12505
GO:0006364	rRNA processing	7.26E-03	22/3460	32/12505
GO:0034984	cellular response to DNA damage stimulus	7.33E-03	80/3460	182/12505
GO:0006352	transcription initiation	8.52E-03	41/3460	77/12505
GO:0022607	cellular component assembly	9.52E-03	217/3460	600/12505
GO:0070647	protein modification by small protein conjugation or removal	1.00E-02	34/3460	60/12505
GO:0051231	spindle elongation	1.04E-02	42/3460	80/12505
GO:0016072	rRNA metabolic process	1.61E-02	22/3460	33/12505
GO:0005996	monosaccharide metabolic process	1.89E-02	43/3460	84/12505
GO:0051186	cofactor metabolic process	2.08E-02	49/3460	100/12505
GO:0006766	vitamin metabolic process	2.48E-02	17/3460	23/12505
GO:0065009	regulation of molecular function	2.74E-02	68/3460	153/12505
GO:0051246	regulation of protein metabolic process	3.90E-02	77/3460	180/12505
GO:0006605	protein targeting	4.13E-02	56/3460	121/12505
GO:0006413	translational initiation	4.26E-02	36/3460	68/12505
GO:0055086	nucleobase, nucleoside and nucleotide metabolic process	4.61E-02	84/3460	201/12505

Table s3.1 The list of low diversity regions in Z-type race

window (10kb)	Z			M			Z score (Z-M)	genes
	size	pi	Z score	size	pi	Z score		
X chromosome (2 windows)								
792	5268	0.0103	-0.1600	5420	0.0112	2.5074	-2.6674	Tbh, CG2233
1430	9074	0.0106	-0.0436	9372	0.0102	2.0115	-2.0551	dpr8
2L chromosome (5 windows)								
100	3309	0.0089	-0.1883	3143	0.0139	2.1212	-2.3095	gus
179	5770	0.0084	-0.3170	5844	0.0141	2.1915	-2.5084	N/A
256	5333	0.0068	-0.8204	5240	0.0128	1.7059	-2.5262	Cyp309a1, Cyp309a2
1048	9741	0.0050	-1.3448	9698	0.0121	1.4411	-2.7859	Rlu2, Grip75, CG7456, CG6144, CG13144
2017	1930	0.0034	-1.8315	1931	0.0087	0.1926	-2.0241	N/A
2R chromosome (4 windows)								
945	9402	0.0102	0.2979	9602	0.0161	2.9602	-2.6624	CG13335
1262	9346	0.0048	-1.1874	9471	0.0114	1.3351	-2.5225	N/A
1263	9538	0.0086	-0.1447	9822	0.0140	2.2385	-2.3832	Sfp53D, CG15617, Acp53C14a, Acp53C14b, Acp53Ea, Acp53C14c, unc-104
1774	9439	0.0059	-0.8757	9339	0.0109	1.1496	-2.0253	CG9294
3L chromosome (1 window)								
1621	9323	0.0029	-1.5179	9166	0.0089	0.5249	-2.0427	CG13073, tRNA:CR32153, CG5018
3R chromosome (10 windows)								
889	9561	0.0041	-1.0138	9360	0.0092	1.1403	-2.1541	sim
922	8870	0.0071	-0.1731	8696	0.0119	2.1914	-2.3645	CG14375, CG14374, CG14377, CG9796, CG33977, yellow-e3
1041	9198	0.0070	-0.1984	9492	0.0127	2.5262	-2.7246	stumps
1405	9529	0.0062	-0.4119	9180	0.0115	2.0538	-2.4658	CG7993, CG7168, CG7998

Table s3.1 (continued)

window (10kb)	Z			M			Z score (Z-M)	genes
	size	pi	Z score	size	pi	Z score		
1433	9009	0.0066	-0.3095	9206	0.0110	1.8493	-2.1588	fru
1633	7559	0.0055	-0.6155	7611	0.0099	1.3884	-2.0039	Or92a, CG4288
1655	9278	0.0022	-1.5718	9395	0.0097	1.3134	-2.8851	CG31205
1656	9798	0.0028	-1.4008	9674	0.0085	0.8327	-2.2335	cdc2c, CG17627, CG42322, CG31199, CG31200
1915	9243	0.0067	-0.2748	9569	0.0109	1.8120	-2.0868	pnt
2559	9316	0.0056	-0.5956	9621	0.0100	1.4315	-2.0271	kay

Table s3.2 The list of low diversity regions in M-type race

window (10kb)	Z			M			Z score (Z-M)	genes
	size	pi	Z score	size	pi	Z score		
X chromosome (42 windows)								
317	8714	0.0164	1.7177	9568	0.0054	-0.2860	2.0036	dnc
490	8975	0.0145	1.1340	9739	0.0040	-0.9531	2.0871	N/A
492	9155	0.0152	1.3343	9717	0.0035	-1.1892	2.5234	N/A
578	9391	0.0140	0.9821	9783	0.0024	-1.7213	2.7034	N/A
693	9069	0.0148	1.2164	9730	0.0041	-0.8793	2.0957	CG12541, CG14427
695	9207	0.0139	0.9409	9890	0.0038	-1.0671	2.0079	CG12541
702	1336	0.0135	0.8163	1450	0.0033	-1.3070	2.1232	N/A
703	9332	0.0120	0.3597	9763	0.0019	-1.9465	2.3061	CR32730
704	9342	0.0113	0.1666	9781	0.0014	-2.2130	2.3796	N/A
716	8297	0.0131	0.6902	9021	0.0028	-1.5467	2.2368	CG1958
718	9416	0.0149	1.2389	9809	0.0019	-1.9307	3.1696	CG1677, CG2059, unc-119
734	9427	0.0113	0.1571	9978	0.0017	-2.0587	2.2158	CG11368
848	9789	0.0114	0.2008	9935	0.0022	-1.8110	2.0118	CG12081, CG12659
931	8466	0.0137	0.8796	8964	0.0034	-1.2593	2.1389	CG42611
935	7798	0.0119	0.3541	8307	0.0023	-1.7451	2.0992	CG42611
936	9148	0.0132	0.7362	9674	0.0031	-1.3843	2.1205	CG42611
981	8049	0.0151	1.3202	8803	0.0043	-0.8088	2.1290	N/A
1016	1299	0.0192	2.5650	1381	0.0033	-1.2607	3.8258	N/A
1071	9197	0.0152	1.3352	9700	0.0033	-1.3043	2.6396	Imp
1099	2713	0.0154	1.4060	2812	0.0030	-1.4185	2.8244	CG42249
1154	6559	0.0127	0.5836	7099	0.0025	-1.6426	2.2262	Ptp10d
1188	9358	0.0152	1.3424	9728	0.0016	-2.1025	3.4449	gd, tsg, CG18130, fw
1193	9046	0.0158	1.5069	9537	0.0045	-0.6916	2.1985	N/A
1196	9526	0.0118	0.3177	9756	0.0017	-2.0583	2.3759	CG32343, CG12721
1197	8778	0.0171	1.9115	9630	0.0035	-1.1763	3.0878	N/A

Table s3.2 (continued)

window (10kb)	Z			M			Z score (Z-M)	genes
	size	pi	Z score	size	pi	Z score		
1198	7844	0.0126	0.5453	8569	0.0018	-1.9891	2.5344	CG15734, CR32657, CR32658
1199	9303	0.0135	0.8269	9730	0.0030	-1.4258	2.2527	CG11356
1207	8359	0.0143	1.0535	9114	0.0039	-1.0184	2.0719	CG1924
1311	9736	0.0131	0.7071	9935	0.0029	-1.4893	2.1964	mew
1358	8331	0.0153	1.3771	9125	0.0038	-1.0514	2.4285	CG9940
1368	7070	0.0170	1.8766	7680	0.0056	-0.1800	2.0566	inaE, CG10993
1509	9170	0.0166	1.7617	9818	0.0053	-0.3462	2.1079	CG32588
1598	9308	0.0124	0.4884	9764	0.0027	-1.5469	2.0352	Tob, CG42354, CG42353
1913	8622	0.0138	0.9217	9933	0.0026	-1.6131	2.5348	CG14196, CG7889, CG7992
1921	8315	0.0154	1.4042	8989	0.0033	-1.2820	2.6862	out
1924	8205	0.0179	2.1684	9174	0.0052	-0.3843	2.5527	gfA, kek5
1971	7617	0.0158	1.5272	9076	0.0049	-0.5228	2.0501	skpC, skpE
1991	9039	0.0133	0.7732	9731	0.0023	-1.7646	2.5378	D2R, tRNA:CR32826
2095	7701	0.0186	2.3732	7914	0.0066	0.2858	2.0874	N/A
2196	2642	0.0175	2.0475	3687	0.0049	-0.5106	2.5581	N/A
2197	4116	0.0251	4.3403	4976	0.0055	-0.2286	4.5689	N/A
2212	4912	0.0170	1.8742	5469	0.0054	-0.2624	2.1366	N/A
2L chromosome (6 windows)								
314	9312	0.0155	1.8058	9619	0.0073	-0.3233	2.1291	toc, CG12400, Mad
519	9766	0.0119	0.7073	9965	0.0046	-1.3207	2.0280	Msp300, snmRNA:765, snmRNA:128
520	9418	0.0137	1.2510	9915	0.0047	-1.2670	2.5180	Msp300, snoRNA:psi18S-525K, snmRNA:158, Cyp28d2

Table s3.2 (continued)

window (10kb)	Z			M			Z score (Z-M)	genes
	size	pi	Z score	size	pi	Z score		
534	7056	0.0183	2.6198	7307	0.0082	0.0071	2.6128	CG12512, nompC
1428	9301	0.0142	1.4203	9821	0.0041	-1.5026	2.9229	wb
1482	9312	0.0122	0.8213	9775	0.0042	-1.4440	2.2654	N/A
2R chromosome (3 windows)								
809	9374	0.0147	1.5451	9467	0.0047	-1.0333	2.5785	Sr-CII
1358	8302	0.0174	2.2656	9389	0.0077	0.0092	2.2563	swi2, rdgBbeta, Uhg1, many snoRNAs
1932	9322	0.0178	2.3819	9744	0.0076	-0.0076	2.3896	Or59a
3L chromosome (1 window)								
230	9132	0.0155	1.4391	9835	0.0054	-0.6117	2.0508	DmsR-2, CG13802
3R chromosome (7window)								
1323	9630	0.0140	1.7981	9733	0.0053	-0.4119	2.2101	CG34053, CG17283, CG5860, CG5863, CG34035
1324	8269	0.0165	2.5055	9620	0.0047	-0.6546	3.1602	CG34035, CG5866, CG33333, CG14332
1767	8545	0.0151	2.1151	9794	0.0064	0.0104	2.1046	Gr93C, Gr93d, glec
2008	9489	0.0126	1.4070	9963	0.0017	-1.8406	3.2476	jar
2009	9404	0.0112	1.0052	9594	0.0036	-1.0964	2.1016	jar, Orct2
2059	9594	0.0106	0.8381	9897	0.0033	-1.1994	2.0375	Ast, CG13631
2286	9560	0.0148	2.0210	9887	0.0054	-0.3784	2.3995	NepYr

Table s3.3 The list of regions with clustered high F_{ST} sites

windows (kb)	corresponding region	number of high FST sites	genes
X chromosome (7 regions)			
1720-1721	1720001..1731000	(30, 30)	CG42666
7027-7038	7027001..7048000	(32, 33, 33, 33, 33, 29, 28, 35, 28, 29, 26, 30)	CR32730
7152-7158	7152001..7168000	(31, 26, 23, 28, 30, 35, 30)	CG1958
7179-7187	7179001..7197000	(31, 36, 38, 41, 37, 37, 34, 30, 32)	CG1677, CG2059, unc-119
7343-7344	7343001..7354000	(31, 30)	CG11368
11977-11982	11977001..11982000	(32, 32, 34, 34, 35, 31)	CG15734, CR32657
12468	12468001..12478000	30	CG11138
2R (1 region)			
17544-17554	1754401..1756400	(30, 40, 45, 49, 43, 48, 52, 51, 46, 32)	N/A
3L (2 regions)			
6122-6130	6122001..6140000	(37, 43, 38, 38, 39, 39, 37, 35, 32)	Lcp65Ag3, Cpr65Au, Lcp65Ag2, Lcp65Ag1, Lcp65Af, Lcp65Ae, Cpr65Av, Cpr65Aw, Lcp65Ad, Lcp65Ac, Lcp65Ab2
17842-17849	17842001..17859000	(33, 33, 32, 36, 35, 40, 40, 33)	CG7430, CG7441, CG5535, CG34002
3R (5 regions)			
14406-14415	14406001..14425000	(32, 33, 33, 40, 39, 34, 31, 30, 32, 31)	fray, CG7694, CG14306, CG14304, CG14305
15111-15113	15111001..15123000	(33, 34, 33)	N/A
17488-17497	17488001..17507000	(46, 48, 48, 49, 46, 36, 41, 40, 41, 38)	CG6353, CG15497, DNApol-alpha180, CG31176
17596-17600	17596001..17610000	(30, 30, 33, 35, 32)	GABA-B-R2, CG6800, RpI12, tsl
18281-18287	18281001..18297000	(30, 33, 36, 36, 34, 35, 33)	CG34376, Rpn7, Ap-50, CG7054, CG18594, CG5377, Nrx-1

Table s3.4 Z>M DEG based on Bonferroni's correction

FBtr#	FBgn#	arm	name	*p*-values			
				Z30 vs. FR	Z56 vs. FR	Z30 vs. CS	Z56 vs. CS
FBtr0081030	FBgn0000120	2L	Arr1-RA	0.00E+00	4.66E-231	0.00E+00	0.00E+00
FBtr0114370	FBgn0031414	2L	eys-RC	1.07E-18	7.16E-05	0.00E+00	0.00E+00
FBtr0081520	FBgn0032946	2L	nrv3-RD	1.13E-210	0.00E+00	1.68E-60	0.00E+00
FBtr0112357	FBgn0085195	2L	CG34166-RA	1.84E-292	0.00E+00	8.45E-36	0.00E+00
FBtr0301855	FBgn0028433	2L	Ggamma30A-RD	1.39E-79	6.16E-43	0.00E+00	7.80E-280
FBtr0079517	FBgn0024290	2L	Slob-RB	4.09E-58	7.26E-60	1.43E-151	1.36E-157
FBtr0077748	FBgn0041337	2L	Cyp309a2-RA	4.28E-04	2.17E-03	2.96E-104	1.67E-104
FBtr0299968	FBgn0259715	2L	CG42369-RA	1.43E-85	9.65E-50	2.83E-141	9.63E-96
FBtr0081303	FBgn0032836	2L	CG10680-RA	5.17E-16	5.87E-09	4.86E-111	1.31E-95
FBtr0080118	FBgn0032297	2L	CG17124-RB	3.62E-61	5.33E-51	1.34E-101	1.41E-89
FBtr0079309	FBgn0025595	2L	GRHR-RB	1.48E-17	2.14E-27	9.66E-47	1.25E-62
FBtr0077489	FBgn0051772	2L	CG31772-RA	1.48E-98	2.12E-79	3.54E-79	1.48E-61
FBtr0080496	FBgn0032472	2L	CG9928-RA	2.79E-40	2.36E-38	2.53E-52	1.55E-50
FBtr0077394	FBgn0031649	2L	hoe2-RA	5.75E-20	8.62E-08	5.89E-73	7.07E-50
FBtr0080222	FBgn0032350	2L	CG6287-RA	8.77E-176	4.12E-112	2.45E-85	3.57E-41
FBtr0089290	FBgn0016930	2L	smi35A-RC	7.43E-25	6.27E-24	5.28E-41	2.30E-40
FBtr0080565	FBgn0053307	2L	CG33307-RA	7.13E-25	6.45E-37	1.72E-24	2.04E-36
FBtr0079071	FBgn0016076	2L	vri-RA	1.50E-147	3.49E-182	1.66E-23	2.39E-36
FBtr0079861	FBgn0032129	2L	jp-RA	3.29E-17	5.94E-21	4.54E-25	1.09E-29
FBtr0077671	FBgn0031489	2L	CG17224-RA	1.32E-58	7.91E-47	1.37E-34	4.85E-25
FBtr0078159	FBgn0031220	2L	CG4822-RB	5.45E-07	9.61E-05	8.81E-28	3.39E-24
FBtr0299969	FBgn0259716	2L	CG42370-RA	3.21E-16	4.66E-18	4.67E-22	3.64E-24
FBtr0077399	FBgn0041150	2L	hoe1-RE	5.52E-41	1.98E-23	3.94E-40	9.81E-23
FBtr0110799	FBgn0031897	2L	CG13784-RC	3.16E-07	2.63E-25	1.23E-05	2.78E-22
FBtr0080718	FBgn0024183	2L	vig-RD	1.01E-14	8.66E-18	2.47E-17	1.16E-20
FBtr0081031	FBgn0002939	2L	ninaD-RA	1.27E-11	3.82E-22	5.09E-10	1.13E-19
FBtr0079079	FBgn0031702	2L	fusl-RA	4.46E-11	1.24E-07	5.65E-24	2.34E-19
FBtr0300331	FBgn0031993	2L	CG8486-RD	2.08E-09	1.64E-12	4.10E-14	6.55E-18
FBtr0081372	FBgn0026756	2L	Ugt37a1-RA	7.09E-16	1.39E-10	2.44E-21	1.84E-15
FBtr0080552	FBgn0012037	2L	Ance-RA	5.13E-27	3.05E-20	3.39E-21	4.60E-15
FBtr0273404	FBgn0032943	2L	Tsp39D-RB	8.04E-08	1.72E-04	7.42E-19	3.61E-14
FBtr0080856	FBgn0024734	2L	PRL-1-RB	4.64E-06	1.34E-16	7.96E-04	6.97E-13
FBtr0273186	FBgn0032109	2L	CG17005-RB	6.95E-06	1.41E-04	4.60E-14	2.28E-12
FBtr0077417	FBgn0031629	2L	CG3244-RA	2.94E-15	3.70E-10	4.59E-17	1.18E-11
FBtr0080294	FBgn0032402	2L	CG14945-RB	5.15E-07	1.44E-03	1.54E-13	5.01E-09
FBtr0079477	FBgn0041181	2L	TepIII-RA	9.83E-06	1.28E-09	5.59E-04	2.39E-07
FBtr0077488	FBgn0051959	2L	CG31959-RB	6.36E-05	1.34E-04	1.96E-07	6.51E-07
FBtr0077816	FBgn0031381	2L	Npc2a-RA	5.01E-50	2.34E-12	9.86E-35	7.48E-05
FBtr0080959	FBgn0040985	2L	CG6115-RA	4.79E-20	6.13E-12	3.40E-10	2.96E-04
FBtr0077647	FBgn0031490	2L	CG17264-RA	7.25E-14	1.51E-07	7.66E-09	1.32E-03
FBtr0087747	FBgn0033820	2R	CG4716-RA	8.15E-135	1.75E-49	0.00E+00	0.00E+00
FBtr0087829	FBgn0004435	2R	Galpha49B-RA	1.75E-76	3.52E-90	7.85E-296	0.00E+00
FBtr0086729	FBgn0034328	2R	IM23-RA	6.78E-304	6.66E-68	0.00E+00	1.07E-297
FBtr0086728	FBgn0034331	2R	CG15067-RA	0.00E+00	0.00E+00	0.00E+00	1.24E-288

Table s3.4 (continued)

FBtr#	FBgn#	arm	name	*p*-values			
				Z30 vs. FR	Z56 vs. FR	Z30 vs. CS	Z56 vs. CS
FBtr0086325	FBgn0034480	2R	CG16898-RA	2.99E-42	2.10E-90	3.12E-179	3.21E-265
FBtr0299943	FBgn0259682	2R	CG42351-RC	2.68E-30	3.84E-25	8.28E-204	5.71E-197
FBtr0086026	FBgn0033054	2R	CG14591-RB	5.92E-27	1.03E-29	5.34E-177	2.23E-189
FBtr0086664	FBgn0025583	2R	IM2-RA	0.00E+00	0.00E+00	6.97E-275	2.33E-123
FBtr0300178	FBgn0004919	2R	gol-RC	2.69E-42	2.27E-52	5.01E-98	1.21E-114
FBtr0088554	FBgn0028473	2R	CG8801-RA	1.69E-59	2.68E-05	2.53E-229	2.55E-103
FBtr0086669	FBgn0034335	2R	GstE1-RA	1.38E-84	1.08E-68	5.29E-107	1.32E-89
FBtr0087893	FBgn0033710	2R	CG17739-RA	4.23E-31	2.00E-05	5.37E-133	2.17E-74
FBtr0086662	FBgn0034329	2R	IM1-RA	0.00E+00	5.66E-140	2.08E-208	6.83E-72
FBtr0114522	FBgn0050054	2R	CG30054-RD	2.03E-18	1.91E-09	7.27E-89	6.53E-71
FBtr0086674	FBgn0063494	2R	GstE6-RA	7.86E-04	2.87E-03	1.36E-65	1.30E-65
FBtr0087653	FBgn0041579	2R	AttC-RA	0.00E+00	8.15E-71	0.00E+00	1.19E-56
FBtr0072073	FBgn0004795	2R	retn-RB	1.58E-25	1.10E-23	7.28E-55	5.21E-53
FBtr0071535	FBgn0003748	2R	Treh-RE	9.32E-124	4.68E-117	7.47E-45	4.20E-39
FBtr0071580	FBgn0003162	2R	Pu-RA	1.44E-33	3.23E-19	2.75E-49	5.13E-32
FBtr0071546	FBgn0003391	2R	shg-RA	2.15E-07	2.47E-04	4.54E-36	2.13E-30
FBtr0086335	FBgn0034475	2R	Obp56h-RA	2.68E-04	6.86E-18	4.63E-10	1.65E-27
FBtr0085991	FBgn0050431	2R	CG30431-RA	4.36E-09	2.84E-04	2.97E-30	4.85E-22
FBtr0086621	FBgn0034407	2R	DptB-RA	0.00E+00	3.38E-117	4.02E-189	4.74E-21
FBtr0086058	FBgn0000099	2R	ap-RA	9.88E-09	9.83E-10	4.52E-19	8.78E-21
FBtr0087386	FBgn0014865	2R	Mtk-RA	0.00E+00	3.97E-30	0.00E+00	1.22E-17
FBtr0086266	FBgn0050148	2R	CG30148-RA	6.90E-06	6.22E-05	2.52E-18	6.31E-17
FBtr0300381	FBgn0050083	2R	CG30083-RB	9.94E-13	1.72E-12	6.05E-16	1.06E-15
FBtr0300942	FBgn0041581	2R	AttB-RB	6.53E-80	1.08E-20	1.04E-66	9.41E-14
FBtr0086665	FBgn0040736	2R	IM3-RA	0.00E+00	4.66E-186	1.46E-70	5.88E-13
FBtr0088640	FBgn0011286	2R	Rya-r44F-RA	2.46E-44	5.98E-38	5.91E-16	1.75E-11
FBtr0071821	FBgn0025878	2R	wrapper-RA	1.49E-21	2.05E-13	1.38E-17	3.64E-10
FBtr0086919	FBgn0034221	2R	CG10764-RA	1.36E-15	4.61E-13	3.24E-12	5.22E-10
FBtr0086620	FBgn0004240	2R	Dpt-RA	3.33E-259	1.12E-92	7.36E-99	1.16E-08
FBtr0072304	FBgn0035020	2R	CG13585-RB	4.42E-17	1.19E-18	2.65E-06	4.48E-07
FBtr0086727	FBgn0040733	2R	CG15068-RA	1.85E-11	1.26E-04	6.94E-14	2.10E-06
FBtr0273356	FBgn0034928	2R	CG13562-RB	2.58E-17	3.99E-12	3.26E-10	6.44E-06
FBtr0088863	FBgn0013307	2R	Odc1-RA	2.59E-10	1.82E-07	1.43E-08	6.95E-06
FBtr0300874	FBgn0034990	2R	CG11406-RC	2.67E-07	1.41E-04	1.22E-08	1.18E-05
FBtr0088337	FBgn0033502	2R	CG12910-RA	5.20E-18	2.11E-05	2.85E-18	1.43E-05
FBtr0086810	FBgn0034293	2R	CG14495-RA	2.51E-03	3.18E-03	2.54E-05	3.18E-05
FBtr0301668	FBgn0034728	2R	rad50-RD	4.75E-09	4.11E-10	8.05E-04	2.27E-04
FBtr0087005	FBgn0010226	2R	GstS1-RB	1.07E-60	7.69E-20	3.39E-31	4.26E-04
FBtr0087920	FBgn0033728	2R	Cpr49Ae-RA	3.87E-30	1.96E-20	2.71E-08	6.69E-03
FBtr0076599	FBgn0000121	3L	Arr2-RA	0.00E+00	0.00E+00	0.00E+00	0.00E+00
FBtr0074949	FBgn0004623	3L	Gbeta76C-RA	2.06E-44	1.50E-05	0.00E+00	0.00E+00
FBtr0076027	FBgn0022959	3L	yps-RA	1.18E-76	4.78E-244	5.96E-21	1.97E-132
FBtr0073073	FBgn0010381	3L	Drs-RA	0.00E+00	0.00E+00	0.00E+00	1.01E-116
FBtr0076798	FBgn0028582	3L	lqf-RE	3.83E-04	8.32E-16	1.13E-74	1.71E-112
FBtr0075369	FBgn0042201	3L	Nplp3-RA	1.13E-62	1.08E-14	3.54E-198	2.20E-105

Table s3.4 (continued)

FBtr#	FBgn#	arm	name	*p*-values			
				Z30 vs. FR	Z56 vs. FR	Z30 vs. CS	Z56 vs. CS
FBtr0074979	FBgn0036876	3L	CG9451-RA	6.62E-161	1.03E-106	7.22E-159	8.31E-105
FBtr0072703	FBgn0035227	3L	CG12090-RA	1.90E-84	1.64E-71	1.68E-107	2.08E-93
FBtr0075553	FBgn0000565	3L	Eip71CD-RA	4.05E-68	4.06E-132	1.51E-32	3.45E-80
FBtr0076093	FBgn0036165	3L	chrb-RC	6.99E-74	1.57E-96	1.30E-58	2.04E-78
FBtr0076466	FBgn0052043	3L	CG32043-RA	1.48E-72	2.49E-141	1.96E-29	4.26E-77
FBtr0075338	FBgn0003250	3L	Rh4-RA	1.80E-155	4.78E-58	2.14E-184	5.82E-77
FBtr0076452	FBgn0035982	3L	CG4461-RA	4.15E-49	1.13E-50	1.31E-73	3.18E-76
FBtr0075174	FBgn0052185	3L	CG32185-RA	3.69E-70	1.07E-37	6.62E-108	5.30E-69
FBtr0073237	FBgn0041630	3L	Hexo1-RD	1.38E-75	5.43E-38	1.09E-109	2.48E-64
FBtr0073061	FBgn0052282	3L	dro4-RA	0.00E+00	0.00E+00	5.46E-36	1.06E-61
FBtr0076119	FBgn0036203	3L	Muc68D-RB	7.82E-33	7.79E-28	3.02E-54	1.85E-48
FBtr0074835	FBgn0004366	3L	rdgC-RD	1.17E-19	4.48E-12	2.96E-59	4.92E-47
FBtr0075348	FBgn0043578	3L	PGRP-SB1-RA	6.35E-160	1.40E-29	5.79E-186	3.61E-42
FBtr0074961	FBgn0022774	3L	Oat-RA	2.95E-13	1.27E-13	8.57E-37	4.50E-38
FBtr0076559	FBgn0035943	3L	CG5653-RA	2.42E-71	1.28E-42	1.32E-65	8.63E-38
FBtr0075512	FBgn0036549	3L	CG10516-RA	2.88E-15	1.63E-14	5.21E-38	1.83E-37
FBtr0299778	FBgn0259224	3L	CG42324-RD	2.32E-43	2.31E-64	1.23E-21	7.80E-37
FBtr0075014	FBgn0036862	3L	CG9619-RA	1.00E-46	9.77E-14	1.16E-79	5.79E-35
FBtr0075426	FBgn0011693	3L	Pdh-RA	2.28E-281	6.28E-205	3.45E-72	5.88E-33
FBtr0072967	FBgn0035344	3L	Cyp4d20-RA	2.19E-39	5.36E-48	4.64E-26	9.28E-33
FBtr0076882	FBgn0035766	3L	eco-RA	0.00E+00	6.80E-159	2.28E-134	1.55E-31
FBtr0072891	FBgn0035338	3L	CG13800-RA	2.79E-21	5.35E-11	1.46E-38	7.62E-25
FBtr0078468	FBgn0014362	3L	mub-RA	2.27E-04	4.39E-11	3.26E-14	1.23E-24
FBtr0075048	FBgn0036833	3L	CG3819-RA	1.44E-09	5.04E-25	1.05E-06	9.50E-21
FBtr0112601	FBgn0085402	3L	Ect4-RG	3.68E-79	1.55E-41	2.73E-50	9.95E-21
FBtr0072923	FBgn0035346	3L	CG1146-RA	1.09E-35	6.33E-59	4.56E-08	1.11E-20
FBtr0072671	FBgn0035207	3L	CG9153-RA	2.62E-21	1.42E-09	2.93E-34	2.28E-19
FBtr0075511	FBgn0036547	3L	CG17032-RA	3.11E-40	1.78E-37	7.99E-20	2.11E-17
FBtr0074820	FBgn0036945	3L	CG6981-RB	4.36E-60	1.52E-45	5.66E-27	1.78E-16
FBtr0113178	FBgn0036683	3L	CG14060-RB	3.03E-05	3.73E-07	7.22E-11	1.56E-13
FBtr0076991	FBgn0020642	3L	Lcp65Ac-RA	6.88E-29	5.40E-17	3.31E-23	2.13E-12
FBtr0075259	FBgn0036673	3L	CG11915-RA	1.62E-04	1.05E-04	6.74E-12	2.33E-12
FBtr0089478	FBgn0036640	3L	nxf2-RA	1.15E-06	5.34E-07	1.02E-11	2.53E-12
FBtr0072727	FBgn0035206	3L	CG9186-RB	1.58E-10	2.36E-14	1.04E-08	3.36E-12
FBtr0076632	FBgn0052355	3L	CG32355-RA	8.29E-25	1.62E-16	2.18E-16	1.66E-09
FBtr0075832	FBgn0023095	3L	caps-RA	2.28E-07	6.79E-04	4.97E-12	9.65E-08
FBtr0112890	FBgn0016797	3L	fz2-RC	4.52E-07	4.35E-10	3.79E-05	1.01E-07
FBtr0072856	FBgn0002872	3L	mu2-RA	9.38E-12	6.32E-14	4.15E-06	1.11E-07
FBtr0076166	FBgn0036149	3L	CG18490-RB	3.44E-14	4.23E-15	5.41E-07	1.84E-07
FBtr0075942	FBgn0036316	3L	CG10960-RB	4.60E-30	1.51E-30	6.69E-05	1.25E-04
FBtr0302087	FBgn0261259	3L	Fhos-RC	2.71E-39	2.75E-27	2.15E-11	1.51E-04
FBtr0076567	FBgn0052029	3L	Cpr66D-RA	1.21E-11	1.46E-08	9.68E-07	3.23E-04
FBtr0075290	FBgn0011293	3L	a10-RA	7.81E-04	8.27E-03	3.10E-05	4.33E-04
FBtr0075471	FBgn0036597	3L	CG4962-RA	1.86E-43	4.08E-35	3.02E-08	4.92E-04
FBtr0075789	FBgn0036391	3L	CG17364-RB	1.06E-18	3.96E-17	5.06E-05	7.73E-04
FBtr0075457	FBgn0036579	3L	CG5027-RA	5.37E-17	6.67E-08	5.10E-11	1.13E-03
FBtr0078404	FBgn0037074	3L	CG7324-RA	5.88E-03	3.68E-03	1.88E-03	1.14E-03

Table s3.4 (continued)

FBtr#	FBgn#	arm	name	*p*-values			
				Z30 vs. FR	Z56 vs. FR	Z30 vs. CS	Z56 vs. CS
FBtr0072822	FBgn0035246	3L	CG13928-RA	2.00E-24	5.32E-05	1.04E-21	1.31E-03
FBtr0299649	FBgn0259175	3L	ome-RE	3.42E-16	2.78E-10	1.55E-07	2.88E-03
FBtr0072828	FBgn0035232	3L	CG12099-RB	2.24E-04	5.32E-03	1.94E-04	5.01E-03
FBtr0073252	FBgn0035512	3L	Cpr64Ac-RA	1.77E-17	9.85E-12	4.55E-07	6.13E-03
FBtr0083857	FBgn0002940	3R	ninaE-RA	0.00E+00	0.00E+00	0.00E+00	0.00E+00
FBtr0085513	FBgn0003861	3R	trp-RA	8.85E-127	2.39E-108	0.00E+00	0.00E+00
FBtr0084585	FBgn0039151	3R	CG13607-RA	9.16E-53	1.55E-56	0.00E+00	0.00E+00
FBtr0085463	FBgn0039682	3R	Obp99c-RA	3.36E-37	3.55E-37	0.00E+00	0.00E+00
FBtr0085778	FBgn0000313	3R	chp-RA	1.77E-45	9.48E-30	0.00E+00	0.00E+00
FBtr0085025	FBgn0040606	3R	CG6503-RA	1.77E-226	9.69E-195	0.00E+00	1.15E-292
FBtr0084949	FBgn0000206	3R	boss-RA	2.17E-98	7.07E-92	3.25E-271	5.20E-266
FBtr0078825	FBgn0087005	3R	retinophilin-RA	9.19E-101	6.74E-23	0.00E+00	1.59E-196
FBtr0113330	FBgn0040629	3R	CG18673-RB	4.71E-180	4.42E-180	6.61E-169	8.06E-169
FBtr0084102	FBgn0038877	3R	CG3308-RA	2.63E-52	4.74E-81	1.23E-55	3.19E-85
FBtr0082324	FBgn0022359	3R	Sodh-2-RA	2.16E-195	2.76E-159	1.12E-109	7.64E-81
FBtr0085832	FBgn0000557	3R	Ef1alpha100E-RA	3.07E-81	2.13E-08	6.40E-179	1.26E-56
FBtr0085460	FBgn0039688	3R	Kul-RA	2.05E-22	3.17E-11	2.82E-69	2.83E-50
FBtr0083966	FBgn0053094	3R	Synd-RB	5.23E-47	3.94E-42	7.26E-53	9.06E-48
FBtr0083154	FBgn0038347	3R	CG18522-RA	5.21E-34	1.19E-22	2.62E-60	1.01E-45
FBtr0082505	FBgn0037974	3R	CG12224-RA	2.03E-31	6.49E-40	3.71E-35	8.43E-44
FBtr0084336	FBgn0046114	3R	Gclm-RA	1.26E-79	5.89E-49	1.84E-67	4.31E-39
FBtr0083998	FBgn0013995	3R	Calx-RA	8.78E-17	2.61E-05	5.07E-58	2.04E-36
FBtr0082103	FBgn0005585	3R	Crc-RA	7.14E-29	3.00E-04	5.80E-80	7.10E-35
FBtr0301977	FBgn0051077	3R	CG31077-RB	1.09E-09	3.46E-09	6.16E-35	1.21E-34
FBtr0078593	FBgn0037410	3R	Osi2-RA	6.15E-55	3.89E-34	3.74E-49	2.52E-29
FBtr0083730	FBgn0038680	3R	Cyp12a5-RA	3.08E-03	2.67E-08	1.32E-17	5.64E-27
FBtr0083262	FBgn0250823	3R	gish-RB	6.99E-09	4.62E-12	7.05E-18	2.43E-22
FBtr0273382	FBgn0038651	3R	CG14299-RC	1.02E-24	7.22E-23	5.31E-24	3.66E-22
FBtr0113405	FBgn0051414	3R	CG31414-RB	1.33E-74	1.71E-76	1.03E-19	1.00E-19
FBtr0083179	FBgn0026616	3R	alpha-Man-IIb-RA	2.09E-08	8.21E-03	3.71E-29	3.40E-19
FBtr0084303	FBgn0039005	3R	CG6969-RA	6.81E-35	5.96E-20	1.53E-33	8.37E-19
FBtr0078823	FBgn0260462	3R	CG12163-RA	2.69E-63	8.07E-44	4.57E-31	4.38E-17
FBtr0085830	FBgn0003870	3R	ttk-RD	1.77E-23	2.02E-32	6.87E-10	1.02E-15
FBtr0084435	FBgn0039099	3R	CG10157-RA	1.93E-29	3.77E-27	1.18E-17	1.41E-15
FBtr0078642	FBgn0037387	3R	CG1213-RB	1.62E-53	8.72E-55	3.22E-15	4.39E-15
FBtr0082060	FBgn0043791	3R	CG8147-RA	1.73E-67	3.45E-03	1.90E-96	4.62E-15
FBtr0111008	FBgn0259685	3R	crb-RB	3.49E-06	5.02E-05	5.69E-16	1.87E-14
FBtr0091531	FBgn0053555	3R	btsz-RC	2.74E-23	7.22E-18	8.80E-19	9.55E-14
FBtr0082438	FBgn0037935	3R	CG6834-RA	8.39E-159	3.16E-170	1.13E-10	9.97E-13
FBtr0300936	FBgn0027930	3R	MP1-RC	2.56E-07	5.30E-09	1.09E-10	1.04E-12
FBtr0084828	FBgn0039319	3R	CG13659-RA	3.34E-28	5.24E-28	6.40E-13	1.45E-12
FBtr0083040	FBgn0051304	3R	CG31304-RA	1.01E-28	2.04E-15	5.70E-25	1.69E-12
FBtr0083585	FBgn0004618	3R	gl-RB	1.91E-14	5.60E-08	9.52E-19	1.54E-11
FBtr0302143	FBgn0038294	3R	Mf-RG	1.47E-85	3.38E-71	9.15E-19	4.71E-11
FBtr0273375	FBgn0051534	3R	CG31534-RC	3.24E-07	3.59E-10	7.94E-08	7.55E-11
FBtr0113289	FBgn0039358	3R	CG5028-RB	2.61E-19	5.78E-17	6.42E-13	8.48E-11
FBtr0084860	FBgn0051288	3R	CG31288-RA	1.88E-22	5.22E-23	6.64E-10	4.42E-10

Table s3.4 (continued)

FBtr#	FBgn#	arm	name	*p*-values			
				Z30 vs. FR	Z56 vs. FR	Z30 vs. CS	Z56 vs. CS
FBtr0300601	FBgn0260386	3R	mtg-RD	1.32E-10	1.99E-07	2.97E-13	6.66E-10
FBtr0083538	FBgn0000477	3R	DNaseII-RA	5.69E-111	5.92E-50	1.52E-46	8.18E-10
FBtr0084316	FBgn0040588	3R	CG13841-RA	2.21E-16	1.45E-13	2.42E-12	1.30E-09
FBtr0078854	FBgn0087012	3R	5-HT2-RA	1.28E-07	7.66E-15	5.73E-04	1.35E-09
FBtr0084459	FBgn0015513	3R	mbc-RA	4.43E-08	5.91E-10	1.69E-06	3.75E-08
FBtr0082405	FBgn0037895	3R	CG6723-RA	1.07E-06	4.67E-03	7.90E-13	5.29E-08
FBtr0082572	FBgn0010041	3R	GstD5-RA	1.87E-25	1.76E-17	1.40E-14	6.94E-08
FBtr0078744	FBgn0250753	3R	exba-RA	1.21E-25	2.56E-16	3.42E-15	7.65E-08
FBtr0085496	FBgn0051038	3R	CG31038-RD	6.04E-18	3.65E-05	1.88E-20	1.05E-06
FBtr0083978	FBgn0038840	3R	CG5621-RA	1.01E-13	1.52E-10	5.99E-09	2.88E-06
FBtr0301147	FBgn0039380	3R	CG5890-RB	9.59E-07	9.83E-04	5.19E-09	1.32E-05
FBtr0085361	FBgn0039628	3R	CG11841-RA	5.35E-43	3.90E-36	4.31E-09	2.42E-05
FBtr0084851	FBgn0039326	3R	CG10562-RA	3.00E-06	1.26E-06	3.82E-05	2.59E-05
FBtr0302187	FBgn0051158	3R	CG31158-RG	1.64E-14	2.02E-06	8.22E-13	3.43E-05
FBtr0113236	FBgn0038286	3R	CG6966-RB	7.86E-09	1.75E-03	5.98E-11	5.15E-05
FBtr0083146	FBgn0019940	3R	Rh6-RB	1.20E-105	4.63E-57	1.64E-27	7.13E-05
FBtr0113224	FBgn0037979	3R	CG3532-RB	5.21E-04	2.69E-05	1.03E-03	7.25E-05
FBtr0082104	FBgn0037721	3R	CG9427-RA	3.25E-17	1.33E-08	5.52E-11	5.31E-04
FBtr0081821	FBgn0040524	3R	CG11052-RA	3.53E-06	4.97E-05	7.50E-05	8.24E-04
FBtr0290056	FBgn0051145	3R	CG31145-RC	5.06E-03	3.58E-04	9.30E-03	8.77E-04
FBtr0083935	FBgn0038820	3R	CG4000-RA	5.43E-297	3.71E-71	4.81E-125	1.26E-03
FBtr0082564	FBgn0003651	3R	svp-RB	1.91E-09	5.06E-05	5.19E-07	4.12E-03
FBtr0113933	FBgn0085520	U	CG40801-RA	1.22E-29	2.13E-23	1.30E-28	1.91E-22
FBtr0301475	FBgn0004625	X	norpA-RE	3.71E-199	5.31E-141	0.00E+00	0.00E+00
FBtr0300200	FBgn0259918	X	inaF-B-RA	9.71E-51	1.21E-29	0.00E+00	1.69E-280
FBtr0071235	FBgn0024943	X	PIP82-RA	2.48E-67	1.44E-31	4.17E-275	1.39E-204
FBtr0073494	FBgn0001145	X	Gs2-RB	5.89E-36	1.87E-09	1.29E-225	6.59E-156
FBtr0077183	FBgn0052523	X	CG32523-RA	3.06E-251	3.50E-188	1.67E-166	9.80E-113
FBtr0073613	FBgn0030332	X	CG9360-RA	5.98E-302	1.25E-248	4.91E-140	1.13E-100
FBtr0070793	FBgn0029769	X	CG3239-RA	8.67E-07	3.50E-09	1.39E-45	2.07E-52
FBtr0073923	FBgn0030555	X	Fbxl4-RA	4.62E-23	1.60E-18	2.22E-55	2.16E-49
FBtr0100644	FBgn0030262	X	Vago-RC	2.10E-32	8.07E-34	2.17E-45	2.02E-47
FBtr0070443	FBgn0040335	X	CG10260-RB	1.14E-30	4.18E-11	1.06E-69	1.59E-39
FBtr0074008	FBgn0026428	X	HDAC6-RA	1.34E-90	3.80E-55	1.02E-57	1.99E-29
FBtr0070463	FBgn0040387	X	PsGEF-RA	1.56E-15	2.02E-12	1.69E-32	1.81E-28
FBtr0070428	FBgn0005670	X	Cyp4d1-RA	2.51E-06	7.41E-07	2.82E-25	1.46E-26
FBtr0073488	FBgn0001624	X	dlg1-RB	9.57E-62	3.09E-88	6.23E-11	9.64E-23
FBtr0074364	FBgn0030773	X	CG9676-RA	0.00E+00	0.00E+00	1.20E-182	1.40E-19
FBtr0070978	FBgn0003390	X	shf-RA	8.38E-06	1.09E-07	1.28E-14	1.29E-17
FBtr0074097	FBgn0030694	X	CG15602-RA	8.50E-28	2.94E-23	7.39E-21	1.19E-16
FBtr0071270	FBgn0011661	X	Moe-RB	5.83E-38	2.41E-42	6.27E-14	4.45E-16
FBtr0073527	FBgn0014133	X	bif-RC	3.98E-19	1.07E-06	4.94E-30	3.16E-14
FBtr0300465	FBgn0259994	X	CG42492-RC	1.98E-11	8.26E-10	9.75E-16	6.23E-14
FBtr0112628	FBgn0259108	X	futsch-RC	4.83E-07	3.53E-17	1.35E-04	2.65E-13
FBtr0300759	FBgn0029930	X	CG12541-RC	1.09E-09	4.86E-13	9.56E-09	1.04E-11
FBtr0301532	FBgn0003218	X	rdgB-RE	8.42E-40	1.63E-32	5.49E-15	5.47E-10
FBtr0070379	FBgn0000382	X	csw-RB	4.21E-11	1.77E-12	1.35E-08	1.01E-09

Table s3.4 (continued)

FBtr#	FBgn#	arm	name	*p*-values			
				Z30 vs. FR	Z56 vs. FR	Z30 vs. CS	Z56 vs. CS
FBtr0071005	FBgn0027108	X	inx2-RA	4.53E-19	1.03E-10	2.26E-16	1.51E-08
FBtr0070808	FBgn0029799	X	CG15772-RA	1.05E-26	9.03E-22	3.56E-12	1.79E-08
FBtr0290086	FBgn0031042	X	CG14221-RB	1.05E-07	4.22E-06	2.85E-10	1.93E-08
FBtr0074694	FBgn0030997	X	CG7990-RB	3.31E-07	2.50E-04	8.66E-12	2.89E-08
FBtr0074634	FBgn0004462	X	Pk17E-RA	2.63E-03	1.25E-03	3.54E-07	1.18E-07
FBtr0074721	FBgn0031023	X	CG14200-RA	4.41E-31	1.16E-23	5.54E-12	6.15E-07
FBtr0074299	FBgn0030755	X	CG9906-RA	4.57E-04	9.12E-03	7.03E-08	2.48E-06
FBtr0070777	FBgn0029766	X	CG15784-RA	6.66E-281	9.68E-263	2.19E-12	2.60E-06
FBtr0073979	FBgn0030593	X	CG9512-RA	2.14E-29	1.46E-28	5.88E-07	4.97E-06
FBtr0073565	FBgn0030339	X	Cyp28c1-RA	2.45E-08	3.30E-07	5.55E-06	6.08E-05
FBtr0074028	FBgn0030615	X	Cyp4s3-RA	1.09E-12	4.04E-11	8.30E-06	1.92E-04
FBtr0073653	FBgn0030398	X	Cpr11B-RA	1.72E-43	6.91E-25	2.19E-15	2.33E-04
FBtr0301703	FBgn0040089	X	meso18E-RB	2.73E-04	6.81E-04	3.61E-04	9.45E-04
FBtr0299526	FBgn0027279	X	l(1)G0196-RK	3.79E-05	4.16E-05	1.43E-03	1.84E-03
FBtr0070137	FBgn0040382	X	CG5273-RB	4.84E-79	2.50E-13	4.22E-53	2.43E-03

Table s3.5 M>Z DEGs based on Bonferroni's correction

FBtr#	FBgn#	arm	name	*p*-values			
				Z30 vs. FR	Z56 vs. FR	Z30 vs. CS	Z56 vs. CS
FBtr0079806	FBgn0012036	2L	Aldh-RA	0.00E+00	0.00E+00	0.00E+00	0.00E+00
FBtr0080030	FBgn0027611	2L	CG6206-RA	0.00E+00	0.00E+00	0.00E+00	0.00E+00
FBtr0100359	FBgn0001125	2L	Got2-RC	1.11E-196	9.84E-214	0.00E+00	0.00E+00
FBtr0079219	FBgn0000052	2L	ade2-RA	4.61E-118	5.92E-189	0.00E+00	0.00E+00
FBtr0079431	FBgn0000053	2L	ade3-RA	4.64E-119	2.41E-169	0.00E+00	0.00E+00
FBtr0080989	FBgn0032652	2L	CG6870-RA	5.35E-34	3.35E-81	3.23E-231	0.00E+00
FBtr0080276	FBgn0032382	2L	CG14935-RA	5.26E-33	9.19E-64	1.95E-230	0.00E+00
FBtr0080449	FBgn0027586	2L	CG5867-RA	1.97E-87	1.22E-134	3.42E-190	7.76E-263
FBtr0077524	FBgn0022073	2L	Thor-RA	2.41E-07	4.54E-37	3.92E-147	3.17E-247
FBtr0079073	FBgn0031701	2L	TotM-RA	2.69E-61	2.77E-69	3.72E-186	6.88E-208
FBtr0078115	FBgn0001142	2L	Gs1-RC	2.12E-79	1.05E-75	2.79E-186	4.57E-186
FBtr0078025	FBgn0002563	2L	Lsp1beta-RA	1.06E-131	1.31E-145	5.28E-157	1.90E-173
FBtr0079925	FBgn0015035	2L	Cyp4e3-RA	1.72E-18	1.42E-16	5.48E-146	4.61E-151
FBtr0077957	FBgn0031306	2L	CG4577-RA	2.03E-37	1.14E-43	3.49E-117	2.76E-132
FBtr0080905	FBgn0086783	2L	Mhc-RL	7.45E-14	9.84E-44	3.26E-55	2.35E-108
FBtr0079606	FBgn0032025	2L	CG7778-RA	2.82E-05	2.26E-05	4.34E-66	1.28E-70
FBtr0079919	FBgn0042174	2L	CG18854-RC	5.78E-05	3.53E-08	8.23E-48	8.90E-59
FBtr0079147	FBgn0001128	2L	Gpdh-RC	0.00E+00	0.00E+00	5.76E-26	1.20E-49
FBtr0077391	FBgn0031645	2L	CG3036-RA	5.06E-14	3.54E-33	1.12E-22	3.46E-46
FBtr0079857	FBgn0028479	2L	CG4389-RB	9.83E-74	3.22E-48	3.25E-71	3.86E-46
FBtr0302160	FBgn0026718	2L	fu12-RC	1.01E-11	6.15E-09	5.63E-42	1.47E-38
FBtr0077731	FBgn0019830	2L	colt-RA	3.95E-23	4.48E-35	9.53E-25	4.12E-37
FBtr0302115	FBgn0000579	2L	Eno-RF	2.79E-41	3.22E-104	3.77E-03	1.40E-31
FBtr0080861	FBgn0020415	2L	Idgf2-RA	1.89E-146	6.74E-168	6.07E-23	8.67E-29
FBtr0077483	FBgn0031589	2L	CG3714-RE	9.50E-22	1.17E-31	3.92E-18	3.14E-27
FBtr0077863	FBgn0040718	2L	CG15353-RA	7.95E-17	1.61E-20	5.94E-21	3.29E-25
FBtr0077751	FBgn0031405	2L	CG4267-RA	2.04E-06	3.09E-11	2.72E-16	4.73E-24
FBtr0079066	FBgn0031693	2L	Cyp4ac1-RA	7.19E-23	5.82E-30	1.04E-17	5.74E-24
FBtr0080281	FBgn0005664	2L	Cry-RA	2.30E-22	2.07E-25	9.60E-20	1.86E-22
FBtr0079106	FBgn0004620	2L	GluRIIA-RI	2.63E-10	3.75E-13	1.66E-17	1.17E-21
FBtr0079894	FBgn0032167	2L	CG5853-RA	6.58E-80	2.48E-61	1.10E-32	1.52E-19
FBtr0079263	FBgn0031824	2L	CG9547-RA	9.72E-03	5.87E-04	5.77E-15	3.59E-18
FBtr0079250	FBgn0015623	2L	Cpr-RA	1.06E-05	6.79E-11	7.12E-11	7.47E-18
FBtr0079471	FBgn0031925	2L	Cyp4d21- RA	4.67E-16	2.48E-19	1.57E-14	1.97E-17
FBtr0080042	FBgn0032253	2L	CG5322-RA	5.28E-29	2.19E-31	4.10E-14	2.58E-15
FBtr0077886	FBgn0031362	2L	CG17646-RA	7.07E-18	2.73E-30	5.36E-07	2.79E-15
FBtr0080017	FBgn0025366	2L	Ip259-RA	5.14E-38	4.80E-63	5.99E-04	5.04E-14
FBtr0080050	FBgn0032237	2L	CG5362-RA	2.19E-13	1.63E-15	1.40E-11	1.61E-13
FBtr0090027	FBgn0032456	2L	MRP-RO	4.74E-04	4.28E-10	6.77E-06	7.64E-13
FBtr0078042	FBgn0000442	2L	Pkg21D-RA	1.33E-16	1.91E-14	8.22E-15	9.50E-13
FBtr0077521	FBgn0021967	2L	Pdsw-RB	7.85E-08	3.83E-13	3.23E-07	2.07E-12
FBtr0079637	FBgn0031998	2L	CG8451-RA	3.46E-69	5.73E-54	2.35E-21	8.27E-12
FBtr0081138	FBgn0051793	2L	CG31793-RA	4.79E-26	6.09E-28	3.25E-10	6.62E-11
FBtr0080866	FBgn0032586	2L	Tpr2-RA	6.21E-03	1.60E-09	2.62E-03	3.43E-10

Table s3.5 (continued)

FBtr#	FBgn#	arm	name	p-values			
				Z30 vs. FR	Z56 vs. FR	Z30 vs. CS	Z56 vs. CS
FBtr0080108	FBgn0032287	2L	CG6415-RA	3.95E-34	9.32E-36	1.53E-08	1.11E-08
FBtr0079642	FBgn0031987	2L	CG12375-RA	5.77E-04	1.08E-05	2.65E-06	1.70E-08
FBtr0079972	FBgn0051755	2L	CG31755-RA	2.19E-05	2.30E-07	3.82E-06	2.91E-08
FBtr0077629	FBgn0031478	2L	CG8814-RA	6.95E-05	2.10E-07	1.01E-04	3.08E-07
FBtr0079032	FBgn0031675	2L	CG9121-RA	2.51E-05	1.30E-09	2.30E-03	5.21E-07
FBtr0114603	FBgn0031813	2L	CG9527-RB	5.85E-05	5.22E-08	7.22E-04	1.16E-06
FBtr0089655	FBgn0028425	2L	JhI-21-RA	2.90E-07	6.91E-11	1.57E-03	3.37E-06
FBtr0081109	FBgn0015808	2L	ScpX-RA	3.82E-05	5.03E-04	2.27E-07	3.84E-06
FBtr0110894	FBgn0083970	2L	CG34134-RA	7.89E-08	1.15E-10	1.30E-03	1.07E-05
FBtr0300709	FBgn0031937	2L	CG13795-RB	1.25E-11	3.65E-09	1.86E-06	2.23E-04
FBtr0087560	FBgn0033926	2R	Arc1-RA	2.46E-116	1.40E-134	0.00E+00	0.00E+00
FBtr0072026	FBgn0034860	2R	CG9812-RC	5.21E-16	1.79E-33	1.10E-158	2.64E-215
FBtr0086625	FBgn0010053	2R	Jheh1-RA	0.00E+00	0.00E+00	1.00E-226	2.96E-203
FBtr0087232	FBgn0001124	2R	Got1-RA	4.20E-65	5.36E-68	3.65E-153	6.00E-162
FBtr0071606	FBgn0034628	2R	Acox57D-p-RA	1.19E-19	6.48E-21	4.53E-112	7.84E-121
FBtr0086935	FBgn0034229	2R	CG4847-RD	7.04E-74	1.18E-86	6.90E-93	6.27E-108
FBtr0087922	FBgn0033730	2R	Cpr49Ag-RA	2.15E-06	4.04E-09	2.97E-91	1.49E-106
FBtr0087004	FBgn0000079	2R	Amy-p-RA	1.37E-17	9.66E-11	1.10E-106	4.50E-96
FBtr0088245	FBgn0027525	2R	CG7686-RA	0.00E+00	0.00E+00	1.27E-63	1.09E-92
FBtr0089970	FBgn0034405	2R	Jheh2-RA	0.00E+00	0.00E+00	9.29E-52	2.61E-78
FBtr0301282	FBgn0027842	2R	CPTI-RD	2.57E-52	5.49E-41	1.22E-90	3.55E-77
FBtr0086292	FBgn0034509	2R	Obp57c-RA	6.26E-23	1.78E-21	4.98E-71	3.89E-71
FBtr0088903	FBgn0001091	2R	Gapdh1-RA	6.70E-06	2.85E-26	1.00E-29	1.30E-66
FBtr0088791	FBgn0053087	2R	CG33087-RC	1.51E-65	5.33E-50	6.24E-77	1.93E-60
FBtr0087309	FBgn0022160	2R	Gpo-1-RA	8.20E-103	5.92E-141	5.23E-36	1.15E-57
FBtr0086327	FBgn0034471	2R	Obp56e-RA	1.33E-12	6.18E-24	5.41E-38	1.97E-57
FBtr0088384	FBgn0033465	2R	CG12140-RA	3.85E-21	1.33E-14	1.50E-59	2.74E-50
FBtr0088611	FBgn0033391	2R	CG8026-RB	1.76E-11	9.87E-26	3.05E-27	3.02E-48
FBtr0072239	FBgn0034909	2R	CG4797-RB	1.63E-18	9.72E-42	4.59E-22	4.64E-47
FBtr0087390	FBgn0034010	2R	CG8157-RA	2.88E-51	9.62E-45	3.91E-51	1.39E-44
FBtr0072226	FBgn0025352	2R	Thiolase-RA	5.01E-28	7.81E-20	4.73E-51	6.76E-41
FBtr0088448	FBgn0033464	2R	CG1441-RA	7.25E-08	8.83E-14	5.34E-26	9.88E-37
FBtr0087450	FBgn0013773	2R	Cyp6a22-RA	4.41E-32	1.48E-37	1.85E-31	1.01E-36
FBtr0089548	FBgn0027572	2R	CG5009-RA	5.74E-52	2.30E-52	5.88E-37	1.18E-36
FBtr0087720	FBgn0033830	2R	CG10814-RA	2.38E-23	1.01E-39	1.50E-20	6.80E-36
FBtr0087732	FBgn0053138	2R	CG33138-RA	3.48E-86	1.05E-76	1.73E-42	1.91E-34
FBtr0087079	FBgn0034155	2R	unc-104-RD	2.33E-17	3.50E-26	5.65E-23	3.09E-33
FBtr0088508	FBgn0017558	2R	Pdk-RA	4.94E-77	2.46E-113	3.10E-14	2.93E-30
FBtr0086639	FBgn0034390	2R	CG15093-RB	2.13E-40	5.51E-60	1.52E-16	4.11E-29
FBtr0086305	FBgn0034494	2R	CG10444-RA	2.68E-13	4.46E-15	2.39E-23	3.56E-26
FBtr0071815	FBgn0013272	2R	Gp150-RC	9.71E-06	1.43E-05	8.92E-24	2.12E-24
FBtr0088593	FBgn0033397	2R	Cyp4p3-RA	1.22E-05	7.38E-04	3.15E-24	4.93E-22
FBtr0289993	FBgn0050050	2R	CG30050-RB	4.98E-05	3.29E-03	2.64E-14	2.10E-12
FBtr0300283	FBgn0034432	2R	CG7461-RB	4.90E-09	3.48E-06	5.94E-15	1.41E-11
FBtr0071928	FBgn0034756	2R	Cyp6d2-RA	1.24E-06	7.13E-08	9.53E-10	3.24E-11
FBtr0089056	FBgn0015038	2R	Cyp9b1-RA	2.54E-03	5.83E-04	1.25E-09	6.36E-11
FBtr0086677	FBgn0063491	2R	GstE9-RA	2.62E-51	1.55E-62	3.14E-06	1.14E-09

Table s3.5 (continued)

FBtr#	FBgn#	arm	name	p-values			
				Z30 vs. FR	Z56 vs. FR	Z30 vs. CS	Z56 vs. CS
FBtr0112670	FBgn0085434	2R	NaCP60E-RC	4.03E-03	1.09E-03	4.51E-08	3.56E-09
FBtr0087644	FBgn0033879	2R	CG6543-RB	2.80E-06	1.24E-09	1.65E-05	1.06E-08
FBtr0072349	FBgn0019886	2R	CG4589-RC	2.87E-03	1.97E-05	2.36E-04	7.82E-07
FBtr0086236	FBgn0034543	2R	CG30152-RA	7.06E-04	8.31E-04	2.15E-05	1.76E-05
FBtr0086699	FBgn0034356	2R	CG10924-RA	6.66E-76	1.15E-81	2.66E-05	3.97E-05
FBtr0088679	FBgn0003074	2R	Pgi-RA	5.93E-134	1.07E-141	1.73E-04	2.47E-04
FBtr0087172	FBgn0034117	2R	CG7997-RA	5.85E-10	6.44E-10	1.40E-04	2.76E-04
FBtr0089324	FBgn0002565	3L	Lsp2-RA	0.00E+00	0.00E+00	0.00E+00	0.00E+00
FBtr0076427	FBgn0036007	3L	path-RA	5.78E-178	3.32E-113	0.00E+00	1.46E-280
FBtr0076810	FBgn0035817	3L	CG7409-RA	3.88E-95	1.71E-98	3.57E-172	7.97E-181
FBtr0075753	FBgn0029167	3L	Hml-RA	7.39E-98	1.69E-59	2.68E-229	1.73E-174
FBtr0075699	FBgn0036449	3L	bmm-RA	8.46E-69	4.10E-91	2.40E-80	6.96E-105
FBtr0078413	FBgn0012034	3L	AcCoAS-RA	1.14E-126	2.45E-88	2.28E-140	2.42E-100
FBtr0076001	FBgn0027843	3L	CAH2-RA	3.37E-49	6.79E-81	7.11E-62	1.32E-97
FBtr0076831	FBgn0035791	3L	CG8539-RA	2.06E-66	2.01E-53	8.32E-100	1.75E-85
FBtr0073301	FBgn0035544	3L	CG15021-RA	7.29E-03	7.61E-11	2.33E-43	1.73E-67
FBtr0078223	FBgn0036995	3L	CG5195-RA	4.14E-07	1.03E-07	5.69E-49	1.24E-53
FBtr0076455	FBgn0035985	3L	Cpr67B-RA	4.94E-07	6.44E-18	3.12E-31	4.58E-52
FBtr0076669	FBgn0001248	3L	Idh-RB	4.86E-94	2.48E-140	3.16E-24	5.95E-48
FBtr0076424	FBgn0010408	3L	RpS9-RB	2.16E-48	6.06E-87	2.87E-18	3.00E-43
FBtr0076526	FBgn0023479	3L	Tequila-RA	0.00E+00	0.00E+00	3.39E-25	5.16E-31
FBtr0074870	FBgn0036935	3L	CG14186-RA	5.72E-05	4.35E-15	1.56E-14	7.74E-30
FBtr0075094	FBgn0040322	3L	GNBP2-RB	3.16E-41	3.61E-46	3.03E-24	1.44E-27
FBtr0076199	FBgn0036116	3L	CG7888-RC	2.41E-17	1.07E-10	1.52E-35	9.52E-27
FBtr0073270	FBgn0035499	3L	Chd64-RB	7.96E-31	2.55E-60	1.18E-07	1.34E-24
FBtr0110866	FBgn0036612	3L	CG4998-RB	1.96E-09	8.17E-12	1.11E-20	1.44E-24
FBtr0076832	FBgn0015033	3L	Cyp4d8-RA	5.08E-24	3.41E-17	9.90E-27	1.02E-19
FBtr0077011	FBgn0004513	3L	Mdr65-RA	5.42E-25	2.59E-52	9.89E-05	1.09E-19
FBtr0112761	FBgn0085484	3L	CG34455-RC	3.21E-13	7.38E-16	6.57E-14	1.32E-16
FBtr0075182	FBgn0036741	3L	CG7510-RA	2.64E-15	4.63E-36	7.74E-03	6.24E-15
FBtr0072978	FBgn0035383	3L	CG2107-RA	1.02E-04	2.69E-03	2.20E-16	1.44E-14
FBtr0073359	FBgn0010349	3L	Dhc64C-RA	5.20E-06	5.61E-12	1.15E-07	2.69E-14
FBtr0077179	FBgn0035588	3L	CG10672-RA	9.50E-09	4.22E-10	1.64E-11	3.44E-13
FBtr0073159	FBgn0035471	3L	Sc2-RA	7.65E-04	9.83E-08	1.27E-07	7.29E-13
FBtr0075046	FBgn0036836	3L	CG11619-RA	1.85E-05	8.38E-09	1.32E-08	1.37E-12
FBtr0300655	FBgn0260388	3L	CG42514-RA	9.11E-16	4.04E-08	9.64E-20	2.70E-11
FBtr0075076	FBgn0036824	3L	CG3902-RA	5.64E-08	5.44E-06	2.06E-13	3.64E-11
FBtr0076936	FBgn0035725	3L	Mis12-RA	9.46E-04	1.93E-06	1.41E-05	6.22E-09
FBtr0072743	FBgn0035233	3L	CG7864-RA	1.05E-04	8.22E-05	1.60E-08	7.77E-09
FBtr0078407	FBgn0037070	3L	CG11309-RA	2.10E-05	1.06E-04	4.60E-09	2.37E-08
FBtr0074972	FBgn0036887	3L	CG9231-RA	3.12E-04	6.84E-08	4.78E-04	1.08E-07
FBtr0072529	FBgn0025592	3L	Gyk-RA	4.07E-08	1.96E-08	6.18E-07	3.29E-07
FBtr0075672	FBgn0036462	3L	mRpL39-RA	2.72E-05	8.28E-08	2.39E-03	1.91E-05
FBtr0076173	FBgn0036157	3L	CG7560-RA	1.77E-35	2.38E-37	2.70E-05	3.14E-05
FBtr0072874	FBgn0040507	3L	ACXD-RA	8.55E-03	3.26E-04	1.86E-03	5.36E-05
FBtr0073077	FBgn0035445	3L	CG12014-RA	8.85E-05	3.21E-04	2.05E-05	7.88E-05
FBtr0072679	FBgn0010786	3L	l(3)02640-RA	5.05E-04	4.36E-04	5.65E-04	4.83E-04

Table s3.5 (continued)

FBtr#	FBgn#	arm	name	p-values			
				Z30 vs. FR	Z56 vs. FR	Z30 vs. CS	Z56 vs. CS
FBtr0076304	FBgn0052055	3L	CG32055-RA	9.91E-04	2.41E-04	4.20E-03	1.11E-03
FBtr0076130	FBgn0036194	3L	CG11652-RA	6.20E-03	8.87E-03	2.89E-03	4.21E-03
FBtr0301802	FBgn0058160	3LHet	CG40160-RE	6.47E-12	1.80E-09	6.69E-14	1.71E-11
FBtr0082660	FBgn0002719	3R	Men-RB	0.00E+00	0.00E+00	0.00E+00	0.00E+00
FBtr0082158	FBgn0002868	3R	MtnA-RA	0.00E+00	0.00E+00	0.00E+00	0.00E+00
FBtr0084847	FBgn0039330	3R	CG11909-RA	4.01E-143	9.38E-210	0.00E+00	0.00E+00
FBtr0084710	FBgn0039241	3R	CG11089-RA	3.66E-93	6.63E-149	0.00E+00	0.00E+00
FBtr0083245	FBgn0027657	3R	glob1-RC	1.19E-16	1.74E-15	0.00E+00	0.00E+00
FBtr0083971	FBgn0028396	3R	TotA-RA	3.88E-06	1.18E-08	0.00E+00	0.00E+00
FBtr0082264	FBgn0020385	3R	pug-RB	4.83E-102	1.27E-156	1.64E-223	0.00E+00
FBtr0082954	FBgn0038236	3R	Cyp313a1-RA	1.99E-121	1.40E-135	1.36E-257	7.17E-286
FBtr0089766	FBgn0038194	3R	Cyp6d5-RA	3.28E-17	9.83E-08	2.74E-267	6.79E-242
FBtr0081996	FBgn0010222	3R	Nmdmc-RB	2.84E-13	1.36E-76	5.14E-86	1.80E-209
FBtr0083038	FBgn0038290	3R	CG6912-RA	6.49E-102	1.23E-119	3.61E-173	8.91E-200
FBtr0083025	FBgn0038291	3R	CG3984-RA	4.52E-44	3.88E-51	1.35E-115	7.27E-131
FBtr0084431	FBgn0039073	3R	CG4408-RA	4.61E-21	1.66E-13	5.72E-132	2.76E-124
FBtr0083036	FBgn0038293	3R	CG6904-RB	5.08E-30	6.73E-52	5.10E-69	1.48E-102
FBtr0084859	FBgn0039321	3R	CG10550-RA	6.58E-28	3.62E-26	7.71E-89	5.37E-89
FBtr0301346	FBgn0086704	3R	stops-RC	2.68E-22	8.21E-42	6.17E-56	1.13E-86
FBtr0085133	FBgn0039486	3R	CG6074-RA	3.38E-07	5.57E-06	3.73E-70	1.63E-71
FBtr0083894	FBgn0038795	3R	CG4335-RA	1.28E-14	6.12E-17	5.99E-62	1.47E-69
FBtr0084285	FBgn0038983	3R	CG5326-RA	3.32E-35	1.83E-38	3.99E-59	1.71E-64
FBtr0113219	FBgn0037872	3R	nocturnin-RD	3.95E-26	7.52E-56	6.41E-31	4.62E-63
FBtr0085715	FBgn0039809	3R	CG15547-RA	2.10E-08	2.96E-10	8.15E-54	2.25E-61
FBtr0082095	FBgn0260463	3R	unc-115-RA	5.01E-51	1.36E-63	2.29E-46	7.09E-58
FBtr0085390	FBgn0014427	3R	CG11899-RA	7.50E-42	7.58E-75	4.47E-20	1.04E-43
FBtr0083790	FBgn0038733	3R	CG11407-RA	6.28E-15	5.08E-38	1.79E-18	1.22E-43
FBtr0085604	FBgn0039737	3R	CG7920-RB	3.87E-15	4.05E-17	1.96E-38	9.29E-43
FBtr0078705	FBgn0037351	3R	RpL13A-RB	1.01E-08	4.39E-23	1.22E-21	1.43E-42
FBtr0084994	FBgn0000064	3R	Ald-RB	2.14E-21	3.75E-49	5.06E-17	2.15E-42
FBtr0084440	FBgn0039102	3R	SPE-RA	6.49E-106	1.11E-144	4.85E-20	2.98E-36
FBtr0082659	FBgn0038083	3R	CG5999-RA	1.79E-14	8.14E-13	1.72E-35	2.58E-35
FBtr0078656	FBgn0011281	3R	Pbprp3-RA	1.05E-07	4.62E-31	8.80E-10	3.35E-35
FBtr0082666	FBgn0001296	3R	kar-RA	1.27E-07	1.90E-13	5.37E-21	1.50E-30
FBtr0083542	FBgn0003499	3R	sr-RA	4.46E-06	1.16E-10	1.04E-19	5.24E-28
FBtr0084691	FBgn0003719	3R	tld-RA	2.68E-21	8.91E-33	4.31E-16	3.72E-26
FBtr0083463	FBgn0038525	3R	CG14329-RA	1.40E-15	4.12E-21	3.95E-19	3.51E-25
FBtr0083889	FBgn0038799	3R	CG4288-RA	7.64E-14	8.50E-12	2.96E-24	4.92E-22
FBtr0084013	FBgn0038858	3R	CG5793-RA	1.28E-38	6.15E-46	1.26E-14	1.43E-18
FBtr0083026	FBgn0038292	3R	CG3987-RA	5.72E-09	8.53E-10	6.38E-17	1.76E-18
FBtr0082093	FBgn0053105	3R	p24-2-RA	4.19E-07	4.16E-06	1.53E-18	6.26E-18
FBtr0085401	FBgn0051445	3R	CG31445-RA	1.64E-13	1.59E-32	1.23E-04	8.38E-18
FBtr0100464	FBgn0037912	3R	CG6782-RD	2.99E-22	1.90E-32	5.47E-09	1.25E-15
FBtr0084186	FBgn0038924	3R	CG6028-RA	7.65E-19	3.72E-25	6.95E-11	1.57E-15
FBtr0082715	FBgn0038115	3R	CG7966-RA	0.00E+00	0.00E+00	3.84E-15	1.80E-13
FBtr0082136	FBgn0037752	3R	RpS29-RA	1.46E-13	1.06E-26	4.88E-04	1.82E-12
FBtr0085798	FBgn0039856	3R	CG1774-RA	2.96E-47	9.46E-64	3.37E-06	2.99E-12

Table s3.5 (continued)

FBtr#	FBgn#	arm	name	p-values			
				Z30 vs. FR	Z56 vs. FR	Z30 vs. CS	Z56 vs. CS
FBtr0082826	FBgn0038180	3R	Cht5-RA	2.38E-08	4.05E-09	1.89E-10	1.49E-11
FBtr0084810	FBgn0039298	3R	to-RA	2.46E-36	1.83E-49	6.24E-06	2.26E-11
FBtr0084109	FBgn0038889	3R	CG7922-RA	3.52E-03	2.70E-07	5.17E-06	3.33E-11
FBtr0082898	FBgn0027563	3R	CG9631-RA	1.18E-03	5.21E-08	5.15E-05	5.34E-10
FBtr0112558	FBgn0085378	3R	CG34349-RA	3.83E-09	5.14E-08	1.08E-10	1.47E-09
FBtr0084317	FBgn0039024	3R	CG4721-RA	5.41E-50	1.96E-35	9.75E-18	1.56E-08
FBtr0290273	FBgn0040493	3R	granny-smith-RD	1.21E-05	4.43E-08	2.13E-05	8.12E-08
FBtr0084690	FBgn0004885	3R	tok-RA	5.88E-03	2.95E-05	5.95E-05	8.43E-08
FBtr0082259	FBgn0024957	3R	Irp-1B-RA	5.13E-19	1.50E-20	7.81E-07	2.37E-07
FBtr0113389	FBgn0051103	3R	CG31103-RB	3.08E-08	3.31E-07	3.43E-07	3.58E-06
FBtr0082111	FBgn0037714	3R	CG9396-RA	5.70E-09	2.91E-10	3.64E-05	4.22E-06
FBtr0302027	FBgn0025701	3R	CG14709-RB	1.65E-06	1.52E-06	4.97E-03	6.07E-03
FBtr0084853	FBgn0039324	3R	CG10553-RA	9.85E-23	1.32E-16	1.02E-06	7.67E-03
FBtr0081795	FBgn0037552	3R	CG7800-RA	4.00E-04	2.20E-03	1.85E-03	9.16E-03
FBtr0071419	FBgn0004045	X	Yp1-RA	0.00E+00	0.00E+00	0.00E+00	0.00E+00
FBtr0070866	FBgn0029831	X	CG5966-RA	0.00E+00	2.12E-167	0.00E+00	0.00E+00
FBtr0073705	FBgn0020513	X	ade5-RA	3.99E-34	1.02E-81	0.00E+00	0.00E+00
FBtr0073908	FBgn0030558	X	CG1461-RA	5.30E-11	5.51E-06	0.00E+00	0.00E+00
FBtr0077304	FBgn0011280	X	Pbprp2-RB	9.90E-66	1.23E-124	1.28E-201	2.78E-305
FBtr0070186	FBgn0040349	X	CG3699-RA	0.00E+00	0.00E+00	1.13E-283	1.63E-301
FBtr0073777	FBgn0030482	X	CG1673-RA	3.00E-04	2.66E-37	2.52E-157	1.08E-277
FBtr0071159	FBgn0030013	X	GIIIspla2-RA	5.82E-25	4.07E-25	4.19E-210	2.66E-223
FBtr0070383	FBgn0023507	X	CG3835-RA	3.37E-12	8.41E-17	5.20E-87	6.37E-103
FBtr0070827	FBgn0029823	X	CG3011-RA	2.29E-24	1.56E-33	2.41E-66	4.47E-83
FBtr0074717	FBgn0027621	X	Pfrx-RB	3.50E-50	1.22E-78	3.67E-41	5.70E-67
FBtr0073778	FBgn0030484	X	CG1681-RA	5.38E-03	2.60E-05	6.31E-55	4.28E-66
FBtr0070916	FBgn0014026	X	RpL7A-RD	3.93E-39	1.29E-127	7.82E-09	5.78E-64
FBtr0071338	FBgn0086450	X	su(r)-RC	1.34E-17	1.09E-32	1.04E-38	7.24E-61
FBtr0070981	FBgn0029897	X	RpL17-RC	2.90E-12	2.72E-50	9.45E-12	2.24E-49
FBtr0070093	FBgn0023537	X	CG17896-RA	2.69E-70	9.02E-92	4.58E-30	2.97E-43
FBtr0071242	FBgn0030040	X	CG15347-RA	8.98E-10	9.39E-05	1.55E-47	3.27E-39
FBtr0073774	FBgn0030478	X	CG1640-RF	1.77E-78	5.82E-96	1.08E-28	4.27E-38
FBtr0073407	FBgn0030245	X	CG1637-RC	1.93E-06	4.14E-05	2.97E-35	4.05E-34
FBtr0070140	FBgn0025621	X	CG16989-RA	1.18E-23	4.94E-40	1.21E-16	1.86E-30
FBtr0112527	FBgn0085354	X	CG34325-RA	8.49E-05	2.57E-08	1.67E-22	4.74E-30
FBtr0074795	FBgn0031069	X	CG12703-RA	1.67E-06	7.18E-10	2.59E-21	1.22E-27
FBtr0071123	FBgn0029990	X	CG2233-RA	4.71E-200	7.30E-54	3.12E-145	2.44E-26
FBtr0112575	FBgn0085388	X	IP3K2-RB	1.61E-10	5.05E-09	6.36E-24	2.17E-22
FBtr0073683	FBgn0011837	X	Tis11-RA	8.26E-15	3.56E-12	5.39E-25	4.24E-22
FBtr0110969	FBgn0030608	X	Lsd-2-RC	1.67E-80	5.41E-37	1.08E-58	5.25E-22
FBtr0073819	FBgn0030519	X	CG11151-RA	3.14E-04	5.45E-09	6.73E-13	1.30E-20
FBtr0073961	FBgn0030607	X	dob-RA	4.96E-35	8.82E-32	5.01E-22	6.11E-19
FBtr0073833	FBgn0052626	X	CG32626-RC	3.60E-07	5.43E-13	2.02E-11	1.32E-18
FBtr0301696	FBgn0026313	X	X11L-RB	8.05E-14	3.71E-19	4.09E-13	2.77E-18
FBtr0070778	FBgn0029768	X	SPR-RA	2.09E-23	1.16E-32	3.33E-11	1.54E-17
FBtr0073510	FBgn0030311	X	CG11699-RA	2.41E-06	9.78E-11	2.25E-10	6.69E-16
FBtr0077312	FBgn0031119	X	CG1812-RA	3.14E-03	2.14E-05	1.76E-11	1.48E-15

Table s3.5 (continued)

FBtr#	FBgn#	arm	name	p-values			
				Z30 vs. FR	Z56 vs. FR	Z30 vs. CS	Z56 vs. CS
FBtr0070446	FBgn0029629	X	CG8636-RA	1.45E-14	5.23E-24	4.65E-08	2.30E-15
FBtr0070115	FBgn0025640	X	CG13369-RA	7.09E-06	1.21E-13	1.08E-04	6.89E-12
FBtr0070387	FBgn0011576	X	Cyp4d2-RA	1.41E-03	2.03E-08	1.83E-05	3.70E-11
FBtr0074654	FBgn0030968	X	CG7322-RA	6.78E-16	7.53E-12	9.21E-15	8.51E-11
FBtr0071224	FBgn0030058	X	CG11294-RA	2.82E-16	1.86E-12	8.02E-13	6.24E-09
FBtr0074258	FBgn0030724	X	Nipsnap-RA	7.23E-12	8.64E-12	1.09E-07	2.02E-07
FBtr0071125	FBgn0003656	X	sws-RA	1.66E-08	9.42E-07	1.01E-08	6.09E-07
FBtr0074053	FBgn0030668	X	CG8128-RA	1.11E-13	4.73E-14	7.57E-07	7.65E-07
FBtr0070558	FBgn0029648	X	CG3603-RA	3.96E-04	7.34E-08	4.44E-03	1.52E-06
FBtr0073903	FBgn0030554	X	CG1434-RA	2.03E-08	3.31E-11	1.02E-03	9.81E-06
FBtr0073794	FBgn0010198	X	RpS15Aa-RD	5.50E-92	4.50E-99	5.08E-04	2.24E-04

Table s3.6 Z>M DEGs based on FDR correction

FBtr#	FBgn#	arm	name	*p*-values			
				Z30-FR	Z56-FR	Z30-CS	Z56-CS
FBtr0081030	FBgn0000120	2L	Arr1-RA	0.00E+00	1.35E-231	0.00E+00	0.00E+00
FBtr0077489	FBgn0051772	2L	CG31772-RA	1.32E-99	1.96E-80	2.12E-80	9.92E-63
FBtr0081520	FBgn0032946	2L	nrv3-RD	1.70E-211	0.00E+00	8.10E-62	0.00E+00
FBtr0079517	FBgn0024290	2L	Slob-RB	1.78E-59	5.31E-61	1.36E-152	2.10E-158
FBtr0080118	FBgn0032297	2L	CG17124-RB	1.72E-62	3.28E-52	9.33E-103	1.34E-90
FBtr0299968	FBgn0259715	2L	CG42369-RA	1.11E-86	5.72E-51	2.58E-142	1.04E-96
FBtr0301855	FBgn0028433	2L	Ggamma30A-RD	9.51E-81	3.22E-44	0.00E+00	1.75E-280
FBtr0080222	FBgn0032350	2L	CG6287-RA	1.13E-176	5.60E-113	1.58E-86	1.73E-42
FBtr0080496	FBgn0032472	2L	CG9928-RA	9.42E-42	1.14E-39	1.06E-53	9.27E-52
FBtr0112357	FBgn0085195	2L	CG34166-RA	3.63E-293	0.00E+00	2.80E-37	0.00E+00
FBtr0077671	FBgn0031489	2L	CG17224-RA	5.80E-60	4.40E-48	4.36E-36	1.66E-26
FBtr0080565	FBgn0053307	2L	CG33307-RA	1.54E-26	2.89E-38	4.30E-26	8.69E-38
FBtr0089290	FBgn0016930	2L	smi35A-RC	1.60E-26	2.03E-25	1.88E-42	1.09E-41
FBtr0079071	FBgn0016076	2L	vri-RA	1.65E-148	7.68E-183	4.05E-25	1.01E-37
FBtr0077399	FBgn0041150	2L	hoe1-RE	1.88E-42	6.27E-25	1.39E-41	3.15E-24
FBtr0079309	FBgn0025595	2L	GRHR-RB	2.55E-19	7.62E-29	3.71E-48	8.71E-64
FBtr0079861	FBgn0032129	2L	jp-RA	5.47E-19	1.74E-22	1.16E-26	4.16E-31
FBtr0299969	FBgn0259716	2L	CG42370-RA	5.19E-18	1.25E-19	1.09E-23	1.21E-25
FBtr0080552	FBgn0012037	2L	Ance-RA	1.18E-28	8.69E-22	7.68E-23	1.03E-16
FBtr0080718	FBgn0024183	2L	vig-RD	1.52E-16	2.27E-19	4.91E-19	3.37E-22
FBtr0081372	FBgn0026756	2L	Ugt37a1-RA	1.13E-17	2.44E-12	5.57E-23	4.21E-17
FBtr0077417	FBgn0031629	2L	CG3244-RA	4.55E-17	6.37E-12	9.10E-19	2.32E-13
FBtr0081031	FBgn0002939	2L	ninaD-RA	1.65E-13	1.14E-23	6.91E-12	3.10E-21
FBtr0300331	FBgn0031993	2L	CG8486-RD	2.40E-11	3.22E-14	7.04E-16	1.66E-19
FBtr0081303	FBgn0032836	2L	CG10680-RA	8.28E-18	9.44E-11	3.94E-112	1.37E-96
FBtr0077394	FBgn0031649	2L	hoe2-RA	1.07E-21	1.32E-09	3.31E-74	4.13E-51
FBtr0079079	FBgn0031702	2L	fusl-RA	5.61E-13	1.88E-09	1.38E-25	6.26E-21
FBtr0110799	FBgn0031897	2L	CG13784-RC	3.17E-09	8.74E-27	1.33E-07	8.75E-24
FBtr0114370	FBgn0031414	2L	eys-RC	1.91E-20	8.71E-07	0.00E+00	0.00E+00
FBtr0077816	FBgn0031381	2L	Npc2a-RA	1.98E-51	4.48E-14	3.16E-36	1.00E-06
FBtr0078159	FBgn0031220	2L	CG4822-RB	5.30E-09	1.15E-06	2.40E-29	1.13E-25
FBtr0077488	FBgn0051959	2L	CG31959-RB	5.10E-07	1.57E-06	2.42E-09	1.01E-08
FBtr0273186	FBgn0032109	2L	CG17005-RB	6.10E-08	1.64E-06	7.83E-16	4.66E-14
FBtr0273404	FBgn0032943	2L	Tsp39D-RB	8.49E-10	1.96E-06	1.57E-20	7.94E-16
FBtr0080959	FBgn0040985	2L	CG6115-RA	9.03E-22	1.15E-13	4.68E-12	3.72E-06
FBtr0079477	FBgn0041181	2L	TepIII-RA	8.48E-08	2.13E-11	5.24E-06	3.81E-09
FBtr0080856	FBgn0024734	2L	PRL-1-RB	4.10E-08	3.34E-18	7.34E-06	1.47E-14
FBtr0077647	FBgn0031490	2L	CG17264-RA	1.04E-15	2.28E-09	1.00E-10	1.53E-05
FBtr0080294	FBgn0032402	2L	CG14945-RB	5.03E-09	1.49E-05	2.56E-15	8.85E-11
FBtr0077748	FBgn0041337	2L	Cyp309a2-RA	3.11E-06	2.18E-05	2.16E-105	1.92E-105
FBtr0080291	FBgn0014019	2L	Rh5-RA	2.20E-15	1.67E-04	1.59E-76	3.18E-49
FBtr0079306	FBgn0025777	2L	homer-RA	6.78E-11	1.70E-04	6.06E-71	5.45E-54
FBtr0300456	FBgn0031694	2L	Cyp4ac2-RB	7.13E-12	1.96E-15	2.55E-04	3.00E-06
FBtr0077544	FBgn0031563	2L	CG10031-RA	2.01E-08	2.90E-04	1.31E-17	2.29E-11

Table s3.6 (continued)

FBtr#	FBgn#	arm	name	*p*-values			
				Z30-FR	Z56-FR	Z30-CS	Z56-CS
FBtr0079475	FBgn0040299	2L	Myo28B1-RA	3.21E-06	2.95E-04	2.38E-28	1.23E-24
FBtr0080923	FBgn0032615	2L	CG6012-RA	6.90E-07	2.67E-13	3.57E-04	2.02E-09
FBtr0290078	FBgn0000256	2L	capu-RF	6.36E-17	1.61E-11	1.43E-07	4.90E-04
FBtr0079849	FBgn0051710	2L	CG31710-RA	1.66E-04	7.79E-05	1.04E-03	6.09E-04
FBtr0301695	FBgn0032549	2L	CG4650-RB	1.58E-07	1.79E-06	2.42E-04	1.27E-03
FBtr0081420	FBgn0032889	2L	CG9331-RC	1.05E-03	1.07E-05	5.12E-17	3.10E-22
FBtr0089956	FBgn0032469	2L	CG9932-RA	1.24E-27	6.62E-20	2.35E-07	1.54E-03
FBtr0079177	FBgn0001942	2L	eIF-4a-RB	1.60E-44	4.85E-08	2.78E-32	1.64E-03
FBtr0079038	FBgn0053113	2L	Rtnl1-RF	1.44E-39	3.04E-15	6.46E-18	1.83E-03
FBtr0078086	FBgn0031258	2L	CG4297-RB	1.74E-05	1.65E-03	2.08E-07	5.12E-05
FBtr0301235	FBgn0031738	2L	CG9171-RD	8.97E-09	1.86E-03	1.86E-12	9.13E-06
FBtr0079649	FBgn0032029	2L	CG17292-RA	5.29E-07	2.13E-03	2.97E-11	2.20E-06
FBtr0077418	FBgn0031627	2L	CG15630-RA	2.12E-04	2.46E-03	7.95E-24	4.98E-22
FBtr0100327	FBgn0032536	2L	Ance-3-RB	1.04E-03	2.50E-03	8.45E-05	1.95E-04
FBtr0081069	FBgn0032685	2L	CG10211-RA	5.82E-17	6.26E-21	4.72E-03	2.44E-04
FBtr0080865	FBgn0032585	2L	CG4580-RA	5.00E-03	1.21E-05	5.91E-03	1.28E-05
FBtr0077796	FBgn0014010	2L	Rab5-RC	6.45E-07	1.38E-03	7.22E-06	7.48E-03
FBtr0100293	FBgn0022893	2L	Df31-RF	5.16E-18	5.65E-10	1.51E-07	8.56E-03
FBtr0079842	FBgn0032135	2L	GlcAT-S-RB	5.72E-05	6.62E-03	8.84E-05	9.39E-03
FBtr0086728	FBgn0034331	2R	CG15067-RA	0.00E+00	0.00E+00	0.00E+00	3.22E-289
FBtr0086664	FBgn0025583	2R	IM2-RA	0.00E+00	0.00E+00	1.17E-275	3.29E-124
FBtr0087829	FBgn0004435	2R	Galpha49B-RA	1.10E-77	3.70E-91	1.43E-296	0.00E+00
FBtr0086669	FBgn0034335	2R	GstE1-RA	1.04E-85	8.57E-70	3.93E-108	1.28E-90
FBtr0086729	FBgn0034328	2R	IM23-RA	1.58E-304	5.20E-69	0.00E+00	3.12E-298
FBtr0086477	FBgn0034470	2R	Obp56d-RA	5.32E-64	1.30E-102	3.05E-215	5.89E-289
FBtr0087653	FBgn0041579	2R	AttC-RA	0.00E+00	6.61E-72	0.00E+00	7.77E-58
FBtr0087747	FBgn0033820	2R	CG4716-RA	8.70E-136	1.02E-50	0.00E+00	0.00E+00
FBtr0300178	FBgn0004919	2R	gol-RC	9.34E-44	1.44E-53	3.38E-99	1.61E-115
FBtr0086325	FBgn0034480	2R	CG16898-RA	1.03E-43	2.25E-91	3.42E-180	6.61E-266
FBtr0071535	FBgn0003748	2R	Treh-RE	9.42E-125	6.75E-118	2.75E-46	1.94E-40
FBtr0086026	FBgn0033054	2R	CG14591-RB	1.35E-28	3.95E-31	5.59E-178	3.81E-190
FBtr0299943	FBgn0259682	2R	CG42351-RC	7.10E-32	1.27E-26	1.13E-204	1.04E-197
FBtr0072073	FBgn0004795	2R	retn-RB	3.47E-27	3.53E-25	3.18E-56	3.22E-54
FBtr0086621	FBgn0034407	2R	DptB-RA	0.00E+00	5.04E-118	4.89E-190	1.43E-22
FBtr0071580	FBgn0003162	2R	Pu-RA	4.20E-35	8.93E-21	1.11E-50	2.03E-33
FBtr0087386	FBgn0014865	2R	Mtk-RA	0.00E+00	1.55E-31	0.00E+00	3.06E-19
FBtr0300942	FBgn0041581	2R	AttB-RB	4.60E-81	3.14E-22	5.18E-68	2.04E-15
FBtr0086665	FBgn0040736	2R	IM3-RA	0.00E+00	1.08E-186	7.89E-72	1.25E-14
FBtr0300381	FBgn0050083	2R	CG30083-RB	1.34E-14	3.36E-14	1.16E-17	2.47E-17
FBtr0088640	FBgn0011286	2R	Rya-r44F-RA	9.05E-46	2.79E-39	1.13E-17	3.43E-13
FBtr0071821	FBgn0025878	2R	wrapper-RA	2.89E-23	4.26E-15	2.76E-19	6.72E-12
FBtr0086919	FBgn0034221	2R	CG10764-RA	2.15E-17	9.31E-15	5.08E-14	9.55E-12
FBtr0114522	FBgn0050054	2R	CG30054-RD	3.58E-20	3.15E-11	4.75E-90	4.97E-72
FBtr0086058	FBgn0000099	2R	ap-RA	1.08E-10	1.65E-11	9.66E-21	2.63E-22
FBtr0086620	FBgn0004240	2R	Dpt-RA	5.67E-260	1.26E-93	5.05E-100	2.02E-10
FBtr0072304	FBgn0035020	2R	CG13585-RB	7.34E-19	3.26E-20	3.03E-08	7.10E-09

Table s3.6 (continued)

FBtr#	FBgn#	arm	name	*p*-values			
				Z30-FR	Z56-FR	Z30-CS	Z56-CS
FBtr0273356	FBgn0034928	2R	CG13562-RB	4.37E-19	7.61E-14	4.52E-12	9.39E-08
FBtr0088863	FBgn0013307	2R	Odc1-RA	3.09E-12	2.71E-09	1.82E-10	1.01E-07
FBtr0087893	FBgn0033710	2R	CG17739-RA	1.16E-32	2.63E-07	4.60E-134	1.73E-75
FBtr0088337	FBgn0033502	2R	CG12910-RA	9.11E-20	2.77E-07	5.89E-20	2.04E-07
FBtr0088554	FBgn0028473	2R	CG8801-RA	7.55E-61	3.46E-07	3.96E-230	2.87E-104
FBtr0086266	FBgn0050148	2R	CG30148-RA	6.06E-08	7.68E-07	5.22E-20	1.53E-18
FBtr0086727	FBgn0040733	2R	CG15068-RA	2.36E-13	1.48E-06	1.16E-15	3.18E-08
FBtr0300874	FBgn0034990	2R	CG11406-RC	2.69E-09	1.64E-06	1.58E-10	1.71E-07
FBtr0086335	FBgn0034475	2R	Obp56h-RA	2.01E-06	1.82E-19	6.33E-12	6.09E-29
FBtr0071546	FBgn0003391	2R	shg-RA	2.19E-09	2.79E-06	1.53E-37	8.31E-32
FBtr0085991	FBgn0050431	2R	CG30431-RA	4.94E-11	3.16E-06	8.60E-32	1.50E-23
FBtr0087005	FBgn0010226	2R	GstS1-RB	5.03E-62	2.15E-21	1.02E-32	5.28E-06
FBtr0301668	FBgn0034728	2R	rad50-RD	5.34E-11	7.05E-12	7.42E-06	2.95E-06
FBtr0086674	FBgn0063494	2R	GstE6-RA	5.54E-06	2.85E-05	6.61E-67	9.43E-67
FBtr0086810	FBgn0034293	2R	CG14495-RA	1.69E-05	3.14E-05	2.66E-07	4.44E-07
FBtr0087920	FBgn0033728	2R	Cpr49Ae-RA	1.02E-31	5.62E-22	3.45E-10	7.10E-05
FBtr0088376	FBgn0033458	2R	CG18446-RA	3.24E-07	3.41E-07	1.19E-04	1.33E-04
FBtr0086034	FBgn0027507	2R	CG1344-RA	4.67E-06	1.27E-07	1.25E-04	4.44E-06
FBtr0087346	FBgn0023441	2R	fus-RE	1.25E-05	1.44E-04	1.31E-06	1.79E-05
FBtr0087748	FBgn0033821	2R	CG10799-RA	1.49E-06	1.80E-04	4.30E-26	3.36E-22
FBtr0071867	FBgn0050269	2R	CG30269-RA	4.45E-12	7.75E-09	6.55E-07	1.96E-04
FBtr0086309	FBgn0004364	2R	18w-RA	1.07E-14	9.97E-15	1.36E-04	2.31E-04
FBtr0087121	FBgn0034141	2R	CG8311-RA	7.58E-27	1.29E-14	1.73E-11	3.88E-04
FBtr0088412	FBgn0004907	2R	14-3-3zeta-RB	8.54E-16	4.44E-04	1.39E-37	2.26E-17
FBtr0112929	FBgn0027596	2R	CG10249-RD	1.27E-08	4.89E-13	5.25E-04	8.75E-07
FBtr0112405	FBgn0085241	2R	CG34212-RA	1.09E-19	4.39E-24	8.05E-04	1.46E-05
FBtr0086673	FBgn0063495	2R	GstE5-RA	4.29E-16	4.27E-14	8.26E-05	1.23E-03
FBtr0087383	FBgn0026370	2R	SRPK-RA	7.71E-13	1.43E-17	1.24E-03	7.94E-06
FBtr0100605	FBgn0004399	2R	psq-RI	4.31E-26	9.39E-77	1.26E-03	1.14E-28
FBtr0100388	FBgn0083919	2R	Zasp52-RF	1.35E-34	3.42E-16	6.67E-14	1.56E-03
FBtr0112596	FBgn0085400	2R	CG34371-RA	1.46E-17	3.96E-16	2.14E-04	1.73E-03
FBtr0086966	FBgn0034179	2R	CG6805-RA	1.22E-03	8.87E-07	6.73E-08	5.92E-13
FBtr0071534	FBgn0034580	2R	Cht8-RA	1.13E-08	1.55E-03	8.18E-13	3.40E-06
FBtr0088915	FBgn0050492	2R	CG30492-RC	3.12E-14	1.66E-03	3.00E-152	3.10E-112
FBtr0086593	FBgn0034417	2R	CG15117-RA	6.76E-04	1.87E-03	3.83E-06	1.16E-05
FBtr0086044	FBgn0033039	2R	gp210-RA	2.77E-03	3.17E-03	7.35E-20	9.10E-21
FBtr0086164	FBgn0033115	2R	CG9460-RA	1.40E-09	6.43E-08	3.27E-04	4.20E-03
FBtr0086306	FBgn0003114	2R	plu-RA	5.00E-03	4.26E-03	5.91E-03	4.97E-03
FBtr0086647	FBgn0034380	2R	CG15087-RA	4.37E-03	6.54E-03	3.63E-03	4.80E-03
FBtr0088428	FBgn0033482	2R	CG1371-RA	5.40E-03	7.09E-04	7.41E-38	1.71E-43
FBtr0087042	FBgn0034162	2R	CG6426-RA	7.20E-35	1.58E-16	4.52E-12	9.61E-03
FBtr0072121	FBgn0034871	2R	CG3906-RA	1.21E-09	9.18E-03	6.10E-22	2.58E-10
FBtr0086662	FBgn0034329	2R	IM1-RA	0.00E+00	9.30E-141	2.94E-209	5.27E-73
FBtr0076599	FBgn0000121	3L	Arr2-RA	0.00E+00	0.00E+00	0.00E+00	0.00E+00
FBtr0073073	FBgn0010381	3L	Drs-RA	0.00E+00	0.00E+00	0.00E+00	1.39E-117
FBtr0074979	FBgn0036876	3L	CG9451-RA	8.29E-162	1.29E-107	7.02E-160	9.79E-106

Table s3.6 (continued)

FBtr#	FBgn#	arm	name	*p*-values			
				Z30-FR	Z56-FR	Z30-CS	Z56-CS
FBtr0072703	FBgn0035227	3L	CG12090-RA	1.39E-85	1.40E-72	1.27E-108	2.10E-94
FBtr0076093	FBgn0036165	3L	chrb-RC	4.17E-75	1.87E-97	6.06E-60	1.77E-79
FBtr0075338	FBgn0003250	3L	Rh4-RA	2.04E-156	3.29E-59	2.46E-185	4.88E-78
FBtr0076452	FBgn0035982	3L	CG4461-RA	1.62E-50	6.88E-52	7.42E-75	2.58E-77
FBtr0073237	FBgn0041630	3L	Hexo1-RD	8.50E-77	2.56E-39	8.66E-111	1.75E-65
FBtr0076559	FBgn0035943	3L	CG5653-RA	1.37E-72	6.63E-44	6.50E-67	3.82E-39
FBtr0075174	FBgn0052185	3L	CG32185-RA	2.06E-71	4.95E-39	5.10E-109	3.92E-70
FBtr0073061	FBgn0052282	3L	dro4-RA	0.00E+00	0.00E+00	1.83E-37	7.16E-63
FBtr0075426	FBgn0011693	3L	Pdh-RA	4.28E-282	1.71E-205	1.91E-73	2.36E-34
FBtr0075553	FBgn0000565	3L	Eip71CD-RA	2.20E-69	6.47E-133	4.68E-34	3.05E-81
FBtr0076882	FBgn0035766	3L	eco-RA	0.00E+00	1.25E-159	2.00E-135	6.07E-33
FBtr0075348	FBgn0043578	3L	PGRP-SB1-RA	7.65E-161	5.30E-31	6.85E-187	1.76E-43
FBtr0076466	FBgn0052043	3L	CG32043-RA	8.68E-74	4.42E-142	5.60E-31	3.63E-78
FBtr0076119	FBgn0036203	3L	Muc68D-RB	2.20E-34	2.81E-29	1.31E-55	1.03E-49
FBtr0072967	FBgn0035344	3L	Cyp4d20-RA	7.07E-41	3.03E-49	1.21E-27	3.69E-34
FBtr0299778	FBgn0259224	3L	CG42324-RD	8.28E-45	1.75E-65	2.83E-23	3.38E-38
FBtr0076027	FBgn0022959	3L	yps-RA	7.48E-78	1.47E-244	1.34E-22	2.86E-133
FBtr0112601	FBgn0085402	3L	Ect4-RG	2.47E-80	7.78E-43	1.12E-51	2.95E-22
FBtr0075511	FBgn0036547	3L	CG17032-RA	1.04E-41	8.15E-39	1.74E-21	5.19E-19
FBtr0074820	FBgn0036945	3L	CG6981-RB	1.97E-61	8.38E-47	1.52E-28	4.26E-18
FBtr0075369	FBgn0042201	3L	Nplp3-RA	5.52E-64	2.44E-16	4.70E-199	2.65E-106
FBtr0075512	FBgn0036549	3L	CG10516-RA	4.49E-17	3.65E-16	1.81E-39	8.02E-39
FBtr0075014	FBgn0036862	3L	CG9619-RA	3.82E-48	2.08E-15	7.04E-81	2.38E-36
FBtr0074961	FBgn0022774	3L	Oat-RA	4.13E-15	2.68E-15	2.95E-38	2.02E-39
FBtr0076991	FBgn0020642	3L	Lcp65Ac-RA	1.68E-30	1.37E-18	8.00E-25	4.38E-14
FBtr0074835	FBgn0004366	3L	rdgC-RD	2.16E-21	8.51E-14	1.39E-60	2.62E-48
FBtr0072891	FBgn0035338	3L	CG13800-RA	5.31E-23	9.51E-13	5.13E-40	2.60E-26
FBtr0072671	FBgn0035207	3L	CG9153-RA	5.00E-23	2.36E-11	9.23E-36	6.14E-21
FBtr0076632	FBgn0052355	3L	CG32355-RA	1.78E-26	3.99E-18	4.27E-18	2.93E-11
FBtr0072727	FBgn0035206	3L	CG9186-RB	1.91E-12	5.20E-16	1.35E-10	6.76E-14
FBtr0072923	FBgn0035346	3L	CG1146-RA	3.29E-37	4.50E-60	5.75E-10	3.23E-22
FBtr0076166	FBgn0036149	3L	CG18490-RB	5.01E-16	9.77E-17	6.57E-09	2.95E-09
FBtr0089478	FBgn0036640	3L	nxf2-RA	1.08E-08	7.70E-09	1.52E-13	5.12E-14
FBtr0075048	FBgn0036833	3L	CG3819-RA	1.68E-11	1.65E-26	1.23E-08	2.83E-22
FBtr0072856	FBgn0002872	3L	mu2-RA	1.22E-13	1.38E-15	4.68E-08	1.80E-09
FBtr0074949	FBgn0004623	3L	Gbeta76C-RA	7.64E-46	1.98E-07	0.00E+00	0.00E+00
FBtr0113178	FBgn0036683	3L	CG14060-RB	2.53E-07	5.47E-09	1.03E-12	3.35E-15
FBtr0112890	FBgn0016797	3L	fz2-RC	4.48E-09	7.44E-12	3.93E-07	1.63E-09
FBtr0075259	FBgn0036673	3L	CG11915-RA	1.24E-06	1.25E-06	1.02E-13	4.74E-14
FBtr0075942	FBgn0036316	3L	CG10960-RB	1.21E-31	5.96E-32	6.81E-07	1.66E-06
FBtr0302087	FBgn0261259	3L	Fhos-RC	8.66E-41	9.63E-29	3.16E-13	2.01E-06
FBtr0078468	FBgn0014362	3L	mub-RA	1.71E-06	7.86E-13	5.64E-16	4.14E-26
FBtr0076798	FBgn0028582	3L	lqf-RE	2.81E-06	1.98E-17	6.48E-76	2.16E-113
FBtr0076567	FBgn0052029	3L	Cpr66D-RA	1.58E-13	2.31E-10	1.14E-08	4.05E-06
FBtr0075471	FBgn0036597	3L	CG4962-RA	6.70E-45	1.80E-36	3.83E-10	6.07E-06
FBtr0075832	FBgn0023095	3L	caps-RA	2.31E-09	7.23E-06	7.65E-14	1.57E-09

Table s3.6 (continued)

FBtr#	FBgn#	arm	name	*p*-values			
				Z30-FR	Z56-FR	Z30-CS	Z56-CS
FBtr0075789	FBgn0036391	3L	CG17364-RB	1.90E-20	1.02E-18	5.20E-07	9.33E-06
FBtr0075457	FBgn0036579	3L	CG5027-RA	8.87E-19	1.03E-09	7.42E-13	1.33E-05
FBtr0072822	FBgn0035246	3L	CG13928-RA	4.22E-26	6.62E-07	2.42E-23	1.52E-05
FBtr0299649	FBgn0259175	3L	ome-RE	5.50E-18	4.84E-12	1.92E-09	3.22E-05
FBtr0078404	FBgn0037074	3L	CG7324-RA	3.72E-05	3.57E-05	1.66E-05	1.33E-05
FBtr0072828	FBgn0035232	3L	CG12099-RB	1.69E-06	5.10E-05	1.88E-06	5.47E-05
FBtr0073252	FBgn0035512	3L	Cpr64Ac-RA	3.01E-19	1.82E-13	5.55E-09	6.57E-05
FBtr0075290	FBgn0011293	3L	a10-RA	5.50E-06	7.72E-05	3.23E-07	5.36E-06
FBtr0074925	FBgn0036910	3L	Cyp305a1-RA	9.98E-11	1.17E-04	3.65E-13	3.30E-06
FBtr0075895	FBgn0036337	3L	CG11255-RA	7.81E-15	1.21E-04	1.33E-17	3.51E-06
FBtr0089420	FBgn0000109	3L	Aprt-RA	2.42E-16	1.57E-17	1.25E-04	5.54E-05
FBtr0077086	FBgn0035620	3L	CG5150-RA	3.00E-07	1.68E-04	3.22E-07	1.82E-04
FBtr0076115	FBgn0036199	3L	Bmcp-RB	2.05E-10	6.67E-08	2.19E-06	2.01E-04
FBtr0076906	FBgn0035734	3L	CG14823-RB	2.48E-71	2.96E-59	8.42E-09	2.20E-04
FBtr0072779	FBgn0067864	3L	Patj-RC	7.53E-10	2.30E-04	1.00E-29	1.45E-19
FBtr0089527	FBgn0036544	3L	CG6114-RA	7.07E-05	2.59E-04	2.50E-27	4.81E-27
FBtr0073329	FBgn0035553	3L	CG13722-RA	2.03E-09	1.62E-08	6.05E-05	3.08E-04
FBtr0075384	FBgn0036620	3L	CG4842-RA	8.28E-13	9.64E-07	3.52E-09	3.33E-04
FBtr0299542	FBgn0036656	3L	CG13026-RB	3.15E-04	3.14E-05	2.30E-10	1.70E-12
FBtr0300426	FBgn0052352	3L	CG32352-RD	2.81E-14	4.69E-04	2.17E-24	6.32E-10
FBtr0076631	FBgn0052353	3L	CG32353-RA	3.32E-05	5.63E-05	3.16E-04	5.36E-04
FBtr0076270	FBgn0036107	3L	CG7949-RA	4.96E-11	2.32E-09	5.77E-05	8.35E-04
FBtr0075399	FBgn0026061	3L	Mipp1-RA	5.10E-11	6.75E-05	2.89E-09	9.90E-04
FBtr0290130	FBgn0036262	3L	CG6910-RB	7.22E-04	5.58E-22	7.89E-32	2.32E-74
FBtr0078454	FBgn0037126	3L	CG14567-RA	9.25E-11	1.26E-03	5.44E-14	1.59E-05
FBtr0075282	FBgn0036697	3L	rogdi-RB	3.41E-04	1.76E-03	3.82E-16	3.69E-15
FBtr0076712	FBgn0035871	3L	CG7188-RB	6.79E-07	1.66E-03	9.20E-07	2.02E-03
FBtr0073285	FBgn0035484	3L	CG11594-RB	1.57E-03	3.48E-14	1.04E-08	9.20E-25
FBtr0076573	FBgn0000358	3L	Cp19-RA	1.57E-03	2.91E-04	2.03E-04	1.72E-05
FBtr0075803	FBgn0036380	3L	CG8757-RA	1.93E-14	2.30E-03	3.36E-53	3.34E-31
FBtr0073106	FBgn0047135	3L	CG32276-RA	1.90E-03	1.67E-03	6.18E-05	3.64E-05
FBtr0076183	FBgn0036152	3L	CG6175-RB	3.58E-07	1.61E-06	8.39E-04	2.84E-03
FBtr0075371	FBgn0036607	3L	CG13059-RA	6.05E-06	4.64E-04	6.70E-05	3.06E-03
FBtr0072630	FBgn0004428	3L	LysE-RA	2.64E-03	3.87E-05	3.14E-03	4.06E-05
FBtr0077044	FBgn0035669	3L	CG6592-RA	2.64E-03	2.76E-03	3.14E-03	3.16E-03
FBtr0078205	FBgn0052425	3L	CG32425-RA	2.54E-09	4.17E-03	7.46E-16	4.69E-07
FBtr0075700	FBgn0036448	3L	mop-RA	3.78E-04	4.63E-03	5.31E-06	1.06E-04
FBtr0089606	FBgn0053493	3L	CG33493-RA	3.72E-09	4.85E-03	5.10E-13	2.72E-05
FBtr0078263	FBgn0040636	3L	CG13255-RA	4.02E-07	3.41E-04	1.79E-05	5.89E-03
FBtr0078354	FBgn0037090	3L	CG7529-RA	3.38E-05	5.27E-03	2.46E-14	1.83E-10
FBtr0078536	FBgn0037186	3L	CG11241-RA	2.33E-10	7.58E-09	7.05E-04	6.49E-03
FBtr0290220	FBgn0035159	3L	CG13896-RB	2.01E-05	7.23E-05	2.15E-03	7.16E-03
FBtr0301435	FBgn0016081	3L	fry-RC	1.98E-07	6.54E-03	4.68E-12	8.13E-06
FBtr0076138	FBgn0086254	3L	CG6084-RB	5.35E-03	2.46E-09	3.59E-08	8.65E-19
FBtr0075437	FBgn0036560	3L	CG5895-RA	2.19E-16	4.78E-06	1.71E-10	8.82E-03
FBtr0075782	FBgn0061515	3L	endos-RA	6.67E-13	6.94E-10	1.60E-04	9.06E-03

Table s3.6 (continued)

FBtr#	FBgn#	arm	name	*p*-values			
				Z30-FR	Z56-FR	Z30-CS	Z56-CS
FBtr0076343	FBgn0025866	3L	CalpB-RA	1.26E-09	9.68E-07	1.25E-04	9.96E-03
FBtr0083857	FBgn0002940	3R	ninaE-RA	0.00E+00	0.00E+00	0.00E+00	0.00E+00
FBtr0085025	FBgn0040606	3R	CG6503-RA	2.77E-227	2.49E-195	0.00E+00	3.16E-293
FBtr0113330	FBgn0040629	3R	CG18673-RB	6.30E-181	9.29E-181	6.70E-170	1.32E-169
FBtr0085513	FBgn0003861	3R	trp-RA	9.23E-128	3.06E-109	0.00E+00	0.00E+00
FBtr0084949	FBgn0000206	3R	boss-RA	1.89E-99	7.80E-93	5.27E-272	1.12E-266
FBtr0082324	FBgn0022359	3R	Sodh-2-RA	3.00E-196	5.32E-160	8.76E-111	6.89E-82
FBtr0084585	FBgn0039151	3R	CG13607-RA	3.78E-54	1.02E-57	0.00E+00	0.00E+00
FBtr0084102	FBgn0038877	3R	CG3308-RA	1.07E-53	4.56E-82	5.48E-57	2.98E-86
FBtr0083966	FBgn0053094	3R	Synd-RB	2.02E-48	2.00E-43	3.09E-54	4.93E-49
FBtr0084336	FBgn0046114	3R	Gclm-RA	8.78E-81	3.40E-50	9.35E-69	1.98E-40
FBtr0085463	FBgn0039682	3R	Obp99c-RA	1.03E-38	1.61E-38	0.00E+00	0.00E+00
FBtr0082505	FBgn0037974	3R	CG12224-RA	5.59E-33	3.16E-41	1.20E-36	4.33E-45
FBtr0085778	FBgn0000313	3R	chp-RA	6.71E-47	3.69E-31	0.00E+00	0.00E+00
FBtr0078593	FBgn0037410	3R	Osi2-RA	2.59E-56	1.68E-35	1.49E-50	9.49E-31
FBtr0078825	FBgn0087005	3R	retinophilin-RA	8.39E-102	2.06E-24	0.00E+00	2.81E-197
FBtr0083154	FBgn0038347	3R	CG18522-RA	1.53E-35	3.60E-24	1.25E-61	5.26E-47
FBtr0273382	FBgn0038651	3R	CG14299-RC	2.17E-26	2.20E-24	1.31E-25	1.15E-23
FBtr0113405	FBgn0051414	3R	CG31414-RB	8.02E-76	1.55E-77	2.20E-21	2.77E-21
FBtr0084303	FBgn0039005	3R	CG6969-RA	2.01E-36	1.69E-21	4.80E-35	2.15E-20
FBtr0078823	FBgn0260462	3R	CG12163-RA	1.34E-64	4.32E-45	1.36E-32	1.07E-18
FBtr0084435	FBgn0039099	3R	CG10157-RA	4.88E-31	1.31E-28	2.38E-19	3.25E-17
FBtr0078642	FBgn0037387	3R	CG1213-RB	6.77E-55	5.58E-56	5.89E-17	9.91E-17
FBtr0091531	FBgn0053555	3R	btsz-RC	5.60E-25	1.91E-19	1.85E-20	2.06E-15
FBtr0084828	FBgn0039319	3R	CG13659-RA	7.93E-30	1.92E-29	1.04E-14	3.01E-14
FBtr0083040	FBgn0051304	3R	CG31304-RA	2.44E-30	4.77E-17	1.44E-26	3.48E-14
FBtr0085460	FBgn0039688	3R	Kul-RA	4.05E-24	5.75E-13	1.45E-70	1.67E-51
FBtr0302143	FBgn0038294	3R	Mf-RG	1.13E-86	2.84E-72	1.91E-20	8.94E-13
FBtr0113289	FBgn0039358	3R	CG5028-RB	4.80E-21	1.46E-18	1.04E-14	1.59E-12
FBtr0082438	FBgn0037935	3R	CG6834-RA	9.80E-160	6.35E-171	1.59E-12	2.09E-14
FBtr0084860	FBgn0051288	3R	CG31288-RA	3.73E-24	1.62E-24	8.97E-12	8.13E-12
FBtr0085830	FBgn0003870	3R	ttk-RD	3.62E-25	8.32E-34	9.22E-12	2.39E-17
FBtr0083538	FBgn0000477	3R	DNaseII-RA	5.47E-112	3.56E-51	5.80E-48	1.48E-11
FBtr0084316	FBgn0040588	3R	CG13841-RA	3.62E-18	3.04E-15	3.81E-14	2.32E-11
FBtr0301977	FBgn0051077	3R	CG31077-RB	1.27E-11	5.62E-11	1.98E-36	4.91E-36
FBtr0083262	FBgn0250823	3R	gish-RB	7.82E-11	8.74E-14	1.43E-19	7.70E-24
FBtr0085832	FBgn0000557	3R	Ef1alpha100E-RA	2.21E-82	3.36E-10	6.80E-180	8.09E-58
FBtr0083585	FBgn0004618	3R	gl-RB	2.82E-16	8.60E-10	1.98E-20	3.02E-13
FBtr0082572	FBgn0010041	3R	GstD5-RA	4.09E-27	4.58E-19	2.46E-16	1.15E-09
FBtr0078744	FBgn0250753	3R	exba-RA	2.70E-27	6.23E-18	6.23E-17	1.26E-09
FBtr0300601	FBgn0260386	3R	mtg-RD	1.61E-12	2.95E-09	4.87E-15	1.21E-11
FBtr0300936	FBgn0027930	3R	MP1-RC	2.59E-09	8.50E-11	1.55E-12	2.17E-14
FBtr0273375	FBgn0051534	3R	CG31534-RC	3.24E-09	6.21E-12	9.96E-10	1.43E-12
FBtr0084459	FBgn0015513	3R	mbc-RA	4.70E-10	1.00E-11	1.95E-08	6.29E-10
FBtr0083978	FBgn0038840	3R	CG5621-RA	1.43E-15	2.67E-12	7.89E-11	4.29E-08
FBtr0085361	FBgn0039628	3R	CG11841-RA	1.87E-44	1.73E-37	5.71E-11	3.41E-07

Table s3.6 (continued)

FBtr#	FBgn#	arm	name	*p*-values			
				Z30-FR	Z56-FR	Z30-CS	Z56-CS
FBtr0083998	FBgn0013995	3R	Calx-RA	1.45E-18	3.40E-07	2.34E-59	8.69E-38
FBtr0084851	FBgn0039326	3R	CG10562-RA	2.70E-08	1.77E-08	3.95E-07	3.63E-07
FBtr0085496	FBgn0051038	3R	CG31038-RD	1.05E-19	4.63E-07	4.18E-22	1.60E-08
FBtr0302187	FBgn0051158	3R	CG31158-RG	2.42E-16	2.79E-08	1.32E-14	4.76E-07
FBtr0111008	FBgn0259685	3R	crb-RB	3.11E-08	6.29E-07	1.10E-17	4.15E-16
FBtr0083146	FBgn0019940	3R	Rh6-RB	1.12E-106	3.10E-58	4.39E-29	9.68E-07
FBtr0082103	FBgn0005585	3R	Crc-RA	1.72E-30	3.32E-06	3.57E-81	2.90E-36
FBtr0078854	FBgn0087012	3R	5-HT2-RA	1.34E-09	1.74E-16	5.35E-06	2.41E-11
FBtr0082104	FBgn0037721	3R	CG9427-RA	5.44E-19	2.11E-10	8.00E-13	6.52E-06
FBtr0081821	FBgn0040524	3R	CG11052-RA	3.14E-08	6.23E-07	7.57E-07	9.85E-06
FBtr0113224	FBgn0037979	3R	CG3532-RB	3.76E-06	3.46E-07	9.30E-06	9.78E-07
FBtr0301147	FBgn0039380	3R	CG5890-RB	9.12E-09	1.03E-05	6.87E-11	1.91E-07
FBtr0083935	FBgn0038820	3R	CG4000-RA	1.13E-297	3.06E-72	4.05E-126	1.47E-05
FBtr0113236	FBgn0038286	3R	CG6966-RB	8.73E-11	1.76E-05	8.61E-13	7.12E-07
FBtr0083730	FBgn0038680	3R	Cyp12a5-RA	2.04E-05	4.20E-10	2.64E-19	2.01E-28
FBtr0082060	FBgn0043791	3R	CG8147-RA	9.26E-69	3.38E-05	1.26E-97	1.03E-16
FBtr0082564	FBgn0003651	3R	svp-RB	2.20E-11	6.34E-07	6.31E-09	4.54E-05
FBtr0082405	FBgn0037895	3R	CG6723-RA	1.01E-08	4.49E-05	1.27E-14	8.84E-10
FBtr0083179	FBgn0026616	3R	alpha-Man-IIb-RA	2.27E-10	7.68E-05	1.05E-30	8.93E-21
FBtr0290056	FBgn0051145	3R	CG31145-RC	3.24E-05	3.92E-06	7.66E-05	1.04E-05
FBtr0084153	FBgn0038914	3R	fit-RA	1.82E-13	6.04E-95	8.43E-05	1.25E-66
FBtr0085419	FBgn0039625	3R	beta4GalNAcTB-RA	9.42E-06	9.17E-06	9.30E-05	9.56E-05
FBtr0078828	FBgn0037298	3R	CG2604-RA	1.03E-04	3.14E-05	3.18E-22	2.17E-24
FBtr0290200	FBgn0039817	3R	CG15553-RB	2.40E-06	3.32E-11	1.71E-04	1.31E-08
FBtr0081729	FBgn0037447	3R	Neurochondrin-RA	1.46E-04	1.90E-07	6.78E-16	4.82E-22
FBtr0083781	FBgn0038722	3R	Nup58-RA	1.15E-05	2.98E-04	1.93E-07	9.85E-06
FBtr0083642	FBgn0004652	3R	fru-RC	1.32E-05	3.80E-07	3.27E-04	1.54E-05
FBtr0083237	FBgn0038395	3R	CG10407-RA	4.24E-07	4.64E-04	1.38E-18	1.09E-13
FBtr0082504	FBgn0037975	3R	CG3397-RA	2.24E-05	4.94E-04	2.93E-07	1.06E-05
FBtr0081942	FBgn0037627	3R	CG13318-RA	9.83E-13	1.02E-07	1.19E-07	6.13E-04
FBtr0114607	FBgn0014001	3R	Pak-RD	1.77E-05	2.70E-05	5.13E-04	7.82E-04
FBtr0084455	FBgn0039114	3R	Lsd-1-RA	9.34E-22	8.28E-04	2.00E-86	6.26E-44
FBtr0084318	FBgn0039023	3R	CG4723-RA	8.11E-04	3.95E-04	3.46E-05	1.04E-05
FBtr0301390	FBgn0039528	3R	dsd-RB	1.02E-11	1.03E-08	1.21E-05	1.40E-03
FBtr0084881	FBgn0011666	3R	msi-RB	1.68E-04	1.32E-03	1.54E-05	1.49E-04
FBtr0089953	FBgn0026620	3R	tacc-RC	1.14E-03	1.45E-05	3.81E-16	3.63E-21
FBtr0084304	FBgn0039006	3R	Cyp6d4-RA	4.29E-04	7.21E-04	1.10E-03	1.74E-03
FBtr0082865	FBgn0016672	3R	Ipp-RA	1.55E-21	1.79E-03	5.85E-24	2.38E-04
FBtr0085126	FBgn0051064	3R	CG31064-RE	1.82E-03	7.67E-04	6.70E-06	1.34E-06
FBtr0083838	FBgn0040571	3R	CG17193-RA	1.47E-05	2.44E-03	4.50E-17	3.96E-13
FBtr0302023	FBgn0039054	3R	CG13830-RD	5.07E-41	3.82E-85	2.43E-03	4.28E-19
FBtr0299661	FBgn0259178	3R	5PtaseI-RC	2.17E-03	1.98E-04	6.92E-04	3.29E-05
FBtr0112908	FBgn0025574	3R	Pli-RC	4.45E-04	2.78E-03	6.37E-08	7.42E-07
FBtr0083225	FBgn0038398	3R	sxe2-RA	6.49E-16	1.13E-06	4.81E-10	3.73E-03
FBtr0083695	FBgn0038654	3R	CG14298-RA	1.41E-06	2.41E-04	6.25E-05	5.34E-03
FBtr0084985	FBgn0051324	3R	CG31324-RA	4.03E-03	1.45E-03	3.88E-03	1.21E-03

Table s3.6 (continued)

FBtr#	FBgn#	arm	name	*p*-values			
				Z30-FR	Z56-FR	Z30-CS	Z56-CS
FBtr0083985	FBgn0044810	3R	TotX-RA	9.51E-07	5.31E-03	1.03E-06	6.28E-03
FBtr0113205	FBgn0037549	3R	CG7878-RA	2.86E-05	8.60E-04	3.29E-04	6.63E-03
FBtr0085348	FBgn0053203	3R	CG33203-RC	2.08E-08	6.15E-03	1.89E-28	4.08E-17
FBtr0082434	FBgn0002906	3R	mus309-RA	3.03E-03	6.86E-04	7.61E-03	1.80E-03
FBtr0082778	FBgn0038129	3R	CG8449-RA	6.32E-05	8.17E-03	1.47E-05	3.14E-03
FBtr0085744	FBgn0002413	3R	dco-RC	1.47E-13	4.28E-16	9.86E-03	1.72E-03
FBtr0301809	FBgn0058198	3R Het	CG40198-RB	2.93E-10	6.01E-06	9.74E-07	2.21E-03
FBtr0089194	FBgn0039927	4	CG11155-RB	8.20E-05	3.35E-03	6.43E-32	2.66E-28
FBtr0113933	FBgn0085520	U	CG40801-RA	3.11E-31	6.69E-25	3.63E-30	6.10E-24
FBtr0301475	FBgn0004625	X	norpA-RE	5.35E-200	9.12E-142	0.00E+00	0.00E+00
FBtr0077183	FBgn0052523	X	CG32523-RA	4.99E-252	8.51E-189	1.66E-167	1.28E-113
FBtr0073613	FBgn0030332	X	CG9360-RA	1.32E-302	4.13E-249	4.38E-141	1.24E-101
FBtr0100644	FBgn0030262	X	Vago-RC	5.82E-34	3.44E-35	8.10E-47	1.08E-48
FBtr0071235	FBgn0024943	X	PIP82-RA	1.31E-68	5.80E-33	7.31E-276	2.64E-205
FBtr0300200	FBgn0259918	X	inaF-B-RA	3.88E-52	4.63E-31	0.00E+00	3.98E-281
FBtr0074008	FBgn0026428	X	HDAC6-RA	1.14E-91	2.47E-56	4.67E-59	7.58E-31
FBtr0074364	FBgn0030773	X	CG9676-RA	0.00E+00	0.00E+00	1.35E-183	3.82E-21
FBtr0073923	FBgn0030555	X	Fbxl4-RA	9.37E-25	4.37E-20	9.84E-57	1.23E-50
FBtr0074097	FBgn0030694	X	CG15602-RA	2.00E-29	9.17E-25	1.66E-22	2.87E-18
FBtr0071270	FBgn0011661	X	Moe-RB	1.82E-39	1.24E-43	1.05E-15	1.05E-17
FBtr0070463	FBgn0040387	X	PsGEF-RA	2.45E-17	3.90E-14	5.17E-34	6.80E-30
FBtr0070443	FBgn0040335	X	CG10260-RB	3.05E-32	7.51E-13	5.60E-71	7.41E-41
FBtr0073488	FBgn0001624	X	dlg1-RB	4.59E-63	3.17E-89	8.89E-13	3.11E-24
FBtr0301532	FBgn0003218	X	rdgB-RE	2.77E-41	6.78E-34	9.85E-17	9.95E-12
FBtr0300465	FBgn0259994	X	CG42492-RC	2.53E-13	1.40E-11	1.84E-17	1.36E-15
FBtr0073494	FBgn0001145	X	Gs2-RB	1.79E-37	3.10E-11	1.94E-226	9.86E-157
FBtr0300759	FBgn0029930	X	CG12541-RC	1.27E-11	9.75E-15	1.25E-10	2.07E-13
FBtr0070379	FBgn0000382	X	csw-RB	5.31E-13	3.44E-14	1.73E-10	1.82E-11
FBtr0071005	FBgn0027108	X	inx2-RA	8.25E-21	1.83E-12	4.42E-18	2.60E-10
FBtr0070808	FBgn0029799	X	CG15772-RA	2.38E-28	2.67E-23	5.55E-14	3.03E-10
FBtr0074721	FBgn0031023	X	CG14200-RA	1.20E-32	3.70E-25	8.48E-14	9.63E-09
FBtr0070793	FBgn0029769	X	CG3239-RA	8.32E-09	5.67E-11	5.23E-47	1.25E-53
FBtr0073527	FBgn0014133	X	bif-RC	7.27E-21	1.51E-08	1.42E-31	6.97E-16
FBtr0070428	FBgn0005670	X	Cyp4d1-RA	2.27E-08	1.05E-08	7.22E-27	5.11E-28
FBtr0070777	FBgn0029766	X	CG15784-RA	1.18E-281	3.72E-263	3.47E-14	3.88E-08
FBtr0290086	FBgn0031042	X	CG14221-RB	1.10E-09	5.73E-08	3.97E-12	3.28E-10
FBtr0073979	FBgn0030593	X	CG9512-RA	5.38E-31	5.45E-30	7.11E-09	7.33E-08
FBtr0070978	FBgn0003390	X	shf-RA	7.30E-08	1.65E-09	2.28E-16	3.21E-19
FBtr0073565	FBgn0030339	X	Cyp28c1-RA	2.64E-10	4.85E-09	6.15E-08	8.30E-07
FBtr0112628	FBgn0259108	X	futsch-RC	4.74E-09	9.10E-19	1.32E-06	5.65E-15
FBtr0074028	FBgn0030615	X	Cyp4s3-RA	1.47E-14	7.30E-13	9.02E-08	2.52E-06
FBtr0073653	FBgn0030398	X	Cpr11B-RA	6.27E-45	2.24E-26	4.07E-17	3.01E-06
FBtr0074694	FBgn0030997	X	CG7990-RB	3.30E-09	2.82E-06	1.30E-13	4.85E-10
FBtr0301703	FBgn0040089	X	meso18E-RB	2.04E-06	7.23E-06	3.45E-06	1.12E-05
FBtr0299526	FBgn0027279	X	l(1)G0196-RK	3.15E-07	5.24E-07	1.28E-05	2.08E-05

Table s3.6 (continued)

FBtr#	FBgn#	arm	name	*p*-values			
				Z30-FR	Z56-FR	Z30-CS	Z56-CS
FBtr0074634	FBgn0004462	X	Pk17E-RA	1.76E-05	1.30E-05	4.33E-09	1.91E-09
FBtr0070137	FBgn0040382	X	CG5273-RB	3.18E-80	5.16E-15	1.81E-54	2.74E-05
FBtr0074299	FBgn0030755	X	CG9906-RA	3.31E-06	8.40E-05	8.79E-10	3.73E-08
FBtr0071020	FBgn0029935	X	CG4615-RA	5.58E-10	1.17E-04	1.84E-21	3.45E-13
FBtr0071398	FBgn0052695	X	CG32695-RA	1.23E-16	1.42E-10	7.41E-09	1.31E-04
FBtr0074047	FBgn0030660	X	CG8097-RA	5.29E-05	1.67E-04	1.45E-06	4.08E-06
FBtr0074388	FBgn0000163	X	baz-RA	4.73E-05	1.96E-05	1.63E-04	6.81E-05
FBtr0070352	FBgn0023511	X	Edem1-RC	1.85E-08	2.18E-04	3.49E-37	1.40E-28
FBtr0089803	FBgn0052656	X	Muc11A-RA	2.24E-04	1.76E-05	4.96E-05	3.01E-06
FBtr0071309	FBgn0030105	X	CG15369-RA	4.27E-05	4.41E-04	1.21E-05	8.21E-05
FBtr0089465	FBgn0052823	X	Sdic3-RB	1.41E-04	5.27E-05	8.16E-04	2.86E-04
FBtr0074635	FBgn0030960	X	CG7053-RA	2.46E-08	4.48E-05	2.40E-06	1.49E-03
FBtr0110791	FBgn0025633	X	CG13366-RB	2.71E-04	1.68E-03	1.10E-08	9.98E-08
FBtr0070840	FBgn0029800	X	lin-52-RA	1.12E-07	2.30E-04	2.25E-06	1.92E-03
FBtr0301058	FBgn0025643	X	CG3588-RE	8.41E-13	8.01E-07	6.95E-08	2.04E-03
FBtr0071058	FBgn0040923	X	CG11368-RA	5.93E-39	2.65E-46	1.80E-03	5.87E-05
FBtr0070480	FBgn0024997	X	CG2681-RA	9.06E-04	2.50E-03	7.67E-15	1.70E-14
FBtr0074579	FBgn0030912	X	CG6023-RA	1.56E-06	1.63E-05	5.35E-04	3.28E-03
FBtr0071444	FBgn0028480	X	CG17841-RA	2.38E-03	2.12E-03	1.08E-51	6.38E-55
FBtr0070147	FBgn0025620	X	CG13360-RA	1.26E-05	3.28E-03	1.36E-45	3.62E-39
FBtr0073818	FBgn0030518	X	CG11134-RA	7.73E-04	3.38E-03	5.71E-08	3.52E-07
FBtr0070930	FBgn0026015	X	Top3beta-RA	4.64E-09	4.00E-03	1.56E-11	1.61E-04
FBtr0089702	FBgn0030657	X	cerv-RA	3.02E-06	1.44E-05	1.61E-03	5.25E-03
FBtr0070436	FBgn0260753	X	pdfr-RA	1.97E-12	1.57E-11	2.08E-03	8.82E-03
FBtr0070254	FBgn0029580	X	CG14778-RA	6.12E-03	1.84E-03	1.19E-03	2.84E-04
FBtr0074626	FBgn0030929	X	CG15043-RA	6.99E-03	5.31E-03	2.75E-08	5.60E-09
FBtr0074531	FBgn0030890	X	CG7536-RA	2.27E-03	9.49E-03	1.50E-03	6.67E-03

Table s3.7 M>Z DEGs based on FDR correction

FBtr#	FBgn#	arm	name	*p*-values			
				Z30-FR	Z56-FR	Z30-CS	Z56-CS
FBtr0079806	FBgn0012036	2L	Aldh-RA	0.00E+00	0.00E+00	0.00E+00	0.00E+00
FBtr0080030	FBgn0027611	2L	CG6206-RA	0.00E+00	0.00E+00	0.00E+00	0.00E+00
FBtr0100359	FBgn0001125	2L	Got2-RC	3.45E-197	2.68E-214	0.00E+00	0.00E+00
FBtr0078025	FBgn0002563	2L	Lsp1beta-RA	2.38E-132	2.03E-146	6.07E-158	1.56E-174
FBtr0079431	FBgn0000053	2L	ade3-RA	8.14E-120	4.98E-170	0.00E+00	0.00E+00
FBtr0080449	FBgn0027586	2L	CG5867-RA	2.30E-88	1.55E-135	4.80E-191	9.47E-264
FBtr0078115	FBgn0001142	2L	Gs1-RC	2.24E-80	6.92E-77	3.80E-187	4.14E-187
FBtr0079073	FBgn0031701	2L	TotM-RA	2.25E-62	1.77E-70	4.91E-187	6.97E-209
FBtr0079857	FBgn0028479	2L	CG4389-RB	9.47E-75	1.40E-49	2.24E-72	1.26E-47
FBtr0077957	FBgn0031306	2L	CG4577-RA	1.24E-38	4.67E-45	3.34E-118	2.08E-133
FBtr0080989	FBgn0032652	2L	CG6870-RA	2.98E-35	2.47E-82	5.80E-232	0.00E+00
FBtr0079147	FBgn0001128	2L	Gpdh-RC	0.00E+00	0.00E+00	1.91E-27	4.31E-51
FBtr0077731	FBgn0019830	2L	colt-RA	1.70E-24	1.52E-36	3.07E-26	1.09E-38
FBtr0080861	FBgn0020415	2L	Idgf2-RA	5.03E-147	1.28E-168	1.82E-24	1.87E-30
FBtr0080281	FBgn0005664	2L	Cry-RA	9.63E-24	5.62E-27	2.49E-21	3.38E-24
FBtr0079894	FBgn0032167	2L	CG5853-RA	7.10E-81	1.42E-62	4.14E-34	2.45E-21
FBtr0077483	FBgn0031589	2L	CG3714-RE	3.89E-23	3.64E-33	9.65E-20	6.52E-29
FBtr0079066	FBgn0031693	2L	Cyp4ac1-RA	3.05E-24	1.75E-31	2.52E-19	1.09E-25
FBtr0077863	FBgn0040718	2L	CG15353-RA	2.71E-18	3.96E-22	1.63E-22	6.46E-27
FBtr0079925	FBgn0015035	2L	Cyp4e3-RA	6.30E-20	3.11E-18	5.73E-147	3.54E-152
FBtr0079471	FBgn0031925	2L	Cyp4d21-RA	1.52E-17	5.93E-21	3.27E-16	2.85E-19
FBtr0080042	FBgn0032253	2L	CG5322-RA	2.69E-30	6.75E-33	8.29E-16	3.33E-17
FBtr0077391	FBgn0031645	2L	CG3036-RA	1.48E-15	1.17E-34	3.30E-24	1.14E-47
FBtr0080905	FBgn0086783	2L	Mhc-RL	2.16E-15	4.08E-45	1.74E-56	1.60E-109
FBtr0078042	FBgn0000442	2L	Pkg21D-RA	4.48E-18	3.85E-16	1.74E-16	1.11E-14
FBtr0079637	FBgn0031998	2L	CG8451-RA	3.23E-70	2.96E-55	6.63E-23	9.37E-14
FBtr0080050	FBgn0032237	2L	CG5362-RA	6.13E-15	3.47E-17	2.47E-13	1.96E-15
FBtr0081138	FBgn0051793	2L	CG31793-RA	2.27E-27	1.79E-29	5.35E-12	7.04E-13
FBtr0079106	FBgn0004620	2L	GluRIIA-RI	6.43E-12	7.07E-15	3.99E-19	2.00E-23
FBtr0302160	FBgn0026718	2L	fu12-RC	2.60E-13	8.77E-11	2.48E-43	3.98E-40
FBtr0080108	FBgn0032287	2L	CG6415-RA	2.23E-35	3.24E-37	2.24E-10	1.03E-10
FBtr0077524	FBgn0022073	2L	Thor-RA	5.07E-09	1.63E-38	4.18E-148	3.73E-248
FBtr0077521	FBgn0021967	2L	Pdsw-RB	1.69E-09	7.21E-15	4.38E-09	2.40E-14
FBtr0077886	FBgn0031362	2L	CG17646-RA	2.55E-19	8.24E-32	7.17E-09	3.60E-17
FBtr0077751	FBgn0031405	2L	CG4267-RA	4.01E-08	5.30E-13	6.01E-18	8.98E-26
FBtr0079250	FBgn0015623	2L	Cpr-RA	1.94E-07	1.14E-12	1.21E-12	1.11E-19
FBtr0079972	FBgn0051755	2L	CG31755-RA	3.87E-07	2.81E-09	4.72E-08	2.62E-10
FBtr0079606	FBgn0032025	2L	CG7778-RA	4.92E-07	2.44E-07	2.70E-67	6.03E-72
FBtr0079919	FBgn0042174	2L	CG18854-RC	9.74E-07	4.71E-10	4.02E-49	3.54E-60
FBtr0077629	FBgn0031478	2L	CG8814-RA	1.16E-06	2.59E-09	1.06E-06	2.57E-09
FBtr0300709	FBgn0031937	2L	CG13795-RB	3.20E-13	5.38E-11	2.35E-08	1.39E-06
FBtr0081109	FBgn0015808	2L	ScpX-RA	6.52E-07	4.81E-06	3.10E-09	2.87E-08
FBtr0090027	FBgn0032456	2L	MRP-RO	7.33E-06	6.71E-12	8.10E-08	9.00E-15
FBtr0080017	FBgn0025366	2L	Ip259-RA	3.15E-39	2.82E-64	5.93E-06	6.19E-16

Table s3.7 (continued)

FBtr#	FBgn#	arm	name	*p*-values			
				Z30-FR	Z56-FR	Z30-CS	Z56-CS
FBtr0079642	FBgn0031987	2L	CG12375-RA	8.78E-06	1.20E-07	3.30E-08	1.56E-10
FBtr0114603	FBgn0031813	2L	CG9527-RB	9.78E-07	6.82E-10	7.08E-06	9.16E-09
FBtr0110894	FBgn0083970	2L	CG34134-RA	1.69E-09	1.89E-12	1.25E-05	7.70E-08
FBtr0089655	FBgn0028425	2L	JhI-21-RA	6.05E-09	1.15E-12	1.49E-05	2.53E-08
FBtr0079032	FBgn0031675	2L	CG9121-RA	4.42E-07	1.96E-11	2.15E-05	4.24E-09
FBtr0302115	FBgn0000579	2L	Eno-RF	1.84E-42	3.18E-105	3.42E-05	3.19E-33
FBtr0080866	FBgn0032586	2L	Tpr2-RA	8.55E-05	2.39E-11	2.42E-05	3.58E-12
FBtr0079263	FBgn0031824	2L	CG9547-RA	1.29E-04	5.58E-06	1.23E-16	5.38E-20
FBtr0080439	FBgn0032482	2L	Pect-RB	1.95E-04	2.96E-10	9.16E-15	2.00E-25
FBtr0078104	FBgn0031217	2L	CG11377-RA	1.39E-07	5.24E-11	2.19E-04	7.52E-07
FBtr0079938	FBgn0032178	2L	CG4804-RA	1.08E-08	5.96E-07	6.17E-06	1.79E-04
FBtr0110872	FBgn0010612	2L	l(2)06225-RB	3.72E-04	2.47E-10	2.95E-04	2.06E-10
FBtr0112637	FBgn0085422	2L	CG34393-RA	4.38E-04	5.34E-05	2.60E-07	1.18E-08
FBtr0081473	FBgn0010100	2L	Acon-RB	7.73E-128	3.32E-205	3.45E-04	4.13E-21
FBtr0081204	FBgn0032779	2L	CG16771-RA	1.90E-12	2.32E-06	3.70E-09	3.86E-04
FBtr0079077	FBgn0031703	2L	CG12512-RA	8.91E-04	5.07E-08	2.65E-18	5.27E-28
FBtr0080134	FBgn0021953	2L	Fatp-RB	8.94E-04	7.53E-05	4.95E-11	3.48E-13
FBtr0079063	FBgn0031692	2L	TpnC25D-RA	7.22E-06	6.63E-08	9.15E-04	3.02E-05
FBtr0080917	FBgn0004797	2L	mdy-RC	1.15E-04	9.36E-04	1.17E-12	2.56E-11
FBtr0300048	FBgn0085209	2L	CG34180-RB	7.84E-04	9.49E-04	1.38E-04	1.80E-04
FBtr0081164	FBgn0002031	2L	l(2)37Cc-RB	3.11E-11	3.57E-25	1.65E-03	1.41E-11
FBtr0079545	FBgn0011230	2L	poe-RA	7.72E-16	5.32E-20	1.91E-03	4.83E-05
FBtr0113018	FBgn0031528	2L	CG15412-RB	2.61E-03	1.24E-03	3.19E-04	1.33E-04
FBtr0079068	FBgn0031695	2L	Cyp4ac3-RA	3.89E-03	1.14E-03	1.54E-04	3.96E-05
FBtr0080397	FBgn0032451	2L	spict-RA	4.99E-03	2.37E-05	2.71E-11	3.62E-16
FBtr0081302	FBgn0032835	2L	CG16772-RA	2.05E-13	5.28E-77	4.53E-03	3.14E-44
FBtr0079322	FBgn0031845	2L	CG9232-RA	1.03E-85	8.87E-86	6.00E-04	4.24E-03
FBtr0079219	FBgn0000052	2L	ade2-RA	7.82E-119	1.29E-189	0.00E+00	0.00E+00
FBtr0080276	FBgn0032382	2L	CG14935-RA	2.88E-34	5.64E-65	3.37E-231	0.00E+00
FBtr0086625	FBgn0010053	2R	Jheh1-RA	0.00E+00	0.00E+00	1.61E-227	2.91E-204
FBtr0087560	FBgn0033926	2R	Arc1-RA	4.05E-117	1.74E-135	0.00E+00	0.00E+00
FBtr0086935	FBgn0034229	2R	CG4847-RD	6.94E-75	9.52E-88	5.74E-94	4.18E-109
FBtr0087232	FBgn0001124	2R	Got1-RA	3.62E-66	3.38E-69	4.09E-154	4.82E-163
FBtr0088245	FBgn0027525	2R	CG7686-RA	0.00E+00	0.00E+00	7.79E-65	6.23E-94
FBtr0089970	FBgn0034405	2R	Jheh2-RA	0.00E+00	0.00E+00	4.79E-53	1.36E-79
FBtr0088791	FBgn0053087	2R	CG33087-RC	1.32E-66	2.39E-51	4.51E-78	7.84E-62
FBtr0087390	FBgn0034010	2R	CG8157-RA	2.21E-52	4.03E-46	1.99E-52	4.42E-46
FBtr0301282	FBgn0027842	2R	CPTI-RD	2.05E-53	2.17E-42	9.77E-92	1.80E-78
FBtr0089548	FBgn0027572	2R	CG5009-RA	4.54E-53	1.12E-53	2.39E-38	3.02E-38
FBtr0087309	FBgn0022160	2R	Gpo-1-RA	1.18E-103	8.33E-142	2.11E-37	4.43E-59
FBtr0087732	FBgn0053138	2R	CG33138-RA	3.97E-87	7.25E-78	7.77E-44	4.53E-36
FBtr0087450	FBgn0013773	2R	Cyp6a22-RA	2.35E-33	5.44E-39	6.81E-33	2.59E-38
FBtr0086292	FBgn0034509	2R	Obp57c-RA	2.68E-24	4.49E-23	3.38E-72	1.86E-72
FBtr0087720	FBgn0033830	2R	CG10814-RA	1.03E-24	3.88E-41	4.04E-22	1.73E-37
FBtr0072226	FBgn0025352	2R	Thiolase-RA	2.49E-29	1.88E-21	2.38E-52	1.91E-42
FBtr0071606	FBgn0034628	2R	Acox57D-p-RA	4.53E-21	1.61E-22	4.06E-113	5.43E-122

Table s3.7 (continued)

FBtr#	FBgn#	arm	name	*p*-values			
				Z30-FR	Z56-FR	Z30-CS	Z56-CS
FBtr0072239	FBgn0034909	2R	CG4797-RB	6.00E-20	3.87E-43	1.32E-23	1.55E-48
FBtr0087079	FBgn0034155	2R	unc-104-RD	8.21E-19	9.76E-28	1.70E-24	7.18E-35
FBtr0086639	FBgn0034390	2R	CG15093-RB	1.37E-41	3.03E-61	3.46E-18	8.98E-31
FBtr0072026	FBgn0034860	2R	CG9812-RC	1.69E-17	5.93E-35	1.33E-159	2.83E-216
FBtr0088384	FBgn0033465	2R	CG12140-RA	1.49E-22	2.70E-16	8.54E-61	9.88E-52
FBtr0088508	FBgn0017558	2R	Pdk-RA	5.04E-78	2.54E-114	6.29E-16	6.52E-32
FBtr0086305	FBgn0034494	2R	CG10444-RA	7.43E-15	9.24E-17	7.31E-25	7.10E-28
FBtr0086327	FBgn0034471	2R	Obp56e-RA	3.57E-14	1.60E-25	2.22E-39	7.49E-59
FBtr0088611	FBgn0033391	2R	CG8026-RB	4.48E-13	2.70E-27	1.05E-28	1.04E-49
FBtr0087004	FBgn0000079	2R	Amy-p-RA	4.89E-19	1.59E-12	9.70E-108	2.65E-97
FBtr0088448	FBgn0033464	2R	CG1441-RA	1.57E-09	1.74E-15	1.78E-27	2.56E-38
FBtr0071928	FBgn0034756	2R	Cyp6d2-RA	2.48E-08	9.18E-10	1.51E-11	3.53E-13
FBtr0087922	FBgn0033730	2R	Cpr49Ag-RA	4.23E-08	5.88E-11	2.42E-92	9.74E-108
FBtr0086677	FBgn0063491	2R	GstE9-RA	2.04E-52	8.97E-64	3.90E-08	1.15E-11
FBtr0300283	FBgn0034432	2R	CG7461-RB	1.16E-10	4.03E-08	1.26E-16	1.60E-13
FBtr0088903	FBgn0001091	2R	Gapdh1-RA	1.25E-07	8.03E-28	3.54E-31	5.71E-68
FBtr0071815	FBgn0013272	2R	Gp150-RC	1.78E-07	1.58E-07	2.74E-25	4.04E-26
FBtr0087644	FBgn0033879	2R	CG6543-RB	5.36E-08	1.87E-11	1.93E-07	9.93E-11
FBtr0086699	FBgn0034356	2R	CG10924-RA	6.64E-77	8.61E-83	3.03E-07	2.71E-07
FBtr0088679	FBgn0003074	2R	Pgi-RA	1.38E-134	1.55E-142	1.77E-06	1.53E-06
FBtr0087172	FBgn0034117	2R	CG7997-RA	1.42E-11	9.94E-12	1.46E-06	1.70E-06
FBtr0088593	FBgn0033397	2R	Cyp4p3-RA	2.20E-07	6.93E-06	9.90E-26	8.71E-24
FBtr0086236	FBgn0034543	2R	CG30152-RA	1.07E-05	7.71E-06	2.46E-07	1.24E-07
FBtr0089056	FBgn0015038	2R	Cyp9b1-RA	3.68E-05	5.54E-06	1.98E-11	6.80E-13
FBtr0289993	FBgn0050050	2R	CG30050-RB	8.44E-07	2.80E-05	5.46E-16	2.43E-14
FBtr0072349	FBgn0019886	2R	CG4589-RC	4.12E-05	2.14E-07	2.41E-06	6.30E-09
FBtr0112670	FBgn0085434	2R	NaCP60E-RC	5.71E-05	9.92E-06	6.47E-10	3.44E-11
FBtr0089055	FBgn0015039	2R	Cyp9b2-RA	9.34E-41	1.49E-28	6.69E-11	6.23E-05
FBtr0301507	FBgn0033988	2R	pcs-RB	1.49E-04	1.72E-06	3.95E-05	3.63E-07
FBtr0088082	FBgn0010516	2R	wal-RA	9.17E-23	2.22E-29	1.29E-04	3.88E-07
FBtr0086775	FBgn0034310	2R	Nup75-RA	1.18E-04	1.13E-04	1.23E-04	1.20E-04
FBtr0088434	FBgn0033476	2R	CG18445-RA	2.96E-06	1.52E-04	2.17E-09	2.56E-07
FBtr0086970	FBgn0023172	2R	RhoGEF2-RF	2.09E-04	9.33E-07	7.65E-06	1.29E-08
FBtr0089050	FBgn0026602	2R	Ady43A-RA	8.17E-05	1.13E-07	3.97E-04	9.49E-07
FBtr0089601	FBgn0034603	2R	Glycogenin-RB	8.30E-04	7.04E-06	5.56E-22	5.68E-28
FBtr0072021	FBgn0034865	2R	Or59b-RA	1.19E-03	2.43E-06	7.74E-07	1.43E-10
FBtr0089053	FBgn0044011	2R	Spn43Ad-RA	2.33E-04	1.40E-03	1.23E-09	1.56E-08
FBtr0113054	FBgn0033246	2R	CG11198-RD	0.00E+00	0.00E+00	8.43E-12	1.44E-03
FBtr0071661	FBgn0034644	2R	CG10082-RA	3.57E-10	1.75E-13	2.09E-03	4.55E-05
FBtr0072400	FBgn0010435	2R	emp-RC	2.93E-03	1.52E-06	3.50E-75	7.61E-95
FBtr0086504	FBgn0034421	2R	hppy-RA	3.13E-03	5.97E-10	5.80E-08	3.53E-18
FBtr0071618	FBgn0050392	2R	CG30392-RA	1.05E-03	3.24E-03	3.00E-09	1.54E-08
FBtr0088652	FBgn0033349	2R	CG8243-RA	5.66E-03	1.52E-03	3.97E-03	1.12E-03
FBtr0088458	FBgn0027580	2R	CG1516-RJ	1.40E-122	3.52E-130	3.72E-03	3.53E-03
FBtr0089938	FBgn0033631	2R	CG9027-RA	6.33E-03	9.18E-04	1.04E-15	2.11E-18
FBtr0088548	FBgn0029092	2R	ced-6-RB	1.46E-08	1.01E-12	5.44E-03	3.23E-05

Table s3.7 (continued)

FBtr#	FBgn#	arm	name	*p*-values			
				Z30-FR	Z56-FR	Z30-CS	Z56-CS
FBtr0071726	FBgn0034674	2R	CG9304-RA	3.02E-07	1.48E-13	5.56E-03	7.49E-07
FBtr0071690	FBgn0034638	2R	CG10433-RA	7.07E-03	3.54E-20	7.94E-10	7.09E-37
FBtr0072111	FBgn0034879	2R	Rrp4-RA	6.98E-08	1.34E-08	6.72E-03	3.14E-03
FBtr0088907	FBgn0033190	2R	CG2137-RA	9.03E-03	6.68E-03	1.02E-04	4.02E-05
FBtr0088591	FBgn0033395	2R	Cyp4p2-RA	1.29E-05	2.80E-06	7.50E-03	3.32E-03
FBtr0072405	FBgn0002607	2R	RpL19-RA	5.61E-22	1.41E-52	8.13E-03	7.32E-16
FBtr0087090	FBgn0011260	2R	Sema-2a-RA	1.18E-05	1.17E-04	1.52E-03	9.14E-03
FBtr0088466	FBgn0260474	2R	CG30002-RA	3.12E-27	2.18E-39	3.29E-04	1.29E-08
FBtr0089324	FBgn0002565	3L	Lsp2-RA	0.00E+00	0.00E+00	0.00E+00	0.00E+00
FBtr0076427	FBgn0036007	3L	path-RA	1.62E-178	3.35E-114	0.00E+00	1.90E-281
FBtr0076810	FBgn0035817	3L	CG7409-RA	4.93E-96	1.61E-99	4.44E-173	7.04E-182
FBtr0078413	FBgn0012034	3L	AcCoAS-RA	2.38E-127	2.09E-89	2.27E-141	1.47E-101
FBtr0075699	FBgn0036449	3L	bmm-RA	7.76E-70	3.56E-92	1.79E-81	4.48E-106
FBtr0075753	FBgn0029167	3L	Hml-RA	9.64E-99	9.18E-61	4.46E-230	1.45E-175
FBtr0076831	FBgn0035791	3L	CG8539-RA	1.86E-67	1.00E-54	7.01E-101	9.36E-87
FBtr0076001	FBgn0027843	3L	CAH2-RA	2.45E-50	4.93E-82	4.26E-63	7.91E-99
FBtr0076526	FBgn0023479	3L	Tequila-RA	0.00E+00	0.00E+00	1.11E-26	1.17E-32
FBtr0075094	FBgn0040322	3L	GNBP2-RB	2.06E-42	1.54E-47	9.64E-26	3.00E-29
FBtr0076669	FBgn0001248	3L	Idh-RB	6.05E-95	3.36E-141	9.90E-26	2.02E-49
FBtr0076424	FBgn0010408	3L	RpS9-RB	1.55E-49	4.96E-88	7.10E-20	8.99E-45
FBtr0076832	FBgn0015033	3L	Cyp4d8-RA	2.29E-25	7.72E-19	3.37E-28	1.67E-21
FBtr0112761	FBgn0085484	3L	CG34455-RC	8.81E-15	1.58E-17	1.31E-15	1.85E-18
FBtr0076199	FBgn0036116	3L	CG7888-RC	8.44E-19	1.75E-12	6.09E-37	1.97E-28
FBtr0110866	FBgn0036612	3L	CG4998-RB	4.70E-11	1.44E-13	3.03E-22	2.77E-26
FBtr0077179	FBgn0035588	3L	CG10672-RA	2.22E-10	6.65E-12	2.87E-13	4.11E-15
FBtr0300655	FBgn0260388	3L	CG42514-RA	2.89E-17	5.37E-10	2.49E-21	2.96E-13
FBtr0073270	FBgn0035499	3L	Chd64-RB	4.20E-32	1.44E-61	1.66E-09	2.60E-26
FBtr0078223	FBgn0036995	3L	CG5195-RA	8.51E-09	1.30E-09	2.81E-50	4.69E-55
FBtr0076455	FBgn0035985	3L	Cpr67B-RA	1.01E-08	1.49E-19	1.14E-32	1.70E-53
FBtr0072529	FBgn0025592	3L	Gyk-RA	8.99E-10	2.70E-10	8.17E-09	2.73E-09
FBtr0075076	FBgn0036824	3L	CG3902-RA	1.23E-09	6.18E-08	4.03E-15	3.94E-13
FBtr0073359	FBgn0010349	3L	Dhc64C-RA	9.74E-08	1.00E-13	1.63E-09	3.34E-16
FBtr0075046	FBgn0036836	3L	CG11619-RA	3.29E-07	1.19E-10	1.93E-10	1.59E-14
FBtr0076173	FBgn0036157	3L	CG7560-RA	1.03E-36	8.68E-39	3.05E-07	2.16E-07
FBtr0074870	FBgn0036935	3L	CG14186-RA	9.63E-07	9.04E-17	3.26E-16	1.71E-31
FBtr0077011	FBgn0004513	3L	Mdr65-RA	2.50E-26	1.25E-53	1.04E-06	1.77E-21
FBtr0078407	FBgn0037070	3L	CG11309-RA	3.72E-07	1.08E-06	6.97E-11	2.14E-10
FBtr0072743	FBgn0035233	3L	CG7864-RA	1.73E-06	8.57E-07	2.32E-10	7.31E-11
FBtr0073077	FBgn0035445	3L	CG12014-RA	1.46E-06	3.14E-06	2.36E-07	5.15E-07
FBtr0074972	FBgn0036887	3L	CG9231-RA	4.96E-06	8.78E-10	4.79E-06	9.45E-10
FBtr0072679	FBgn0010786	3L	l(3)02640-RA	7.72E-06	4.21E-06	5.59E-06	2.92E-06
FBtr0073159	FBgn0035471	3L	Sc2-RA	1.15E-05	1.24E-09	1.76E-09	8.63E-15
FBtr0076936	FBgn0035725	3L	Mis12-RA	1.41E-05	2.25E-08	1.67E-07	5.91E-11
FBtr0075672	FBgn0036462	3L	mRpL39-RA	4.75E-07	1.06E-09	2.23E-05	1.34E-07
FBtr0072978	FBgn0035383	3L	CG2107-RA	1.69E-06	2.33E-05	4.91E-18	1.81E-16
FBtr0076304	FBgn0052055	3L	CG32055-RA	1.47E-05	2.40E-06	3.78E-05	6.44E-06

Table s3.7 (continued)

FBtr#	FBgn#	arm	name	*p*-values			
				Z30-FR	Z56-FR	Z30-CS	Z56-CS
FBtr0075182	FBgn0036741	3L	CG7510-RA	8.27E-17	1.62E-37	6.71E-05	7.93E-17
FBtr0076185	FBgn0036150	3L	Ir68a-RA	2.82E-11	2.74E-10	6.08E-06	5.51E-05
FBtr0076130	FBgn0036194	3L	CG11652-RA	8.55E-05	7.13E-05	2.65E-05	2.32E-05
FBtr0073301	FBgn0035544	3L	CG15021-RA	9.96E-05	1.27E-12	1.05E-44	7.86E-69
FBtr0072874	FBgn0040507	3L	ACXD-RA	1.14E-04	3.19E-06	1.76E-05	3.62E-07
FBtr0078235	FBgn0028978	3L	trbl-RA	2.24E-04	1.39E-06	4.08E-22	5.80E-28
FBtr0089942	FBgn0025682	3L	scf-RA	6.92E-04	1.47E-16	6.87E-23	7.45E-50
FBtr0089491	FBgn0035976	3L	PGRP-LC-RB	2.14E-17	7.61E-26	7.00E-04	1.36E-07
FBtr0076529	FBgn0043806	3L	CG32032-RA	9.95E-04	1.06E-09	3.06E-04	1.48E-10
FBtr0076469	FBgn0052037	3L	CG32037-RA	1.04E-04	7.84E-04	7.98E-47	5.10E-47
FBtr0073124	FBgn0035398	3L	Cht7-RA	3.09E-04	1.43E-09	9.19E-04	1.39E-08
FBtr0076892	FBgn0035753	3L	RpL18-RA	1.59E-04	5.26E-17	1.16E-03	6.00E-15
FBtr0072762	FBgn0035252	3L	CG7970-RA	3.91E-05	4.26E-06	1.40E-03	2.66E-04
FBtr0074976	FBgn0036882	3L	CG9279-RB	5.21E-07	3.59E-15	1.67E-03	2.83E-09
FBtr0075997	FBgn0036257	3L	RhoGAP68F-RA	3.17E-06	2.42E-03	7.07E-11	7.42E-07
FBtr0073215	FBgn0035501	3L	CG1299-RA	3.46E-04	2.53E-03	1.20E-10	2.60E-09
FBtr0075190	FBgn0036752	3L	Adgf-A-RA	5.03E-03	3.89E-03	6.92E-05	4.55E-05
FBtr0075845	FBgn0260049	3L	flr-RA	6.07E-03	6.80E-04	1.44E-14	2.38E-17
FBtr0076319	FBgn0036043	3L	CG8177-RG	6.85E-03	2.63E-06	4.33E-20	8.40E-30
FBtr0074940	FBgn0036888	3L	CG9330-RA	1.13E-05	6.29E-19	5.86E-03	7.68E-13
FBtr0072915	FBgn0026570	3L	CG5704-RA	7.52E-03	4.49E-03	3.30E-05	1.12E-05
FBtr0072556	FBgn0035147	3L	CG12030-RA	3.38E-06	9.84E-06	2.00E-03	4.88E-03
FBtr0075460	FBgn0052154	3L	CG32154-RA	7.70E-05	1.84E-04	2.75E-03	5.39E-03
FBtr0072562	FBgn0035146	3L	CG13893-RA	9.03E-03	7.04E-06	2.17E-07	1.24E-12
FBtr0072983	FBgn0040308	3L	Jafrac2-RB	7.07E-03	9.36E-03	1.03E-03	1.31E-03
FBtr0301097	FBgn0260657	3L	CG42540-RC	2.24E-06	1.12E-03	2.66E-45	1.68E-38
FBtr0301802	FBgn0058160	3L Het	CG40160-RE	1.69E-13	2.68E-11	1.33E-15	1.90E-13
FBtr0082660	FBgn0002719	3R	Men-RB	0.00E+00	0.00E+00	0.00E+00	0.00E+00
FBtr0082158	FBgn0002868	3R	MtnA-RA	0.00E+00	0.00E+00	0.00E+00	0.00E+00
FBtr0084847	FBgn0039330	3R	CG11909-RA	1.02E-143	2.40E-210	0.00E+00	0.00E+00
FBtr0082954	FBgn0038236	3R	Cyp313a1-RA	3.60E-122	1.84E-136	2.54E-258	9.75E-287
FBtr0082264	FBgn0020385	3R	pug-RB	6.75E-103	2.12E-157	2.53E-224	0.00E+00
FBtr0083038	FBgn0038290	3R	CG6912-RA	8.84E-103	1.31E-120	4.63E-174	8.51E-201
FBtr0084710	FBgn0039241	3R	CG11089-RA	4.45E-94	1.07E-149	0.00E+00	0.00E+00
FBtr0083025	FBgn0038291	3R	CG3984-RA	3.05E-45	1.81E-52	1.24E-116	5.38E-132
FBtr0084285	FBgn0038983	3R	CG5326-RA	1.92E-36	6.98E-40	2.24E-60	7.39E-66
FBtr0083036	FBgn0038293	3R	CG6904-RB	2.63E-31	3.23E-53	3.36E-70	9.18E-104
FBtr0084859	FBgn0039321	3R	CG10550-RA	3.27E-29	1.00E-27	6.07E-90	2.96E-90
FBtr0113219	FBgn0037872	3R	nocturnin-RD	1.89E-27	3.99E-57	2.31E-32	1.95E-64
FBtr0301346	FBgn0086704	3R	stops-RC	1.11E-23	3.31E-43	3.34E-57	6.12E-88
FBtr0085390	FBgn0014427	3R	CG11899-RA	4.99E-43	4.91E-76	1.17E-21	3.21E-45
FBtr0084440	FBgn0039102	3R	SPE-RA	9.79E-107	1.66E-145	1.26E-21	7.56E-38
FBtr0084994	FBgn0000064	3R	Ald-RB	8.54E-23	1.65E-50	1.19E-18	6.18E-44
FBtr0084691	FBgn0003719	3R	tld-RA	1.05E-22	2.92E-34	9.47E-18	7.38E-28
FBtr0083245	FBgn0027657	3R	glob1-RC	4.05E-18	3.68E-17	0.00E+00	0.00E+00

Table s3.7 (continued)

FBtr#	FBgn#	arm	name	*p*-values			
				Z30-FR	Z56-FR	Z30-CS	Z56-CS
FBtr0083463	FBgn0038525	3R	CG14329-RA	4.39E-17	1.03E-22	9.99E-21	6.84E-27
FBtr0085604	FBgn0039737	3R	CG7920-RB	1.20E-16	9.02E-19	8.13E-40	2.77E-44
FBtr0083790	FBgn0038733	3R	CG11407-RA	1.92E-16	1.92E-39	4.46E-20	3.72E-45
FBtr0084013	FBgn0038858	3R	CG5793-RA	7.95E-40	2.60E-47	2.64E-16	2.20E-20
FBtr0083894	FBgn0038795	3R	CG4335-RA	3.83E-16	1.35E-18	3.62E-63	6.82E-71
FBtr0082715	FBgn0038115	3R	CG7966-RA	0.00E+00	0.00E+00	8.25E-17	2.18E-15
FBtr0084431	FBgn0039073	3R	CG4408-RA	1.78E-22	3.22E-15	5.56E-133	1.99E-125
FBtr0081996	FBgn0010222	3R	Nmdmc-RB	7.84E-15	9.21E-78	3.91E-87	1.87E-210
FBtr0082659	FBgn0038083	3R	CG5999-RA	5.26E-16	1.51E-14	6.85E-37	6.38E-37
FBtr0083889	FBgn0038799	3R	CG4288-RA	2.21E-15	1.49E-13	9.47E-26	8.71E-24
FBtr0084186	FBgn0038924	3R	CG6028-RA	2.84E-20	1.00E-26	1.18E-12	2.06E-17
FBtr0100464	FBgn0037912	3R	CG6782-RD	1.23E-23	5.99E-34	8.26E-11	1.66E-17
FBtr0083026	FBgn0038292	3R	CG3987-RA	1.34E-10	1.31E-11	1.50E-18	2.70E-20
FBtr0084317	FBgn0039024	3R	CG4721-RA	3.99E-51	6.69E-37	2.37E-19	1.44E-10
FBtr0078705	FBgn0037351	3R	RpL13A-RB	2.34E-10	1.13E-24	3.45E-23	4.13E-44
FBtr0085715	FBgn0039809	3R	CG15547-RA	4.77E-10	4.70E-12	4.24E-55	9.33E-63
FBtr0082826	FBgn0038180	3R	Cht5-RA	5.32E-10	5.88E-11	3.16E-12	1.68E-13
FBtr0112558	FBgn0085378	3R	CG34349-RA	9.08E-11	6.74E-10	1.82E-12	1.46E-11
FBtr0089766	FBgn0038194	3R	Cyp6d5-RA	1.14E-18	1.24E-09	5.34E-268	7.72E-243
FBtr0078656	FBgn0011281	3R	Pbprp3-RA	2.24E-09	1.41E-32	1.41E-11	8.17E-37
FBtr0082666	FBgn0001296	3R	kar-RA	2.70E-09	3.66E-15	1.49E-22	3.38E-32
FBtr0082259	FBgn0024957	3R	Irp-1B-RA	1.91E-20	3.71E-22	1.01E-08	2.00E-09
FBtr0113389	FBgn0051103	3R	CG31103-RB	6.84E-10	4.02E-09	4.62E-09	2.68E-08
FBtr0085798	FBgn0039856	3R	CG1774-RA	2.10E-48	5.72E-65	4.17E-08	3.44E-14
FBtr0082093	FBgn0053105	3R	p24-2-RA	8.59E-09	4.79E-08	3.84E-20	9.34E-20
FBtr0083971	FBgn0028396	3R	TotA-RA	7.34E-08	1.65E-10	0.00E+00	0.00E+00
FBtr0085133	FBgn0039486	3R	CG6074-RA	7.02E-09	6.27E-08	2.50E-71	7.88E-73
FBtr0083542	FBgn0003499	3R	sr-RA	8.45E-08	1.90E-12	2.67E-21	1.12E-29
FBtr0084810	FBgn0039298	3R	to-RA	1.47E-37	8.12E-51	7.51E-08	2.49E-13
FBtr0290273	FBgn0040493	3R	granny-smith-RD	2.18E-07	5.87E-10	2.45E-07	7.09E-10
FBtr0082111	FBgn0037714	3R	CG9396-RA	1.34E-10	4.63E-12	4.00E-07	3.14E-08
FBtr0085401	FBgn0051445	3R	CG31445-RA	4.62E-15	5.05E-34	1.28E-06	1.24E-19
FBtr0082136	FBgn0037752	3R	RpS29-RA	4.13E-15	3.02E-28	4.87E-06	2.12E-14
FBtr0082898	FBgn0027563	3R	CG9631-RA	1.74E-05	6.82E-10	5.60E-07	5.49E-12
FBtr0084109	FBgn0038889	3R	CG7922-RA	5.01E-05	3.28E-09	6.28E-08	3.62E-13
FBtr0302027	FBgn0025701	3R	CG14709-RB	3.29E-08	1.78E-08	4.40E-05	3.29E-05
FBtr0084853	FBgn0039324	3R	CG10553-RA	4.15E-24	2.89E-18	1.30E-08	4.12E-05
FBtr0081795	FBgn0037552	3R	CG7800-RA	6.27E-06	1.95E-05	1.75E-05	4.86E-05
FBtr0084690	FBgn0004885	3R	tok-RA	8.17E-05	3.15E-07	6.42E-07	7.37E-10
FBtr0085249	FBgn0027579	3R	CG5508-RA	7.04E-187	1.36E-197	4.35E-05	6.36E-05
FBtr0081763	FBgn0014930	3R	CG2846-RA	1.40E-04	6.43E-06	5.03E-19	1.04E-22
FBtr0084550	FBgn0039156	3R	CG6178-RA	6.42E-07	4.55E-06	2.20E-05	1.26E-04
FBtr0085015	FBgn0039430	3R	CG5455-RA	2.19E-04	1.67E-07	7.71E-17	1.64E-23
FBtr0085080	FBgn0051075	3R	CG31075-RA	3.64E-04	7.89E-06	0.00E+00	0.00E+00
FBtr0085623	FBgn0015221	3R	Fer2LCH-RB	3.73E-04	1.15E-09	6.53E-154	5.96E-194
FBtr0301283	FBgn0037817	3R	Cyp12e1-RC	3.91E-04	2.46E-04	1.13E-19	8.04E-21

Table s3.7 (continued)

FBtr#	FBgn#	arm	name	*p*-values			
				Z30-FR	Z56-FR	Z30-CS	Z56-CS
FBtr0113311	FBgn0039827	3R	CG1544-RC	5.30E-10	3.14E-04	2.39E-33	5.18E-22
FBtr0085405	FBgn0062442	3R	CG1458-RA	5.01E-04	3.28E-04	5.53E-09	1.87E-09
FBtr0083128	FBgn0038311	3R	CG14864-RA	6.89E-04	2.10E-05	7.46E-06	9.77E-08
FBtr0085003	FBgn0039417	3R	CG6073-RA	8.96E-04	1.44E-05	3.00E-04	3.96E-06
FBtr0301477	FBgn0011672	3R	Mvl-RD	1.11E-03	3.19E-14	4.87E-04	6.47E-15
FBtr0100012	FBgn0053970	3R	CG33970-RA	1.16E-03	4.38E-09	5.93E-04	1.74E-09
FBtr0081869	FBgn0037592	3R	CG11737-RA	1.24E-03	1.13E-05	1.77E-04	8.73E-07
FBtr0082825	FBgn0038179	3R	CG9312-RA	8.15E-06	1.25E-03	3.38E-12	7.47E-09
FBtr0082569	FBgn0010038	3R	GstD2-RA	1.81E-03	1.60E-04	8.69E-15	1.11E-17
FBtr0084367	FBgn0051052	3R	Nha2-RA	9.08E-28	1.80E-32	1.75E-03	1.46E-04
FBtr0078937	FBgn0051523	3R	CG31523-RA	1.37E-04	1.91E-03	5.65E-15	4.82E-13
FBtr0083986	FBgn0038839	3R	CG10830-RA	4.44E-04	3.12E-03	3.80E-13	1.07E-11
FBtr0084830	FBgn0051436	3R	CG31436-RA	1.61E-31	2.20E-35	3.32E-03	7.79E-04
FBtr0084224	FBgn0038959	3R	CG13856-RA	5.46E-03	2.10E-03	3.02E-05	8.19E-06
FBtr0084289	FBgn0038981	3R	CG5346-RA	6.61E-03	1.31E-03	7.50E-10	1.46E-11
FBtr0081540	FBgn0015570	3R	alpha-Est2-RA	7.03E-61	7.12E-38	1.12E-11	5.51E-03
FBtr0083122	FBgn0038318	3R	CG6236-RA	9.90E-03	1.30E-03	1.20E-07	2.65E-09
FBtr0084352	FBgn0039052	3R	CG6733-RA	1.83E-17	1.37E-15	2.41E-04	7.41E-03
FBtr0082095	FBgn0260463	3R	unc-115-RA	3.78E-52	8.11E-65	1.09E-47	2.76E-59
FBtr0113417	FBgn0052000	4	CG32000-RH	4.61E-04	1.67E-03	8.10E-07	4.29E-06
FBtr0300992	FBgn0052017	4	CG32017-RB	1.64E-30	3.62E-20	3.57E-07	8.86E-03
FBtr0071419	FBgn0004045	X	Yp1-RA	0.00E+00	0.00E+00	0.00E+00	0.00E+00
FBtr0070186	FBgn0040349	X	CG3699-RA	0.00E+00	0.00E+00	2.40E-284	2.30E-302
FBtr0070866	FBgn0029831	X	CG5966-RA	0.00E+00	3.83E-168	0.00E+00	0.00E+00
FBtr0077304	FBgn0011280	X	Pbprp2-RB	8.80E-67	1.38E-125	1.86E-202	4.10E-306
FBtr0074717	FBgn0027621	X	Pfrx-RB	2.61E-51	8.66E-80	1.57E-42	2.55E-68
FBtr0073705	FBgn0020513	X	ade5-RA	2.23E-35	7.77E-83	0.00E+00	0.00E+00
FBtr0070093	FBgn0023537	X	CG17896-RA	2.55E-71	8.02E-93	1.63E-31	8.97E-45
FBtr0073774	FBgn0030478	X	CG1640-RF	1.83E-79	5.39E-97	3.76E-30	1.14E-39
FBtr0071123	FBgn0029990	X	CG2233-RA	1.55E-200	3.73E-55	3.18E-146	5.01E-28
FBtr0071159	FBgn0030013	X	GIIIspla2-RA	2.66E-26	1.09E-26	6.26E-211	2.94E-224
FBtr0070827	FBgn0029823	X	CG3011-RA	1.04E-25	5.23E-35	1.52E-67	2.36E-84
FBtr0110969	FBgn0030608	X	Lsd-2-RC	1.83E-81	1.93E-38	5.96E-60	9.24E-24
FBtr0073961	FBgn0030607	X	dob-RA	2.83E-36	2.76E-33	1.43E-23	9.48E-21
FBtr0071338	FBgn0086450	X	su(r)-RC	4.80E-19	3.53E-34	4.38E-40	2.97E-62
FBtr0070140	FBgn0025621	X	CG16989-RA	5.24E-25	1.92E-41	2.78E-18	4.15E-32
FBtr0301696	FBgn0026313	X	X11L-RB	2.31E-15	8.81E-21	7.90E-15	4.19E-20
FBtr0073683	FBgn0011837	X	Tis11-RA	2.51E-16	6.42E-14	1.75E-26	7.61E-24
FBtr0070383	FBgn0023507	X	CG3835-RA	8.89E-14	1.85E-18	4.02E-88	4.02E-104
FBtr0070981	FBgn0029897	X	RpL17-RC	7.72E-14	1.23E-51	1.69E-13	7.91E-51
FBtr0070778	FBgn0029768	X	SPR-RA	9.23E-25	3.69E-34	5.72E-13	2.25E-19
FBtr0074654	FBgn0030968	X	CG7322-RA	2.17E-17	1.33E-13	1.93E-16	9.00E-13
FBtr0112575	FBgn0085388	X	IP3K2-RB	3.98E-12	7.24E-11	1.97E-25	3.93E-24
FBtr0071224	FBgn0030058	X	CG11294-RA	9.36E-18	3.40E-14	1.51E-14	5.91E-11
FBtr0070916	FBgn0014026	X	RpL7A-RD	2.47E-40	1.52E-128	1.17E-10	2.46E-65
FBtr0070446	FBgn0029629	X	CG8636-RA	4.28E-16	1.37E-25	6.67E-10	3.00E-17

Table s3.7 (continued)

FBtr#	FBgn#	arm	name	*p*-values			
				Z30-FR	Z56-FR	Z30-CS	Z56-CS
FBtr0074258	FBgn0030724	X	Nipsnap-RA	1.87E-13	1.50E-13	1.53E-09	1.73E-09
FBtr0073833	FBgn0052626	X	CG32626-RC	7.44E-09	1.01E-14	3.52E-13	2.03E-20
FBtr0074053	FBgn0030668	X	CG8128-RA	3.16E-15	9.37E-16	9.82E-09	6.15E-09
FBtr0071125	FBgn0003656	X	sws-RA	3.81E-10	1.12E-08	1.49E-10	4.94E-09
FBtr0074795	FBgn0031069	X	CG12703-RA	3.33E-08	1.11E-11	7.21E-23	2.57E-29
FBtr0073510	FBgn0030311	X	CG11699-RA	4.64E-08	1.61E-12	3.72E-12	9.05E-18
FBtr0073908	FBgn0030558	X	CG1461-RA	1.33E-12	6.23E-08	0.00E+00	0.00E+00
FBtr0073407	FBgn0030245	X	CG1637-RC	3.82E-08	4.37E-07	1.16E-36	9.47E-36
FBtr0071242	FBgn0030040	X	CG15347-RA	2.17E-11	9.67E-07	7.46E-49	8.96E-41
FBtr0112527	FBgn0085354	X	CG34325-RA	1.41E-06	3.47E-10	4.84E-24	1.05E-31
FBtr0070115	FBgn0025640	X	CG13369-RA	1.32E-07	2.37E-15	1.13E-06	7.89E-14
FBtr0073777	FBgn0030482	X	CG1673-RA	4.79E-06	9.61E-39	2.98E-158	1.37E-278
FBtr0073819	FBgn0030519	X	CG11151-RA	4.98E-06	7.79E-11	1.28E-14	2.19E-22
FBtr0073794	FBgn0010198	X	RpS15Aa-RD	6.55E-93	4.35E-100	5.06E-06	1.39E-06
FBtr0073903	FBgn0030554	X	CG1434-RA	4.63E-10	5.64E-13	9.76E-06	7.10E-08
FBtr0070387	FBgn0011576	X	Cyp4d2-RA	2.07E-05	2.78E-10	2.13E-07	4.00E-13
FBtr0077312	FBgn0031119	X	CG1812-RA	4.49E-05	2.32E-07	3.06E-13	1.96E-17
FBtr0070558	FBgn0029648	X	CG3603-RA	6.23E-06	9.43E-10	3.98E-05	1.18E-08
FBtr0073778	FBgn0030484	X	CG1681-RA	7.56E-05	2.78E-07	3.34E-56	1.87E-67
FBtr0299514	FBgn0259101	X	CG42249-RC	1.25E-04	6.29E-07	1.00E-04	4.91E-07
FBtr0074682	FBgn0259834	X	out-RA	1.59E-05	1.16E-04	6.22E-09	6.80E-08
FBtr0301628	FBgn0083228	X	Frq2-RC	2.33E-04	4.92E-06	2.66E-07	1.31E-09
FBtr0070913	FBgn0014031	X	Spat-RA	2.41E-04	2.59E-04	1.76E-08	1.45E-08
FBtr0071002	FBgn0029922	X	CG14431-RA	3.52E-04	2.59E-04	2.24E-05	1.20E-05
FBtr0070106	FBgn0040369	X	CG13377-RA	6.08E-04	5.45E-04	9.16E-05	7.45E-05
FBtr0074487	FBgn0030850	X	CG8408-RA	1.04E-03	1.91E-09	1.07E-04	5.18E-11
FBtr0071241	FBgn0014032	X	Sptr-RA	1.30E-03	2.36E-07	1.57E-06	1.83E-11
FBtr0070081	FBgn0004648	X	svr-RB	4.27E-03	7.21E-12	8.01E-07	3.85E-19
FBtr0070824	FBgn0029821	X	CG4020-RA	1.13E-08	4.59E-07	1.39E-04	2.79E-03
FBtr0074678	FBgn0040068	X	vav-RB	2.10E-03	3.50E-03	5.87E-05	1.15E-04
FBtr0077233	FBgn0031170	X	CG1718-RA	6.09E-03	2.65E-03	3.73E-03	1.72E-03
FBtr0073845	FBgn0030512	X	CG9940-RA	5.37E-09	4.89E-03	1.50E-15	5.03E-07
FBtr0074452	FBgn0030853	X	CG5703-RA	7.97E-07	2.44E-12	6.43E-03	2.11E-06
FBtr0073730	FBgn0029133	X	REG-RA	6.87E-03	1.26E-04	8.92E-03	1.97E-04

Table s3.8 The GO terms enrich in Z>M DEGs based on FDR correction

rank	terms		*p*-values	sampled frequency	background frequency
1	GO:0007602	phototransduction	2.28E-11	16/308	48/12665
2	GO:0009583	detection of light stimulus	1.35E-10	16/308	53/12665
3	GO:0050896	response to stimulus	2.18E-10	78/308	1345/12665
4	GO:0009582	detection of abiotic stimulus	6.49E-10	16/308	58/12665
5	GO:0007601	visual perception	1.58E-09	14/308	43/12665
6	GO:0050953	sensory perception of light stimulus	2.26E-09	14/308	44/12665
7	GO:0009416	response to light stimulus	2.42E-09	20/308	108/12665
8	GO:0009581	detection of external stimulus	2.67E-09	16/308	63/12665
9	GO:0016056	rhodopsin mediated signaling pathway	1.87E-08	10/308	20/12665
10	GO:0009314	response to radiation	2.56E-08	20/308	122/12665
11	GO:0009605	response to external stimulus	6.51E-07	23/308	194/12665
12	GO:0007603	phototransduction, visible light	7.07E-07	9/308	20/12665
13	GO:0051606	detection of stimulus	2.74E-06	16/308	97/12665
14	GO:0009586	rhodopsin mediated phototransduction	4.51E-06	8/308	17/12665
15	GO:0007186	G-protein coupled receptor protein signaling pathway	7.33E-06	22/308	201/12665
16	GO:0009584	detection of visible light	1.16E-05	9/308	26/12665
17	GO:0016059	deactivation of rhodopsin mediated signaling	5.14E-05	7/308	15/12665
17	GO:0022400	regulation of rhodopsin mediated signaling pathway	5.14E-05	7/308	15/12665
19	GO:0050908	detection of light stimulus involved in visual perception	5.34E-05	8/308	22/12665
20	GO:0009628	response to abiotic stimulus	6.58E-05	23/308	246/12665
21	GO:0050962	detection of light stimulus involved in sensory perception	8.01E-05	8/308	23/12665
22	GO:0003008	system process	1.04E-04	39/308	623/12665
23	GO:0008277	regulation of G-protein coupled receptor protein signaling pathway	1.18E-04	8/308	24/12665
24	GO:0007165	signal transduction	1.19E-04	23/308	254/12665
25	GO:0023060	signal transmission	1.61E-04	36/308	557/12665
26	GO:0023046	signaling process	1.76E-04	36/308	559/12665
27	GO:0050877	neurological system process	2.68E-04	37/308	594/12665
28	GO:0006952	defense response	8.56E-04	18/308	181/12665
29	GO:0019731	antibacterial humoral response	3.22E-03	9/308	47/12665
30	GO:0042051	compound eye photoreceptor development	4.41E-03	10/308	62/12665
31	GO:0042462	eye photoreceptor cell development	5.13E-03	10/308	63/12665

Table s3.9 The GO terms enrich in M>Z DEGs based on FDR correction

rank	terms		*p*-values	sampled frequency	background frequency
1	GO:0044281	small molecule metabolic process	4.60E-24	75/318	715/12665
2	GO:0043436	oxoacid metabolic process	1.60E-14	37/318	263/12665
2	GO:0019752	carboxylic acid metabolic process	1.60E-14	37/318	263/12665
2	GO:0006082	organic acid metabolic process	1.60E-14	37/318	263/12665
5	GO:0042180	cellular ketone metabolic process	1.88E-13	37/318	283/12665
6	GO:0055114	oxidation reduction	3.20E-12	46/318	473/12665
7	GO:0032787	monocarboxylic acid metabolic process	2.46E-11	20/318	84/12665
8	GO:0006066	alcohol metabolic process	9.53E-09	24/318	169/12665
9	GO:0005975	carbohydrate metabolic process	2.76E-08	35/318	373/12665
10	GO:0044262	cellular carbohydrate metabolic process	2.40E-07	23/318	180/12665
11	GO:0044282	small molecule catabolic process	2.69E-07	18/318	107/12665
12	GO:0008152	metabolic process	8.42E-07	181/318	5060/12665
13	GO:0044283	small molecule biosynthetic process	1.17E-06	27/318	266/12665
14	GO:0019318	hexose metabolic process	1.95E-06	15/318	80/12665
15	GO:0005996	monosaccharide metabolic process	2.04E-06	16/318	93/12665
16	GO:0044242	cellular lipid catabolic process	9.13E-06	9/318	25/12665
17	GO:0044271	cellular nitrogen compound biosynthetic process	1.34E-05	24/318	239/12665
18	GO:0006629	lipid metabolic process	2.35E-05	26/318	285/12665
19	GO:0016042	lipid catabolic process	3.94E-05	10/318	38/12665
20	GO:0044255	cellular lipid metabolic process	1.02E-04	19/318	171/12665
21	GO:0006635	fatty acid beta-oxidation	1.78E-04	6/318	11/12665
22	GO:0009062	fatty acid catabolic process	3.49E-04	6/318	12/12665
22	GO:0019395	fatty acid oxidation	3.49E-04	6/318	12/12665
24	GO:0009056	catabolic process	5.48E-04	30/318	424/12665
25	GO:0006090	pyruvate metabolic process	6.35E-04	6/318	13/12665
25	GO:0034440	lipid oxidation	6.35E-04	6/318	13/12665
27	GO:0044106	cellular amine metabolic process	6.78E-04	18/318	174/12665
28	GO:0009156	ribonucleoside monophosphate biosynthetic process	9.09E-04	7/318	21/12665
28	GO:0009161	ribonucleoside monophosphate metabolic process	9.09E-04	7/318	21/12665
30	GO:0016052	carbohydrate catabolic process	1.37E-03	12/318	81/12665
31	GO:0006631	fatty acid metabolic process	2.08E-03	9/318	44/12665
32	GO:0006006	glucose metabolic process	2.35E-03	10/318	57/12665
33	GO:0009308	amine metabolic process	3.02E-03	24/318	319/12665
34	GO:0046395	carboxylic acid catabolic process	3.09E-03	9/318	46/12665
34	GO:0016054	organic acid catabolic process	3.09E-03	9/318	46/12665
36	GO:0009127	purine nucleoside monophosphate biosynthetic process	4.21E-03	6/318	17/12665
36	GO:0009167	purine ribonucleoside monophosphate metabolic process	4.21E-03	6/318	17/12665
36	GO:0009168	purine ribonucleoside monophosphate biosynthetic process	4.21E-03	6/318	17/12665
36	GO:0009126	purine nucleoside monophosphate metabolic process	4.21E-03	6/318	17/12665
40	GO:0006519	cellular amino acid and derivative metabolic process	6.00E-03	18/318	202/12665

Table s3.10 List of shared high F_{ST} sites summarized by their belonging transcripts

FBtr#	FBgn#	name	arm	location and type of substitution*				
				5	3	R	S	U
FBtr0077498	FBgn0021800	l(2)k16918-RB	2L	0	1	0	0	0
FBtr0301863	FBgn0010473	tutl-RF	2L	0	0	0	1	0
FBtr0300471	FBgn0260952	Msp-300-RG	2L	0	0	1	4	0
FBtr0080695	FBgn0028926	NC2beta-RA	2L	0	0	0	1	0
FBtr0080905	FBgn0086783	Mhc-RL	2L	0	2	0	0	0
FBtr0087450	FBgn0013773	Cyp6a22-RA	2R	0	0	0	1	0
FBtr0086916	FBgn0034215	CG4802-RA	2R	0	0	0	1	0
FBtr0086504	FBgn0034421	hppy-RA	2R	0	1	0	0	0
FBtr0071661	FBgn0034644	CG10082-RA	2R	0	0	0	2	0
FBtr0114541	FBgn0034887	CG5428-RB	2R	0	0	0	1	0
FBtr0300749	FBgn0035444	CG12012-RB	3L	1	0	0	0	0
FBtr0073202	FBgn0035489	Rcd5-RA	3L	0	0	0	2	0
FBtr0073212	FBgn0003206	Ras64B-RA	3L	0	1	0	0	0
FBtr0073294	FBgn0035542	CG11347-RD	3L	0	0	0	1	0
FBtr0112601	FBgn0085402	Ect4-RG	3L	0	0	3	3	0
FBtr0076622	FBgn0035904	CG6776-RA	3L	0	0	0	1	0
FBtr0076529	FBgn0043806	CG32032-RA	3L	0	0	0	1	0
FBtr0076532	FBgn0035966	nwk-RA	3L	0	0	0	1	0
FBtr0075693	FBgn0036451	CG9425-RB	3L	0	0	0	2	0
FBtr0100458	FBgn0038156	CG14372-RB	3R	0	0	0	1	0
FBtr0082832	FBgn0000454	Dip-B-RC	3R	1	0	0	1	0
FBtr0300037	FBgn0000634	Fas1-RF	3R	0	0	0	1	0
FBtr0083637	FBgn0023083	fray-RA	3R	0	0	1	0	0
FBtr0083700	FBgn0261113	Xrp1-RB	3R	1	0	1	1	0
FBtr0083729	FBgn0038679	CG6040-RA	3R	0	0	0	1	0
FBtr0110915	FBgn0260003	Dys-RD	3R	0	0	0	1	0
FBtr0083786	FBgn0051216	CG31216-RA	3R	0	0	0	1	0
FBtr0083819	FBgn0014006	Pk92B-RB	3R	1	0	0	0	0
FBtr0083882	FBgn0038788	Sirt2-RA	3R	0	0	1	1	0
FBtr0299771	FBgn0259222	CG42322-RI	3R	0	0	0	1	0
FBtr0100124	FBgn0038890	CG7956-RB	3R	0	0	0	1	0
FBtr0113269	FBgn0039026	CG7029-RB	3R	1	0	0	0	0
FBtr0084337	FBgn0017590	klg-RA	3R	0	0	0	1	0
FBtr0084459	FBgn0015513	mbc-RA	3R	0	0	0	1	0
FBtr0111008	FBgn0259685	crb-RB	3R	0	1	1	2	0
FBtr0301865	FBgn0039234	nct-RC	3R	0	0	0	1	0
FBtr0084710	FBgn0039241	CG11089-RA	3R	0	0	0	1	0
FBtr0301134	FBgn0039466	CG5521-RB	3R	1	0	0	0	0
FBtr0070064	FBgn0000316	cin-RB	X	0	0	0	1	0
FBtr0070166	FBgn0052815	CG32815-RA	X	0	0	1	1	0
FBtr0070167	FBgn0040340	TRAM-RB	X	0	0	0	1	0
FBtr0070259	FBgn0025381	CG14782-RA	X	1	0	0	0	0

Table s3.10 (continued)

FBtr#	FBgn#	name	arm	location and type of substitution*				
				5	3	R	S	U
FBtr0100557	FBgn0026086	Adar-RC	X	0	0	0	1	0
FBtr0114454	FBgn0026873	MED18-RC	X	0	1	0	0	0
FBtr0070311	FBgn0014411	Vps26-RA	X	1	0	0	0	0
FBtr0070312	FBgn0023514	CG14805-RA	X	0	0	1	1	0
FBtr0070316	FBgn0023510	CG17766-RA	X	0	1	0	1	0
FBtr0070326	FBgn0010110	east-RB	X	0	0	0	1	0
FBtr0070376	FBgn0040395	Unc-76-RB	X	3	0	0	0	0
FBtr0301058	FBgn0025643	CG3588-RE	X	0	0	1	1	0
FBtr0301123	FBgn0026083	CG4857-RE	X	0	0	0	1	0
FBtr0070707	FBgn0011760	ctp-RC	X	0	1	0	0	0
FBtr0301793	FBgn0004368	Ptp4E-RC	X	0	0	0	1	0
FBtr0070821	FBgn0029820	CG16721-RA	X	0	0	0	1	0
FBtr0070858	FBgn0029824	CG3726-RA	X	0	0	0	0	1
FBtr0070905	FBgn0029867	CG3847-RA	X	0	2	0	0	0
FBtr0070908	FBgn0029870	Marf-RA	X	0	1	0	0	0
FBtr0071047	FBgn0029942	CG2059-RA	X	0	0	1	0	0
FBtr0071092	FBgn0029976	CG1514-RA	X	0	0	0	1	0
FBtr0071168	FBgn0020653	Trxr-1-RB	X	0	1	0	0	0
FBtr0071171	FBgn0030030	CG1636-RA	X	0	0	0	1	0
FBtr0071207	FBgn0002968	Nrg-RA	X	0	1	0	1	0
FBtr0071213	FBgn0030049	Trf4-1-RE	X	0	0	0	1	0
FBtr0071218	FBgn0030053	CG12081-RA	X	0	0	0	1	0
FBtr0071219	FBgn0025864	Crag-RA	X	0	0	1	4	0
FBtr0071222	FBgn0030056	CG11284-RA	X	0	0	0	1	0
FBtr0071365	FBgn0030145	CG3099-RB	X	0	0	0	0	1
FBtr0112976	FBgn0030234	CG15211-RC	X	1	0	0	0	0
FBtr0073448	FBgn0030286	CG1657-RA	X	0	0	0	1	0
FBtr0073454	FBgn0000499	dsh-RA	X	0	0	0	1	0
FBtr0073503	FBgn0030304	Cyp4g15-RA	X	0	0	0	1	0
FBtr0301020	FBgn0052666	CG32666-RC	X	0	1	0	1	0
FBtr0073509	FBgn0030310	PGRP-SA-RA	X	0	0	0	1	0
FBtr0073518	FBgn0030318	rho-4-RB	X	0	0	0	2	0
FBtr0073527	FBgn0014133	bif-RC	X	0	0	0	2	0
FBtr0301501	FBgn0011754	PhKgamma-RE	X	0	0	1	0	0
FBtr0073552	FBgn0030330	Tango10-RB	X	1	0	0	0	0
FBtr0273257	FBgn0030343	ATP7-RB	X	0	0	0	0	1
FBtr0073621	FBgn0030364	CG15735-RA	X	1	0	0	0	0
FBtr0073683	FBgn0011837	Tis11-RA	X	0	0	0	1	0
FBtr0073774	FBgn0030478	CG1640-RF	X	0	3	0	0	0
FBtr0073778	FBgn0030484	CG1681-RA	X	0	1	0	0	0
FBtr0073779	FBgn0030486	Set2-RA	X	0	0	1	0	1
FBtr0073808	FBgn0030505	NFAT-RA	X	0	0	0	2	0
FBtr0073810	FBgn0030508	CG15760-RA	X	0	0	0	1	0
FBtr0073821	FBgn0004047	Yp3-RA	X	0	0	0	1	0
FBtr0290021	FBgn0030575	CG5321-RB	X	0	0	1	0	0

Table s3.10 (continued)

FBtr#	FBgn#	name	arm	location and type of substitution*				
				5	3	R	S	U
FBtr0073959	FBgn0030603	CG5541-RB	X	0	0	0	1	0
FBtr0112983	FBgn0030613	rab3-GEF-RB	X	0	0	0	1	0
FBtr0074053	FBgn0030668	CG8128-RA	X	0	0	0	2	0
FBtr0111036	FBgn0003392	shi-RH	X	0	0	0	2	0
FBtr0301666	FBgn0030706	CG8909-RC	X	0	0	0	1	0
FBtr0074127	FBgn0010240	Lcch3-RA	X	0	0	0	1	0
FBtr0074134	FBgn0030717	CG8931-RA	X	0	0	0	1	1
FBtr0074136	FBgn0000611	exd-RC	X	0	1	0	0	0
FBtr0301696	FBgn0026313	X11L-RB	X	0	1	0	2	0
FBtr0074462	FBgn0030870	CG6398-RA	X	0	2	0	0	0
FBtr0074515	FBgn0030895	CG7135-RA	X	0	0	0	1	0
FBtr0301628	FBgn0083228	Frq2-RC	X	0	1	0	0	0
FBtr0074563	FBgn0030921	CG6290-RA	X	0	0	1	0	0
FBtr0074717	FBgn0027621	Pfrx-RB	X	0	0	0	1	0
FBtr0070007	FBgn0031092	CG9577-RA	X	0	0	0	1	0
FBtr0070008	FBgn0031094	CG9578-RA	X	0	0	1	2	0

* 5 for 5’ end UTR, 3 for 3’ end UTR, R for replacement substitution, S for synonymous substitution, and U for undetermined substitution between R and S

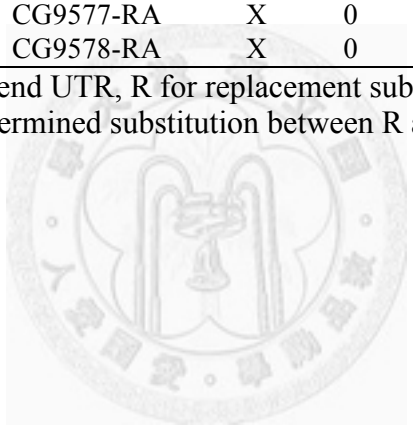

Table s3.11 The list of regions with clustered high F_{ST} sites by RNA-seq data

windows (kb)	corresponding region	number of high FST sites	genes
X chromosome (14 regions)			
2375-2377	2375001..2387000	(32, 32, 31)	trol
2516-2520	2516001..2530000	(31, 37, 40, 40, 34)	CG9904, CG13762, CG10620, sgg
6133-6138	6133001..6148000	(30, 31, 33, 34, 33, 30)	CG14445, Rbcn-3A
7175	7175001..7185000	30	CG1677, CG2059, unc-119
8135-8138	8135001..8148000	(32, 34, 34, 30)	CG2147, sni, Trxr-1, ND75, CG1632
10814-10818	10814001..10828000	(33, 31, 31, 31, 31)	CG11203, v, CG2145
10962	10962001..10972000	31	CG15203, sev
11217-11225	11217001..11235000	(39, 47, 47, 48, 48, 53, 53, 48, 36)	l(1)10Bb, CG1657, Kap3, CG34348
14120-14124	14120001..14134000	(33, 41, 39, 34, 30)	CG11138
14720-14723	14720001..14733000	(31, 31, 32, 32)	mRpL38, CG42271, Fbx14, CG1434
15803-15807	15803001..15817000	(32, 33, 34, 34, 33)	CycD, CG8909, CG8916
17550-17555	17550001..17565000	(33, 33, 33, 33, 33, 33)	CG8211, beta-Spec, CG12990
18276	18276001..18286000	30	betaCop, Tsf1, CG32549
18681-18684	18681001..18694000	(30, 30, 30, 30)	CG6961, Pk17E, CG7053, bnb
2L (3 regions)			
7009-7015	7009001..7025000	(30, 30, 30, 30, 30, 31, 31)	uif, CG13776, ade3, Pcp, CG31908
8052-8059	8052001..8069000	(33, 36, 43, 44, 47, 43, 38, 32)	CG7466, poe
9644-9648	9644001..9658000	(32, 34, 37, 36, 34)	CG15828, CG33299
2R (1 region)			
20007	20007001..20017000	31	CG3257, CG13569, tamo
3L (18 regions)			
989	989001..999000	31	CG13908, CG12938, trio
1300-1310	1300001..1320000	(30, 31, 33, 31, 33, 37, 39, 37, 30)	Scf, Rac1, CG9149, CG2277, CG2469, CG9186, CG9153
1491-1496	1491001..1506000	(33, 27, 26, 26, 27, 31)	CG12804, pUf68, Psa, cue
1531-1535	1531001..1545000	(33, 31, 32, 32, 33)	Ir62a, CG12090, CG12091, CG7852, CG3231
1590-1597	1590001..1607000	(38, 38, 44, 44, 42, 40, 37, 33)	CG13917, CG12104, CG 33791, CG 18170

Table s3.11 (continued)

windows (kb)	corresponding region	number of high FST sites	genes
2036-2042	2036001..2052000	(30, 30, 33, 34, 36, 34, 30)	CG42355, sls
2125-2134	2125001..2144000	(33, 34, 29, 32, 33, 34, 37, 33, 31, 31)	zormin
2768-2771	2768001..2781000	(35, 37, 33, 30)	CG1240, CG9977, CG12093, Atg2, mRpS3
3356-3361	3356001..3371000	(35, 34, 36, 32, 32, 30)	kst, Drs
4058-4067	4058001..4077000	(30, 25, 25, 25, 25, 29, 34, 35, 35, 31)	CG1136, CG18869, dib, wit, CG32259, Faa, Gad1
4801-4810	4801001..4820000	(30, 37, 37, 44, 47, 46, 49, 49, 46, 34)	CG7509, CG18808, Dhc64c
6958-6963	6958001..6973000	(30, 30, 30, 30, 30, 31)	CG10064, Mis12, CG9953, CG10063, G-ialpha65A, CR32385
8551-8559	8551001..8569000	(33, 40, 41, 41, 42, 42, 41, 41, 37)	rhea, CG6638
9073-9082	9073001..9092000	(30, 37, 41, 44, 46, 54, 52, 52, 53, 39)	Tequila, CG32032, CG13015
9127-9132	9127001..9142000	(30, 36, 30, 30, 30, 30)	Dhpr, Use1, nwk, CG4641
9621-9626	9621001..9636000	(35, 36, 42, 42, 41, 35)	Or67b, CG8336, fry, CG8329, CG18179, CG18180
9769-9775	9769001..9785000	(32, 32, 32, 32, 32, 31, 30)	CG8177, CG14168
13845-13847	13845001..13857000	(36, 37, 33)	Hml, CG8745
3R (1 region)			
17848-17850	17848001..17860000	(30, 32, 31)	CG6455, mRpL35, CG6028, Cch1, ND42, CG13409, CG6015